Stem cell control through tailored ion release profiles from resorbing calcium phosphate materials

Nigel De Melo, MSc



The University of Nottingham, School of Medicine

A thesis submitted to The University of Nottingham

for the degree of Doctor of Philosophy

March 2020

Acknowledgements

I would like to express my gratitude towards my supervisors, Dr. Virginie Sottile and Dr. Ifty Ahmed for their constant and invaluable guidance throughout my PhD.

My heartfelt thanks go out to my colleagues and friends, Anaid Lugo, Sarah Marsh and Zubair Ahmed who have shown me nothing but kindness, support, and wisdom, and without whom I would not have made it this far.

I would also like to thank the members of the Adult Stem Cell group (CBS) and Advanced Materials Research group (Wolfson) for their experimental, analysis and manufacturing assistance with a special mention to Laura Macri-Pellizzeri, Lauren Murrell and Towhidul Islam.

Finally, a special thanks to my family for their boundless love, support and encouragement, no matter how far they may be.

Abstract

Control of stem cell fate has been traditionally enacted by applications of proteins, cytokines, and small molecules. Recent studies suggest that inorganic ions can similarly influence stem cell behaviour and fate. Phosphate based glasses (PBGs) demonstrate tailorable dissolution rates for the local release of these ions, demonstrating potential for both hard and soft tissue regeneration. PBG microspheres have been proposed as a promising biomaterial for orthopaedic applications due to their chemical similarity to the inorganic phase of bone and the potential for their ionic dissolution products to promote bone healing and repair. This project explored the effects of ionic dissolution products on human mesenchymal stem cells (hMSCs) *in vitro* and how they may be used to control stem cell fate.

This was investigated though the application of precursor compounds in isolation and in combination onto hMSCs to optimize metabolic and osteogenic effects of the core components of a PBG system. Solid and porous PBG microspheres of seven different formulations were produced and characterized for elemental composition, thermal properties and Q^n species distribution before testing with hMSC culture. hMSC were cultured on PBGs directly to investigate the effects of PBG formulation on adhesion. PBGs were also indirectly tested through the application of ionic dissolution products into hMSC culture to identify effects on metabolic activity, alkaline phosphatase activity (ALP), matrix mineralization and gene expression changes though the use of TaqMan Low Density Arrays (TLDAs).

Compound and indirect PBG treatments demonstrated that phosphate content in culture exhibited a dose specific cytotoxic effect on hMSC (>1.25 mM) that could be reversed through the application of calcium (5 mM), magnesium (5 mM) or both in combination. Specific phosphate species such as pyrophosphate and polyphosphate likely contributed to the promotion of ALP activity while inhibiting matrix

mineralization. This suggested that a balance between pyrophosphate/polyphosphate and orthophosphate may need to be targeted to promote ALP activity without inhibiting matrix mineralization due to oversaturation. Direct hMSC culture on PBG discs revealed significant increases in cell adhesion with decreasing PBG degradation rate. Indirect studies and gene expression analysis on hMSCs revealed no cytotoxicity from the dissolution products, and no upregulation of integrin gene expression with increasing calcium and magnesium content in the PBGs tested. These findings suggest that degradation of the glass surface itself may be responsible for the lowered number of adherent cells through surface destabilization or creation of high pH/osmolarity layer at the material-cell interface. This study also investigated the previously unexplored strategy of PBG microsphere mixing. Utilizing two different formulations of PBG microspheres allowed for the leveraging of their respective properties of faster degradation and higher calcium content from one formulation, while promoting nominal metabolic activity from the other. Finally, analysis of gene expression following PBG treatment revealed the promotion of β-catenin destabilization through Notch receptor and secreted frizzled related protein 1 (*SFRP1*) upregulation which may result in the disruption of RUNX2 and β-catenin activity, key osteoblastic promoter genes.

Table of Contents

Acknowledgements i
Abstract ii
Table of Contents iv
Table of Figures ix
Table of Tables xiii
Abbreviations xiv
Chapter 1 - Introduction 1
1.1 Introduction 1
1.2 Literature review 2
1.2.1 Biomaterials 2
1.2.1.1 A brief history of orthopaedic biomaterials 2
1.2.1.2 45S5 Bioglass® 4
1.2.1.3 S53P4 5
1.2.1.4 Calcium phosphate glasses 6
1.2.1.5 Structure of phosphate-based glasses 7
1.2.1.6 Applications of PBGs 10
1.2.2 Structure and maintenance of bone 13
1.2.2.1 Bone structure and function 13
1.2.2.2 Bone Remodelling 14
1.2.2.3 Genetic pathways modulating osteogenic differentiation 16
1.2.3 Regenerative medicine 19
1.2.3.1 Mesenchymal stem cells 19
1.2.3.2 MSC applications and challenges 20
1.2.4 Ion-cell interactions 22
1.2.4.1 Phosphate 22
1.2.4.2 Calcium 23
1.2.4.3 Magnesium 25
1.2.4.4 Other inorganic ions 26
1.3 Aims and hypothesis 28
1.4 Objectives: 28
Chapter 2 - Methods 29
2.1 Cell culture 29
2.1.1 Cells 29
2.1.2 Passaging 30
2.1.3 Precursor compound supplementation 30

2.1.4 Indirect PBG testing 31
2.1.5 Direct PBG testing 31
2.1.6 Metabolic Activity 31
2.1.7 Alkaline phosphatase 31
2.1.8 Alizarin red 32
2.2 Molecular Biology 33
2.2.1 RNA Extraction 33
2.2.2 cDNA Synthesis 33
2.2.3 Reverse Transcription PCR 34
2.2.4 Agarose Gel Electrophoresis 34
2.2.5 TaqMan Low Density Arrays 34
2.3 Imaging 37
2.3.1 Bright field 37
2.3.2 Fluorescent microscopy 37
2.3.3 Scanning election microscopy 38
2.4 Materials manufacture 38
2.4.1 Glass production 38
2.4.2 Microsphere production 39
2.4.3 Glass disc production 39
2.4.4 Energy-dispersive x-ray spectroscopy 40
2.4.5 Thermal analysis 40
2.4.6 X-Ray powder diffraction 40
2.4.7 Nuclear Magnetic Resonance 41
2.4.8 Viscosity Measurement 42
2.4.9 Mass Loss 43
2.5 Statistical analysis 43
Chapter 3 - Optimization of ion concentration *in vitro* for hMSC application 44
3.1 Introduction 44
3.2 Aims and hypotheses 44
3.3 Results 46
3.3.1 Direct ion application utilizing chemical precursors 46
3.3.1.1 Effects of singular ions on hMSC 46
3.3.1.2 Effects of combinatorial ion supplementation on hMSC 52
3.3.1.3 Effects of ions on hMSC gene expression 55
3.3.1.3.1 Proliferative markers 56
3.3.1.3.2 Integrin markers 57

3.3.1.3.3 Osteoblast markers 58
3.3.1.3.4 Notch markers 60
3.3.1.3.5 TGFβ and BMP markers 61
3.3.1.3.6 Wnt markers 63
3.4 Discussion 64
3.4.1 Assessment of direct ion application to hMSC 64
3.4.1.1 Singular ion dose optimization on hMSC 64
3.4.1.2 Combinatorial dose optimization on hMSC 68
3.4.2 Effects of direct ion application on hMSC gene expression 70
3.4.2.1 Proliferation Markers 70
3.4.2.2 Integrin Markers 71
3.4.2.3 Osteoblastic Markers 72
3.4.2.4 Notch Markers 74
3.4.2.5 TGF-β and BMP Markers 75
3.4.2.6 Wnt Markers 77
3.5 Summary 79
Chapter 4 - Biological impact of phosphate for calcium substitution in PBGs 81
4.1 Introduction 81
4.2 Aims and hypotheses 81
4.3 Results 83
4.3.1 Material characterization 83
4.3.2 hMSC adhesion to PBG discs 88
4.3.3 Indirect microsphere application 91
4.3.3.1 Effects of microsphere degradation products on hMSC 91
4.3.3.2 Effects of microsphere degradation products on hMSC gene expression 94
4.3.3.2.1 Proliferative markers 95
4.3.3.2.2 Integrin marker 96
4.3.3.2.3 Osteoblast markers 96
4.3.3.2.4 Notch markers 98
4.3.3.2.5 TGFβ and BMP markers 99
4.3.3.2.6 Wnt markers 101
4.4 Discussion 103
4.4.1 Material characterization 103
4.4.2 hMSC adhesion on PBG glass 104
4.4.3 Effects of indirect treatment of PBG on hMSC 107

4.4.4 Effects of indirect treatment on hMSC gene expression 110
4.4.4.1 Proliferation markers 110
4.4.4.2 Integrin markers 111
4.4.4.3 Osteoblastic markers 111
4.4.4.4 Notch markers 115
4.4.4.5 TGF-β and BMP markers 116
4.4.4.6 Wnt markers 117
4.5 Summary 119
Chapter 5 - Microsphere formulation mixing 122
5.1 Introduction 122
5.2 Aims and hypotheses 122
5.3 Results 124
5.3.1 Material characterization 124
5.3.2 Material Spheroidization 127
5.3.3 Indirect microsphere application and mixture 129
5.3.3.1 Effects of microsphere degradation products on hMSC 129
5.3.3.2 Effects of mixed microsphere degradation products on hMSC gene expression 132
5.3.3.2.1 Proliferative markers 133
5.3.3.2.2 Integrin markers 134
5.3.3.2.3 Osteoblast markers 135
5.3.3.2.4 Notch markers 136
5.3.3.2.5 TGFβ and BMP markers 138
5.3.3.2.6 Wnt markers 140
5.4 Discussion 141
5.4.1 Material characterization 141
5.4.2 Effects of indirect treatment of PBG on hMSC 142
5.4.3 Effects of indirect treatment on hMSC gene expression 146
5.4.3.1 Proliferation markers 146
5.4.3.2 Integrin markers 147
5.4.3.3 Osteoblastic markers 148
5.4.3.4 Notch markers 149
5.4.3.5 TGF-β and BMP markers 150
5.4.3.6 Wnt markers 150
5.5 Summary 154
Chapter 6 - Microsphere formulation optimization for osteogenic response 157

6.1 Introduction 157
6.2 Aims and hypotheses 157
6.3 Results 159
6.3.1 Material characterization 159
6.3.2 Material Spheroidization 162
6.3.3 Indirect microsphere application 163
6.3.3.1 Effects of P45 microsphere degradation products on hMSC 163
6.3.3.2 Effects of mixed microsphere degradation products on hMSC gene expression 166
6.3.3.2.1 Proliferative markers 167
6.3.3.2.2 Integrin markers 168
6.3.3.2.3 Osteoblast markers 169
6.3.3.2.4 Notch markers 170
6.3.3.2.5 TGFβ and BMP markers 172
6.3.3.2.6 Wnt markers 174
6.4 Discussion 176
6.4.1 Material characterization 176
6.4.2 Effects of indirect treatment of PBG on hMSC 177
6.4.3 Effects of indirect treatment on hMSC gene expression 180
6.4.3.1 Proliferation markers 180
6.4.3.2 Integrin markers 180
6.4.3.3 Osteoblastic markers 180
6.4.3.4 Notch markers 183
6.4.3.5 TGF-β and BMP markers 184
6.4.3.6 Wnt markers 184
6.5 Summary 186
Chapter 7 - Final Discussion 188
7.1 Possible role of PBGs in β-catenin destabilization 188
7.2 Pyrophosphate and its role in matrix mineralization 192
7.3 PBG design for adhesion or osteogenic differentiation 194
7.4 Future work 196
7.5 Final conclusions 198
References: 199
Appendix I – PrestoBlue Optimization 231
Appendix II – cDNA validation 232

Table of Figures

Figure 1.1 (A) The phosphate tetrahedra and (B) its combination with other tetrahedra to form a polymerized phosphate anion chain. 7

Figure 1.2. Q^n species structure as the number of BO (n) are reduced. 8

Figure 1.3 (A) Addition of a modifier oxide (CaO) to a phosphate bond and (B) its formation of ionic crosslinking between the two phosphate chains creating non-bridging oxygen bonds (NBO). 9

Figure 1.4. Scanning electron micrographs of an L3 vertebra in (A) a 31-year-old woman and (B) a 70-year-old woman. Adapted from Poole and Compston (2006). ..11

Figure 1.5. Diagram indicating the proposed mode of action of PBG microspheres when injected into osteoporotic bone. 12

Figure 1.6. Schematic of the basic multicellular unit (BMU) illustrating key cells and stages involved in bone remodelling.....15

Figure 1.7. Major regulatory pathways involved in osteogenic differentiation 17

Figure 1.8. Overview of cell responses to dissolution products of bioactive glasses. Adapted from Hoppe et al. (2011). 22

Figure 3.1. (A) The metabolic (day 2, 7 and 11), (B) ALP (day 11) and (C) ALZ intensity (day 21) of hMSC treated with 5, 10 and 20mM calcium.....47

Figure 3.2. (A) The metabolic (day 2, 7 and 11), (B) ALP (day 11) and (C) ALZ intensity (day 21) of hMSC treated with 5, 10 and 20mM magnesium 48

Figure 3.3. (A) The metabolic (day 2, 7 and 11), (B) ALP (day 11) and (C) ALZ intensity (day 21) of hMSC treated with 5, 10 and 20mM phosphate 49

Figure 3.4. Alizarin red staining on hMSCs treated with 5, 10 and 20 mM calcium, magnesium and phosphate on day 21 50

Figure 3.5. (A) The metabolic (day 2, 7 and 11), (B) ALP (day 11) and (C) ALZ intensity (day 21) of hMSC treated with 5, 2.5 and 1.25 mM phosphate 51

Figure 3.6. (A) The metabolic (day 2, 7 and 11), (B) ALP (day 11) and (C) ALZ intensity (day 21) of hMSC treated with combinations of 5 mM calcium, 5 mM magnesium and 1.25 mM phosphate 53

Figure 3.7. (A) The metabolic (day 2, 7 and 11), (B) ALP (day 11) and (C) ALZ intensity (day 21) of hMSC treated with combinations of 5 mM calcium, magnesium and phosphate.....54

Figure 3.8. hMSC proliferation marker expression after 11 days of OM and 555 treatment normalized to the standard medium (SM) control. 56

Figure 3.9. Heatmap of hMSC integrin gene expression after 11 days of OM and 555 treatment normalized to the standard medium (SM) control. 57

Figure 3.10. hMSC osteoblastic gene expression after 11 days of OM and 555 treatment normalized to the standard medium (SM) control. 59

Figure 3.11. hMSC notch gene expression after 11 days of OM and 555 treatment normalized to the standard medium (SM) control 60

Figure 3.12. hMSC TGFB and BMP gene expression after 11 days of OM and 555 treatment normalized the standard medium (SM) control.....62

Figure 3.13. hMSC WNT gene expression after 11 days of OM and 555 treatment normalized to the standard medium (SM) control. 63

Figure 4.1. Glass characterization of P40, P35 and P30. (A) Thermal analysis traces via DSC of the PBG formulations showing T_g, T_c and T_m. (B) XRD spectra confirming the amorphous nature of P40, P35 and P30 glasses produced. 84

Figure 4.2. ^{31}P NMR spectra of the P40, P35 and P30 formulations. 86

Figure 4.3. Adherence of MSC analysed at 24 hours after seeding on P40, P35, P30 and TCP control.....89

Figure 4.4. Average mass loss per cm^2 of P40, P35 and P30 discs over 30 days (A) and average rate of loss (B).....90

Figure 4.5. (A) The metabolic (day 2, 7 and 11), (B) ALP (day 11) and (C) ALZ intensity (day 21) of hMSC treated with the dissolution products of P40, P35 and P30 compared to standard medium (SM) and osteogenic medium (OM).....92

Figure 4.6. (A) The metabolic (day 2), (B) ALP (day 11) and (C) ALZ intensity (day 21) of hMSC treated with the dissolution products of P40, P35 and P30 incubated in standard medium (SM) and osteogenic medium without β-glycerophosphate (OM-) compared to SM, OM and OM- controls.....93

Figure 4.7. hMSC proliferation marker expression after 11 days of P40 and P40OM- treatment normalized to the standard medium (SM) control 95

Figure 4.8. hMSC integrin gene expression after 11 days of P40 and P40OM- treatment normalized to the standard medium (SM) control 96

Figure 4.9. hMSC osteoblast gene expression after 11 days of P40 and P40OM- treatment normalized to the standard medium (SM) control 97

Figure 4.10. hMSC notch gene expression after 11 days of P40 and P40OM- treatment normalized to the standard medium (SM) control 99

Figure 4.11. hMSC TGFβ and BMP gene expression after 11 days of P40 and P40OM- treatment normalized to the standard medium (SM) control 100

Figure 4.12. hMSC Wnt gene expression after 11 days of P40 and P40OM- treatment normalized to the standard medium (SM) control 102

Figure 4.13. Alignment of P40, P35 and P30 to the predictions presented by Wazer and Fluck (1959). 104

Figure 5.1. Glass characterization of P50Ca50, P50Ca50Mg50 and P50Mg50. (A) Thermal analysis traces via DSC of the PBG formulations showing T_g, T_c and T_m. (B) XRD spectra confirming the amorphous nature of P50Ca50, P50Ca50Mg50 and P50Mg50 glasses produced. 125

Figure 5.2. ^{31}P NMR spectra of the P50Ca50, P50Ca25Mg25 and P50Mg50 formulations 127

Figure 5.3. SEM scans of resin embedded sections of (A) P50Ca50, (B) P50Ca25Mg25, (C) P50Mg50 and (D) viscosity of the P40 and P50Ca50 PBGs via a high temperature viscometer 128

Figure 5.4. The metabolic activity of hMSC treated with the dissolution products of (A) P50Ca50, P50Ca25Mg25 and P50Mg50 and (B) mixes of 0-100% P50Ca50 mixed with P40 compared to standard media (SM) and osteogenic media (OM)..... 130

Figure 5.5. The metabolic (A; day 2, 7 and 11), ALP (B; day 11) and ALZ activity (C; day 21) of hMSC treated with the dissolution products of P40 mixed with 0-25% of P50Ca50 compared to standard medium (SM) and osteogenic medium (OM) 131

Figure 5.6. hMSC proliferation gene expression after 11 days of Mix and MixOM- treatment normalized to SM control 133

Figure 5.7. hMSC Integrin gene expression after 11 days of Mix and MixOM- treatment normalized to SM control 134

Figure 5.8. hMSC osteoblast gene expression after 11 days of Mix and MixOM- treatment normalized to SM control 136

Figure 5.9. hMSC Notch gene expression after 11 days of Mix and MixOM- treatment normalized to SM control 137

Figure 5.10. hMSC TGFβ and BMP gene expression after 11 days of Mix and MixOM- treatment normalized to SM control 139

Figure 5.11. hMSC Wnt gene expression after 11 days of Mix and MixOM- treatment normalized to SM control 140

Figure 6.1. Glass characterization of P45. (A) Thermal analysis traces via DSC showing T_g, T_c and T_m. (B) XRD spectra confirming the amorphous nature of P45 and P50Ca25Mg25. 160

Figure 6.2. ^{31}P NMR spectra of the P45 and P50Ca25Mg25 PBG formulations..... 161

Figure 6.3. SEM scans of resin embedded sections of (A) P45 and (B) P40. 162

Figure 6.4. (A) The metabolic (day 2, 7 and 11), (B) ALP (day 11) and (C) ALZ intensity (day 21) of hMSC treated with the dissolution products of P45 compared to SM and OM 164

Figure 6.5. (A) The metabolic (day 2), (B) ALP (day 11) and (C) ALZ intensity (day 21) of hMSC treated with the dissolution products of P45 incubated in SM and OM- compared to SM, OM and OM- controls 165

Figure 6.6. hMSC proliferation gene expression after 11 days of P45 and P45OM- treatment normalized to SM control. 167

Figure 6.7. hMSC integrin gene expression after 11 days of P45 and P45OM- treatment normalized to SM control 168

Figure 6.8. hMSC osteoblast gene expression after 11 days of P45 and P45OM- treatment normalized to SM control 170

Figure 6.9. hMSC Notch gene expression after 11 days of P45 and P45OM- treatment normalized to SM control. *$p<0.05$ 171

Figure 6.10. hMSC TGFβ and BMP gene expression after 11 days of P45 and P45OM- treatment normalized to SM control 173

Figure 6.11. hMSC Wnt gene expression after 11 days of P45 and P45OM- treatment normalized to SM control 175

Figure 7.1. Illustration demonstrating (A) The successful activation of the Wnt pathway through the binding of a Wnt ligand to the LRP-FZD coreceptors resulting in the inhibition of the GSK3 destruction complex and accumulation of β-catenin (β-cat) in the nucleus which binds to TCF/LEF and promotes gene transcription. (B) The proposed mechanism of PBG mediated β-catenin destabilization through the binding of Wnt ligands by SFRP1, preventing them from activating the LRP-FZD coreceptors resulting in the phosphorylation and destruction of β-catenin (β-cat) by the GSK3 destruction complex. (C) The second proposed mechanism of PBG mediated β-catenin destabilization through the binding of the Notch target gene Hes1 to Groucho, preventing the accumulated β-catenin (β-cat) from Wnt signalling from promoting transcription. 191

Table of Tables

Table 2.1 Precursor compounds used for medium supplementation 30

Table 2.2. TLDA gene list 36

Table 2.3. PBGs manufactured 38

Table 3.1 Index of gene groups analysed in chapter 3 55

Table 4.1. EDX measurements of glass compositions against target formulation (mol%) ± standard error of the mean (SEM). 83

Table 4.2. Glass transition (T_g), onset of crystallisation (T_c), melting temperature (T_m) and calculated thermal processing window (Tc_{onset}) for P40, P35 and P30. 85

Table 4.3. Distribution of Qn species across PBG formulations 87

Table 4.4. Index of gene groups analysed in chapter 4 94

Table 5.1. EDX measurements of P50Mg50, P50Ca25Mg25 and P50Ca50 against target formulation (mol%) ± standard error of the mean (SEM). 124

Table 5.2. Glass transition (T_g), onset of crystallisation (T_c), melting temperature (T_m) and calculated thermal processing window (Tc_{onset}) for each of the PBG glass formulations explored. 126

Table 5.3. Distribution of Q^n species across PBG formulations 127

Table 5.4. Index of gene groups analysed in chapter 5 132

Table 6.1. EDX measurements of P45 and P50Ca25Mg25 against target formulation (mol%) ± standard error of the mean (SEM). 159

Table 6.2. Glass transition (T_g), onset of crystallization (T_c), melting temperature (T_m) and calculated thermal processing window (Tc_{onset}) for P45 and P50Ca25Mg25 160

Table 6.3. Distribution of Q^n species across PBG formulations 161

Table 6.4. Index of gene groups analysed in chapter 6 166

Abbreviations

555	5 mM calcium, magnesium and phosphate
ALP	Alkaline phosphatase
ALZ	Alizarin red
ASC	Adult stem cells
BGLAP	Osteocalcin
BMP	Bone morphogenic protein
BO	Bridging oxygen
CaP	Calcium phosphate
CaSR	Calcium sensing receptor
CCND1	Cyclin D1
DLX	Distal-less homeobox
DMEM	Dulbecco's modified eagle medium
DSC	Differential scanning calorimeter
DSL	Delta/Serrate/Lag2 ligands
ECM	Extracellular matrix
EDTA	Ethylenediaminetetraacetic acid
EDX	Energy dispersive x-ray spectroscopy
ESC	Embryonic stem cells
FBS	Fetal bovine serum
FGF	Fibroblast growth factor
GvHD	Graft versus host disease
HA	Hydroxyapatite
HES	Hairy/Enhancer-Of-Split
HEY	Hairy/Enhancer-Of-Split Related with YRPW Motif
HLA	Human leukocyte antigen
hMSC	Human mesenchymal stem cell
hMSC-GFP	Green fluorescent protein positive hMSC
iPSC	Induced pluripotent stem cell
ITGA	Integrin α subunit
ITGB	Integrin β subunit
LEF	Lymphoid enhancer factor

MGP	Matrix gla protein
MIK67	Marker Of proliferation Ki-67
Mix	SM conditioned with 10% P50Ca50 and 90% P40
MixOM-	OM- conditioned with Mix
MO	Modifier oxides
MSC	Mesenchymal stem cell
NBO	Non-bridging oxygen
OM	Osteogenic medium
OM-	Osteogenic medium without β-glycerophosphate
OPN	Osteopontin
OSX	Osterix
P40	SM conditioned with P40
P40OM-	OM- conditioned with P40
P45	SM conditioned with P45
P45OM-	OM- conditioned with P45
PBG	Phosphate based glass
PBS	Phosphate buffered solution
PCNA	Proliferating cell nuclear antigen
PPAR-γ	Peroxisome proliferator activated receptor γ
PTH	Parathyroid hormone
RUNX	Runt related transcription factor
SDW	Sterile distilled water
SEM	Standard error of the mean
SM	Standard medium
SPP1	Osteopontin
TAE	Tris-acetate-EDTA
TCF	T-cell factor
TCP	Tissue culture plastic
TGF-β	Transforming growth factor β
TLDA	TaqMan Low Density Array
XRD	X-ray powder diffraction

Chapter 1 - Introduction

1.1 Introduction

There is increasing interest in the use of phosphate-based glasses (PBGs) for bone fillers, scaffolds, and tissue engineering applications due to compositions being developed with a chemical similarity to the inorganic phase of bone. PBGs have been demonstrated to be both bioactive and resorbable and increasing evidence suggests that the ionic dissolution products from degrading PBGs can influence stem cell function and fate (Hoppe et al., 2011; Kasuga, 2005; Murphy et al., 2014).

The following subsection contains a literature review covering topics relevant to this study: (1.2.1) Biomaterials with a focus on bioactive glasses, their structure and applications, (1.2.2) The structure and homeostasis of bone, (1.2.3) Regenerative medicine, its applications and challenges, and finally (1.2.4) PBG ion dissolution products and their interactions with stem cells. Following the literature review, the aims and objectives of this PhD thesis are presented (1.3 and 1.4).

1.2 Literature review

1.2.1 Biomaterials

Biomaterial development is driven by the need to replace and repair damaged tissue. This need for restoration of biological function can be aided or accomplished using biomaterials for the creation of implants, promotion of tissue restoration and drug delivery systems. The following subsections contains a brief overview of biomaterial history as well as a focused review of PBG structure and applications.

1.2.1.1 A brief history of orthopaedic biomaterials

First generation biomaterials were developed for use *in vivo* and were largely prostheses, engineered for their bioinert nature and mechanical strength (Hench and Thompson, 2010). These biomaterials were developed with a biomimetic approach, attempting to mimic the structural and physical properties of the host tissue with minimal toxic response (Hench, 1980). These materials largely consisted of commercially existing single phase materials of higher purity to minimize the toxic effects of corrosion (Hench and Thompson, 2010). Composite materials were later seen in the 1980s in a push toward materials that closely resembled the mechanical properties of bone. Hapex is a successful example of a composite biomaterial utilized for the replacement of middle ear bone. It is comprised of 40% hydroxyapatite (HA) within a high-density polyethylene matrix and was demonstrated to approach the lower bounds of stiffness compared to cortical bone (4.4 GPa vs 7 GPa) (Dalby et al., 2003; Deb et al., 1996).

Second generation biomaterials shied away from attempting to be bioinert and instead controlled bioactive responses were sought. These responses were developed to encourage the bonding of the implant and the host tissue. Bioactive glasses developed

during this time explored this interface formation between the host tissue and material, and was largely reliant on the formation of a hydroxy-carbonate apatite layer (Hench et al., 1971). This new layer at the material surface was demonstrated to be similar to that of the mineral phase of bone which provided an ideal interface for cell-material bonding (Hench and Thompson, 2010). Soluble HA coatings were also used to promote osteoconduction along the material-bone interface, eliciting bone growth around the coating, promoting stronger interface bonding (Hench and Thompson, 2010). A number of these biomaterials have been approved for clinical use such as NovaBone (45S5), BonAlive (S53P4), StronBone and TheraGlass, and this review has briefly detailed the 45S5 and S53P4 formulations in the next subsection.

It is important to note the significant shift in philosophy that accompanied the transition from second to third generation biomaterials. Hench and Thompson (2010) highlighted not only the successes but also the failures of bioinert and bioactive implants. They noted the failure rates being a large detriment to their efficacy and the lack of significant improvements to the growing issue. After recognition of the limits of tissue replacement; the inherent impossibility of attempting to engineer a material to withstand ever-changing physical loads, biochemical stimuli, managing material toxicity and longevity, the emphasis transitioned from attempting to replace tissues to the regeneration of tissues (Hench and Thompson, 2010).

With these issues in mind, third generation biomaterials were produced that combined the core faculties of prior materials. These new materials were often both resorbable and bioactive, more so than their predecessors, eliciting much deeper biological responses from increased proliferation to differentiation.

1.2.1.2 45S5 Bioglass®

The mineral phase of bone is largely formed from hydroxyapatite ($Ca_{10}(PO_4)_6(OH)_2$) and as such fabricated materials often utilize chemically similar components such as calcium phosphates and tricalcium phosphates (Dorozhkin, 2010; Hoppe et al., 2011). Funded by the US Army Medical Research and Development Command, Bioglass® was developed to replace traditional metallic and synthetic prosthesis materials due to the high risk of rejection. Bioglass® attempted to repair bone using ceramic implants that were in part measured in their success by the formation of a HA interface between the implant and the host tissue as seen in the testing of an early formulation of Bioglass® in 1971 (Hench, 2006). 45S5 was first approved for clinical use in 1985 as a middle ear bone prosthesis to treat conductive hearing loss (Merwin, 1986). It saw further use as a particulate (Biogran and PerioGlas) to be mixed with a liquid to allow for a viscous mouldable consistency that could then be implanted into a defect (Baino et al., 2018).

The 45S5 Bioglass® composition ($45SiO_2{\cdot}24.5CaO{\cdot}24.5Na_2O{\cdot}6P_2O_5$ wt%) demonstrated a surface reaction leading to the release of soluble ionic species including calcium and phosphate, as well as the formation of a hydrated silica gel layer. This layer then adsorbs amorphous calcium phosphate which is then crystalized to form a hydroxy-carbonate apatite layer at the material interface (Gunawidjaja et al., 2012; Hench and Thompson, 2010; Kokubo, 1998). This layer is suggested to promote adsorption of growth factors, proliferation and the mineralization of the matrix (Hott et al., 1997; Shu et al., 2003). It is later shown that Bioglass® 45S5 is not only osteoconductive (Yuan et al., 2001), but also promotes osteoblast specific protein activity stimulated by the dissolution products of the degrading glass (Xynos et al., 2001). Increasing evidence suggests that these released ions play a far greater role in osteogenesis and other biological processes than previously thought (Barradas et al., 2012; Rodrigues et al., 2014; Saltman and Strause, 1993; Srivastava et al., 2013; Yang et al., 2011; Yoshizawa

et al., 2014a). There have been numerous studies testing the role of various ions such as calcium (Barradas et al., 2012; Danoux et al., 2015; Navarro et al., 2003b), strontium (Strobel et al., 2013; Yang et al., 2011, 2011) and magnesium (Solomons and Styner, 1969; Yoshizawa et al., 2014a, 2014b) in bone metabolism, which are detailed in subsection 1.2.4 within this review.

1.2.1.3 S53P4

S53P4 ($53SiO_2 \cdot 20CaO \cdot 23Na_2O \cdot 4P_2O_5$ wt%) is a bioactive glass used to treat bone infections with a 90% success rate due to its antibacterial properties (van Gestel et al., 2019, 2015). S53P4 in fluid initiates ion exchange with its local environment. This ion exchange increases the local pH and osmotic pressure resulting in the inhibition of bacterial growth while generating a silica gel layer at the glass surface. Calcium and phosphate then precipitate onto the silica layer and crystalize to form HA, enabling bone bonding (van Gestel et al., 2015). S53P4 has been used as a bone graft substitute for a number of clinical applications such as craniofacial surgeries, osteomyelitis treatments and grafting of bone tumour defects (van Gestel et al., 2015). While S53P4 demonstrated efficacy in clearing the majority of infections in bone graft applications, the slow dissolution rate resulted in the presence of S53P4 up to 10 years after implantation that may have negative effects on bone remodelling (Lindfors et al., 2010).

1.2.1.4 Calcium phosphate glasses

As mentioned previously, there is significant interest in using calcium phosphates for the formation of these biomaterials due to its chemical similarity to the inorganic phase of bone and their tailorable solubility. While extremely well characterized, 45S5 and S53P4 are silica based bioactive glasses, notable for their low dissolution rates (Abou Neel et al., 2009). In contrast, phosphate based glasses (PBGs) can be completely solubilized and the time taken to do so can be tailored from a few days to months by manipulating its composition (Navarro et al., 2003b). This increased solubility, and thus faster ion release profile, may prove effective in utilizing the released ions such as calcium and magnesium to drive stem cell commitment and differentiation. There is increasing investigation into the use of PBGs and their dissolution products for the control and manipulation of cell activity. Studies have demonstrated their potential for wound healing (Sghayyar et al., 2020), tissue defect infiltration (McLaren et al., 2019), promotion of osteogenic genes (Lin et al., 2020) and neurite outgrowth among others (Kim et al., 2015).

1.2.1.5 Structure of phosphate-based glasses

PBGs consist of a three-dimensional network of phosphate tetrahedra that comprise the basic building blocks of these glasses (Ahmed et al., 2018). Oxygen atoms covalently bridge these phosphate tetrahedra, giving rise to P-O-P bonds, enabling their formation. Unlike silicate glasses, the phosphate tetrahedra contain a single terminal double bonded oxygen, reducing its network connectivity (Islam et al., 2017). The tetrahedral phosphate structure and chain formation are illustrated in Figure 1.1.

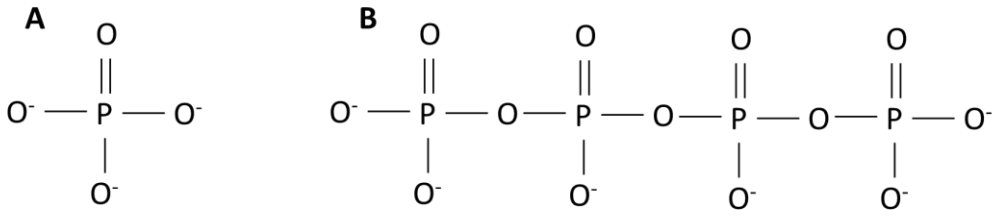


Figure 1.1 (A) The phosphate tetrahedra and (B) its combination with other tetrahedra to form a polymerized phosphate anion chain.

Phosphate tetrahedra are classified using Q^n terminology where n represents the number of bridging oxygen (BO) per tetrahedron (Figure 1.2) (Brow, 2000). Q^3 to Q^0 denotes a gradual decrease in structural connectivity and influences the range of phosphate structures that are produced. Figure 1.2 illustrates the Q^n species that can be formed and the decrease of BO as Q^3 transitions to Q^0.

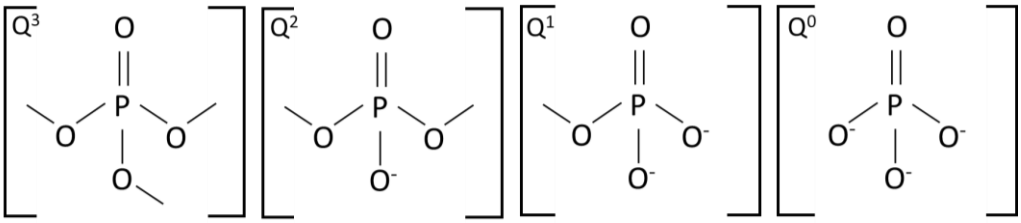


Figure 1.2. Q^n species structure as the number of BO (n) are reduced.

As PBGs can incorporate various oxides such as CaO, MgO and NaO as network modifiers, using specific oxides can confer cellular benefits when released in addition to modifying glass properties (Murphy et al., 2014). These modifier oxides (MO) can act to crosslink phosphate chains and gradual addition of MOs typically causes a shift from Q^3 to Q^0 as the oxides disrupt the structural connectivity within the PBG, effectively depolymerizing it and generating non-bridging oxygen bonds (NBO) (Hoppe et al., 2000). MOs have been added to PBGs to modify their properties, including to control their degradation rates, viscosity and thermal stability (Hossain et al., 2014; Parsons et al., 2015a). Figure 1.3 illustrates the introduction of CaO to a phosphate glass network and the crosslinking that occurs.

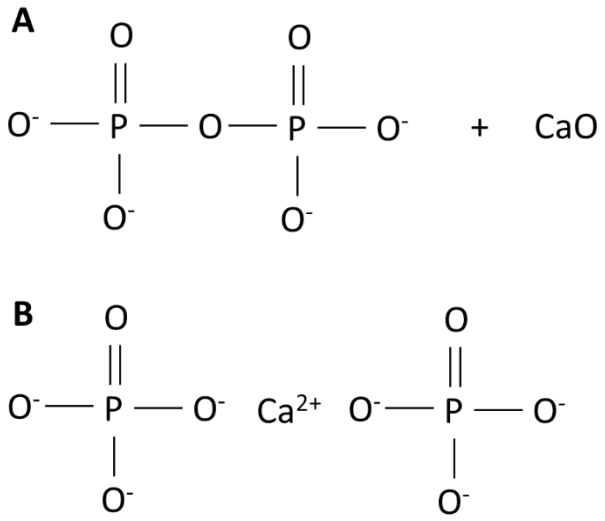


Figure 1.3 (A) Addition of a modifier oxide (CaO) to a phosphate bond and (B) its formation of ionic crosslinking between the two phosphate chains creating non-bridging oxygen bonds (NBO).

PBGs typically demonstrate rapid degradation in water, however, their degradation occurs through two distinct mechanisms, hydration and hydrolysis (Bunker et al., 1984). Hydration occurs when ions such as Na^+ are exchanged with H^+ from water, resulting in the formation of a hydrated layer on the glass surface. Water also attacks the glass by hydrolysing P-O-P bonds producing terminating P-OH groups, thereby reducing number of BOs and disrupting the glass network (Bunker et al., 1984; Gao et al., 2004). Glass dissolution can also be aided by acid/base catalysis in which ionic bonds between phosphate chains are disrupted by the local pH (Bunker et al., 1984).

1.2.1.6 Applications of PBGs

Due to their rapid and controllable solubility compared to silica based glasses, numerous applications have been investigated for PBGs including the delivery of antibacterial ions, tissue engineering, orthopaedic materials and even as trace element supplements for animals (Knowles, 2003). By doping PBGs with ions known to have deleterious effects on microbes such as silver or copper, PBGs can be developed to have long-term antimicrobial effects as the PBG degrades (Ahmed et al., 2006; Foroutan et al., 2019; Jung et al., 2008). The controllable release rates of PBGs allow for a sustained delivery of antimicrobial ions when implanted into a wound or graft site, decreasing bacterial infections and the need for revision surgery (Foroutan et al., 2019). Similarly, the controlled release of ions from PBGs have been demonstrated to elicit a variety of cellular responses such as proliferation, adhesion and matrix mineralization (Murphy et al., 2014). Triggering cellular responses such as these through the use of inorganic ions without the use of growth factors demonstrates immense potential for hard and soft tissue regeneration.

Hard tissue regeneration has been previously explored with calcium phosphate containing materials due to their ability to bond bone at the material interface (Bohner and Lemaitre, 2009). PBGs have been investigated to provide this bioactive effect in composites, however, due to their complete solubility they are able to degrade once healing is complete (Lapa et al., 2020). PBG composites show potential for use as bioresorbable fixation devices that degrade over time, slowly shifting the load onto newly generated bone (Felfel et al., 2013; Haque et al., 2010). PBGs also demonstrate great potential for soft tissue regeneration in a variety of cell types. Kim et al. (2015) demonstrated the ability of PBG fibres to promote neuronal growth in a rat model, demonstrating increased motor function recovery 8-weeks after implantation and Lin

et al. (2020) demonstrated the ability of PBG fibres to promote osteogenic differentiation in murine osteoblast cells over 21 days.

Calcium phosphate glass microspheres could potentially be used for bone tissue regeneration in the treatment of a number of bone metabolic diseases and defects (Hossain et al., 2015). Osteoporosis is one such musculoskeletal disease that significantly increases the risk of fragility fractures, due to decreased bone mineral density and microarchitectural deterioration that compromises the strength of the tissue (Kanis et al., 2013; Willson et al., 2015). Figure 1.4 compares the vertebral bone architecture of a woman without (31-year-old, Figure 1.4A) and with (70-year-old, Figure 1.4B) osteoporosis, demonstrating the loss in structural connectivity.

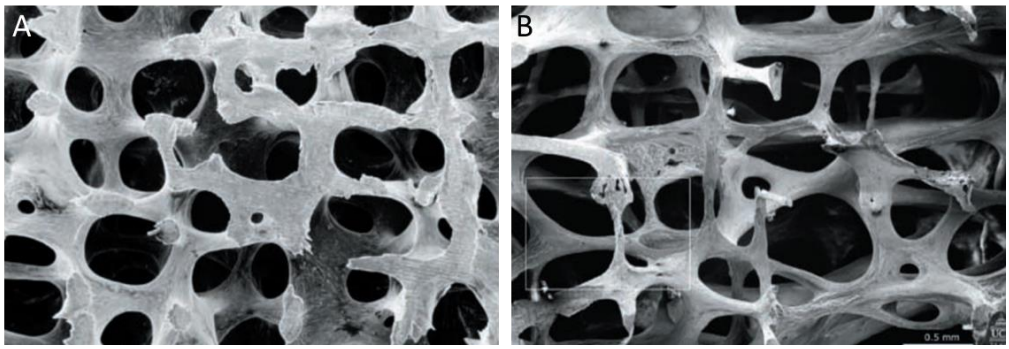


Figure 1.4. Scanning electron micrographs of an L3 vertebra in (A) a 31-year-old woman and (B) a 70-year-old woman. Adapted from Poole and Compston (2006).

To combat low bone mass, PBGs can be produced in spherical geometries which have been demonstrated to have numerous advantages over fixed geometry implants such as the ability to be injected in a minimally invasive way, enhanced surface area and increased tissue infiltration (Cai et al., 2013; Gupta et al., 2018; Hossain et al., 2015; Matamoros-Veloza et al., 2020; McLaren et al., 2019). McLaren et al. (2019) demonstrated the ability of porous PBG microspheres to fill an induced bone defect in

sheep and promote tissue ingrowth as well as increased osteoid tissue content 13 weeks post-implantation. To further support its use as an injectable therapy, Matamoros-Veloza et al. (2020) demonstrated the injectability of PBG microspheres using a delivery agent such as xanthan gum to allow for their injection through a 18-14G needle.

If used as a prophylactic agent, these microspheres could reduce risk and incidence of fracture through the controlled dissolution of inorganic ions into the osteoporotic bone as proposed in Figure 1.5. These inorganic ions may be used to promote bone regeneration, strengthening the osteoporotic bone and thereby reducing risk of fracture. The mechanisms of bone homeostasis and the influence of ions on stem cells are reviewed below.

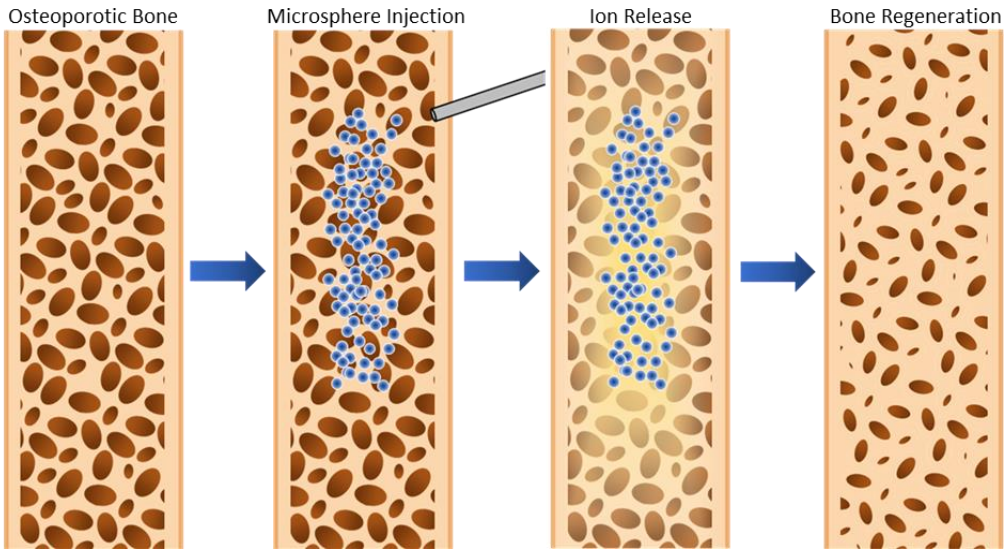


Figure 1.5. Diagram indicating the proposed mode of action of PBG microspheres when injected into osteoporotic bone.

1.2.2 Structure and maintenance of bone

1.2.2.1 Bone structure and function

Bone is a rigid, mineralized organ that plays a variety of significant roles within the body such as locomotion, protection and structural support (Florencio-Silva et al., 2015). Bone is comprised of both organic and inorganic materials. Organic materials such as collagen and fibronectin provide tensile strength while inorganic materials such as hydroxyapatite comprise the majority of the bone and provide tissue stiffness (Boskey, 2013; Chang et al., 2017). The outer layer of bone is compact and strong, typically comprised of 90% bone and 10% pore space which are represented by Haversian canals. This dense outer layer houses cancellous bone defined by its honeycomb structure. Cancellous bone is less dense than cortical tissue and is typically comprised of only 25% bone due to its honeycomb structure. The cortical bone defines the bone shape while its firm exterior provides sufficient support for tendons. The interior spongy structure provides significant structural support and surface area for mineral exchange (Mechiche Alami et al., 2016).

1.2.2.2 Bone Remodelling

Bone is a metabolically active and highly adaptive tissue that is capable of responding to mechanical stimuli and self-repair (Robling et al., 2006). It is composed of four unique cell types, osteoblasts, bone lining cells, osteocytes and osteoclasts (Buckwalter et al., 1996; Florencio-Silva et al., 2015). These cells work in conjunction to maintain the bone remodelling process. These four cell types can be further characterized into bone forming, resorbing and maintenance cells. Osteocytes and bone lining cells work to maintain bone while the function of osteoblasts and osteoclasts is to carry out bone formation and resorption respectively (Robling et al., 2006).

Osteoblasts are derived from undifferentiated mesenchymal cells (MSCs) within the marrow. They tightly line the surface of bone and actively secrete organic matrix that is then later mineralized (Marks and Popoff, 1988). Osteocytes are osteoblasts that have become trapped within the bone matrix they synthesize and represent 90-95% of all bone cells (Bellido, 2014; Rochefort et al., 2010). These osteocytes are linked through their distinct dendritic morphology and have been thought to play a role in the response to physical stimuli due to their strain sensitive nature (Bellido, 2014; Bonewald, 2005). Alternatively, osteoblasts can form bone lining cells through metabolic inactivity (Downey and Siegel, 2006). These thin elongated cells cover most bone surfaces, they function as a barrier between bone and other compartments and assist in the bone remodelling process. Osteoclasts resorb mineralized bone and cartilage and are located on the surface of bone near large vascular channels (Marks and Popoff, 1988).

As it ages, bone begins to lose its structural integrity and requires constant maintenance through resorption of old bone and synthesis of new bone. Though carried out by osteoclasts and osteoblasts respectively, bone resorption and synthesis

are not independent processes. Temporary anatomic structures called basic multicellular units (BMU) that consist of osteoclasts, osteoblasts, a blood supply and connective tissue carry out the bone remodelling process through coordination of these cell types (Jilka, 2003; Visconti et al., 2019). Production of collagenase by the bone lining cells exposes the bone surface to osteoclastic bone resorption (Hauge et al., 2001). As the BMU advances, the osteoclasts resorb the exposed bone while the osteoblasts within the BMU begin to synthesis new bone in a process taking up to four months (Jilka, 2003). As mentioned earlier, the osteoblasts that synthesize bone eventually encase themselves within the matrix they produce to form osteocytes or flatten out and become quiescent bone lining cells to layer the newly produced bone surface (Hauge et al., 2001). The process of bone formation by the BMU is illustrated in Figure 1.6.

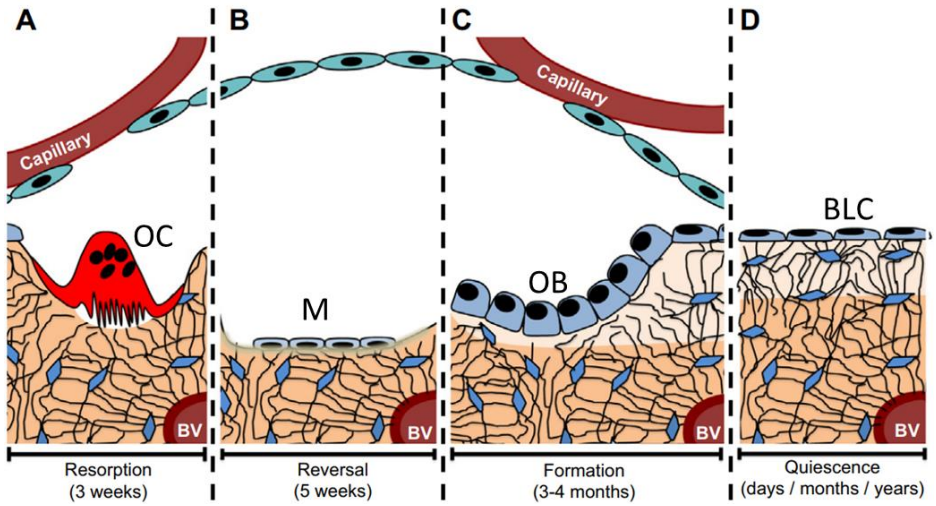


Figure 1.6. Schematic of the basic multicellular unit (BMU) illustrating key cells and stages involved in bone remodelling. (A) Initiation of bone resorption by osteoclasts (OC) under the capillary connected canopy. (B) Reversal by macrophages (M) which prime the resorption surface for bone formation. (C) Osteoblasts (OB) generate new osteoid to fill the degraded pit which is mineralized over time. (D) Completion of the bone remodelling process, covering the new bone surface with bone lining cells (BLC). Adapted from (Sims and Martin, 2020).

1.2.2.3 Genetic pathways modulating osteogenic differentiation

The coordinated function of osteoblasts and osteoclasts in both bone synthesis and resorption is critical for the maintenance of bone. MSCs are the precursors to osteoblasts and their commitment and differentiation down the osteogenic lineage strongly influences bone homeostasis. Runt-related transcription factor 2 (RUNX2) is a master regulator of osteogenic differentiation and is acted upon by a number of signalling pathways. Komori et al. (1997) highlighted the importance of RUNX2 in detailed studies on homozygous RUNX2 knockout mice which resulted in a fatal phenotype due to complete ablation of mineralization and arrest of osteoblast differentiation. This section briefly discusses the mechanisms of the main pathways involved in osteogenic differentiation and how they influence RUNX2 activity. These pathways are illustrated in Figure 1.7.

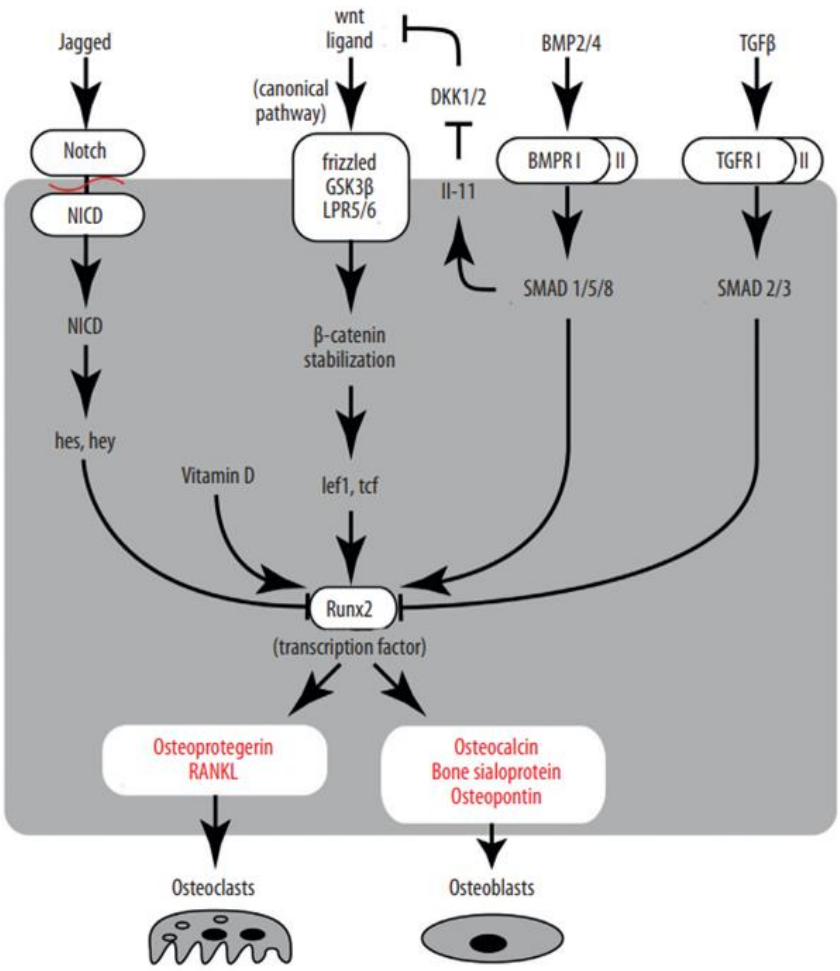


Figure 1.7. Major regulatory pathways involved in osteogenic differentiation, adapted from Rutkovskiy et al. (2016)

The Wnt pathway plays a central role in the activation of RUNX2 and subsequent modulation of osteogenic differentiation. Through the binding of Wnt ligands to co-receptors, the β-catenin destruction complex GSK3β is inhibited, preventing the phosphorylation and ubiquitination of β-catenin, allowing for its translocation into the nucleus where it facilitates activation and expression of RUNX2 (Shares et al., 2018).

In contrast to the Wnt signalling is Notch signalling which, upon activation, inhibits both β-catenin and RUNX2 transcriptional activity (Deregowski et al., 2006). This activity is mediated by Notch downstream target genes HEY1 and HES1 which inhibit

the transcriptional activity through the formation of a complex with Groucho/TFC and RUNX2, limiting the transcriptional activity of β-catenin and RUNX2 (Lin and Hankenson, 2011; Xu et al., 2015; Zanotti and Canalis, 2016). Lawal et al. (2017) demonstrated through the deletion of Notch ligand JAG1, that Notch signalling inhibits the transition of osteoprogenitor cells into pre-osteoblasts. Therefore, though inhibitory to osteogenic differentiation, Notch signalling plays a vital part in the maintenance of the osteoprogenitor pool in vivo (Weber and Calvi, 2010).

The transforming growth factor β (TGF-β) signalling pathway functions through the use of ligands such as bone morphogenic protein (BMP) and TGF-β, heteromeric receptor complexes, and SMADs intracellular signalling transducers (Wu et al., 2016). Depending on the ligand-receptor interaction, either BMP or TGF-β to their respective receptor complexes, promotion or inhibition of osteogenic differentiation is observed (Rutkovskiy et al., 2016). BMP ligand-receptor activation leads to the translocation of SMAD1, 5 and 8 to the nucleus where it recruits RUNX2 to promote the expression of osteogenic genes. Conversely, TGF-β ligand-receptor activation leads to the translocation of SMAD2 and 3 into the nucleus which represses the function of RUNX2.

The transition from MSCs to bone forming osteoblast cells is a complicated process that relies on the signalling, crosstalk, and transcriptional regulation of many different molecular pathways. The effects of PBG dissolution products on a number of the major pathways such as Wnt, Notch and TGF-β/BMP pathways are explored in this thesis.

1.2.3 Regenerative medicine

1.2.3.1 Mesenchymal stem cells

Stem cells are cells possessing the ability to self-renew and differentiate (Wei et al., 2013). Self-renewal allows the cells to replicate while maintaining their undifferentiated state and the capacity to differentiate allows the cells to specialize into mature cells with specific functions from different lineages. There are numerous types and sources of stem cells that have varying levels of potency however these can be largely categorized into the following groups: i) embryonic stem cells (ESC), ii) induced pluripotent stem cells (iPSC) and iii) adult stem cells (ASC). Typically isolated from the inner cell mass of a blastocyst, ESC are pluripotent and have the capacity to differentiate into mature cells from the three germ layers (Evans and Kaufman, 1981). iPSC are adult somatic cells that have been reprogrammed into a pluripotent state through the expression of several key transcription factors (Takahashi et al., 2007). Finally, ASC are stem cells which have unipotent or multipotent capacity, largely only able to differentiate into a limited number of mature cell types compared to the pluripotent nature of ESC or iPSC (Horwitz et al., 2005). Despite the difference in potency, ASC have a number of benefits over ESC and iPSC such as the ability to be easily sourced, cultured and demonstrate minimal ethical and fewer clinical concerns (Ullah et al., 2015).

Mesenchymal stem cells (MSC) are a type of ASC residing in the bone marrow, dental pulp, adipose tissue and umbilical cord among other areas and are responsible for wound healing, tissue growth and replenishing mature cells within their residing tissue (Berebichez-Fridman and Montero-Olvera, 2018). MSC have demonstrated plastic adherence, self-renewal and the ability to differentiate into mature cells from neuronal, hepatic, chondral and osteogenic lineages (Berebichez-Fridman et al., 2017). For tissue engineering and regenerative medicine, MSCs are typically obtained from

the bone marrow due the accessibility of bone marrow aspirate, MSC content and well characterized nature (Bobis et al., 2006; Corsi et al., 2007).

1.2.3.2 MSC applications and challenges

Due to their capacity to differentiate into a variety of mature cell types, MSCs have been investigated for use in nerve regeneration (Fairbairn et al., 2015), treatment of bone pathologies (Jäger et al., 2010), myocardial infarctions (Roura et al., 2012) and even autoimmune diseases (González et al., 2009).

MSCs have demonstrated potential for bone synthesis therapies, particularly in cases of problematic non-union fractures or patients with low bone mass and high risk of fracture (Oryan et al., 2017; Phetfong et al., 2016). Their application solves specific issues involving lack of MSC migration to a defect site and declining numbers of MSC population in an elderly patient (Block et al., 2017; Oryan et al., 2017). Supplementation of these MSC therapies with growth factors such as BMP2 further promote MSC differentiation and production of bone (Vo et al., 2012).

MSCs for cell therapies are derived in two ways, autologous and allogeneic transplants, each with its own challenges. Autologous transplants use MSC sourced from the patient, expanded in culture and transplanted back into a patient to promote bone regeneration at a target site (Talaat et al., 2018). While autologous therapies have significantly reduced risk of graft versus host disease (GvHD) and rejection, patient cell condition itself may influence the success of the transplant (Champlin, 2003). For example, patients with obesity or rheumatoid arthritis may have cells whose therapeutic function is compromised (Lukomska et al., 2019). Furthermore, elderly patients that are most at risk from low bone mass and fragility fractures have

decreased number of MSC cells, making sourcing sufficient numbers of cells difficult (Block et al., 2017).

Conversely, allogeneic transplants provide disease free cells that can be collected in adequate concentrations (Block et al., 2017). However, allogeneic transplants are accompanied by greater risk of GvHD and rejection despite human leukocyte antigen (HLA) matching. Interestingly, the immunomodulatory properties of MSCs make them desirable as a therapeutic agent for allogeneic transplants due to their demonstrated ability to treat GvHD (Le Blanc and Mougiakakos, 2012).

Finally, endogenous growth factors provide signals needed for the growth and maintenance of tissue. Exogenous application of these growth factors such as fibroblast growth factor 2 (FGF2), BMP2 and BMP7 have been explored for the promotion of differentiation and tissue repair in cases where endogenous activity is insufficient (Kuroda et al., 2019). Their use in bone regeneration has been extensively explored and while their efficacy has been demonstrated, their limited periods of activity due to low half-life, difficulty in maintaining optimal concentrations *in vivo*, cost and regulatory issues limit their widespread adoption (El Bialy et al., 2017; Kuroda et al., 2019; Schliephake, 2013).

The ability to influence stem cells through PBG dissolution without the reliance on exogenous biological factors provides a potential strategy for bone regeneration that would overcome many of the hurdles growth factor applications are currently facing.

1.2.4 Ion-cell interactions

There is increasing interest in investigating the effects of ionic dissolution products from inorganic materials on cells and how they may regulate stem cell function and fate (Murphy et al., 2014). Figure 1.8 illustrates some of the ways inorganic ions released from bioactive glasses may influence cell behaviour.

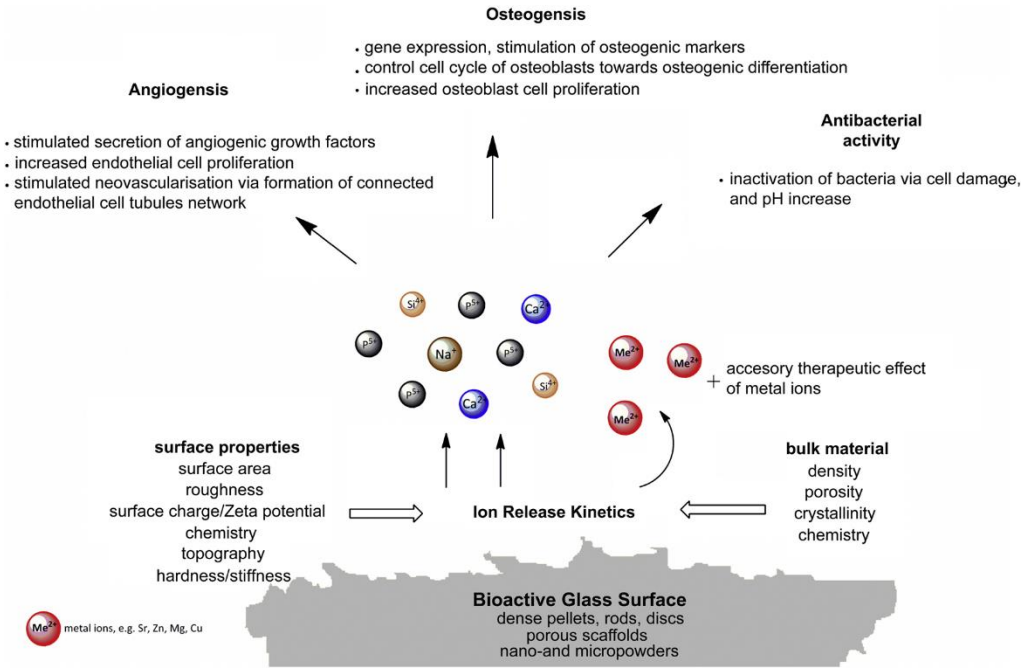


Figure 1.8. Overview of cell responses to dissolution products of bioactive glasses. Adapted from Hoppe et al. (2011).

1.2.4.1 Phosphate

The process of bone reabsorption involves the breakdown of bone by osteoclasts, resulting in a local increase in not only calcium but also inorganic phosphate (Khoshniat et al., 2011a). Additional increases in local phosphate can also be attributed to alkaline phosphatase (ALP), an enzyme that regulates osteoblastic mineralization through the hydrolysis of pyrophosphates (Terkeltaub, 2001). The local phosphate concentration

has been shown to alter osteogenic gene expression (Beck et al., 2000), proliferation (Kanatani et al., 2002), mineralization (Julien et al., 2007) and high concentrations have even been linked to apoptosis of osteoblasts (Magne et al., 2003; Meleti et al., 2000). This apoptosis functions as a method of aiding bone resorption through the creation of a localized ion gradient (Meleti et al., 2000).

An interesting aspect of PBG degradation is the release of various phosphate species such as pyrophosphates and metaphosphates or even polyphosphate chains (Ahmed et al., 2005). These species demonstrate differing functional effects on *in vitro* osteogenic differentiation. Pujari-Palmer et al. (2016) demonstrated that pyrophosphate can promote ALP despite its well documented inhibitory effects on matrix mineralization (Addison et al., 2007; Orriss et al., 2016). Polyphosphates have demonstrated to behave in a similar inhibitory manner to pyrophosphates though recent studies suggest that while they may inhibit matrix mineralization activity, they may promote the upregulation of β-catenin, a key osteogenic gene (Ardeshirylajimi et al., 2018; Hoac et al., 2013). ALP has also been demonstrated to act on pyrophosphate and polyphosphate species, cleaving them to generate orthophosphates which can be incorporated into the collagen matrix, thus preventing the inhibition of matrix mineralization by the other phosphate species (Hoac et al., 2013; Omelon et al., 2013).

1.2.4.2 Calcium

Bone remodelling relies heavily on the homeostasis of calcium ions within the local area. The bone itself serves as store for calcium as it undergoes the exchange of bound and free ions along its large surface area. The sequestration of free calcium ions is required by osteoblasts to secrete osteoid, a specialized extracellular matrix (ECM) (Duncan et al., 1998). The ECM produced by osteoblasts contains nucleation sites that

allow for mineral deposition comprised of calcium and phosphate. Homeostasis of the local environment is maintained through the secretion of parathyroid hormone (PTH) as a response to calcium ion levels in serum (Barradas et al., 2012; Duncan et al., 1998). Influxes of free calcium ions occur through the resorption of bone and increased renal and intestinal absorption maintain homeostatic calcium levels (Duncan et al., 1998). Pathological states then arise as a result of the disruption of the aforementioned homeostatic environment.

Calcium ions play a fundamental role in the activation of calcium ion channels as a result of the responses to external and hormonal stimuli in both osteoblasts and osteoclasts (Duncan et al., 1998). Maeno et al. (2005) showed that low concentrations of calcium (2-6 mM) promote survival and proliferation of mouse osteoblasts (mOBs) while higher concentrations of (6-10 mM) favour differentiation and matrix mineralization. Concentrations higher than 10mM result in decrease of survival. Calcium reaches 20 mM near sites of reabsorption, 20-fold higher than that of standard serum (Silver et al., 1988). This extracellular signalling ion activates G-protein coupled calcium signalling receptors (CaSR) and is known to regulate proliferation, differentiation and apoptosis (Khoshniat et al., 2011a). However, some studies suggest that osteoblastic cells contain a unique calcium sensing receptor (Pi et al., 2005). Barradas et al. (2012) proposed a calcium ion channel mediated mechanism of transcription through which after influx of calcium into the cell, a signalling cascade is activated, leading to a c-Fos and c-Jun mediated transcription of BMP2, a key gene in maintaining bone homeostasis.

Calcium was also shown to significantly increase the rate of mineralization and promoted adhesion and an upregulation of the vascular growth factors *Ang1/2* (at 5 mM) in murine osteoblast like cells (MC3T3E1) (Nakamura et al., 2010). *Ang1* is noted

to promote the structural integrity of blood vessels while *Ang2* promotes blood vessel growth (Maisonpierre et al., 1997; Suri et al., 1996). Angiogenesis plays a key roles in bone formation and upregulation of vascular growth factors such as Ang1/2 have shown to increase alkaline phosphatase activity, osteocalcin production and mineral deposition (Jeong et al., 2010, p. 1; Suzuki et al., 2007).

Due to the concomitant nature of calcium and inorganic phosphate within the bone microenvironment, it was theorized that that calcium plays a role in the modulation of inorganic phosphate effects (Adams et al., 2001). Khoshniat et al. (2011a) later showed the complete abolishing of the osteoblast gene upregulating effects of inorganic phosphate in the absence of calcium in a murine osteoblast cell line. Interestingly, this activation of subsequent inorganic phosphate pathways was incited not by CaSR but by the formation of calcium phosphate precipitate which activates the *Erk1/2* pathways.

1.2.4.3 Magnesium

Magnesium ions have been shown to play a vital role in vascularization through the upregulation of nitric oxide synthase (Maier et al., 2004). The increase in nitric oxide, a mediator for angiogenesis inhibits *angiostatin*, an angiogenesis antagonist (Cooke and Losordo, 2002; Matsunaga et al., 2002). Angiogenesis and osteogenesis are fundamentally linked, osteogenesis can't be undertaken without adequate blood supply and as such, magnesium ions likely play a significant albeit indirect role in aiding bone repair (Carano and Filvaroff, 2003; Gerber and Ferrara, 2000). Animal studies corroborate this by showing that magnesium deficiency results in osteoporosis in rats (Stendig-Lindberg et al., 2004). Furthermore, addition of magnesium to calcium

phosphate biomaterials showed increases in osteoblastic attachment, proliferation and osteoblastic properties (Landi et al., 2008; Xue et al., 2008).

1.2.4.4 Other inorganic ions

Many inorganic ions exhibit effects on MSC that may prove useful for integration into PBGs for the promotion of bone formation. While ions such as strontium, zinc and gallium are briefly reviewed here, they are not explored further in this study.

Strontium has long been suggested as an agent for bone repair with many studies detailing its effects on bone remodelling (Shorr and Carter, 1952; Xue et al., 2008). Strontium, like calcium, is largely found in bone as its localized sink within the body (Hodges et al., 1950). It has a high affinity for bone and incorporates itself into it via surface exchange or ionic substitution (Dahl et al., 2001). It acts beneficially on bone formation, increasing bone mass and decreasing resorption when delivered in low doses in rodents (Grynpas and Marie, 1990; Marie, 2003; Marie et al., 1993). This promotion of osteogenic activity may be a result of the increased internalization of calcium ions into cells through interaction with membrane bound calcium receptors reported by some studies (Shoback et al., 1995).

While essential for animals, zinc has shown to play a key role in bone development. Inhibition of bone growth and abnormal skeletal development is seen in cases of zinc deficiency (Hurley, 1981; Oner et al., 1984). Zinc is known to be a constituent of key bone proteins such as ALP and has even demonstrated to play a role in the upregulation of key osteogenic genes such as *RUNX2* (Coleman, 1992; Park et al., 2018). Finally, zinc excretion has been suggested as a marker for osteoporosis as patients had lower levels of bone zinc content than controls while urinary zinc was found to substantially increase (Yamaguchi, 1998).

Cerium ions have been reported to promote proliferation of osteoblasts yet had concentration dependent effects on osteogenic differentiation (Babenko et al., 2012; Zhang et al., 2010). Cerium was additionally shown to increase expression of *RUNX2, ALP, BSP and BMP2* at lower doses (Hu et al., 2014; Zhang et al., 2010).

Unlike the other ions discussed that promote osteogenic activity, gallium interacts with osteoclasts. It displays an inhibitory effect on osteoclast differentiation and formation, thereby combating the effects of bone resorption (Verron et al., 2010). A decrease in osteoclastic markers are seen with cells cultured with biomaterials incorporated with gallium, promoting total defect filling and additionally enhanced the bone density in ovariectomized rats (LI et al., 2016; Strazic Geljic et al., 2018). This inhibitory effect on osteoclast activity could be utilized in biomaterial design to tackle fracture risk from another angle. Disrupting bone resorption rather than simply promoting bone formation which may prove to be an effective strategy in decreasing fracture risk.

1.3 Aims and hypothesis

This thesis aimed to investigate the effects of PBGs and their dissolution products on human stem cell behaviour in order to drive the differentiation of stem cells down an osteogenic lineage. It was hypothesized that controlled release of PBG dissolution products (particularly calcium, magnesium and phosphate ions) would influence stem cell behaviour and genes linked to differentiation.

1.4 Objectives:

- Identification and optimization for metabolic and osteogenic activity, the ion concentrations of the core elements of a PBG system through the application of its chemical precursors on human mesenchymal stem cells (hMSCs).

- Combinatorial assessment of PBG chemical precursors on metabolic, osteogenic activity and gene expression in hMSCs.

- Investigation of the effects of decreasing phosphate content in PBG systems on direct hMSC adhesion.

- Investigation of the effects of decreasing phosphate content in PBG systems on indirect hMSC metabolic activity, osteogenic activity and gene expression.

- Exploration of the biological benefits of mixing microspheres of two PBG formulations through observations on metabolic, osteogenic activity and gene expression.

- Development of a PBG microsphere formulation optimized to promote metabolic activity and osteogenic activity in hMSC.

Chapter 2 - Methods

2.1 Cell culture

A class II microbiological safety cabinet (ThermoFisher) was used to perform all cell culture. All cells were maintained at 37°C and 5% CO_2 in a Hera Cell 150 incubator (Thermo Electron Corporation).

Reagents were purchased from ThermoFisher Scientific unless otherwise stated.

2.1.1 Cells

A human mesenchymal stem cell (hMSC) line (Okamoto et al., 2002) was primarily used within this project. An inhouse transduction of green fluorescent protein gene allowed for the use of a GFP positive variant of the hMSC line (hMSC-GFP) (Macri-Pellizzeri et al., 2018). Both hMSC cell types were cultured in standard medium (SM) consisting of Dulbecco's Modified Eagle Medium (DMEM), supplemented with 10% (v/v) fetal bovine serum (FBS), 1% (v/v) L-glutamine, 1% (v/v) non-essential amino acids and 1% (v/v) penicillin streptomycin. Where osteogenic differentiation was required, osteogenic medium (OM) was used. OM consists of SM supplemented with 100 nM dexamethasone, 10 mM β-glycerophosphate (Sigma-Aldrich), 0.05 mM L-ascorbic acid (Sigma-Aldrich). Where stated, OM was used without β-glycerophosphate (OM-) to evaluate the effect of phosphates released from PBGs without masking their activity. The medium was refreshed every 48 hours and up to 21 days for osteogenic differentiation.

2.1.2 Passaging

hMSC were passaged upon reaching 80% confluency. After a phosphate buffered solution (PBS) wash, 0.25% (v/v) trypsin/0.02% (v/v) ethylene diaminetetraacetic acid (EDTA) was added to the monolayer for 2 minutes at 37°C. After incubation, mechanical stimulation was used to detach the remaining cells from the flask surface and fresh SM was added to neutralize the trypsin. The cell suspension was then centrifuged for 5 minutes at 200 g in a Sigma 3-16 centrifuge. The cell pellet was then resuspended in fresh SM and a 1:4 split was seeded into a new tissue culture flask.

2.1.3 Precursor compound supplementation

Each compound was used to produce stock solutions of specific concentration in sterile distilled water (SDW). The compounds used are listed in Table 2.1. The stock solutions were then filtered through a 0.22 µm pore filter and diluted to the relevant concentration per experiment in SM. The medium was refreshed every 48 hours for up to 21 days for osteogenic differentiation.

Table 2.1 Precursor compounds used for medium supplementation

Ion	Compound	Company
Calcium	$CaCl_2$	Sigma-Aldrich
Magnesium	$MgSO_4$	Thermo Fisher Scientific
Inorganic Phosphate	$Na_2HPO_4*H_2O$	Thermo Fisher Scientific

2.1.4 Indirect PBG testing

PBG microspheres were sterilized through two 15-minute washes in 70% ethanol and allowed to dry for 24 hours at room temperature in a sterile environment. Microspheres were added to SM at a concentration of 100 mg/ml and incubated at 37°C for 48 hours. The conditioned media was collected and filtered through a 0.22 µm pore filter before aliquoting 300 µl into each well of hMSC. SM on the PBG microspheres was refreshed and the media was replaced every 48 hours.

2.1.5 Direct PBG testing

PBG discs (9 mm diameter) were sterilized through two 15-minute washes in ethanol 70% and allowed to dry for 24 hours at room temperature in a sterile environment. Discs were placed in a well plate before seeding with hMSC-GFP at a density of 8000 cells/cm^2 before analysis after 24 hours.

2.1.6 Metabolic Activity

The metabolic activity of the cells was analysed using PrestoBlue Cell Viability Reagent (PB). Working PB solution was prepared by diluting the stock reagent in 90% SM. After washing the cells in PBS, 300 µl of prepared reagent was added to the cells and incubated for 40 minutes at 37°c and 5% CO_2 (optimization detailed in appendix). The solution was then transferred to a 96-well plate for its fluorescence to be measured on a plate reader (Tecan Infinite 200; 560nm and 590nm ex/em).

2.1.7 Alkaline phosphatase

Alkaline Phosphatase (ALP) working solution was made by dissolving 1 mg/ml p-Nitrophenyl phosphate and 0.2M Tris buffer tablets (SIGMAFAST p-Nitrophenyl

phosphate Tablets, Sigma-Aldrich) in 20 ml of SDW. After two PBS washes, 300 µl of the solution was dispensed into each well of a 48-well plate. The plates are then loaded into a plate reader and read (5 readings/well in a cross pattern) every 2 minutes for 24 minutes (Tecan Infinite 200; Abs: 405nm). The solution was then removed, the cells are washed twice with PBS and fresh medium was added. Data is presented as rate of change in absorbance over time.

2.1.8 Alizarin red

Cells were fixed after 10 minutes of incubation with 4% paraformaldehyde (PFA) at 4°C. After fixation the cells were washed twice with PBS and once with deionized water. 200 µl Alizarin Red S 1% (w/v) aqueous solution was added to each well and incubated for 15 minutes at room temperature. Excess stain was removed through multiple washes with deionized water. Incubating 200 µl of de-staining solution (20 % methanol, 10 % acetic acid in deionized water) per well for 20 minutes at room temperature was used to extract the mineral stain. The solution was then transferred to a 96-well plate and its absorbance was read on a plate reader (Tecan Infinite 200; Abs: 405nm)

2.2 Molecular Biology

2.2.1 RNA Extraction

On day 11 of culture, hMSCs were washed twice with PBS and incubated with Tri-reagent for 30s at room temperature. Cell scrapers were used to release the monolayer which was collected and frozen at -80°C. Before RNA extraction, the collected cells were thawed at room temperature and centrifuged in an Eppendorf 5415R microcentrifuge at 3000g for 5 minutes. The supernatant was collected and chloroform (Fisher Scientific) was added in a 1:5 ratio, vortexed and incubated at room temperature for 10 minutes to facilitate phase separation. Samples were then centrifuged at 12000g for 15 minutes and the nucleic acid phase was collected. 1:1 70% ethanol was added to the collected samples and vortexed before transferring to a RNeasy MinElute spin column from a RNeasy Micro Kit (Qiagen). RNA was extracted from the column using the manufacturer's instructions with the addition of a DNase I treatment step to reduce DNA contamination from the samples. Finally, RNA was eluted in 20 µl of SDW. The purity and concentration of the collected RNA was assessed using a SimpliNano Spectrophotometer (GE Healthcare).

2.2.2 cDNA Synthesis

A High Capacity RNA-to-cDNA Kit (ThermoFisher) was used to synthesize cDNA from the collected RNA samples according to the manufacturer's instructions. A reaction mix of reverse transcriptase, buffer and RT-enzyme was mixed with the RNA samples and incubated at 37°C for 1 hour in a heat block. Subsequently, the samples were incubated at 95°C for 5 minutes in a heat block to halt the reaction. cDNA samples were stored at -20°C.

2.2.3 Reverse Transcription PCR

cDNA samples were validated using RT-PCR with the housekeeping gene β-Actin (primer sequence in appendix). RT-PCR was carried out using a reaction mixture consisting of 0.15 µl Platinum Taq DNA polymerase 100 ng cDNA, 2µl 10x PCR buffer (Invitrogen), 0.6 µl $MgCl_2$ (Invitrogen), 0.6 µl dNTPs, 0.75 µl 5 mM forward primer, 0.75 µl 5 mM reverse primer and made up to 20 µl with SDW. PCR was carried out using a Labnet Multigene Thermal Cycler (Labnet International Inc., USA) using an initial 90°C 5 minute denature step followed by 35 cycles of 94°C for 30s, 60°C for 45s and 72°C for 60s and a final extension step of 72°C for 10 minutes. Reactions were held at 4°C until analysed using agarose gel electrophoresis.

2.2.4 Agarose Gel Electrophoresis

A 2% agarose gel was prepared using Tris-acetate-EDTA (TAE) buffer and ethidium bromide for the visualization of RT-PCR samples. Once prepared, the gel was allowed to set for 30 minutes. RT-PCR samples were mixed with 5x loading dye (Qiagen) and loaded alongside a 50bp hyperladder (Bioline) to determine sample product size. The gel was run for 1 hour at 85V and 400mA in TAE buffer after which it was visualized using a FujiFilm LAS 4000 imager (FujiFilm UK LTD, UK).

2.2.5 TaqMan Low Density Arrays

Custom TaqMan Low Density Array (TLDA) 384-well microfluidic cards (ThermoFisher) were designed for the analysis of gene expression. The 64 x 2 sample format was used and probes from ThermoFisher were selected and preloaded onto the card. Where possible, probes that spanned an exon boundary, were not within an untranslated

region (UTR) and did not detect gDNA were chosen. The selected genes can be seen in Table 2.2.

800 ng of each cDNA sample was diluted in a total of 200 µl RNase free water and mixed with 200 µl TaqMan Universal Master Mix II with UNG in a Lightsafe microcentrifuge tube. Samples were vortexed and 100µl of the mix were loaded into each reservoir of the TLDA plate. The plate was then centrifuged twice at 200g for 1 minute using a Sorvall ST40 centrifuge (ThermoFisher) after which it was sealed. A 7900HT Fast Real Time PCR System was used with SDS RQ Manager Software (Applied Biosystems) to run the sealed TLDA plates with the following settings: hold at 50°C for 2 minutes, hold at 94.5°C for 10 minutes and 40 cycles of 92°C for 15 seconds and 60°C for 1 minute.

Table 2.2. TLDA gene list

Gene Group	Gene	Name
Housekeeping	GAPDH	Glyceraldehyde-3-phosphate dehydrogenase
	ACTB	Actin beta
	GUSB	Glucuronidase beta
	18s rRNA	18S ribosomal RNA
Proliferation	CCND1	Cyclin D1
	PCNA	Proliferating cell nuclear antigen
	MKI67	Marker of proliferation Ki-67
Integrin	ITGA1	Integrin subunit alpha 1
	ITGA3	Integrin subunit alpha 3
	ITGB1	Integrin subunit beta 1
Osteogenic	RUNX2	Runt related transcription factor 2
	PPARG	Peroxisome proliferator activated receptor gamma
	SP7	Sp7 transcription factor
	ALPL	Alkaline phosphatase, liver/bone/kidney
	COL1A1	Collagen type I alpha 1
	BGLAP	Bone gamma-carboxyglutamate protein
	MSX2	Msh homeobox 2
	DLX5	Distal-less homeobox 5
	SPP1	Secreted phosphoprotein 1
	TNFRSF11B	TNF receptor superfamily member 11b
Osteoclastic	TNFSF11	Tumour necrosis factor superfamily member 11
	CTSK	Cathepsin K
	MMP9	Matrix metallopeptidase 9
	NFATC1	Nuclear factor of activated T-cells 1
	OSTF1	Osteoclast stimulating factor 1
TGF-β/BMP	BMP2	Bone morphogenetic protein 2
	BMP4	Bone morphogenetic protein 4
	BMP6	Bone morphogenetic protein 6
	BMP7	Bone morphogenetic protein 7
	GDF2	Growth differentiation factor 2
	SMAD1	SMAD family member 1
	SMAD3	SMAD family member 3
	SMAD4	SMAD family member 4
	SMAD6	SMAD family member 6
	SMAD7	SMAD family member 7
	TGFB1	Transforming growth factor beta 1
	TGFB2	Transforming growth factor beta 2
	TGFB3	Transforming growth factor beta 2
	NOG	Noggin
WNT	LRP5	LDL receptor related protein 5
	LRP6	LDL receptor related protein 6
	CTNNB1	Catenin beta 1

	FZD1	Frizzled class receptor 1
	WNT3A	Wnt family member 3A
	WNT5A	Wnt family member 5A
	WNT10B	Wnt family member 10B
	ROR2	receptor tyrosine kinase like orphan receptor 2
	SFRP1	Secreted frizzled related protein 1
Notch	NOTCH1	Notch 1
	NOTCH2	Notch 2
	NOTCH3	Notch 3
	NOTCH4	Notch 4
	JAG1	Jagged 1
	JAG2	Jagged 2
	DLL1	Delta like canonical Notch ligand 1
	DLL3	Delta like canonical Notch ligand 3
CaSR	CASR	Calcium sensing receptor
	PTH	Parathyroid hormone
	PTHLH	Parathyroid hormone like hormone
	MAPK3	Mitogen-activated protein kinase 3
	MAPK1	Mitogen-activated protein kinase 1
	IGF2	Insulin like growth factor 2
	PTGES2	Prostaglandin E synthase 2
	CDH1	Cadherin 1

2.3 Imaging

2.3.1 Bright field

Bright field images were taken using a Nikon Eclipse TS100 microscope with a Nikon Coolpix S10 camera attached.

2.3.2 Fluorescent microscopy

Fluorescent images were taken using a Nikon Eclipse TS2 with a Nikon D3300.

2.3.3 Scanning election microscopy

Samples were embedded in resin (EpoFix Resin and Epofix Hardener, Struer) and metallographic abrasive paper (P240, P400, P800 and P1200), followed by 6 µm and 1 µm polishing pads and diamond pastes were used to polish the surface and create a section of each sample. The embedded samples were then coated in 10 nm carbon and imaged using a Quanta Q650 SEM (Thermo Scientific) in SE mode at an acceleration voltage of 20 kV.

2.4 Materials manufacture

2.4.1 Glass production

The precursors P_2O_5, NaH_2PO_4, Na_2CO_3, $CaHPO_4$, $CaCO_3$ and $MgHPO_4.3H_2O$ were used to fabricate PBGs listed in Table 2.3. The precursors were mixed and placed within a 100ml Pt/5% Au crucible (Birmingham Metal Company, UK).

The crucible was placed into a furnace ramped to 350°C at 10°C/min then held for 30 minutes. A second ramp at 10°C/min was used to heat to 1150°C then held for 90 minutes. The melts were then poured and quenched onto a steel plate and left to cool to room temperature.

Table 2.3. PBGs manufactured

Glass Code	**P_2O_5 (mol%)**	**CaO (mol%)**	**MgO (mol%)**	**Na_2O (mol%)**
P40	40	16	24	20
P35	35	21	24	20
P30	30	26	24	20
P50Ca50	50	50	0	0
P50Ca25Mg25	50	25	25	0
P50Mg50	50	0	50	0
P45	45	30	25	0

2.4.2 Microsphere production

To manufacture microspheres, a planetary zirconia ball mill (Retsch Planetary Mill PM100) was used to grind the quenched glass for 2 minutes at 500 rpm. Stainless steel sieves (VWR International, UK) were then used to sieve the glass particles into a size range of 63-125 µm. Non-porous microspheres were prepared by funnelling the glass powders into the flame (3200°C) of an oxy-acetylene flame spray gun (MK 74, Metallisation Ltd, UK). Porous PBG microspheres were prepared by thoroughly mixing the glass powders with $CaCO_3$ in a 1:3 ratio before funnelling into the flame of the thermal spray gun (oxy-acetylene ratio of 3:3). After cooling, the microspheres were collected from the cooling trays and porous microspheres were acid washed in 5 mM acetic acid for 2 minutes followed by a deionized water wash for 5 minutes and then dried in a 50°C oven for 24 hours.

2.4.3 Glass disc production

To produce glass discs, molten glass from each formulation was poured into pre-heated graphite moulds with 9 mm diameter rod cut outs and held at 10 °C above the glass transition temperature (T_g, see Table 4.3) for each composition for 1 hour before being allowed to cool to room temperature overnight. After cooling, the glass rods were removed from the moulds and cut using a diamond saw blade to 2 mm width. Metallographic abrasive paper (P240, P400, P800 and P1200), followed by 6 µm and 1 µm polishing pads and diamond pastes were used to polish the surfaces of the glass discs. Industrial methylated sprit was used as a lubricant.

Once prepared, the discs were sterilized through two 15-minute washes in ethanol 70% and allowed to dry for 24 hours at room temperature in a sterile environment.

2.4.4 Energy-dispersive x-ray spectroscopy

To confirm the glass formulations produced, chemical analysis was conducted via Energy-dispersive x-ray spectroscopy (EDX). Microspheres were embedded in resin (EpoFix Resin and Epofix Hardener, Struers) and then polished to expose their cross-sectional surfaces, before applying carbon coating. Samples were then analysed at a 10 mm working distance using a 10kV beam using a FEI/Philips XL30 SEM.

2.4.5 Thermal analysis

A Differential Scanning Calorimeter (DSC, TA instruments, Q600) was used to determine the glass transition (T_g), onset crystallization ($T_{c,ons}$), peak crystallization (T_c) and glass melting temperature (T_m) points of the produced glass formulations. The processing window for the different glasses was determined using the following equation:

$$\text{Processing window} = (T_{c,\,ons} - T_g)$$

20 mg of powdered glass samples were added to a platinum sample pan and heated from room temperature to 1100°C at a ramp of 10°C /min. A second blank platinum pan was used for a baseline to correct the thermal traces of the samples.

2.4.6 X-Ray powder diffraction

X-ray powder diffraction (XRD) was used to confirm the amorphous nature of the PBGs produced. Ground glass powder samples were run using a DVA-Da Vinci Advantage over a 2 theta range from 5 degrees to 70 degrees with a 0.02-degree step size and a step time over 4s.

2.4.7 Nuclear Magnetic Resonance

NMR was used to resolve the distribution of different Q^n species within the PBGs produced. Solid-state ^{31}P NMR spectra were recorded for the produced PBGs at room temperature using a Varian Chemagnetics Infinity plus spectrometer set to operate at a Larmor frequency of 121.468 MHz. The glass samples were packed into 4 mm Magic Angle Spinning (MAS) probe before being spun at 12kHz. The resulting spectra were then set into Gaussian lines to quantify the proportions of the different Q environments of each sample, with data handling being performed using the Varian Chemagnetics software Spinsight Version 3.5.2.

2.4.8 Viscosity Measurement

Viscosity of the glasses were measured at high temperatures using a rotational viscometer (Brookfield DV-III UTRA, USA). The viscosity was quantified by measuring the force required to rotate a spindle in a fluid. The viscosity was determined by measuring the shear stress and the shear rate exerted by the viscous fluid on a rotating cylindrical platinum spindle according to the following equation:

$$\eta=\tau/\gamma$$

where, η is the viscosity in poise, τ is the shear stress in dynes/cm^2 and γ is the rate of shear in sec^{-1}.

In order to derive a viscosity curve for glasses, the fixed viscosity at glass transition temperature and the viscosity data obtained via rotational method were used and fitted to the Vogel–Fulcher–Tammann (VFT) by a least squares calculations in the equation below:

$$\mathrm{Log}(\eta)=A+B/(T-To)$$

where, T is the temperature in °C, η is the viscosity in Pa·s and A, B and To are constants.

2.4.9 Mass Loss

PBG disc dimensions and weight were recorded and placed in 500 µl ultra-pure water at room temperature for 30 days. The discs were dried completely overnight before the new weight was recorded and the disc placed into fresh ultra-pure water. Mass loss was normalized to surface area of the discs used.

2.5 Statistical analysis

GraphPad Prism 8 (GraphPad Software, San Diego, CA) was used to carry out statistical analysis. All results are presented as mean ± standard error of the mean.

Cell culture data was analysed using a One-way ANOVA with Dunnett's multiple comparison test. $p<0.05$ with *$p<0.05$, **$p<0.01$, ***$p<0.001$ and ****$p<0.0001$.

Gene expression analysis was carried out using a Kruskal-Wallis test followed by an uncorrected Dunn's test for post hoc multiple comparisons. $p<0.05$ with *$p<0.05$, **$p<0.005$, ***$p<0.001$ and ****$p<0.0001$.

Replicates (n) refer to biological replicates unless otherwise stated.

Chapter 3 - Optimization of ion concentration *in vitro* for hMSC application

3.1 Introduction

Human bone is a complex and dynamic tissue comprised of numerous cells including osteoblasts and osteoclasts that work together to constantly remodel and repair bone (Allen and Burr, 2019). These functions are regulated by a variety of hormones, growth factors and physical stimuli (Huang et al., 2007; Rutkovskiy et al., 2016). Additionally, a number of inorganic ions such as calcium, magnesium and phosphate have demonstrated to play a role in bone homeostasis and osteoblast differentiation (Hoppe et al., 2011; Khoshniat et al., 2011b; Maeno et al., 2005; Wolf and Cittadini, 1999). The physiological role these ions play in bone growth makes their use as therapeutic agents attractive and PBGs allow for the utilization of these inorganic ions as a therapeutic agent for the promotion of bone growth (Hossain et al., 2015).

3.2 Aims and hypotheses

Existing literature indicates that MSCs have a variety of dose specific responses to various inorganic ions, for example, requiring 6-8 mM calcium to promote osteogenic differentiation, 10 mM phosphate to promote matrix gla protein (MGP) expression and 0.5 mM magnesium to promote cellular proliferation (Julien et al., 2007; Maeno et al., 2005; Wolf and Cittadini, 1999). Studies also indicated combinatorial effects of ions on cells when applied together *in vitro*, for example, Adams et al. (2001) demonstrated how increases in calcium concentration (0-1 mM) caused rapid increases in phosphate dependent osteoblast apoptosis. Additionally, Khoshniat et al. (2011) demonstrated the necessity of both phosphate (10 mM) and calcium (1.8 mM) for the stimulation of matrix mineralization genes such as osteopontin (*OPN*) and MGP in MC3T3-E1 cells .

The aims of this chapter were to identify the effects of and optimize the ion concentrations of the core elements of a PBG system for osteogenic differentiation. This was achieved through the application of its chemical precursors on hMSC to allow for dose optimization. To further explore the effects that are triggered through use of multiple ions, combinatorial tests of the of the optimized precursor doses were undertaken. Metabolic and osteogenic activity were measured using presto blue, alkaline phosphatase (ALP) and alizarin red (ALZ) assays to optimize for cytotoxicity, ALP activity and matrix mineralization.

Once an optimized combination of ions was identified, cells grown under this treatment were collected and processed for molecular evaluation using TaqMan Low Density Arrays. Markers for osteogenic, Notch, Wnt, BMP and proliferative signalling markers were analysed to gain insight into the effects of the precursor chemical compound combinations applied to hMSCs in culture.

3.3 Results

3.3.1 Direct ion application utilizing chemical precursors

3.3.1.1 Effects of singular ions on hMSC

Many inorganic ions such as calcium, magnesium and phosphate among others, have been shown to play key roles in bone metabolism, angiogenesis and mineralization of bone tissue. To investigate the effects of these ions directly on hMSCs, metabolic and osteogenic activity were analysed after treatment with media conditioned with the relevant ions. Precursor compounds (see Table 2.1) were added to cell culture media and refreshed on hMSC every 48 hours for 21 days.

Figure 3.1 below shows the effects of varying calcium concentrations on hMSCs. 5 mM calcium showed an increase in metabolic activity compared to both the SM control and 20 mM treatment on day 11 (Figure 3.1A). While ALP activity was significantly lower than the control (Figure 3.1B), the ALZ intensity was substantially higher in both 5 and 10 mM doses compared to the SM control and showed no significant difference from the OM positive control (Figure 3.1C). From the concentrations investigated 5 mM calcium dose was demonstrated to be the most effective for metabolic and ALZ response on hMSC.

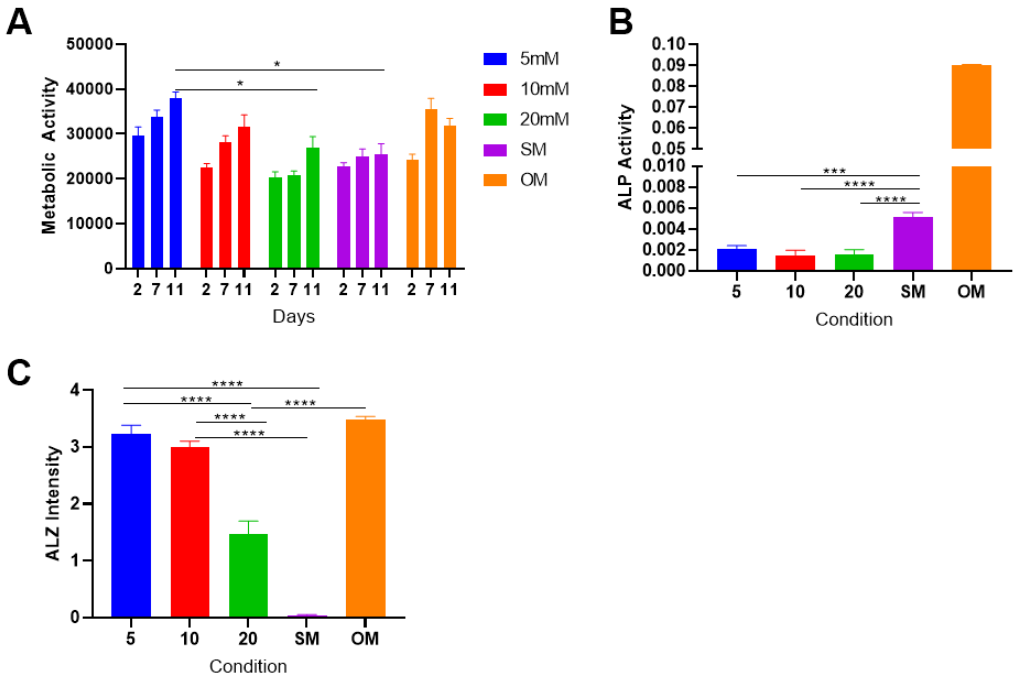


Figure 3.1. (A) The metabolic (day 2, 7 and 11), (B) ALP (day 11) and (C) ALZ intensity (day 21) of hMSC treated with 5, 10 and 20mM calcium, compared to standard medium (SM) and osteogenic medium (OM) controls. *p<0.05, ***p<0.001, ****p<0.0001 (n=2).

Figure 3.2 below shows the effects of varying magnesium concentrations on hMSCs. No significant changes to metabolic activity were seen on day 11 of magnesium supplementation (Figure 3.2A). However, ALP activity decreased with increasing magnesium, with the 5 mM magnesium treatment showing significant increase when compared to the SM control while the 10 mM and 20 mM magnesium concentrations significantly decreased ALP activity compared to the 5 mM dose (Figure 3.2B). Despite the high levels of ALP seen, little to no ALZ intensity was seen in any of these treatments, when compared to the untreated control (Figure 3.2C and 3.4). Out of the doses tested, 5 mM magnesium showed the most effective response due to its ALP activity while no changes in activity were seen in metabolic activity and mineral deposition between the concentrations.

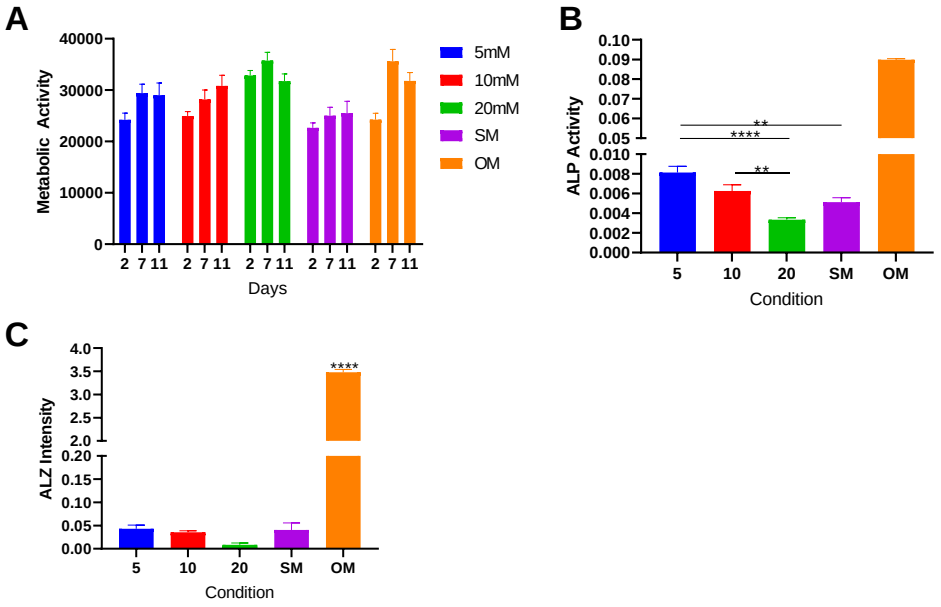


Figure 3.2. (A) The metabolic (day 2, 7 and 11), (B) ALP (day 11) and (C) ALZ intensity (day 21) of hMSC treated with 5, 10 and 20mM magnesium, compared to standard medium (SM) and osteogenic medium (OM) controls. **p<0.01, ****p<0.0001 (n=2).

Figure 3.3 below shows the effects of varying phosphate concentrations on hMSCs. All concentrations of phosphate treatment showed significant reductions in metabolic activity, almost completely disrupting the cell monolayer in all doses, demonstrating a decreasing trend in activity with increasing phosphate concentration (Figure 3.3A). The effect of ALP and ALZ intensity on phosphate treated cells was difficult to accurately quantify due to the disruption of the monolayer observed, though some level of ALZ stain could be seen at 5 mM (Figure 3.4). Despite its negative activity at all doses, the 5 mM phosphate showed to be the least disruptive dose with the monolayer still being partially intact on day 21 (Figure 3.4).

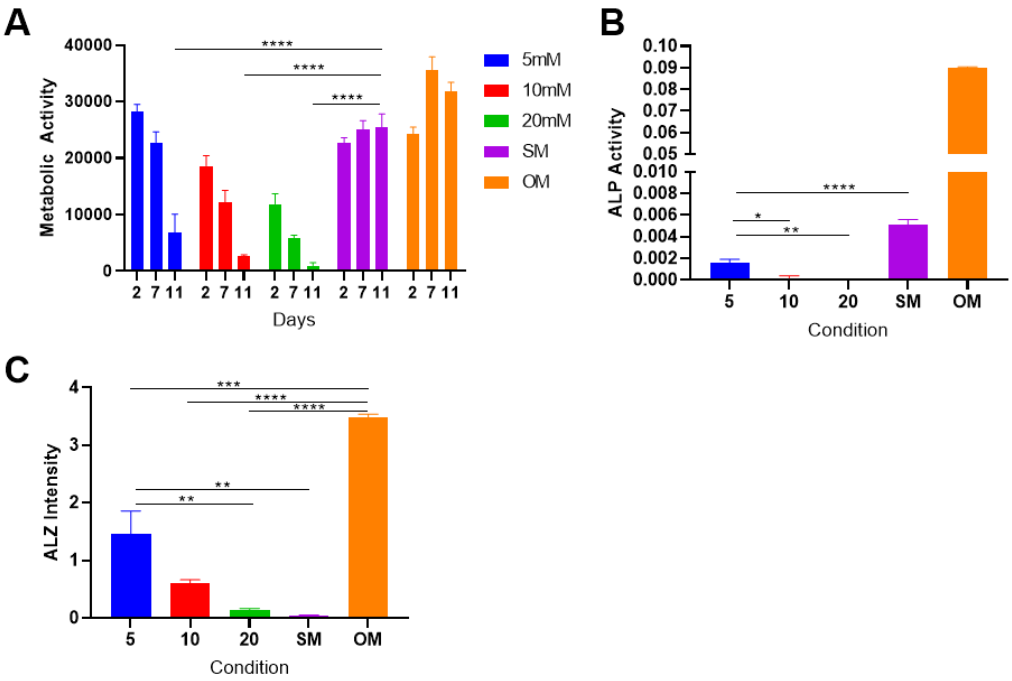


Figure 3.3. (A) The metabolic (day 2, 7 and 11), (B) ALP (day 11) and (C) ALZ intensity (day 21) of hMSC treated with 5, 10 and 20mM phosphate, compared to standard medium (SM) and osteogenic medium (OM) controls. *p<0.05, **p<0.01, ***p<0.001, ****p<0.0001 (n=2).

The lowest concentrations of all the ions investigated above demonstrated to be the most effective, revealing promotion of metabolic activity and ALZ intensity for calcium, increases in alkaline phosphatase activity for magnesium and minimal disruption to cell activity in phosphate at 5 mM.

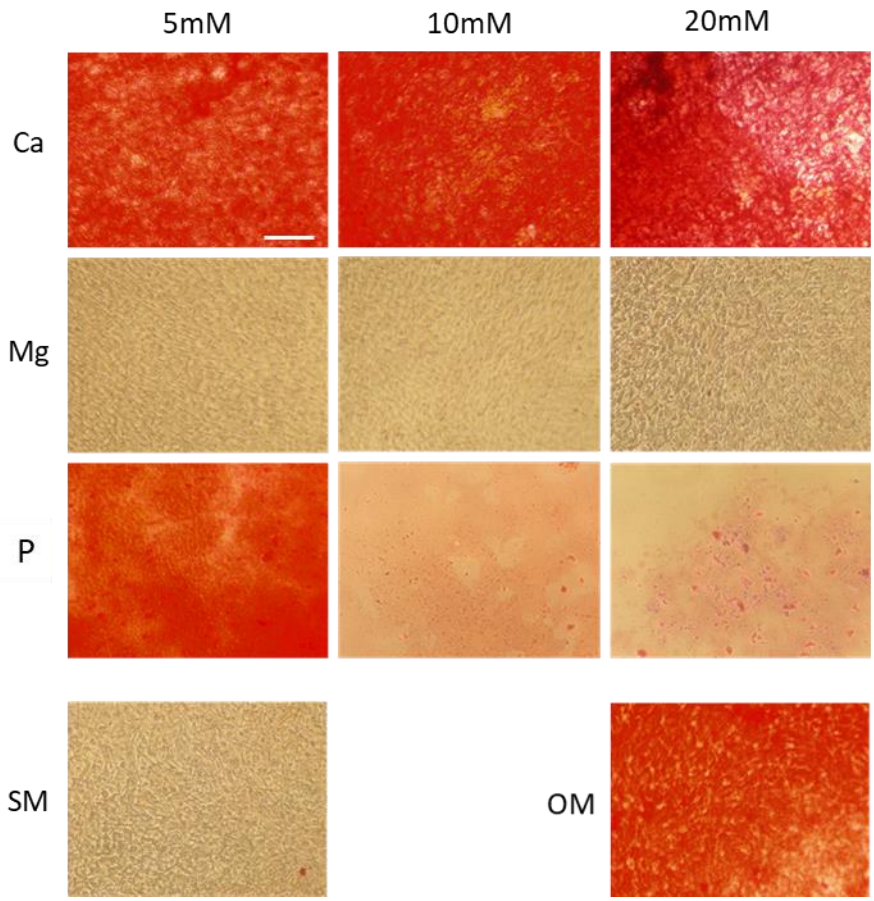


Figure 3.4. Alizarin red staining on hMSCs treated with 5, 10 and 20 mM calcium, magnesium and phosphate on day 21, compared to standard medium (SM) and osteogenic medium (OM) controls. Scale bar = 250 µm.

Due to the inhibitory and monolayer disrupting activity of the inorganic phosphate concentrations explored (5-20 mM), further optimizations were carried out to identify a more appropriate dose. Lower doses of phosphate were tested (Figure 3.5) and a trend of increasing metabolic activity was seen with decreasing phosphate concentrations, with a significant difference seen between 5 mM and 1.25 mM doses (Figure 3.5A). Osteogenic activity also showed a sharp increase with a significant spike in ALP and ALZ intensity in the 1.25 mM dose (Figure 3.5B and 3.5C). The reduced 1.25 mM dose also showed significantly better activity in all cases compared to the original 5 mM dose.

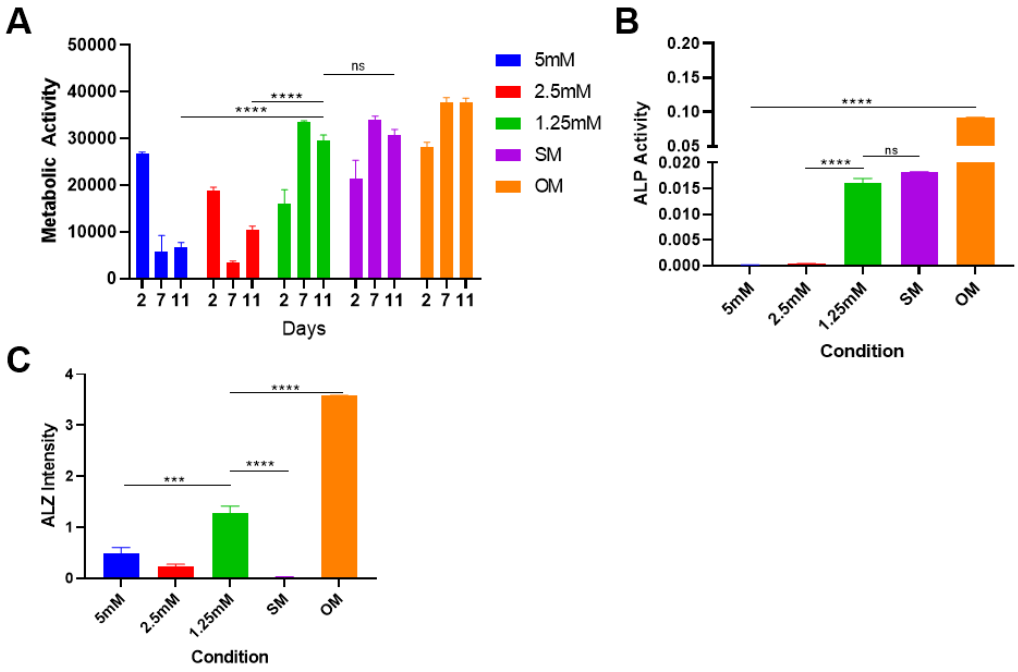


Figure 3.5. (A) The metabolic (day 2, 7 and 11), (B) ALP (day 11) and (C) ALZ intensity (day 21) of hMSC treated with 5, 2.5 and 1.25 mM phosphate, compared to standard medium (SM) and osteogenic medium (OM) controls. ***p<0.001, ****p<0.0001 (n=3 technical replicates).

3.3.1.2 Effects of combinatorial ion supplementation on hMSC

Literature studies show that the co-dependent nature of inorganic ions, where two or more ions are present at the necessary doses, can activate and/or amplify specific cellular pathways (Adams et al., 2001; Murphy et al., 2014). To investigate the potential complementary effects of ions on cells, the previously tested singular ion doses were combined for hMSC treatment. Singular ion testing showed that 5 mM calcium, 5 mM magnesium and 1.25 mM phosphate resulted in the best metabolic and osteogenic activity and these concentrations of ions was taken forward for combinatorial tests (Figure 3.1, 3.2 and 3.5).

Figure 3.6 shows that the metabolic activity of the mixed ion concentrations containing 5 mM calcium, 5 mM magnesium and 1.25 mM inorganic phosphate showed significantly better metabolic activity compared to the SM control and the calcium and magnesium ion mix at day 11. Furthermore, combination of phosphate and magnesium resulted in superior metabolic performance than combinations of phosphate and calcium at day 11. Significant increases in ALP activity were seen in the magnesium and phosphate mix compared to the SM control however all other mixes showed inhibited ALP performance compared to the SM control (Figure 3.6B). The magnesium and phosphate mix demonstrate the previously seen increase in ALP activity of magnesium in isolation while the addition of calcium appears to completely ablate this activity. Similarly, the calcium phosphate mix demonstrated the best ALZ intensity compared to the SM control while all other formulations showed no ALZ stain, indicating that the addition of magnesium to the calcium and phosphate mix reduces the ALZ intensity (Figure 3.6C).

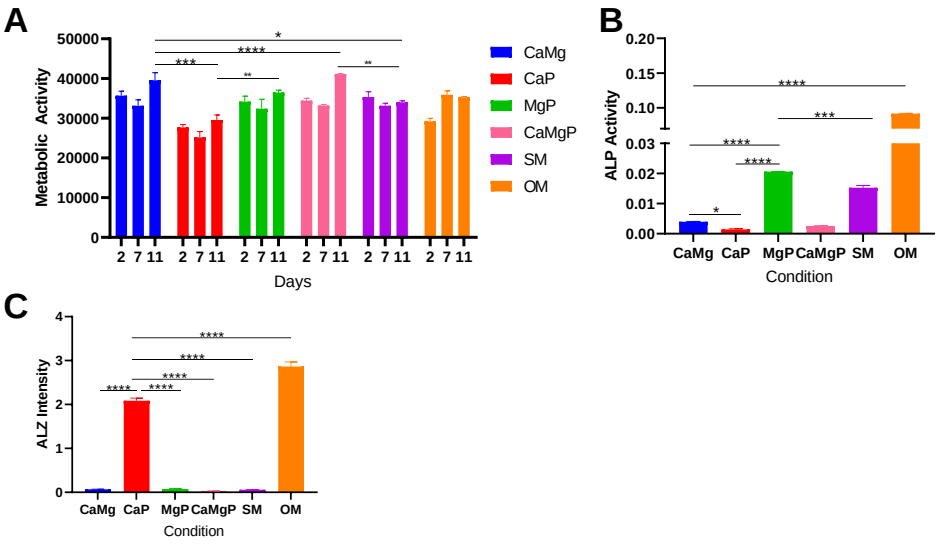


Figure 3.6. (A) The metabolic (day 2, 7 and 11), (B) ALP (day 11) and (C) ALZ intensity (day 21) of hMSC treated with combinations of 5 mM calcium, 5 mM magnesium and 1.25 mM phosphate, compared to standard medium (SM) and osteogenic medium (OM) controls. *p<0.05, **p<0.01, ***p<0.001, ****p<0.0001 (n=3 technical replicates).

Observing how the ions can promote or inhibit either metabolic activity or osteogenic activity depending on the combination, the previously tested 5 mM phosphate was combined with 5 mM calcium and 5 mM magnesium as can be seen in Figure 3.7. This mix further demonstrates the ability of calcium and magnesium to rescue hMSC when treated with higher doses of phosphate previously shown to result in significant decreases in metabolic activity when tested in isolation (Figure 3.3A). Figure 3.7A shows that combination of 5 mM phosphate with calcium still results in significantly lower metabolic activity compared to the SM control while combination with magnesium greatly improves its metabolic activity. Furthermore, combination of all three ions together at 5 mM results in the best metabolic activity (figure 3.7A). Similar to the previous test, the 5 mM phosphate mixed with 5 mM magnesium demonstrated

the best alkaline phosphatase activity as seen previously with 1.25 mM phosphate while other combinations of calcium, magnesium and phosphate result in inhibited ALP activity compared to the SM control (Figure 3.6B and 3.7B). Finally, Figure 3.7C demonstrates that using 5 mM phosphate results in increases in ALZ intensity in the three compound mix where previously in the 1.25 phosphate mix, no ALZ stain was seen.

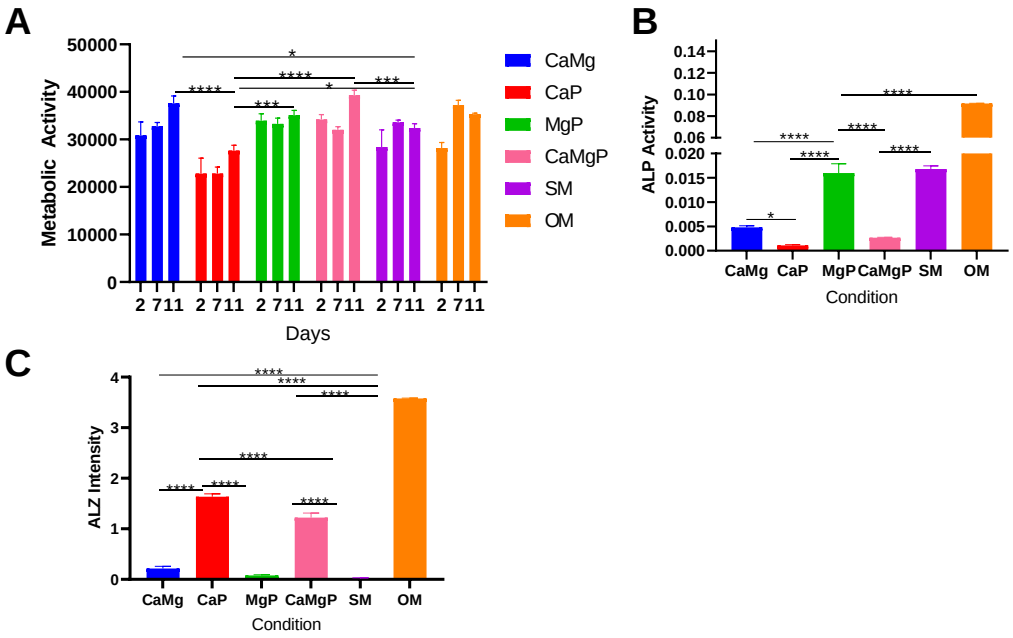


Figure 3.7. (A) The metabolic (day 2, 7 and 11), (B) ALP (day 11) and (C) ALZ intensity (day 21) of hMSC treated with combinations of 5 mM calcium, magnesium and phosphate, compared to standard medium (SM) and osteogenic medium (OM) controls. *p<0.05, ***p<0.001, ****p<0.0001 (n=2).

3.3.1.3 Effects of ions on hMSC gene expression

When tested at lower concentrations in isolation, 1.25 mM phosphate demonstrated superior metabolic and osteogenic activity compared to higher doses, despite this, the use of 1.25 mM phosphate in combination with 5 mM calcium and magnesium resulted in no ALZ stain. Using a higher dose of 5 mM phosphate along with 5 mM calcium and 5 mM magnesium allowed for increased ALZ intensity compared to the lower phosphate combination. To further investigate the effects of direct application of 5 mM calcium, magnesium and phosphate (henceforth titled 555) on hMSC, TaqMan Low Density Arrays (TLDAs) were used to measure changes in gene expression on 555 treated cells. Table 3.1 indexes all the gene groups analysed in this subsection.

Table 3.1 Index of gene groups analysed in chapter 3

Section Number	**Gene Group**
3.3.1.3.1	Proliferative
3.3.1.3.2	Integrin
3.3.1.3.3	Osteoblastic
3.3.1.3.4	Notch
3.3.1.3.5	TGF-β and BMP
3.3.1.3.6	Wnt

3.3.1.3.1 Proliferative markers

Changes to expression in proliferative gene markers *CCND1*, *PCNA* and *MKI67* were analysed after 11 days of direct ion treatment with 555 on hMSC cells *in vitro* (Figure 3.8). hMSC treated with 555 demonstrated no significant changes to proliferative gene expression compared to the SM control. 555 treated cells did show significant upregulation of *CCND1* compared to OM treated cells, in which decreased expression was seen. No significant changes in expression were noted in *MKI67* and *PCNA* expression in either treatment.

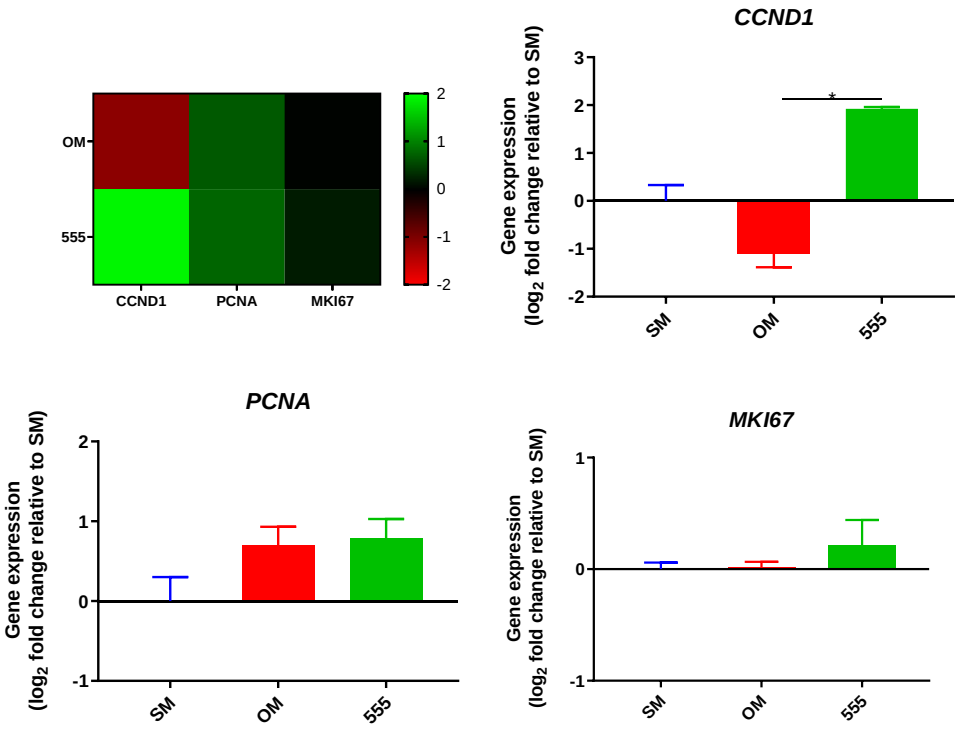


Figure 3.8. hMSC proliferation marker expression after 11 days of OM and 555 treatment normalized to the standard medium (SM) control. *p<0.05 (n=2).

3.3.1.3.2 Integrin markers

Gene expression of integrin subunits *ITGA1*, *ITGA3* and *ITGB1* were analysed for changes after 11 days of 555 treatment of hMSC *in vitro* (Figure 3.9). 555 treated samples demonstrated no significant changes to integrin gene expression compared to the SM or OM controls.

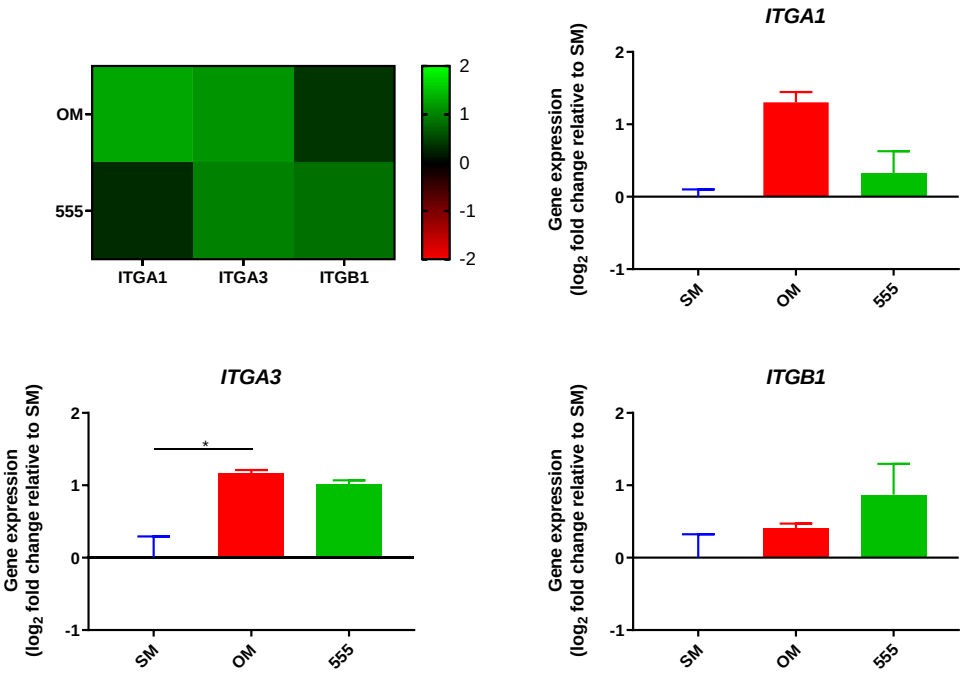


Figure 3.9. Heatmap of hMSC integrin gene expression after 11 days of OM and 555 treatment normalized to the standard medium (SM) control. *p<0.05 (n=2).

3.3.1.3.3 Osteoblast markers

Gene expression changes to key osteoblastic markers *RUNX2, ALPL, COL1A1, BGLAP, MSX2, DLX5 and SPP1* were analysed on cells cultured *in vitro* to discern the effects of direct ion application of 555 on hMSC differentiation after 11 days of treatment (Figure 3.10). Additionally, while not directly influencing osteoblast differentiation *PPAR-γ* and *TNFRSF11* were observed for changes in expression during osteoblast differentiation. 555 treatment demonstrated no significant changes to osteoblast gene expression compared to the SM control. 555 treatment did not alter ALPL gene expression contrary to the decrease in ALP activity noted previously. Additionally, 555 treated cells did show significant upregulation of *SPP1* and *BGLAP* compared to the OM control.

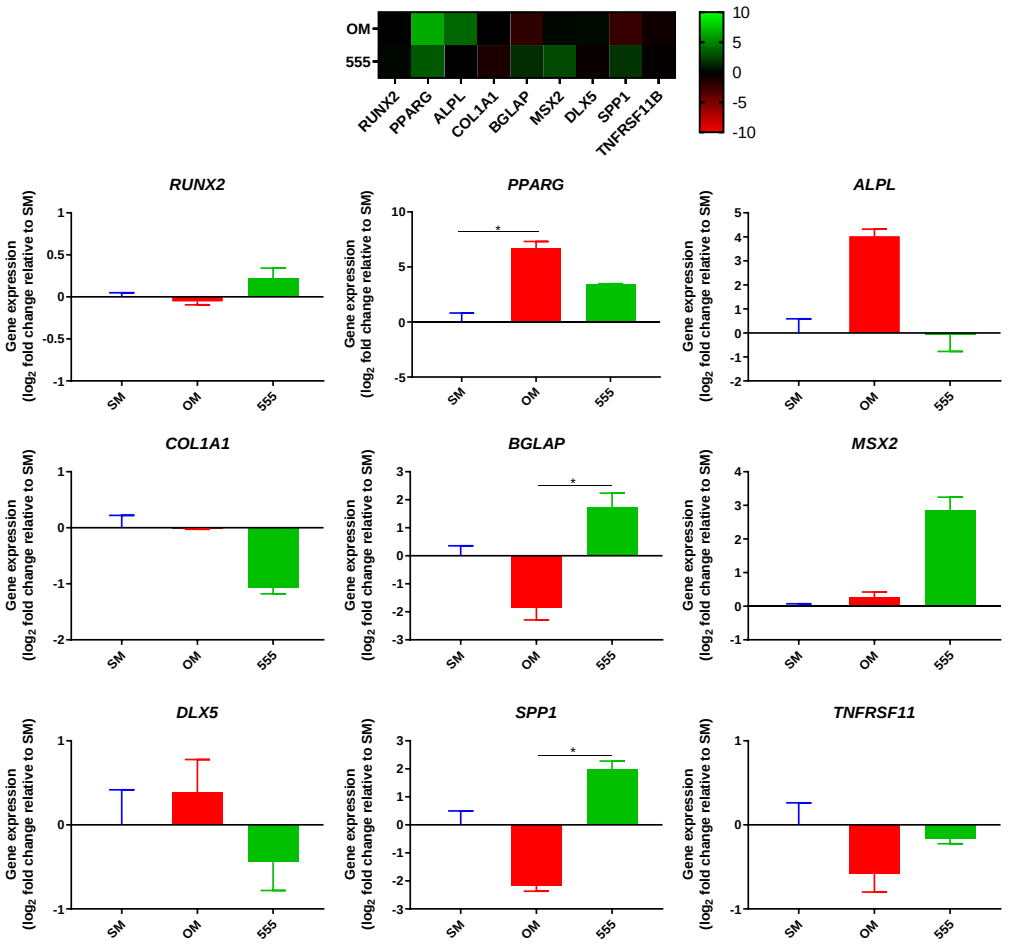


Figure 3.10. hMSC osteoblastic gene expression after 11 days of OM and 555 treatment normalized to the standard medium (SM) control. *p<0.05 (n=2).

3.3.1.3.4 Notch markers

Notch gene expression markers were analysed at 11 days after direct ion treatment of hMSC with 555 *in vitro* to discern its effects on Notch signalling (Figure 3.11). The genes analysed included Notch receptors (*NOTCH1, NOTCH2* and *NOTCH3*), ligands (*JAG1, JAG2* and *DLL1*) and a Notch regulator (*DLL3*). No significant changes to Notch gene expression were observed in 555 treated cells compared to the SM and OM controls.

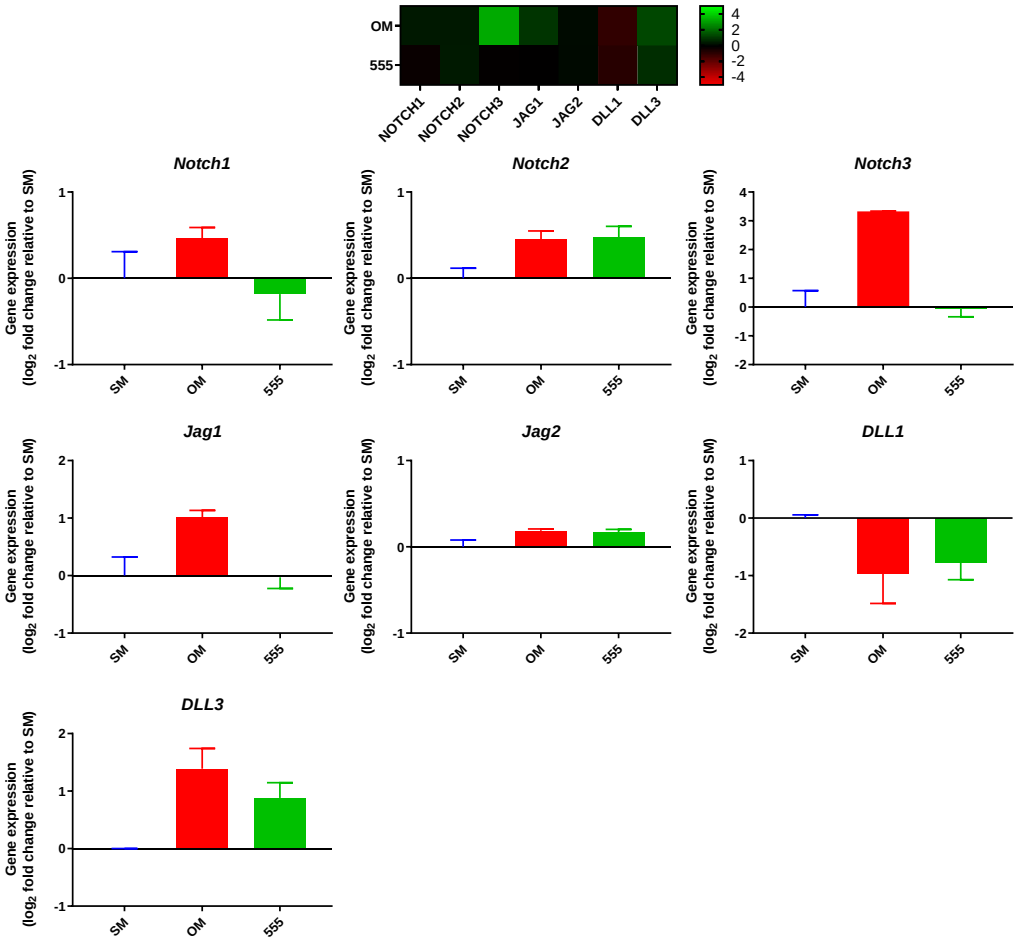


Figure 3.11. hMSC notch gene expression after 11 days of OM and 555 treatment normalized to the standard medium (SM) control. *p<0.05 (n=2).

3.3.1.3.5 TGFβ and BMP markers

The expression of BMP and TGFβ markers were analysed after direct ion treatment of hMSC with 555 after 11 days to discern their effects on BMP signalling (Figure 3.12). Genes analysed included BMP ligands (*BMP2, BMP4* and *BMP5*), TGFβ ligands (*TGFβ1, TGFβ2, TGFβ3*), SMADs (*SMAD1, SMAD3, SMAD4, SMAD6* and *SMAD7*) and Noggin (*NOG*). 555 treatment demonstrated no significant changes in TGFβ and BMP gene expression compared to the SM control. However, significant increases in expression were observed in *BMP2* and *SMAD6* compared to the OM control.

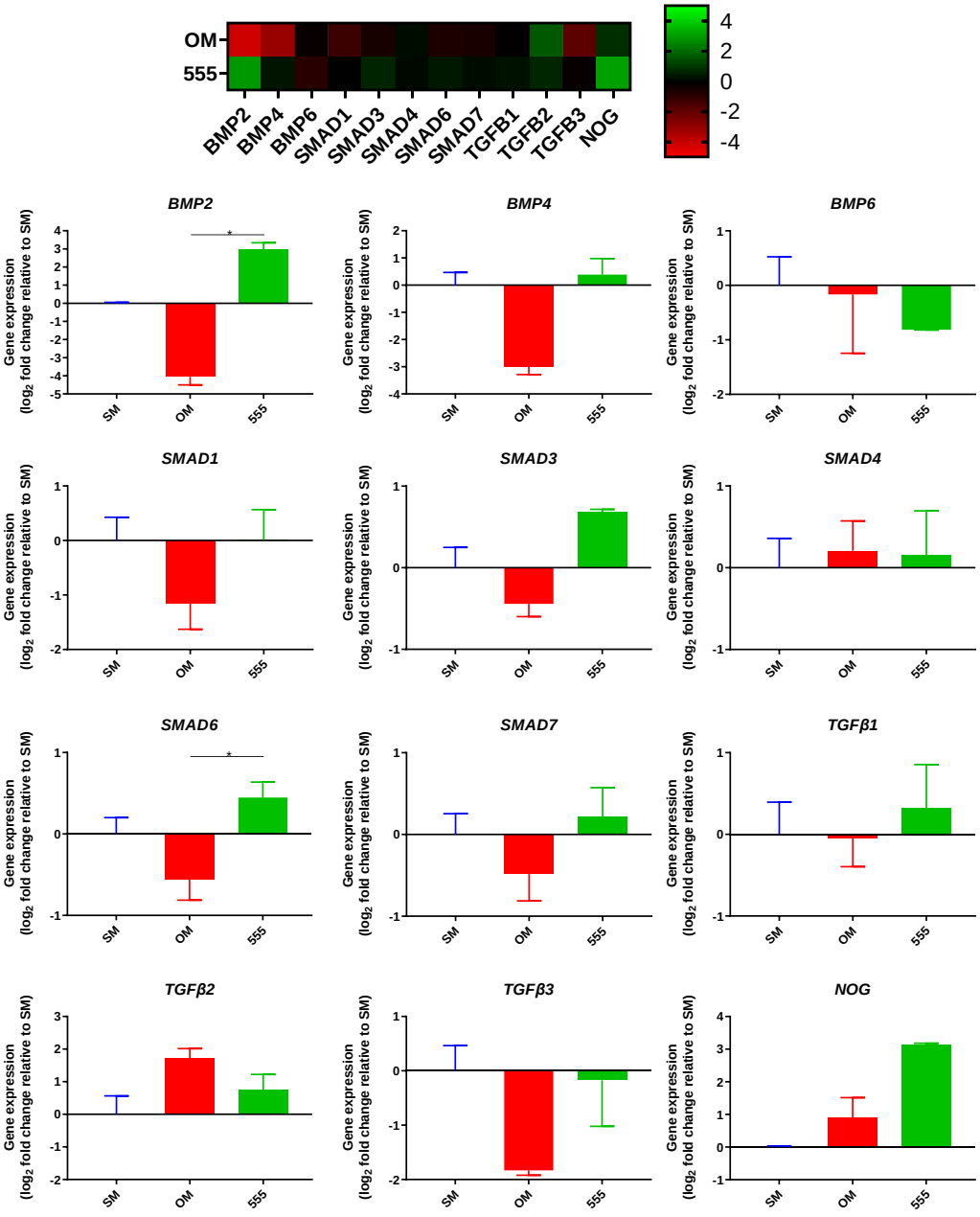


Figure 3.12. hMSC TGFB and BMP gene expression after 11 days of OM and 555 treatment normalized the standard medium (SM) control. *p<0.05 (n=2).

3.3.1.3.6 Wnt markers

Markers for Wnt gene expression were analysed after direct ion treatment of hMSC with 555 for 11 days to observe for changes in expression within the Wnt pathway (Figures 3.13). Wnt co-receptors (*LRP5, LRP6, FZD1* and *ROR2*), ligands (*WNT5A, WNT10B*), inhibitor *SFRP1* and transcriptional activator *CTNNB1* were observed for changes in expression. *SFRP1* showed a significant upregulation in 555 treated cells compared to the SM control. No other Wnt genes demonstrated changes to expression compared to both the SM and OM controls.

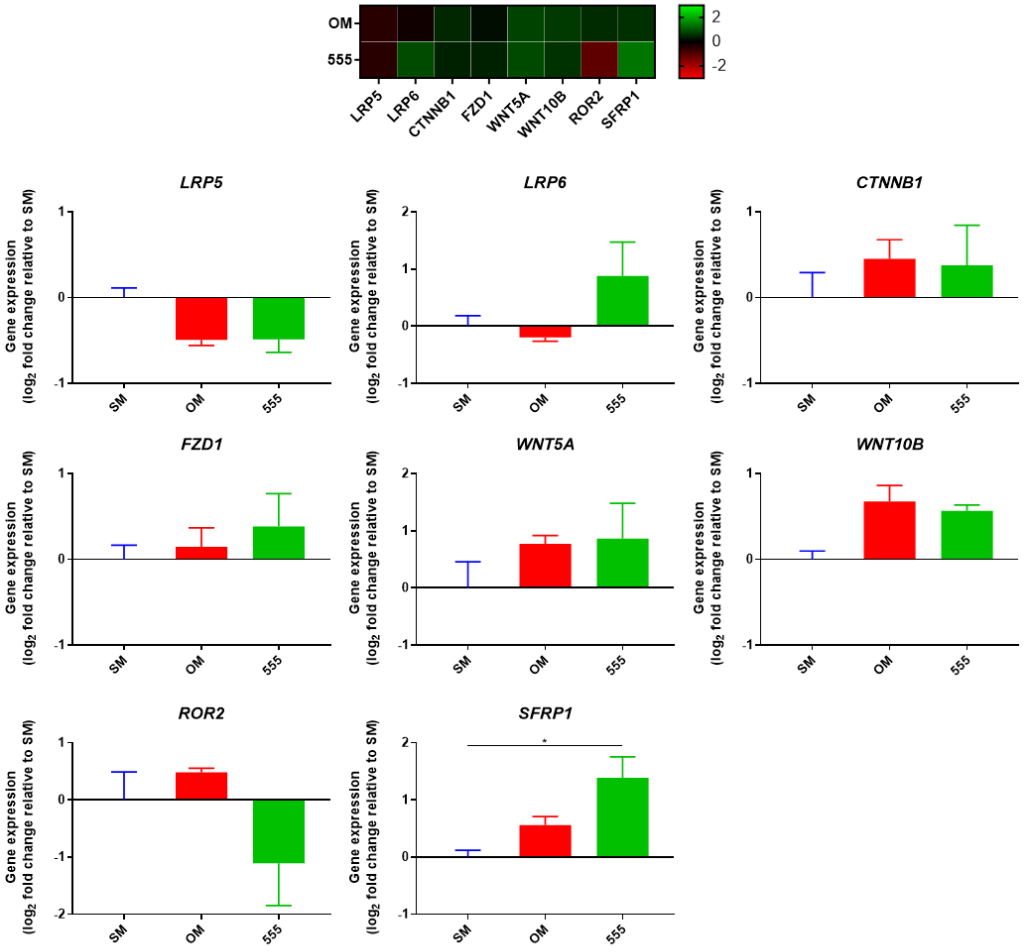


Figure 3.13. hMSC WNT gene expression after 11 days of OM and 555 treatment normalized to the standard medium (SM) control. *p<0.05 (n=2).

3.4 Discussion

PBGs allow for the tailorable, controlled release of inorganic ions such as calcium, magnesium and phosphate as the glass degrades. These ions can interact with hMSC and have been noted to promote proliferation, adhesion and differentiation (Hoppe et al., 2011). As such, the response of hMSC to the ionic components of PBGs is of key importance in PBG development. This chapter investigates the metabolic and osteogenic response of hMSC to PBG ionic precursors, in isolation and in combination to identify an optimal concentration of ions for the promotion of osteogenic differentiation.

3.4.1 Assessment of direct ion application to hMSC

3.4.1.1 Singular ion dose optimization on hMSC

Direct calcium application of 5 mM resulted in increases of metabolic activity and ALZ intensity compared to the SM control. These increases in metabolic activity and ALZ intensity decreased as the calcium concentration was increased to 20 mM. Maeno et al. (2005) demonstrated that concentrations of calcium between 2-4 mM demonstrated better osteoblast proliferation while higher concentrations of 6-8 mM were superior for osteoblast differentiation and matrix mineralization. The results presented here correlate with the effect of calcium on metabolic activity, yet 20 mM of calcium did not promote more ALZ intensity. This may be attributed to the use of an immortalized human line while Maeno et al. (2005) used primary mouse osteoblast cells.

The results shown here also correlate with a study by Danoux et al. (2015), who showed that calcium application via $CaCl_2$ promoted cell proliferation at both 4 mM and 8 mM. However, unlike Danoux et al. (2015) and despite promoting ALZ intensity, ALP was significantly inhibited across all treatments. This is also in contrast with studies

which indicate the necessity of ALP for mineralization, however, the time-dependent nature of ALP expression should be noted as standard osteogenic differentiation demonstrates a sharp level of ALP increase on day 11 followed by downregulation (Golub and Boesze-Battaglia, 2007; Orimo, 2010). Due to the levels of ALZ stain intensity seen, it is possible that the necessary increase in ALP expression for matrix mineralization is delayed, resulting in tests on day 11 not reflecting the increase in ALP that may occur several days later. However, it may also be possible that the ALZ stain seen is not due to active cellular matrix mineralization but due to passive deposition of calcium and phosphate precipitate.

Magnesium application to hMSC cultures resulted in no significant changes to metabolic activity across all doses explored. Studies have indicated magnesium's capacity to promote growth and its deprivation was demonstrated to cause cell cycle arrest (Wolf and Cittadini, 1999). Despite this, only minimal changes in metabolic activity were noted. Due to these minor non-significant increases seen with increasing dose, it is likely that the pathways that are contingent on a minimal magnesium dose may be saturated due to the 0.81 mM of magnesium present in DMEM and additional magnesium present in serum which was added to the cells during typical culture. Studies have shown the key role Mg^{2+} plays in ATP synthesis however, Rubin (1975) suggested that while 0.1-0.8 mM magnesium is required for the binding to adenosine, increase in magnesium beyond this point likely result in no increases to cell proliferation due to the saturation of all adenosine present (Ko et al., 1999).

The ALP enzyme consists of two magnesium ions within its structure, making it necessary for the production of ALP (Coleman, 1992). Furthermore, Dean (2002) demonstrated how the addition of increasing concentration of magnesium ions via

$MgCl_2$ up to 5 mM causes an increase in ALP. Olorunniji et al. (2007) also demonstrated the increase in ALP activity with the addition of $MgCl_2$ up to 4 mM magnesium, after which an increase in concentration to 8 mM magnesium inhibited the activity of ALP. These results in the literature corroborate the results presented in this study. Olorunniji et al. (2007) also suggests that further increases of magnesium past the promoting effect seen at 4 mM causes Mg^{2+} to displace Zn^{2+} ions from the catalytic site of ALP causing decreased activity as both ions are required for ALP to function effectively (Hung and Chang, 2001). The results presented here and in the literature indicate that magnesium promotes ALP activity up to 5 mM after which an inhibitory effect is observed, while no changes to metabolic activity were noted compared to the SM control.

Phosphate supplementation showed the greatest impact on cells, causing visible disruption to the monolayer at doses higher than 5 mM after 48 hours and resulting in significant decreases in metabolic activity readings across all doses by day 11. Further decreases to the doses applied at 2.5 mM and 1.25 mM demonstrated significantly less impact on cell viability as the dose was reduced. Meleti et al. (2000) demonstrated similar results where increasing phosphate concentrations from 1-7 mM in media induced apoptosis of osteoblast like cells, with the highest dose causing complete monolayer failure.

Inhibition of osteogenic activity was seen with increasing concentration of phosphate from 1.25 mM to 20 mM. At the lowest dose of 1.25 mM, minimal ALP inhibition was seen along with significant matrix mineralization. Contrasting information about the effects of phosphate on ALP activity are present in the literature. Dean (2002) describes a competitive inhibition of 1 mM sodium phosphate on ALP activity while

Danoux et al. (2015) demonstrated much higher levels of ALP activity in 4 mM treated cells of a donor compared to the untreated control. The contradictory effect of ALP activity could also be attributed cell differences, while both studies use hMSCs, Danoux et al. (2015) worked with primary cells as opposed to the immortalized cell line used in this study. However, increases in matrix mineralization were observed at lower doses, once again suggesting a potentially delayed ALP activity curve or non-biological deposition. Additionally, due to the apoptotic nature of phosphate at higher concentrations (Meleti et al., 2000), it is possible that phosphate treatments do not inhibit osteogenic activity directly but decrease the number of cells within the monolayer at higher concentrations, which decreases the overall activity measured by the assay.

Calcium treatment promoted significant increases to metabolic activity, magnesium treatments promoted significant increases to ALP activity and phosphate demonstrated its dose dependant cytotoxic effect on hMSC. Ultimately, the significant biological impact on hMSC by PBG precursors has been demonstrated and as PBGs will deliver all three ionic components during its dissolution, multiplexed tests with the three precursors was undertaken to observe any combinatorial effects between the three ions on hMSC.

3.4.1.2 Combinatorial dose optimization on hMSC

Combinatorial tests of 5 mM calcium, magnesium and phosphate showed significant differences between the various treatments by day 11. Keeping in mind the sizeable disruption of metabolic activity seen in the singular phosphate 5 mM treatment, the combinatorial results observed with 5 mM phosphate, calcium and magnesium showed significantly improved metabolic activity compared to all other mixes investigated. A study by Magne et al. (2003) demonstrated the apoptotic effects of 4 mM phosphate concentration in the presence of 2.4 mM calcium (by supplementing media with NaH_2PO_4 and Na_2HPO_4 and $CaCl_2$). However, the mentioned study was carried out on murine ATDC5 cells of the chondrogenic lineage which may explain the differences in cell death where, when applied in isolation, 2.4 mM calcium and 4 mM phosphate had no effect on cell viability while in combination, triggered an apoptotic event.

A study by Adams et al. (2001) suggested that the synergistic apoptotic pathway works through calcium ions facilitating inorganic phosphate entry into cells resulting in disruption of the mitochondrial transmembrane potential. Calcium in DMEM used for hMSC feeds (1.80 mM) along with calcium present in serum would likely saturate the calcium dependent apoptotic pathway proposed by Magne et al. (2003). As such, excess calcium added through testing would likely not contribute to this potentially saturated pathway.

Calcium and magnesium have been noted to promote cell viability and proliferation and appear to rescue combinatorial treatments with 5 mM phosphate (Danoux et al., 2016; Hoppe et al., 2011; Wolf and Cittadini, 1999). The combined treatment using all three compounds resulted in the greatest promotion of metabolic activity even when compared to the control while calcium and phosphate in combination resulted in the weakest activity under the *in vitro* conditions explored.

Lowering phosphate concentration to 1.25 mM showed significantly improved metabolic activity both singularly and when combined. The calcium and phosphate mix which showed the weakest metabolic activity at 5 mM phosphate showed a non-significant difference from the control when 1.25 mM phosphate was used, suggesting decreased promotion of the previously described apoptotic pathway. Identical trends in ALP activity were seen between the 5 mM and 1.25 mM combinatorial phosphate applications, with the magnesium phosphate combination showing the highest activity when compared to the control.

However, using a lower dose of phosphate resulted in complete ablation of matrix mineralization activity of the tertiary formulation, indicating a requirement of specific phosphate levels to elicit a mineralization response. This is supported by Khoshniat et al. (2011) who demonstrated the calcium and phosphate dependence of ERK1/2 phosphorylation and MGP/OPN expression where 10 mM phosphate and 1.8 mM calcium was required for the promotion of the noted mineralization genes.

The data presented in this study suggests that optimization in isolation may not be an efficient way to evaluate the effectiveness or potential of various ions, and may only give indicators as to how these ions may behave in combination when applied to cells.

3.4.2 Effects of direct ion application on hMSC gene expression

Using precursor compounds revealed that calcium (5 mM) and magnesium (5 mM) can promote metabolic activity and ALP activity respectively. Phosphate however, at doses higher than 1.25 mM, resulted in significant cell toxicity. Combinatorial tests revealed that using a lower dose of phosphate (1.25 mM) results in complete ablation of ALZ intensity. Calcium and magnesium (5 mM) demonstrated their ability to rescue cells treated with 5 mM phosphate allowing for the use of higher doses of phosphate than when tested in isolation. As such, 5 mM calcium, magnesium and phosphate (555) was taken forward for gene expression analysis due to its promotion of metabolic activity and ALZ stain intensity.

3.4.2.1 Proliferation Markers

Three proliferative genes were analysed on day 11 for changes when treated with 555. 555 treated cells showed increased expression of proliferation gene marker *CCND1* compared the OM control. *CCND1* (cyclin D1) is a notable proliferative marker shown to promote cellular proliferation in a number of cell types due its control of the progression through the G1 phase of the cell cycle (Ahlin et al., 2017; Marquez et al., 2017; Wang et al., 2012). Although *MKI67* (marker Of proliferation Ki-67) and *PCNA* (proliferating cell nuclear antigen) are notable proliferative markers, they showed no significant change in expression compared to the SM control in 555 treated cells at day 11 (Akino et al., 2003; Sasaki et al., 1987; Yang et al., 2018). Interestingly, while *CCND1* was upregulated in the 555 treatment, it was downregulated in the OM treatment. The upregulated proliferative marker in addition to the significant increase in metabolic activity compared to the SM control suggests that the 555 application had a pro-proliferative effect on hMSC.

Osteoblast differentiation occurs in three key stages: early, mid and late stage differentiation. The early stage differentiation is classified by increases in proliferation and the initial expression of pro-osteogenic genes. The initiation of matrix maturation and differentiation begins with the exit of the cell cycle (Rutkovskiy et al., 2016). Proliferation and differentiation are typically antagonistic processes where terminal differentiation results in a permanent exit from the cell cycle (Ruijtenberg and van den Heuvel, 2016). Additionally, Chang et al. (2009) demonstrated how supplementary BMP4 triggers differentiation in osteoblast-like cells though G_0/G_1 cell cycle arrest. Given the need of exit from the cell cycle for mid and late stage differentiation, the increased expression of *CCND1* in 555 treated cells suggests that the cells are still within the initial early stage of differentiation or have not begun commitment.

3.4.2.2 Integrin Markers

Differentiation and function of tissue can be controlled by the extracellular matrix (ECM) and adhesion along with cell-ECM interactions which are largely controlled through integrin signalling (Brunner et al., 2011; Rozario and DeSimone, 2010). Osteoblast cells typically express several integrin subunits including α1, α3 and β1 (Clover et al., 1992). Due to its integral role in adhesion these integrins were analysed on day 11 for changes to expression after treatment with 555. 555 treatment demonstrated similar *ITGA3* (α3 subunit) expression to OM treated samples but ultimately did not cause significant changes to expression compared to the SM control. Calabrese et al. (2016) demonstrated significant upregulation (4.5-fold increase) of *ITGA1* at day 11 of osteogenic differentiation of human MSCs isolated form adipose tissue. Furthermore, Olivares-Navarrete et al. (2017) noted the typically lower levels of *ITGA1* and *ITGB1* expression (up to 1 fold) in hMSC compared to human osteoblast cells when grown on copolymer surfaces of varying stiffness. The different levels of

expression seen between the data shown here and those presented by Calabrese et al. (2016) may be attributed to difference in cell source and the use of a premade osteogenic differentiation kit (Osteogenic Differentiation Medium BulletKit™, Lonza). It is worth noting that despite the minimal changes to expression, the application of treatments to the cells was performed in an indirect manner, surface properties of any biomaterial may further augment or inhibit the levels of integrin expression and as such a direct culture would likely result in changes to integrin expression and activity (Boyan and Schwartz, 2006). For the intended application, PBG microspheres are to be injected into osteoporotic bone in which they will serve as a surface for cell growth in addition to releasing ions into the local environment (McLaren et al., 2019). While the ions tested in this study displayed minimal changes to integrin gene expression, indirect testing of ions on monolayers may not accurately reflect the true extent of the impact to integrin expression PBG will have when in direct contact with cells.

3.4.2.3 Osteoblastic Markers

Analysis of osteoblastic marker expression on day 11 after 555 treatment demonstrated no changes to *ALPL* (ALP) expression compared to the SM control, in line with the results seen prior with 555 treatment resulting in decreased ALP activity in hMSC cells (3.3.1.2). Factors downstream from mRNA expression may explain the significant decreases in enzyme activity compared to the control despite no major downregulation from the gene being seen on the same timepoint. Dean (2002) demonstrated how sodium phosphate acts as a competitive inhibitor for the ALP enzyme, which may explain its decreased activity in 5 mM phosphate solution despite no observable drop in ALPL gene expression.

BGLAP (osteocalcin) and *SPP1* (osteopontin) are significantly upregulated in 555 treated samples compared to the OM control. Both *BGLAP* and *SSP1* are notable markers for osteogenic differentiation. Zhang et al. (2007) demonstrated the increased expression of *BGLAP* in primary hMSC after 20 days of treatment with OM. The difference in expression within the OM control presented here may be attributed to the earlier timepoint tested and the use of a cell line in this study. Lee et al. (2018) reported a 40-fold increases in *SPP1* expression after three days of treatment with 8 mM $CaCl_2$. While a 2-fold upregulation was observed in this study, differences may be attributed to the use of murine cells (C3H10T1/2), increased calcium concentration as well as the application of only $CaCl_2$ with no other ions supplemented in. While upregulation of these two bone matrix proteins correlated with the data presented in this study, their upregulation at the tested timepoint (day 11) is odd as osteocalcin and osteopontin are both expressed by late stage mature osteoblasts. The upregulation of both bone matrix proteins is likely due in part to the elevated levels of calcium within the culture, this is typically seen at sites of bone resorption, acting as a chemoattractant and promoting matrix deposition within the local area of resorption to prepare for bone formation (Lee et al., 2018).

Furthermore, osteopontin and osteocalcin play key roles in matrix formation and adhesion at sites of bone remodelling, their overexpression and calcium binding nature may help to explain the dissonance between the lack of ALP activity seen despite significant ALZ stain intensity observed (McKee and Nanci, 1996; Sodek et al., 2000; Zoch et al., 2016). Sage et al. (2011) demonstrated that an increase of from 1.2 mM to 1.6 mM of calcium (via $CaCl_2$) significantly increases the levels of calcium deposition when phosphate is at 2 mM. The high concentrations of phosphate and calcium in the 555 condition may result in non-biological deposition of calcium phosphate which would then bind to the increased levels of osteopontin and osteocalcin in culture. Both

the osteocalcin and osteopontin proteins exhibit high affinity to Ca^{2+}, which would prevent them from being removed through the rigorous washing steps involved within the ALZ assay (Kläning et al., 2014). The now retained deposition would also be bound by the calcium targeting ALZ stain, generating a false positive ALZ result (Gregory et al., 2004; Puchtler et al., 1969).

The 555 treatment demonstrates significant upregulation of *BGLAP* and *SPP1* compared to the OM control. These upregulations may contribute to the potential non-biological mineralization/deposition created by the treatment. Additionally, the 555 treatment does not promote upregulation of other early stage osteoblast genes such as *RUNX2* and *ALPL*.

3.4.2.4 Notch Markers

The Notch intercellular signalling pathway is notable for its contribution to cell fate and differentiation of osteoblasts. However, its exact role in differentiation remains controversial (Muguruma et al., 2017). The pathway contains four Notch receptors and five Delta/Serrate/Lag2 (DSL) ligands (Zanotti and Canalis, 2016). This study observed the effects of hMSC treated with 555 on day 11 on the expression of three receptors: *NOTCH1*, *NOTCH2* and *NOTCH3* as well as four DSL ligands: *JAG1*, *JAG2*, *DLL1* and the Notch regulator *DLL3*. No significant changes to Notch expression are observed between the 555 treatment and the SM or OM controls. Wang et al. (2019) reported a significant 1.5-fold increase in *JAG1* expression and a 2-fold increase in *NOTCH1* expression in rat bone marrow MSCs at day 1 of culture on hydroxyapatite followed by a significant decrease to control levels by day 7. The present data suggests that 555 treatment has no significant impact on Notch gene expression on day 11. However, as indicated by Wang et al. (2019), a sharp spike of Notch activation through ligand and

receptor upregulation may be occurring during early treatment and additional timepoints may help identify any transient promotion of Notch expression.

3.4.2.5 TGF-β and BMP Markers

The BMP signalling pathway plays a critical role in the regulation of the osteoblast differentiation and subsequent bone formation (Beederman et al., 2013). The 20 key BMP ligands belong to the TGF-β family and are divided into four distinct categories BMP2 and 4, BMP5-8, BMP9 and 10, and BMP12-14 (Carreira et al., 2014). This study has analysed the first subfamily, *BMP2* and *BMP4* as well as *BMP6* for changes to expression on day 11 after treatment with 555. *BMP2*, *BMP4* and *BMP6* were chosen due to their notable impact in promoting bone formation and fracture healing in osteoblasts as reviewed by Marsell and Einhorn (2009).

555 treated samples showed no significant upregulation of BMP genes compared to the SM control. However, 555 demonstrated significant upregulation of *BMP2* compared to the OM control. Aquino-Martínez et al. (2017) demonstrated that mice MSCs grown on 3D gelatin scaffolds with different extracellular concentrations of calcium (0-10 mM $CaCl_2$) showed increased levels of *BMP2* and *BMP4* expression with concentration (up to 4-fold increase with 5 mM calcium) at 10 days of culture. While a similar 3-fold increase in *BMP2* expression was observed in this study, no upregulation of *BMP4* was seen. As suggested by Aquino-Martínez et al. (2017) and correlated by the data presented here, extracellular levels of Ca^{2+} appear to promote upregulation of *BMP2* in culture. It was further suggested that Ca^{2+} and *BMP2* cooperatively promotes osteoblast differentiation by triggering SMAD pathways and enhancing *BGLAP*, *RUNX2* and *SP7* gene expression. However, the data presented in this study showed that while *BGLAP* was upregulated, *RUNX2* and *BMP4* were not. These

differences may be attributed to the differences in cell source (primary mice), culture method (2D vs 3D), surface (TCP vs gelatin) and the addition of additional ion precursors (5 mM phosphate and magnesium). It is likely then that *BMP2* is promoted by increased levels of calcium in culture, though further BMP expression analysis of hMSC treated with phosphate and magnesium with calcium may help elucidate their effects on minimal levels of *BMP4* upregulation seen.

Three TGF-β ligands are known in mammals, TGF-β1, TGF-β2 and TGF-β3 (G. Chen et al., 2012). Unlike BMPs which bind to heteromeric complexes of ActR and BMPR subunits, TGF-β ligands are only capable of binding to TβR receptor complexes (Feng and Derynck, 2005). Maeda et al. (2004) demonstrated using a mouse myoblast cell line C2C12 that TGF-β signalling inhibits osteoblast maturation through the promotion of inhibitor SMAD (SMAD6 and 7) upregulation. 555 treatment demonstrated no significant changes to TGF-β ligand gene expression compared to the SM or OM controls.

SMAD transcription factors play a role after BMP or TGF-β activation of its receptor. Three key SMAD subfamilies interact downstream of BMP activation to regulate osteogenic expression; receptor-regulated SMADs (SMAD1, 2, 3, 5 and 8), common-mediator SMADs (SMAD 4) and inhibitory SMAs (SMAD 6 and 7) (Carreira et al., 2014; Massagué et al., 2005). Receptor-regulated SMADs are activated by BMP (SMAD1, 5 and 8) or TGF-β (SMAD2 and 3) binding to its receptor causing association with the common-mediator SMAD4 for translocation into the nucleus. However, inhibitory SMADs can prevent this association through phosphorylation. This study looked at the changes to expression of *SMAD1, 3, 4, 6* and *7*. 555 treatment demonstrated no significant changes to SMAD gene expression compared to SM however, *SMAD6* showed significant upregulation compared to the OM control. As suggested by Maeda

et al. (2004), this increase in inhibitor *SMAD* upregulation compared to the OM control may have negative consequences on osteoblast maturation due to its negative impact on BMP signalling during late stage maturation.

The 555 treatment demonstrated the ability to upregulate *BMP2* expression yet lack of significant changes to *TGF-β* expression and upregulation of *SMAD6* suggests that any positive influence on osteoblast differentiation the promoted BMP pathway may have may be attenuated due to increased SMAD phosphorylation and may explain the decreased levels of ALP activity seen in 555 treated cells.

3.4.2.6 Wnt Markers

The Wnt signalling pathway plays a key role in bone formation and maintenance (Lerner and Ohlsson, 2015). It operates through two principle pathways, the canonical β-catenin dependant and non-canonical β-catenin independent pathways. The canonical pathway has been demonstrated to play a key role in osteogenic differentiation due to the transcriptional activity of β-catenin (Chen and Long, 2013). This chapter investigated the effects of 555 treatment on several key Wnt signalling genes including co-receptors (*LRP5, LRP6, FZD1 and ROR2*), ligands (*WNT5A, WNT10B*) and inhibitor *SFRP1.*

555 treatment demonstrated no significant changes to Wnt expression markers compared to the SM control with the exception of *SFRP1*, which was upregulated. *SFRP1* acts as an antagonist of Wnt signalling and is one of the few known WNT signalling inhibitors (Yao et al., 2010). By binding to the Wnt protein it prevents receptor activation leading to inhibition of bone formation through attenuation of the Wnt signalling pathway (Kawano and Kypta, 2003; Yao et al., 2010). Studies such as

those done by Yao et al. (2010) demonstrate the negative effects of long term overexpression of *SFRP1* on inhibition of bone formation and osteoblast maturation, and even further demonstrating a 30% loss of ALP activity in cells overexpressing *SFRP1*.

The 555 treatment demonstrates a potential negative impact on canonical Wnt signalling and thus β-catenin stabilization through its attenuation by *SFRP1* upregulation. These results corelate with the ALP activity data which showed significant reduction of ALP activity in 555 treated cells compared to the SM control. This potential inhibition of maturation suggests that the 5 mM calcium treatment plays a role in SFRP1 activity as decreased ALP activity is observable in isolated treatments as well as combinatorial tests where the only combination of ions that did not inhibit ALP activity were 5 mM magnesium and 5 mM phosphate, without the addition of any calcium.

3.5 Summary

The above studies demonstrated the significant biological responses exhibited by calcium, magnesium and phosphate ions. Phosphate demonstrated significant cytotoxicity at concentrations greater than 1.25 mM however, when combined with either calcium or magnesium at 5 mM, allowed for rescue and growth of cells treated with 5 mM phosphate. Magnesium at 5 mM demonstrated upregulation of ALP activity however, this promotion of activity was abolished upon combination with either 5 mM calcium, phosphate or both. Calcium demonstrated the most interesting effect on hMSC, promoting increased metabolic activity at 5 mM while inhibiting ALP activity at any concentration. ALZ stain intensity was also observed at all concentrations of calcium treatment however this was likely not biological integration into a collagen matrix but precipitation out of solution followed by possible binding to secreted osteopontin and osteocalcin. Osteopontin and osteocalcin were demonstrated to exhibit not only upregulation upon increased extracellular calcium levels but also share a high affinity for calcium, likely contributing to the retainment of calcium despite no true matrix mineralization being seen. It is also likely that calcium in the 555 treatment promoted upregulation of *BMP2* and *SMAD6* suggesting an overall negative impact on TGF-β and BMP due to SMAD6 working in an antagonistic manner against the signalling cascade. Finally, *SFRP1* was significantly upregulated in the 555 treatment, its inhibitory nature towards Wnt signalling, β-catenin stabilization and thus osteoblast differentiation suggests its involvement towards the loss of ALP activity in the 555 treatment. Furthermore, similar inhibitory trends in ALP activity seen in all calcium treatments and mixes suggests that it may be calcium that promotes *SFRP1* expression at this timepoint.

This study highlighted the significant effects various concentrations of calcium, magnesium and phosphate can have on metabolic activity, osteogenic differentiation

and how, when combined, these effects can be further controlled. Calcium (5 mM) was demonstrated to play a role in the upregulation of BGLAP and SPP1 matrix proteins and *SFRP1* which was identified as a potential inhibitor of osteogenic differentiation through Wnt signalling attenuation.

Chapter 4 - Biological impact of phosphate for calcium substitution in PBGs

4.1 Introduction

PBGs are promising highly versatile materials that have been explored for numerous applications such as wound healing, bone regrowth and acting as an anti-microbial agent (Ahmed et al., 2006; McLaren et al., 2019; Sghayyar et al., 2020). Studies have demonstrated their suitability for bone formation and osteogenic differentiation of bone marrow MSC through their dissolution and release of a various inorganic ions (Hoppe et al., 2011). As such, their use as microspheres in a bone defect filling application is of particular interest due to not only their promotion for bone growth but their ability to act as a surface for cell growth, behaving as a scaffold for tissue ingrowth which is further promoted by a novel manufacturing process allowing for highly porous PBG microspheres (Hossain et al., 2018; McLaren et al., 2019).

4.2 Aims and hypotheses

To explore the hypothesis that new PBG formulations promoting bone growth can be developed, this study explored the effects of a previously developed PBG microsphere formulation P40 ($40P_2O_5{\cdot}16CaO{\cdot}20Na_2O{\cdot}24MgO$) on hMSC (Hossain et al., 2018). Numerous studies showed the beneficial properties of decreasing PBG solubility through decreasing phosphate content (Uo et al., 1998a) or increasing titanium doping (Abou Neel et al., 2014). The previous chapter demonstrated the cytotoxic nature of increasing phosphate content (1.25-20 mM) and how calcium content (5 mM) can promote metabolic activity and even rescue hMSC treated with high doses of phosphate. This chapter aims to investigate the effect of decreasing phosphate

content through calcium substitution ((40-x)P_2O_5·(16+x)CaO·20Na_2O·24MgO) on cell adhesion, metabolic and osteogenic activity.

hMSC were tested with three formulations of PBG in a direct and indirect manner (see Table 4.1). Direct testing was carried out by seeding cells onto the PBG discs to observe how changing PBG formulations affected cell adhesion rates. These same formulations were then tested indirectly, to observe the impact of their degradation products and ion release rates on hMSC when not in direct contact with the PBG surfaces (i.e. without the added effect of surface degradation and topography). Finally, TaqMan Low Density Arrays (TLDAs) were utilized to analyse the proliferative, osteogenic and integrin gene expression of hMSC when treated with the dissolution products of P40 in standard medium (SM) and osteogenic medium without β-glycerophosphate (OM-).

4.3 Results

4.3.1 Material characterization

EDX analysis

The glass formulations developed are highlighted below in Table 4.1. To confirm PBG composition, EDX analysis was conducted on each formulation and the measurements for P40, P35 and P30 confirmed that the materials were within 1-4 mol% of the target formulation (Table 4.1). P_2O_5 was substituted for the equivalent mol% CaO through the formulations while the remaining components (MgO and Na_2O) remained unchanged.

Table 4.1. EDX measurements of glass compositions against target formulation (mol%) ± standard error of the mean (SEM).

		P_2O_5 (mol%)	CaO (mol%)	MgO (mol%)	Na_2O (mol%)
P40	Target	40	16	24	20
	Measured	39.4 ± 0.7	16.6 ± 0.6	24.0 ± 0.6	20.0 ± 0.7
P35	Target	35	21	24	20
	Measured	34.0 ± 0.4	25.5 ± 1.7	21.9 ± 1.0	18.7 ± 0.7
P30	Target	30	26	24	20
	Measured	28.2 ± 0.3	24.3 ± 0.7	26.0 ± 0.5	21.6 ± 0.5

DSC analysis

Differential scanning calorimeter (DSC) analysis was carried out to determine the thermal properties of the glasses explored, in particular, the glass transition (T_g), crystallisation (T_c) and melting (T_m) temperatures of each formulation. Figure 4.1A shows the DTA traces of the three formulations. The T_g, T_c and T_m values for the traces are presented in Table 4.2. Phosphate content substitution for calcium resulted in increases in T_g, and initially decreased the T_c from 592 °C to 557 °C going from P40 to P35. For P30, two secondary crystallisation peaks were seen for the P35 and P30 formulations at 637 °C and 654 °C, followed by two melting peak events (T_m).

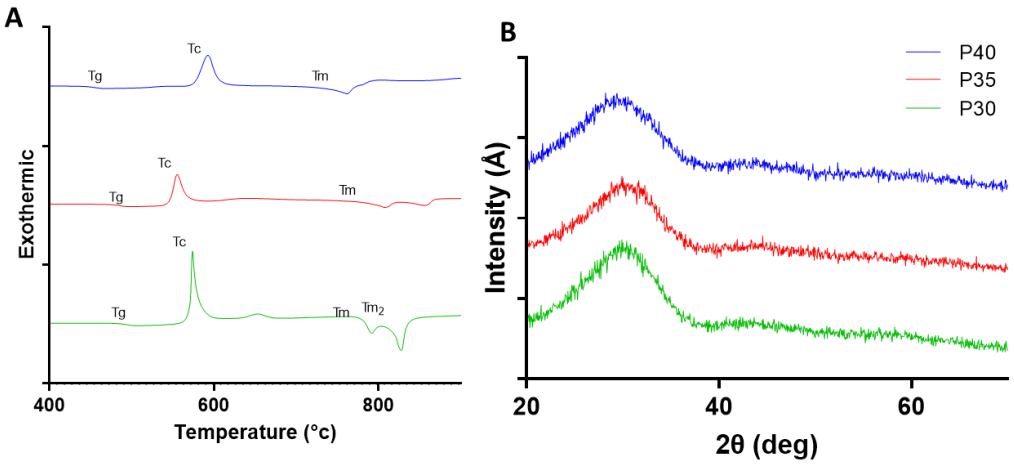


Figure 4.1. Glass characterization of P40, P35 and P30. (A) Thermal analysis traces via DSC of the PBG formulations showing T_g, T_c and T_m. (B) XRD spectra confirming the amorphous nature of P40, P35 and P30 glasses produced.

XRD analysis

XRD was carried out to identify any crystalline peaks within the tested formulations. PBGs are typically lacking in crystalline peaks due to their amorphous nature. XRD analysis on the three formulations revealed the absence of crystalline peaks confirming the amorphous nature of the glasses as can be seen in Figure 4.1B.

Table 4.2. Glass transition (T_g), onset of crystallisation (T_c), melting temperature (T_m) and calculated thermal processing window (Tc_{onset}) for P40, P35 and P30.

	T_g	*T_c*			*T_m*		*Window*
	Onset	Onset	1	2	1	2	Tc_{onset}- Tg
P40	445	563	592		761	838	118
P35	476	533	557	637	805	853	57
P30	485	553	578	654	790	825	68

^{31}P NMR spectroscopy

NMR analysis was used to resolve the distribution of different Q^n species within the different PBG formulations. The NMR spectra for P40 showed two dominant peaks representing Q^1 (-8.6 ppm) and Q^2 (-22.8 ppm) units (Brow, 2000; Shih et al., 2003)(Figure 4.2). P35 also demonstrated similar peaks identified as Q^1 (-8.1 ppm) and Q^2 (-21.4 ppm) units. The slight shift in peaks associated with the Q^2 species was suggested to be due to substitution of 5 mol% phosphate for calcium and a decrease in Q^2 species content from 49% to 6% followed by equivalent increases in Q^1 species.

When the level of phosphate content decreased to 30 mol% in the P30 formulation, a shift from Q^2 and Q^1 to the Q^0 (2.6 ppm) fractions was seen, with P30 showing orthophosphate content, which were absent from the other two formulations explored (see Table 4.3).

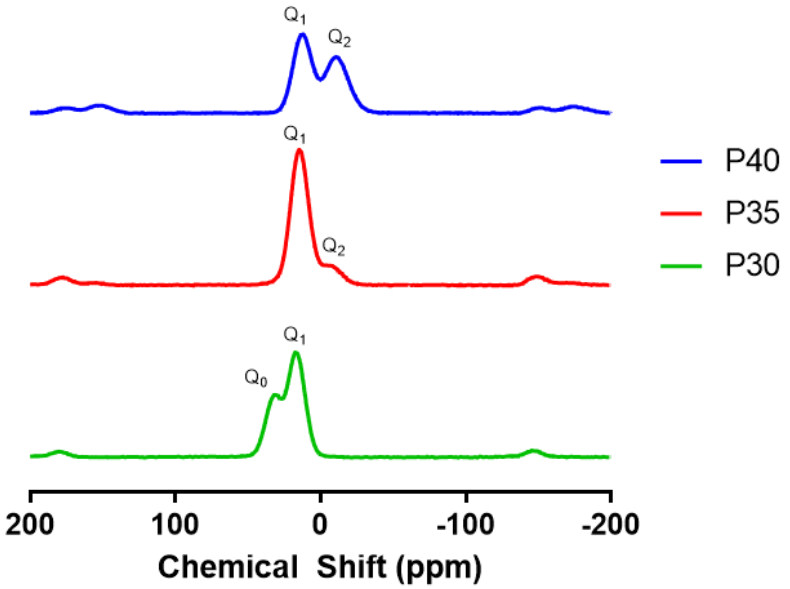


Figure 4.2. ^{31}P NMR spectra of the P40, P35 and P30 formulations. Data provided by Lauren Murrell.

Table 4.3. Distribution of Qn species across PBG formulations.

	Q^0	Q^1	Q^2
P40	0	51	49
P35	0	94	6
P30	39	61	0

4.3.2 hMSC adhesion to PBG discs

An investigation was conducted to identify the impact of altering phosphate and calcium content of PBG on their capacity for cell adhesion and viability. To this end, GFP-labelled MSCs were seeded onto discs (9x2 mm) made from the three PBG formulations with TCP as a control and cultured for 24 hours. hMSC were able to attach to all three formulations tested, however, there were notable differences.

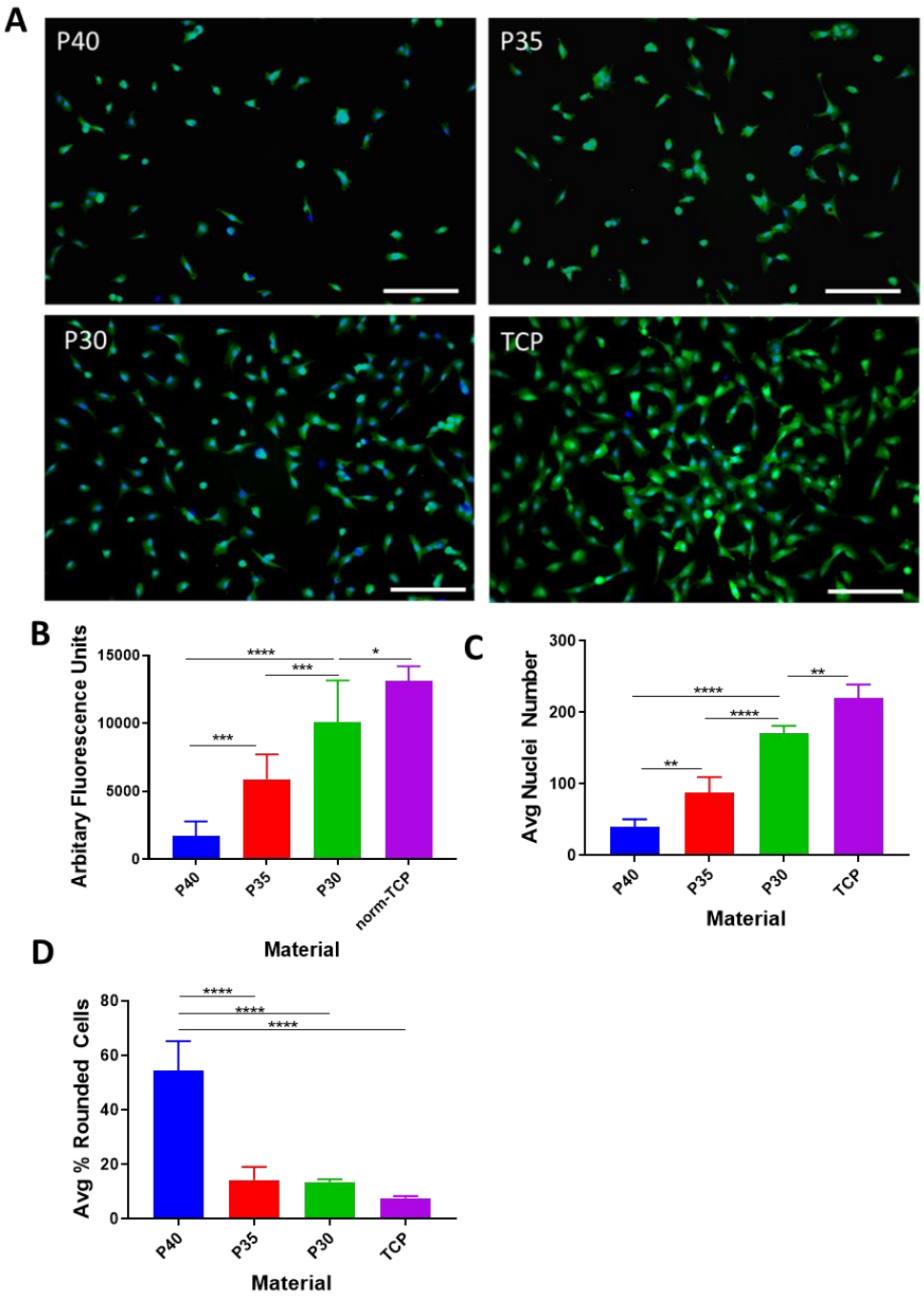


Figure 4.3. Adherence of MSC analysed at 24 hours after seeding on P40, P35, P30 and TCP control. (A) Fluorescent images showing GFP-labelled cells (green) and Hoechst stained nuclei (blue). (B) Metabolic activity assay (norm-TCP shows TCP activity normalized to disc surface area). (C) Average nuclei count per field of view at 24 hours. (D) Average count of rounded cells per field of view at 24 hours. Scale bar = 250 µm. *p<0.05, **p<0.01, ***p<0.001 and ****p<0.0001. (n=3).

Cells seeded on the P40 formulation showed the lowest cell density while cells seeded on the P30 formulation showed the highest (Figure 4.3A). Furthermore, many of the cells on the P40 formulation displayed a rounded morphology, characteristic of cells with low substrate attachment (Okano et al., 1995). The proportion of these rounded cells decreased on the P35 and P30 formulations, whilst a significantly increased proportion of rounded cells are seen on the P40 formulation (Figure 4.3D). The increasing number of adhered cells observed were in the order P30>P35>P40 and was supported by results from the metabolic activity and nuclei count assays performed at 24 hours (Figure 4.3B and 4.3C). The numbers of cells attached to the P40 discs after 24 hours were significantly lower compared to P35, P30 and to the TCP controls. Similarly, cells grown on the P40 formulation showed significantly lower metabolic activity when compared to the other two formulations and the control of TCP (Figure 4.3B).

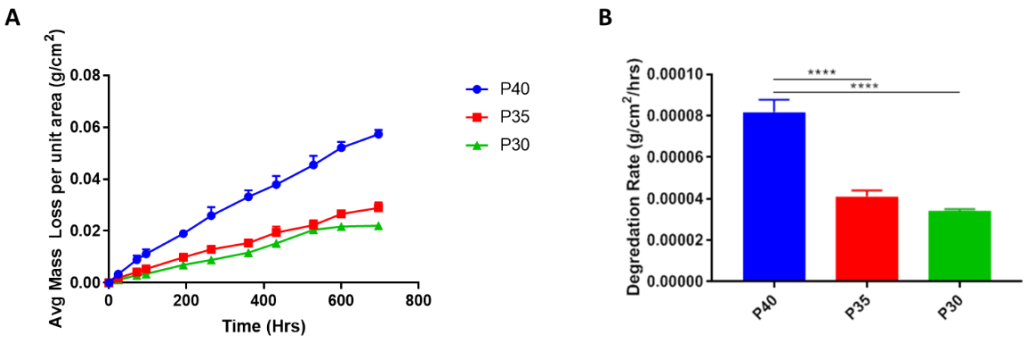


Figure 4.4. Average mass loss per cm^2 of P40, P35 and P30 discs over 30 days (A) and average rate of loss (B). *p<0.05, **p<0.01, ***p<0.001 and ****p<0.0001. (n=3).

Due to the rate of surface degradation, likely having effects on cell adhesion, the degradation profiles of P40, P35 and P30 discs in ultra-pure water were investigated over 30 days (Figure 4.4). P40 was observed to degrade significantly faster than both P35 and P30 (Figure 4.4B). As the modifier fraction was increased and phosphate content decreased, the rate of mass loss was significantly reduced. Further substitution of phosphate for calcium in the P30 formulation was associated with a further decrease in the rate of mass loss. However, no statistically significant difference compared to P35 was seen.

4.3.3 Indirect microsphere application

4.3.3.1 Effects of microsphere degradation products on hMSC

To identify the effects of the PBG dissolution product on hMSC, indirect treatment of hMSCs was also carried out by treating cells with the dissolution products of PBG microspheres added every 48 hours for 21 days. Unlike the notable difference observed with direct seeding on the different PBG disc formulations, no significant differences were seen between the formulations on day 2. However, statistically significant differences were observed on day 11 with this indirect model between cells treated with P40 and P35 conditioned media (Figure 4.5A). Testing for osteogenic activity showed that indirect treatments with all three glass formulations resulted in no changes observed in osteogenic activity from the control in ALP or for mineral deposition (Figure 4.5B and 4.5C).

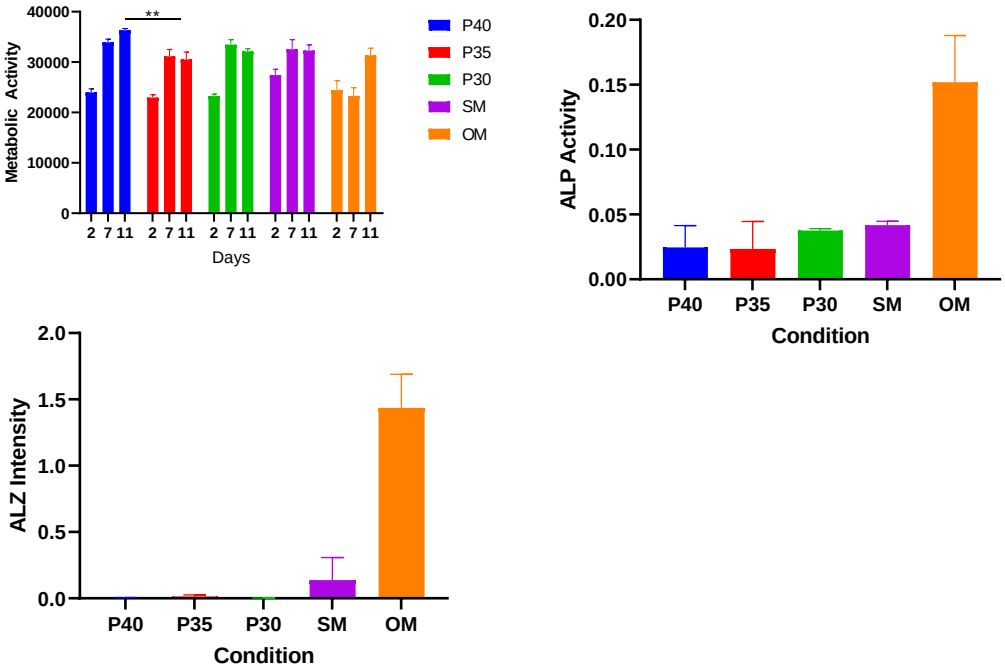


Figure 4.5. (A) The metabolic (day 2, 7 and 11), (B) ALP (day 11) and (C) ALZ intensity (day 21) of hMSC treated with the dissolution products of P40, P35 and P30 compared to standard medium (SM) and osteogenic medium (OM). **p<0.01. (n=2).

Whilst medium conditioned from all formulations demonstrated no significant impact on the osteogenic parameters measured, P40 resulted in significantly higher metabolic activity than P35 on day 11 and due to it being previously explored in the literature *in vivo* (McLaren et al., 2019), was taken forward for further experimentation. To further explore the effects of P40, it was also incubated in OM- medium (osteogenic media without β-glycerophosphate). β-glycerophosphate is the phosphate source for the mineralized matrix in osteogenically differentiating cell as such it was not used in OM- order to better elucidate the effectiveness of phosphate release on hMSC by preventing any competitive effects that may appear between two independent

phosphate sources. An increase in ALP activity was noted in P40OM- (P40 degraded in OM-) and interestingly, demonstrated higher activity than that of both OM- and P40 in isolation (Figure 4.6). Despite the ALP activity seen in P40OM- treated cells, no matrix mineralization was observed in either P40OM- or P40 in isolation.

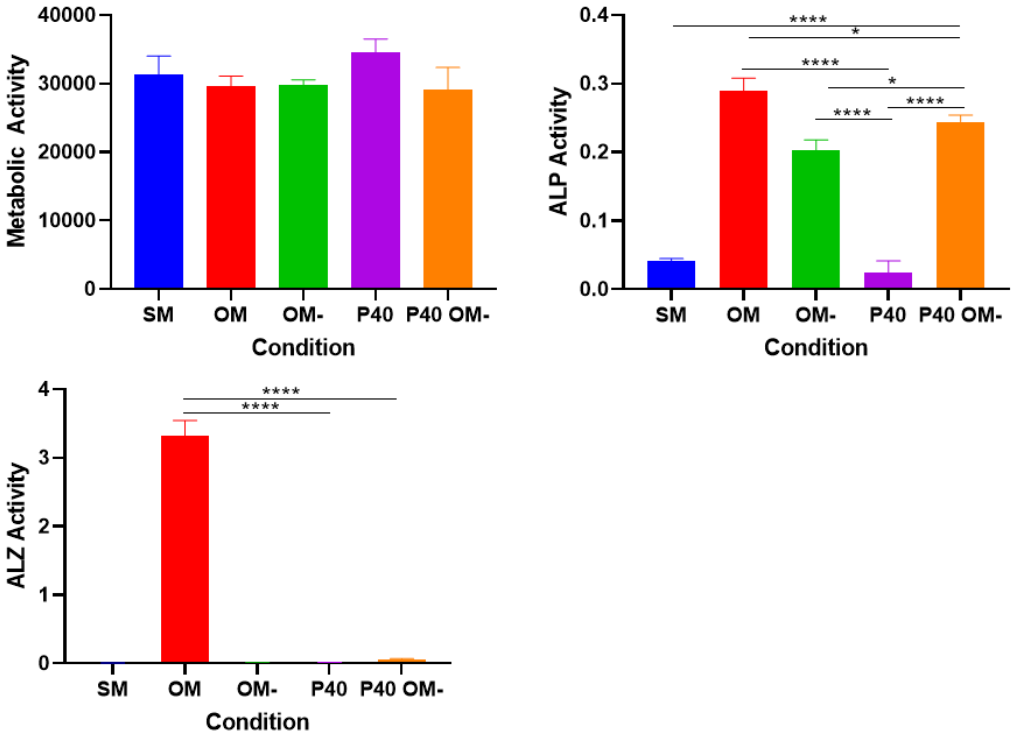


Figure 4.6. (A) The metabolic (day 2), (B) ALP (day 11) and (C) ALZ intensity (day 21) of hMSC treated with the dissolution products of P40, P35 and P30 incubated in standard medium (SM) and osteogenic medium without β-glycerophosphate (OM-) compared to SM, OM and OM- controls.*p<0.05, **p<0.01, ***p<0.001 and ****p<0.0001. (n=3 technical replicates).

4.3.3.2 Effects of microsphere degradation products on hMSC gene expression

TaqMan Low Density Arrays (TLDAs) were used to facilitate analysis of hMSC gene expression on day 11 after indirect treatment with the dissolution products of P40 in SM or OM- (OM without β-glycerophosphate). OM- was used to observe the effects of PBG dissolution products without masking the effects of phosphate released with β-glycerophosphate. Table 4.4 indexes all the gene groups analysed in this subsection.

Table 4.4. Index of gene groups analysed in chapter 4

Section Number	**Gene Group**
4.3.3.2.1	Proliferative
4.3.3.2.2	Integrin
4.3.3.2.3	Osteoblastic
4.3.3.2.4	Notch
4.3.3.2.5	TGF-β and BMP
4.3.3.2.6	Wnt

4.3.3.2.1 Proliferative markers

Proliferative gene expression markers *CCND1*, *PCNA* and *MKI67* were observed after 11 days of indirect treatment of hMSC with P40 in SM and OM- media (Figure 4.7). P40 treatment demonstrated no significant changes to proliferative gene expression compared to the SM control. Similarly, the P40OM- treatment demonstrated no significant changes to the OM- control. The P40OM- treatment did show significant downregulation of *CCND1* and upregulation of *PCNA* compared to the SM control.

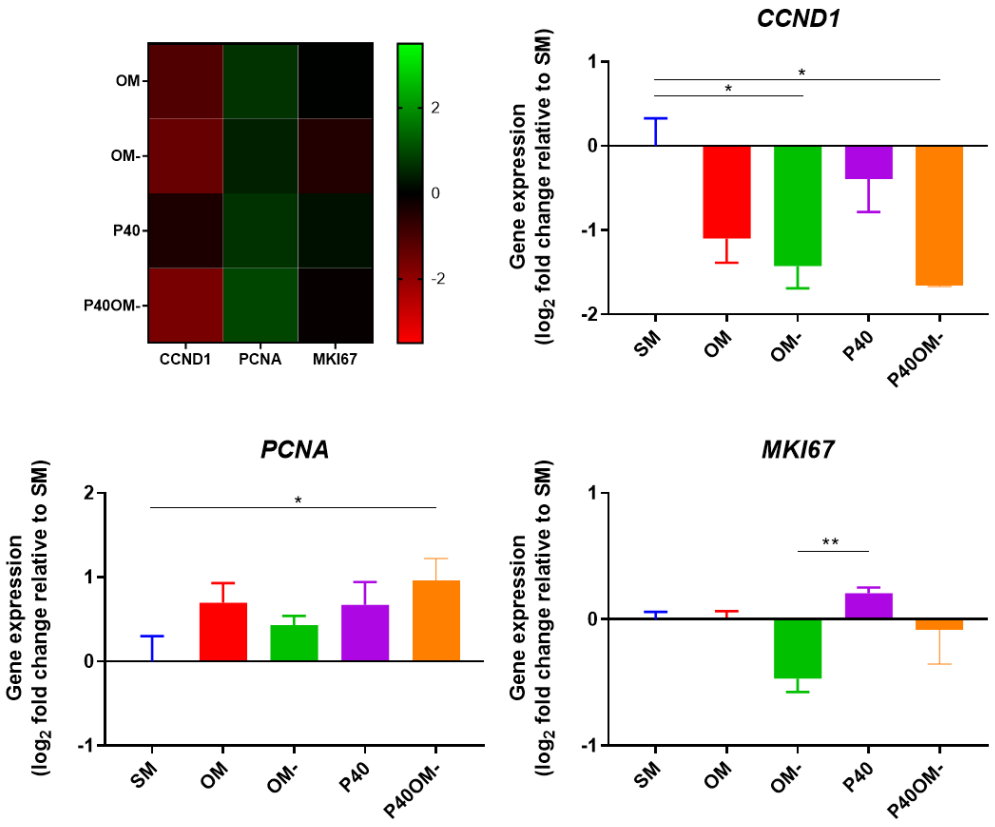


Figure 4.7. hMSC proliferation marker expression after 11 days of P40 and P40OM- treatment normalized to the standard medium (SM) control. *p<0.05, **p<0.005 (n=2).

4.3.3.2.2 Integrin marker

Integrin subunits *ITGA1*, *ITGA3* and *ITGB1* were observed for changes in expression after 11 days of indirect treatment with P40 in SM and OM- media (Figure 4.8). No significant changes in integrin expression are observed between P40 and the SM control and P40OM- and the OM- control.

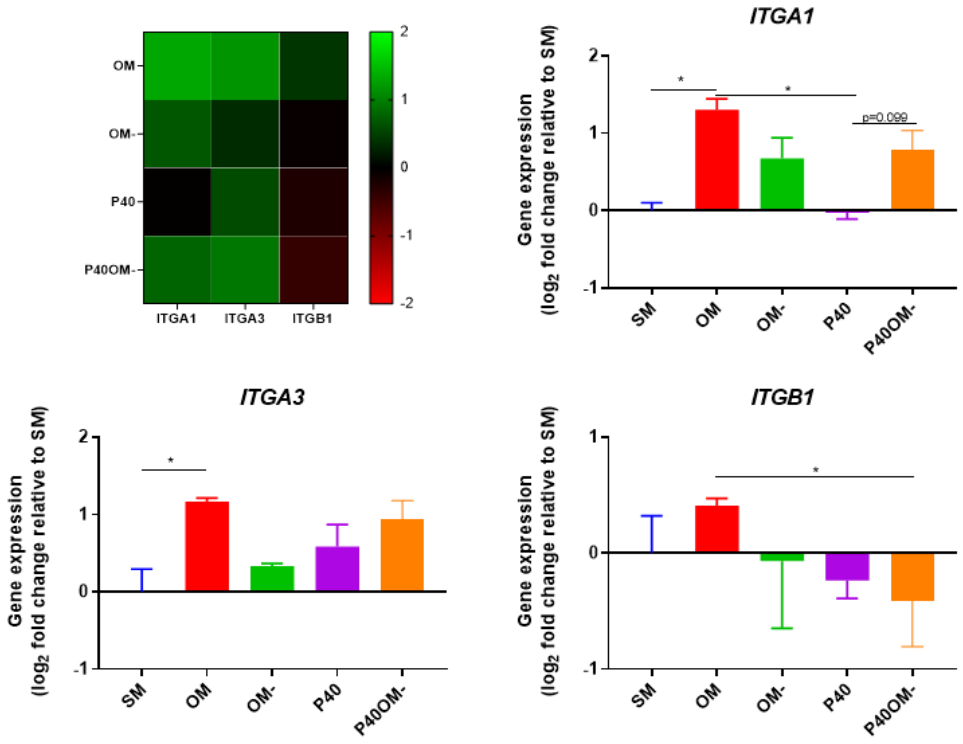


Figure 4.8. hMSC integrin gene expression after 11 days of P40 and P40OM- treatment normalized to the standard medium (SM) control. *p<0.05 (n=2).

4.3.3.2.3 Osteoblast markers

Osteoblast genes *RUNX2, ALPL, COL1A1, BGLAP, MSX2, DLX5* and *SPP1* were observed for changes in expression after 11 days of indirect treatment of hMSC with P40 in SM and OM- (Figure 4.9). Additionally, while not directly influencing osteoblast differentiation *PPAR-γ* and *TNFRSF11* were also observed for changes in expression during indirect treatment with P40 and P40OM-. No significant changes to osteoblast

gene expression are observed in P40 treated samples compared to the SM control. P40OM- treated samples, however, demonstrate significant upregulation of *RUNX2* and *DLX5* compared to the OM- control. P40OM- treatment also demonstrates significant upregulation of *PPAR-γ* and *ALPL* compared to the SM control suggesting minimal contribution of the P40 dissolution products to the upregulation of these genes.

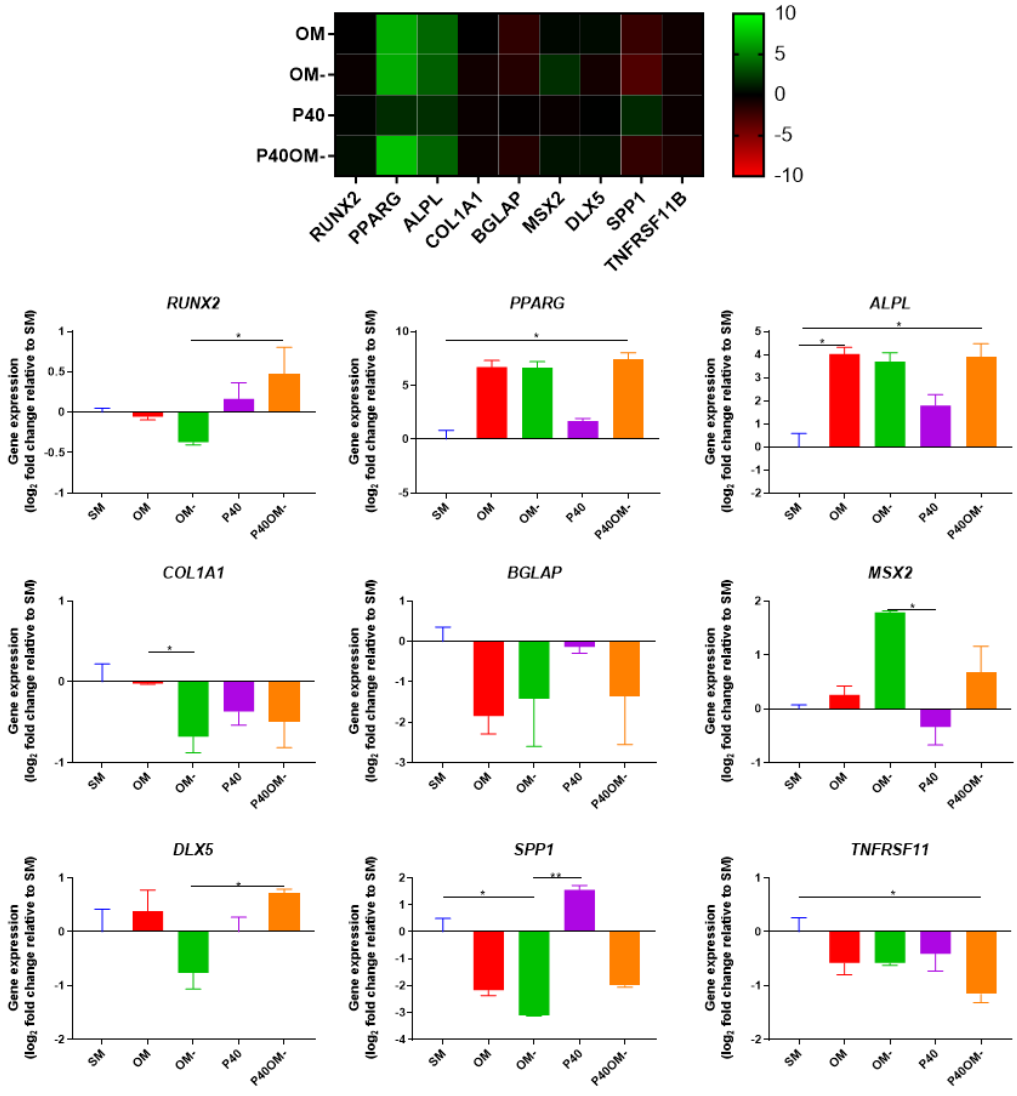


Figure 4.9. hMSC osteoblast gene expression after 11 days of P40 and P40OM- treatment normalized to the standard medium (SM) control. *p<0.05, **p<0.005 (n=2).

4.3.3.2.4 Notch markers

Expression changes for the Notch pathway were analysed after 11 days of indirect treatment of hMSC with P40 in SM and OM- (Figure 4.10). The genes analysed included Notch receptors (*NOTCH1*, *NOTCH2* and *NOTCH3*), ligands (*JAG1*, *JAG2* and *DLL1*) and a Notch regulator (*DLL3*). P40 treatment did not significantly alter Notch gene expression compared to the SM control. P40OM- treatment showed that *NOTCH2* was significantly upregulated compared to the OM- control while Notch3 was upregulated compared to the SM control. *NOTCH1, JAG1, JAG2, DLL1* and *DLL3* showed no significant changes in expression in the P40 and P40OM- treatments.

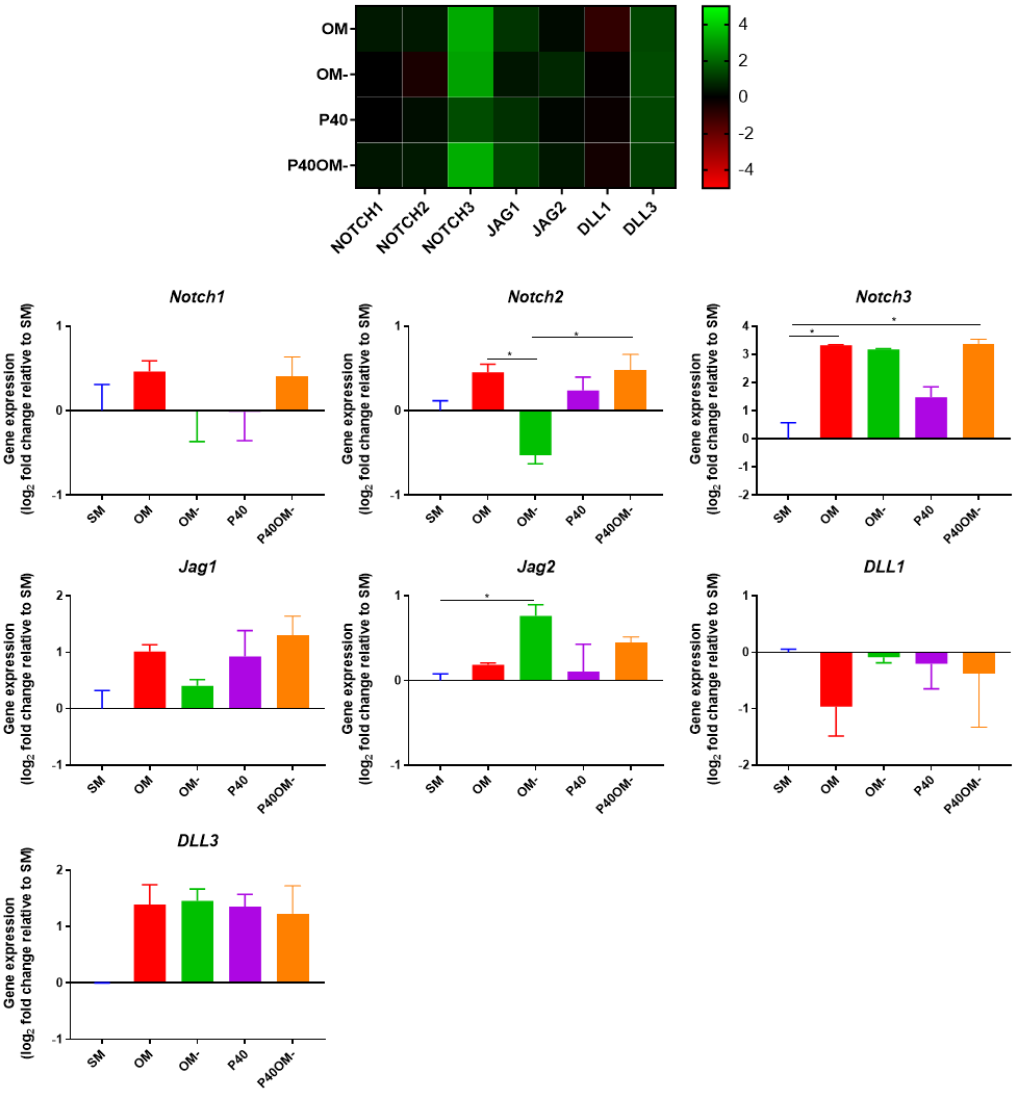


Figure 4.10. hMSC notch gene expression after 11 days of P40 and P40OM- treatment normalized to the standard medium (SM) control. *p<0.05 (n=2).

4.3.3.2.5 TGFβ and BMP markers

TGFβ and BMP genes were analysed for changes in expression after 11 days of P40 treatment in SM, OM and OM- (Figure 4.11). Genes analysed included BMP ligands (*BMP2, BMP4* and *BMP5*), TGFβ ligands (*TGFβ1, TGFβ2, TGFβ3*), SMADs (*SMAD1, SMAD3, SMAD4, SMAD6 and SMAD7*) and Noggin (*NOG*). No significant changes in expression of TGFβ and BMP markers were observed between P40 and the SM control

and P40OM- and the OM- control. *BMP2* was significantly downregulated in the P40OM- treatment compared to the SM control.

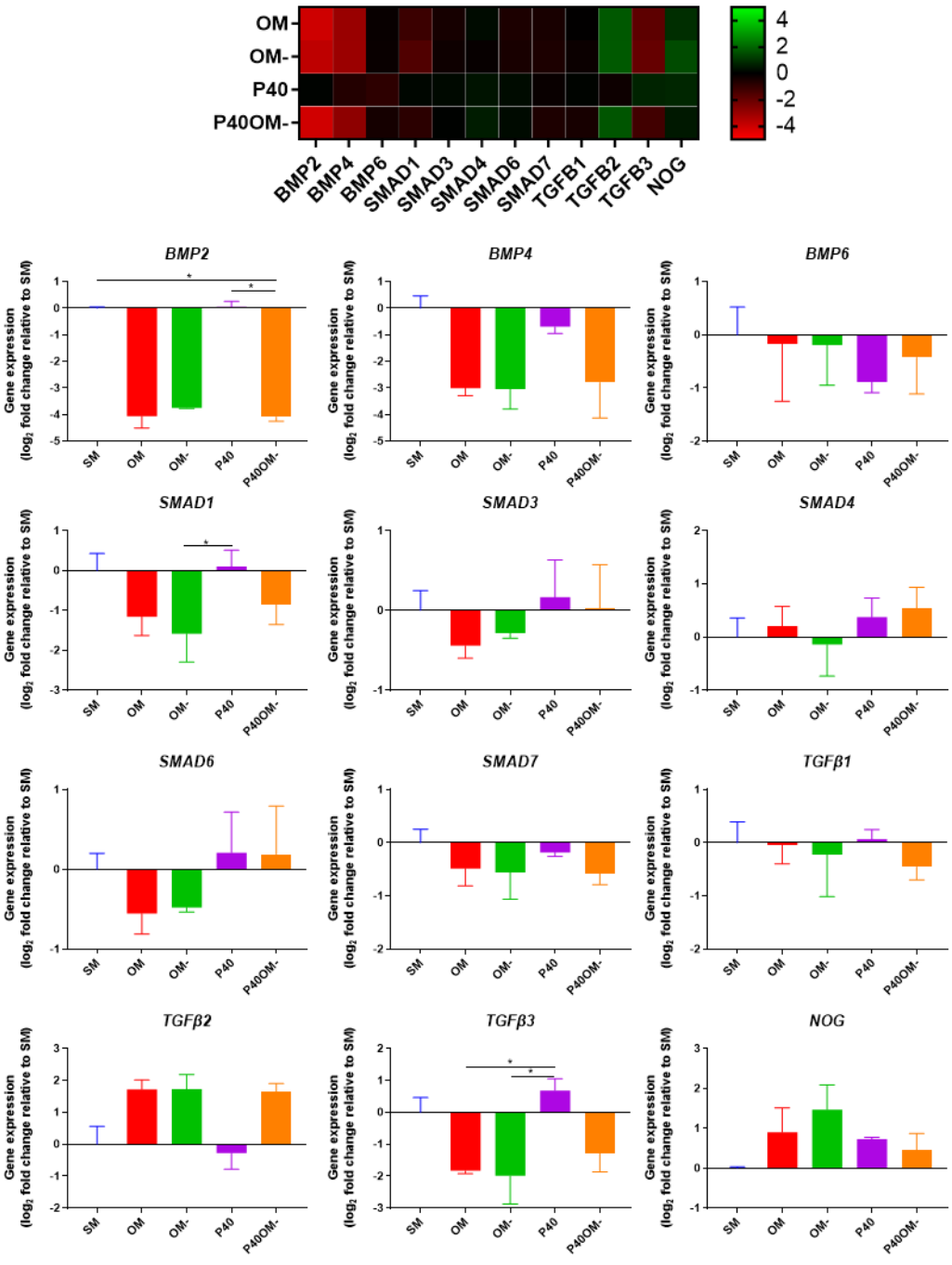


Figure 4.11. hMSC TGFβ and BMP gene expression after 11 days of P40 and P40OM- treatment normalized to the standard medium (SM) control. *p<0.05 (n=2).

4.3.3.2.6 Wnt markers

Wnt genes were analysed for changes in expression after 11 days of indirect treatment with P40 in SM and OM- (Figure 4.12). Wnt co-receptors *(LRP5, LRP6, FZD1* and *ROR2*), ligands (*WNT5A, WNT10B*), inhibitor *SFRP1* and transcriptional activator *CTNNB1* were observed for changes in expression. P40 treatment showed no significant changes to Wnt gene expression compared to the SM control. P40OM- treatment upregulated *ROR2* compared to the OM- control. P40OM- treatment also causes the upregulation of *FZD1 Wnt5A, Wnt10B* and *ROR2* compared to the SM control.

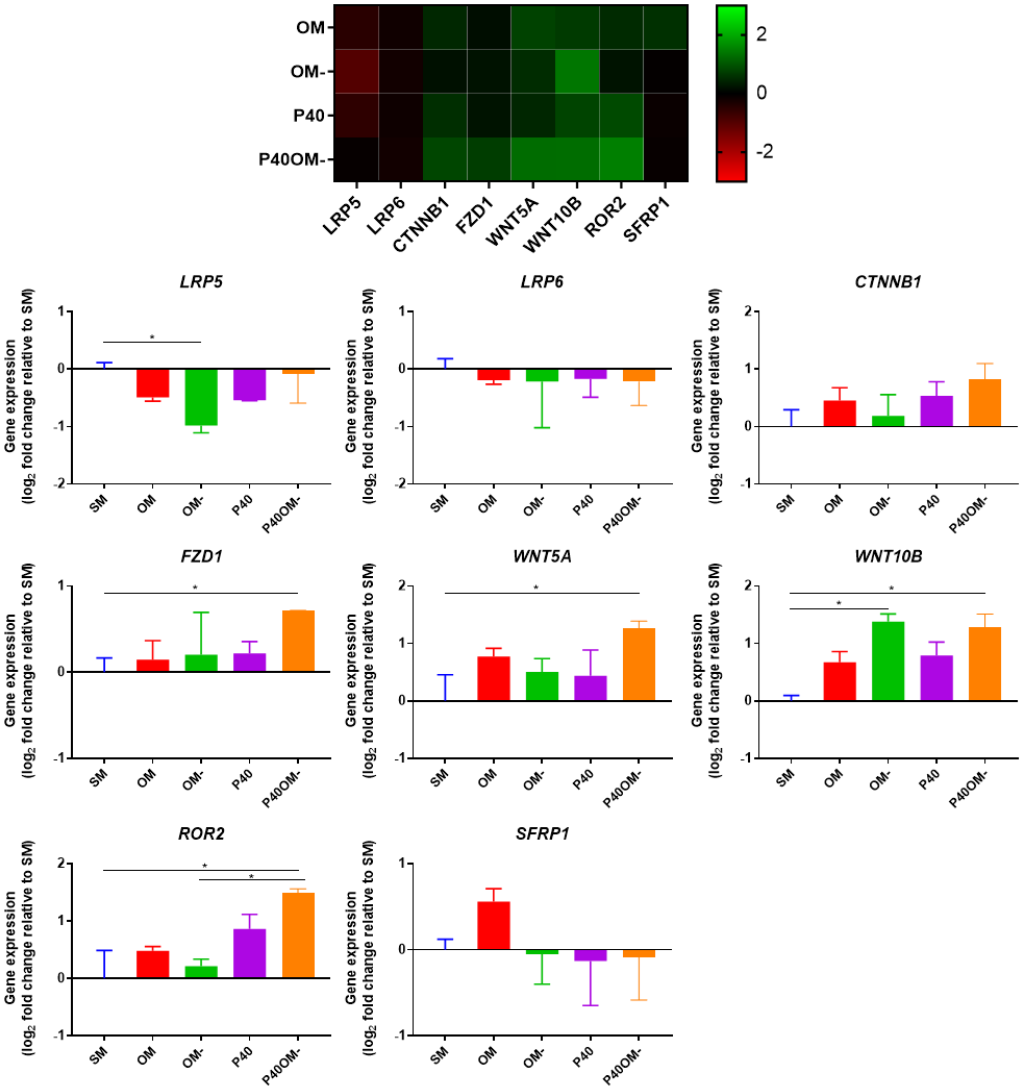


Figure 4.12. hMSC Wnt gene expression after 11 days of P40 and P40OM- treatment normalized to the standard medium (SM) control. *p<0.05 (n=2).

4.4 Discussion

Studies have explored the osteogenic and proliferative promoting properties of PBGs. Recently, McLaren et al. (2019) demonstrated not only their biocompatibility *in vivo* but their capacity to act as a scaffold to promote tissue ingrowth. The previous chapter demonstrated the negative impact of high phosphate content on cell viability in addition to showing the ability of calcium to rescue cells treated with high levels of phosphate. As such, this chapter investigates the metabolic activity, osteogenic activity and adhesion potential of the PBG formulation $(40\text{-}x)P_2O_5{\cdot}(16+x)CaO{\cdot}20Na_2O{\cdot}24MgO$ (x=0, 5 and 10) as phosphate is substituted for calcium.

4.4.1 Material characterization

Compositional analysis of P40, P35 and P30 using EDX confirmed their composition to be within 1-4% of the target formulation. This was expected and has been seen for other PBG investigated in the literature, particularly P40 (Hossain et al., 2018). No crystallization peaks were observed for all three glass formulations, confirming their amorphous nature. Thermal analysis indicated a linear increase in T_g as phosphate content was substituted for calcium. This was likely due to the increase in divalent calcium cations, resulting in increased cross-linking of the phosphate chains within the glass structure (Ahmed et al., 2004; Okura et al., 2006; Uo et al., 1998a). This correlates with data presented by Franks et al. (2001) who demonstrated a linear increase in T_g as calcium was added to the $45P_2O_5{\cdot}(8+x)CaO{\cdot}(47\text{-}x)Na_2O$ (x=2-32) PBG system and Ahmed et al. (2008) who demonstrated a similar linear increase in T_g with calcium addition into the PBG system $50P_2O_5{\cdot}(50+x)CaO{\cdot}(x)Na_2O$ (x=0-50). ^{31}P NMR analysis revealed Q^2 species content decreased as phosphate content was reduced and substituted for calcium (49, 6 and 0%), resulting initially in significantly increased Q^1 species (as seen with P35). With further decrease in phosphate content, the Q^1 species

were observed to have decreased (94 to 61%), with introduction of Q^0 (i.e. orthophosphate) species, with complete loss of Q^2 species for the P30 formulation. The Q^n species distribution in all three PBGs aligned relatively closely with the model predictions defined by Wazer and Fluck (1959) as demonstrated by Figure 4.13.

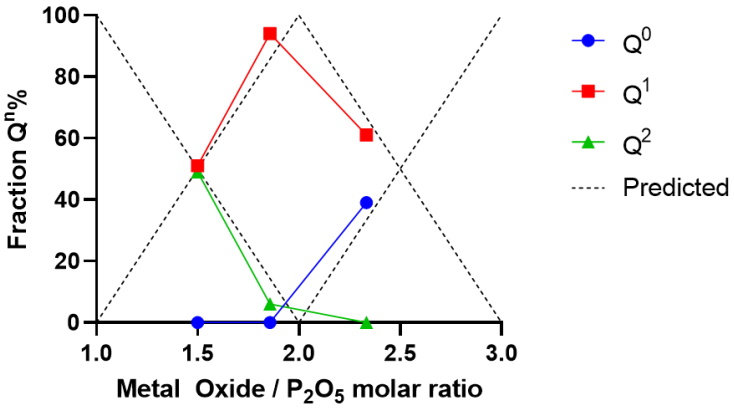


Figure 4.13. Alignment of P40, P35 and P30 to the predictions presented by Wazer and Fluck (1959).

4.4.2 hMSC adhesion on PBG glass

Cell adhesion was analysed using polished glass discs to evaluate the impact of the phosphate to calcium substitutions on the cell response to the material. All formulations were shown to support cell adhesion, with P30 demonstrating the highest capacity for cell adhesion and P40 demonstrating the lowest. These results were attributed to the degradation profile and hence ion release profiles of the PBG formulations developed.

Ion-cell interactions occur due to the role calcium ions play in cell adhesion events by triggering the macromolecular calcium-sensing receptor (CaSR)/integrin complexes that promote adhesion (Tharmalingam et al., 2011; Tharmalingam and Hampson,

2016). Akin to the CaSR, some integrins are also stimulated directly by divalent cation binding, particularly α-subunit containing integrins (Xiong et al., 2002). It is worth noting that all the disc formulations used also contained magnesium, which is also a divalent cation, and could be capable of activating the low conformation state of the heterodimer integrins (Mould et al., 1995). However, the ratio of MgO was constant among the PBG formulations tested here though it should be noted that with increasing degradation profiles, the release of magnesium ions would also have been increased. Conversely, a negative or inhibitory effect due to released ions may also be taking place. For example, Meleti et al. (2000) demonstrated a dose-dependent decrease in cell viability of up to 60% when osteoblast-like cells were treated with increasing phosphate content (1-7 mM) in culture medium, with a similar trend being seen in the direct ion optimization study presented earlier in this thesis. Furthermore, while a negative impact of increasing phosphate content was seen, we have previously demonstrated that calcium and magnesium content can rescue phosphate induced cytotoxicity in hMSC suggesting increased cell health in formulations containing lower phosphate and higher magnesium and/or calcium.

In addition to ion-cell interactions, material degradation properties are also likely to play a role in the results observed due to the impact degradation has on the local micro-environment, such as causing changes to pH and osmotic pressure. Abou Neel et al. (2007) showed increased adhesion and proliferation rate of an osteosarcoma cell line (MG63) on PBG discs containing increasing mol% of titanium through NaH_2PO_4 substitution for TiO_2 (0-5% in $CaO{\cdot}Na_2O{\cdot}P{\cdot}Ti$). Bitar et al. (2004) also demonstrated increased adhesion and proliferation of human osteoblasts on PBG discs with increasing mol% of calcium through Na_2O substitution for CaO (30-34% in $CaO{\cdot}Na_2O{\cdot}P{\cdot}Ti$). A common correlation with these studies, and in the data presented here, was an increase in cellular adhesion with decreasing glass solubility. Substituting

sodium with calcium or titanium likely resulted in a decrease of degradation rates through increased depolarization of the phosphate network, ultimately decreasing their dissolution rates (Parsons et al., 2010; Skelton et al., 2007a). In both studies above, the P_2O_5 content was fixed at 30 and 50 mol% respectively, whereas in the data presented in this study, phosphate itself was substituted with calcium, further increasing phosphate network depolymerization and thus solubility. This could explain the differences in adhesion seen between formulations. Navarro et al. (2003) suggested that local variations in the liquid environment near the glass surface may be negatively impacting cells due to changes in pH and ionic levels. Skelton et al. (2007) who showed increased cell adhesion in a formulation containing more calcium mol% (48 mol%) than other formulations in the $50P{\cdot}(40+x)CaO{\cdot}(10-x)Na_2O$ glass system, suggested similar methods of cell loss, citing potential contribution from: surface integrity, ion-cell interactions and pH/osmolarity change at the material-cell interface. A study by Tošić et al. (2013) using scanning electron micrograph images of an immersed glass surface, demonstrated the disruption of the glass surface through the formation of pits followed by their expansion in size and number by 24 hours. Naturally, a slower degrading glass would result in a more stable glass-medium interface. In addition to this, the physical surface of the glass itself is breaking down would likely inhibit adhesion events.

The data presented here suggests that substituting phosphate content for calcium content promotes cell adhesion. As PBGs with slower solubility, lower phosphate content and high calcium content promotes cell adhesion, it is likely that this promotion occurred through a combination of a number of mechanisms: i) calcium or magnesium promotion of integrin activity, ii) cytotoxic effects of phosphate on hMSC, iii) alteration of pH/osmotic pressure at the cell-material interface and iv) loss of PBG surface integrity as degradation occurs. The effects of ion dissolution products on

hMSC metabolic, osteogenic activity as well as proliferation and integrin gene expression are discussed in the subsequent sections of this study to further explore the effects of PBGs on hMSC activity.

4.4.3 Effects of indirect treatment of PBG on hMSC

Indirect treatment of hMSC with PBG dissolution products resulted in no significant impacts to metabolic activity compared to SM. Furthermore, despite the significant impact on cell adhesion seen with direct seeding, 48-hour analysis of metabolic activity demonstrated no significant changes between the formulations. On the other hand, by day 11, P40 had demonstrated significant increases in metabolic activity compared to P35 yet no formulation demonstrated significant variation from the SM control. Ahmed et al. (2010) showed that a similar glass formulation to P40, $40P_2O_5{\cdot}25CaO{\cdot}10MgO{\cdot}25Na_2O$ demonstrated a relatively neutral pH profile (pH 7.5). The data presented by Ahmed et al. (2010) and the indirect data presented here indicate that it was likely not overall pH of the media that contributed to cell loss on P40 discs. The results here represent a disconnect between the effects of the material surface and the dissolution products on cells, indicating that it was likely activity at the cell-material interface rather than the dissolution products interacting with hMSC which resulted in the loss of cells from the PBG disc surface in formulations with higher phosphate content compared to the TCP control. Lack of osteogenic activity was also noted across all formulations. The results presented here correlate with those of Patel et al. (2019) who showed that P40 PBG microspheres demonstrated no significant changes in ALP activity when hMSC were cultured on them.

No significant changes to metabolic activity were noted when P40 was degraded in OM- media however notable increases to ALP activity were seen. P40OM-

demonstrated higher ALP activity than that of OM- and P40 in isolation however despite this, no ALZ stain intensity was observed. Similarly, Abou Neel et al. (2014) demonstrated a significant increase in ALP activity of human osteosarcoma cells cultured on PBG discs with 50 μg/ml ascorbic acid and 5 mM β-glycerophosphate ($P_2O_5{\cdot}CaO_5{\cdot}Na_2O{\cdot}5TiO_2$). However, in contrast to the results presented here, Lin et al. (2020) demonstrated that growth of MC3T3-E1 cells in media with 50 μg/ml ascorbic acid, 10 mM β-glycerophosphate and 1 mg/ml of PBG fibres ($50P_2O_5{\cdot}40CaO_5{\cdot}5Na_2O{\cdot}5Fe_2O_3$) resulted in elevated levels of both ALP and ALZ intensity. This lack of matrix mineralization in cells treated with P40OM- may be attributed to a combination of two factors, the levels of pyrophosphate observed in the tested PBG formulations and the lack of complete differentiation which culminates in matrix mineralization. Pyrophosphate is a known promoter of ALP activity, as demonstrated by Pujari-Palmer et al. (2016) who showed the increases to ALP activity seen in MC3T3 cells at 0.1 μM and 100 μM doses of sodium pyrophosphate. However, it was also shown to inhibit matrix mineralization activity through its ability to sequester calcium and also block matrix mineralization sites (Addison et al., 2015). Its promotion of ALP activity however, allows for the cleavage of pyrophosphate, allowing for and eventually promoting matrix mineralization (Pujari-Palmer et al., 2016; Xu et al., 1991). It is possible then that sites of matrix mineralization are blocked due to oversaturation of pyrophosphate or lack of ALP protein quantity required for its removal.

The data presented here suggests that it is not the ionic dissolution products interacting with cells that causes loss of adhesion when cultured directly onto the surface of the PBG disc. Instead is likely that the degradation of glass surface itself contributes to the loss of cells seen. Furthermore, the dissolution products of P40 combined with the pro-osteogenic effects of OM- significantly increase the levels ALP

activity seen in hMSC. This promotion can likely be attributed in part, to the high pyrophosphate content of the P40 formulation which may also contribute to the lack of matrix mineralization observed in P40OM- treated cells. Subsequent sections on gene expression analysis on day 11 using TLDAs may help clarify the true differentiation state of hMSC differentiation and potential impact of pyrophosphate after P40 and P40OM- treatment.

4.4.4 Effects of indirect treatment on hMSC gene expression

4.4.4.1 Proliferation markers

Proliferative gene expression was not significantly altered through indirect application of P40 alone. In P40OM- treated samples, significant downregulation was seen between *CCND1* expression compared to the SM control. CCND1 controls cell progression through the G1 cell cycle phase (Ahlin et al., 2017). Its downregulation in P40OM- treated cells indicates a decrease in proliferative activity compared to the SM control. The inhibition of proliferative activity is required for cell differentiation due to the antagonistic nature of proliferation and differentiation (Ruijtenberg and van den Heuvel, 2016). OM treated cells demonstrated strong osteogenic differentiation capacity while displaying the same levels of *CCND1* expression as that of P40OM- treated cells. Conversely, *PCNA* expression of P40OM- treated samples was significantly upregulated compared to the SM control. This contrast between changes in proliferation markers *CCND1* and *PCNA* is odd. However, studies by Maga and Hübscher (2003) and Paunesku et al. (2001) discussed that while *PCNA* is typically upregulated in periods of cell proliferation, it also controls a number of other intracellular processes from DNA repair to methylation depending on the regulatory state of a number of other genes such as *P21*. As such, the data presented in this study suggests a potential decrease in proliferative activity of P40OM- treated cells due to the significant downregulation of *CCND1*. However, as P40 alone demonstrated no changes to proliferative gene expression activity while OM- treated cells expressed proliferative gene activity similar to that of P40OM- treated cells, it is likely that the ion release products of the P40 PBG did not significantly influence proliferative gene expression.

4.4.4.2 Integrin markers

Integrins play a critical role in cell adhesion, and as such, integrin subunits α1, α3 and β1 were analysed for changes in expression after 11 days of indirect treatment with P40 in SM and OM- media. P40 treatment in either SM or OM- showed no significant changes to observed integrin subunit expression at the mRNA level. The lack of significant downregulation of integrin gene expression by P40 dissolution products is a result that does not directly align with the data seen previously which showed that direct culture of hMSC on P40 resulted in 82% loss of cells from the surface compared to hMSC cultured on TCP. Skelton et al. (2007) suggested that the degradation of the PBG disrupts the material surface, decreases local pH and osmotic pressure, which can negatively affect cell viability and adhesion. Studies like those done by Chen et al. (2012) and Donnelly et al. (2018) demonstrate the importance of surface nanotopology and its effect it promoting cellular adhesion and controlling cell behaviour. Loss of this cell adhered surface due to active PBG degradation would likely impact adhesion events and the retainment of cells on the PBG surface. This data correlates with prior indirect metabolic assays with P40 and suggests that it is not the interaction of ionic products released from P40 with hMSC that influence cellular detachment, but the glass surface itself, and its degradation, that caused a significant loss of cells with increasing degradation rate.

4.4.4.3 Osteoblastic markers

ALPL gene expression showed significant increases in activity over the SM control in P40OM- treated cells, demonstrating expression levels similar to that of both OM and OM-. In isolation however, without OM-, P40 did not trigger a significant increase over the SM control. Prior ALP assays on hMSC also demonstrated that while P40OM- treatment caused an increase in ALP activity significantly higher than that of OM-, this

activity was not as high as that of OM, suggesting that factors downstream from mRNA expression inhibit the ALP protein production or activity. Dean (2002) suggested that sodium phosphate can act as a competitive inhibitor of the ALP assay, decreasing the rate of substrate conversion. This competitive inhibition could explain the results seen by the ALP assay in which P40OM- showed decreased levels of ALP activity compared to OM despite having similar levels of *ALPL* expression. P40 also demonstrates a relatively high pyrophosphate content (51%) yet no significant increases to ALPL gene expression over the OM or OM- controls are seen despite increases in ALP activity observed compared to the OM- control. Pujari-Palmer et al. (2016) demonstrated that pyrophosphate promotes both ALP protein activity and gene expression at 0.1 µM of sodium pyrophosphate on MC3T3 cells on day 10. However, upon increasing the dose to 100 µM, only protein activity was promoted suggesting a biphasic response to pyrophosphate dose on ALP gene expression. It may be likely then that the pyrophosphate distribution did not promote ALP gene expression but promoted ALP protein activity in culture. Ultimately, P40 alone did not significantly increase *ALPL* expression compared to the SM control and P40OM- demonstrated similar levels of *ALPL* expression to that of OM- suggesting that OM-, and not the P40 dissolution products, are influencing the changes to expression of this gene and pyrophosphate may be contributing to promotion of protein activity rather than gene expression when released from P40.

While not an osteoblastic marker, *PPAR-γ* expression was significantly upregulated by P40OM- treatment, demonstrating similar levels of expression to that of OM and OM- treated cells. PPAR-γ is a notable adipogenic marker, acting to regulate MSC differentiation down either adipogenic or osteogenic lineages depending on its regulatory state (Zhuang et al., 2016). Dexamethasone used in OM plays a key role in both osteogenic and adipogenic differentiation through the regulation of osterix

expression (Mikami et al., 2011; Yuasa et al., 2015). Dexamethasone is known to increase the expression of *PPAR-γ* and as a result of its use in differentiation media, all treatments with dexamethasone (OM, OM- and P40OM-) resulted in increased levels of *PPAR-γ* (Kelmendi-Doko et al., 2017; Vidal-Puig et al., 1997). Studies demonstrate that using strong differentiation media such as this, containing 100 nM dexamethasone, causes upregulation of *PPAR-γ*. For example Ghali et al. (2015) demonstrated similar increases in *PPAR-γ* expression in osteogenic differentiated primary murine cells with 100 nM dexamethasone by day 14 while still maintaining an osteogenic phenotype with ALP activity and mineralized matrix demonstrated. As such, the upregulation of *PPAR-γ*, despite being an adipogenic marker, was likely a side effect of dexamethasone in the osteogenic differentiation media. Treatment of hMSC with P40 alone caused no change to *PPAR-γ* expression. Furthermore, OM- and P40OM- demonstrated similar levels of *PPAR-γ* expression suggesting minimal contribution of P40 to *PPAR-γ* upregulation. Though *PPAR-γ* was upregulated, the increased expression of *RUNX2* suggests the beginning of differentiation down an osteogenic pathway and analysis at further timepoints may confirm the decrease of *PPAR-γ* as osteogenic differentiation continues (van Zoelen et al., 2016).

Interestingly, both *RUNX2* and *DLX5* showed significant upregulation in expression of P40OM- treated cells compared to OM- alone, indicating complementary effects of OM- and the dissolution products of P40 in the promotion of these genes. *DLX* genes play critical roles as transcription factors in osteogenesis and chondrogenesis (Samee et al., 2007). Typically expressed in early stages of bone development, *DLX5* plays a critical role in driving *RUNX2* expression and subsequently, osteogenic differentiation (Holleville et al., 2007; Lee et al., 2005). *DLX5* null mice were shown to exhibit numerous skeletal defects (Acampora et al., 1999). However, the critical role *DLX5* plays is in its ability to upregulate *RUNX2*. *RUNX2* acts to induce osteogenic lineage

determination and deficient mice demonstrated complete ablation of ossification and presence of bone, resulting in a lethal phenotype owing to the arrest of osteoblast maturation (Komori et al., 1997; Otto et al., 1997). A study by Lin et al. (2020) highlighted the ability of PBG fibres to promote osteoblast adhesion and proliferation as well as osteogenic differentiation due to the upregulation of osteogenic marker genes *ALP*, *RUNX2* and *COL1A1* among others. Lin et al. (2020) reported a 2-3 fold upregulation of *RUNX2*, while a 1.39 fold increase in expression was seen in this study. The differences in expression can be attributed to difference in formulation ($50P_2O_5{\cdot}40CaO_5{\cdot}5Na_2O{\cdot}5Fe_2O_3$ vs $40P_2O_5{\cdot}16CaO{\cdot}20Na_2O{\cdot}24MgO$), timepoint (21 days vs 11 days) and cell type (MC3T3-E1 vs hMSC). Regardless, a clear difference was seen between P40OM- and OM- treated cells in both *RUNX2* and *DLX5* expression suggesting that the dissolution products from P40 in combination with OM- play a key role in the upregulation of these genes. A similar 1.5 fold increase in *RUNX2* expression was seen through applications of 7.5 mM $CaCl_2$ by Aquino-Martínez et al. (2017) in mouse bone marrow derived MSC by day 10. The data presented here supports the findings of other studies in the literature, demonstrating the capacity of PBG dissolution products to promote *RUNX2* expression in MSC cells. This increase in expression was likely attributed to calcium ions, as demonstrated by Aquino-Martínez et al. (2017), and promote increases in *RUNX2* through *DLX5* as it is an upstream regulator of *RUNX2* (Rutkovskiy et al., 2016).

In isolation, P40 demonstrated no significant changes to osteoblastic gene expression at day 11, however, combination with OM- showed that it promoted *RUNX2*, *DLX5* and *ALPL*, demonstrating potential initiation of osteogenic differentiation.

4.4.4.4 Notch markers

Dissolution products of P40 in SM appeared to cause no significant changes to Notch receptor or ligand gene expression compared to the SM control. *NOTCH2* in P40OM- treated cells in demonstrated significantly higher expression compared to OM- indicating the capacity of PBG dissolution products to support *NOTCH2* expression in the absence of β-glycerophosphate, as similar levels of expression were noted in OM treated cells. *NOTCH2* has been tied to the suppression of osteoblastogenesis and promotion of bone resorption in mice (Zanotti and Canalis, 2016) suggesting negative contribution towards osteogenic differentiation.

P40OM- treated cells also expressed significantly increased *NOTCH3* expression compared to the SM control. The levels of expression seen are similar to that of OM and OM- treated cells indicating a significant contribution to expression from OM- media and no inhibition from the P40 dissolution products as P40 in isolation did not cause significant changes to *NOTCH3* expression. Upregulation of Notch receptors suggests promotion of the Notch pathway which has been noted to have inhibitory effects on the promotion of osteogenic differentiation through the attenuation of β-catenin activity and RUNX2 modulation (Hilton et al., 2008; Lin and Hankenson, 2011). These inhibitory effects have been suggested to be enacted by Notch target genes *HEY1* and *HES1* which bind to RUNX2 and β-catenin nuclear target TCF/LEF to form inhibitory complexes which attenuate RUNX2 and β-catenin activity (Deregowski et al., 2006; Xu et al., 2015).

The P40 ionic dissolution products showed potential in regulating Notch receptor gene activity when in a pro-osteogenic environment such as that of OM- at day 11. While promotion of the Notch pathway may have negative effects on osteogenic differentiation, additional time points or targets downstream of Notch signalling may

be required to identify the impact of P40 dissolution products on Notch gene expression.

4.4.4.5 TGF-β and BMP markers

BMP2, BMP4 and *BMP6* were observed for changes to gene expression after 11 days of indirect treatment with P40 dissolution products. P40 caused no significant changes in *BMP2* expression compared to the SM control while P40OM- resulted in decreases in BMP2 expression. These decreases in expression align with that of the osteogenic controls. No differences were noted between P40OM- and OM- and minimal P40 activity indicates that no changes to *BMP2* expression were caused due to P40 dissolution products.

P40 caused no changes to SMAD expression compared to the SM control. *SMAD1* however, demonstrated a significant decrease in expression in OM treated samples compared to the P40 treatment. Similarly, *TGFβ3* was also downregulated in the osteogenic controls compared to the P40 treatment again indicating the lack of influence of P40 on the BMP/ TGF-β pathways.

P40 demonstrated no significant changes to TGF-β and BMP gene expression after 11 days of indirect treatment in SM. When combined with OM- media, TGF-β and BMP genes demonstrated levels of expression similar to that of the OM or OM- controls suggesting minimal impact of the P40 dissolution products on TGF-β and BMP gene activity.

4.4.4.6 Wnt markers

FZD1, *WNT5A*, *WNT10B* and *ROR2* demonstrated significant upregulation in the P40OM- treated samples compared to the SM control. P40, OM and OM- treated samples showed no significant upregulation, with the exception of *WNT10B* in OM- treated samples. These results suggest that P40 dissolution products in OM- media are capable of upregulating these Wnt factors where P40 and OM- in isolation cannot. Unlike *FZD1*, *WNT5A* and *ROR2*, the upregulation of *WNT10B* in the P40OM- treatment may be caused due to the OM- media used rather than the application of P40 due to the equivalent increases seen in the OM- treatment.

Billiard et al. (2005) also demonstrated through cell lines representing the various osteoblast stages that *ROR2* is expressed in a biphasic pattern, showing high levels of expression in pre-osteoblasts (1-fold) and late stage osteoblasts (0.6-fold increase) with minimal levels of expression seen in early osteoblasts at day 0. The 2.9-fold increase in ROR2 expression correlates with the levels of expression observed in pre-osteoblast cells with differences in expression intensity likely being attributed to timepoint (day 11 vs 0).

ROR2 has been described to play multiple roles in both the canonical and non-canonical Wnt pathways (Maeda et al., 2012; Oishi et al., 2003). Billiard et al. (2005) demonstrated that ROR2 can bind to both WNT1 and WNT3 ligands to promote a tyrosine kinase mediated action on Wnt target genes. WNT1 binding was suggested to promote β-catenin activity on target gene upregulation while WNT3 was suggested to inhibit this activity. In addition Billiard et al. (2005) noted that interaction of Wnt ligands with ROR2 ultimately sequesters them away from canonical Wnt signalling required for the stabilization of β-catenin. ROR2 was also suggested to increase intracellular Ca^{2+} levels due to its function as a receptor for WNT5A in the non-canonical Ca^{2+} pathway (De, 2011; Thiele et al., 2016). The activation of this pathway

has also been suggested to antagonize the β-catenin dependent pathway through the promotion of the ubiquitin ligase SIAH2 which degrades β-catenin (De, 2011; Ishitani et al., 2003; Topol et al., 2003). Conversely, ROR2 has also demonstrated pro-osteogenic effects through the promotion of osteoblast commitment and increased bone formation (Liu et al., 2007). Ultimately, ROR2 plays many different roles in Wnt signalling and its ultimate effect of osteogenic differentiation will likely be determined by the levels of expression of the specific Wnt ligands to which it binds.

This promotion of Wnt signalling (*FZD1* and *WNT5A*) in P40OM- treatments in part correlates with findings by Lin et al. (2020) who demonstrated the use of phosphate glass fibres of the composition $50P_2O_5{\cdot}40CaO_5{\cdot}5Na_2O{\cdot}5Fe_2O_3$ and reported calcium induced Wnt signalling due to the degradation of the PBG fibres and release of calcium ions into the media. The mentioned study noted increases in *RUNX2*, *β-catenin* and *SP7*. The reported *β-catenin* upregulation was seen at day 7 followed by downregulation at day 14 and a large upregulation at day 21. The modulation of *β-catenin* expression coincides with the results presented in this study which demonstrated increases in specific Wnt gene markers by P40OM- yet no increases to *β-catenin* activity at day 11.

It appears that P40OM- treatment promotes multiple Wnt pathways, possibly through the upregulation of the multirole *FZD1* and *ROR2* receptors as well as through more direct promotion of non-canonical pathways through *WNT5A* expression increases, subsequently antagonizing β-catenin signalling through its degradation. Such non-specific changes to Wnt activation may in part be the cause of lack of mineralization seen despite *ALPL* upregulation. Further analysis at later time points and potential observation of genes downstream of both the canonical and non-canonical pathways (CDX2/NFAT) would help elucidate the mechanisms of PBG mediated Wnt activation.

4.5 Summary

Material analysis revealed a linear increase in T_g as 5 and 10% phosphate was substituted for calcium in P40, P35 and P30. This expected linear increase was likely due to increased crosslinking of phosphate chains within the glass structure. The suggested increases in crosslinking are further supported by the distribution of Q^n species observed which demonstrated a shift from 49% Q^2 in P40 to 6% in P35 and eventually a complete loss of Q^2 species in P30 as more calcium is substituted in for phosphate. This increase in phosphate crosslinking was also observable in the trend of decreasing degradation rates as calcium content is increased.

The PBG discs demonstrated a linear response of increasing cell adhesion as phosphate was substituted for calcium with P40 demonstrating 76.6% fewer adhered cells than the P30 formulation. This trend in adhesion activity likely occurred due to a number of mechanisms: i) ion dissolution products promoting integrin activity, ii) phosphate cytotoxicity, iii) pH/osmotic changes at the cell-material interface and iv) loss of PBG surface integrity. Indirect treatment of hMSC with PBG microspheres demonstrated no cytotoxic effects to cell health at any time point suggesting minimal contribution of ionic dissolution products to cell loss. Further investigation into gene expression revealed no changes to integrin gene expression however, it may still be possible that promotion of integrin protein activity occurred with increased calcium or magnesium content. Ultimately, the increased calcium content and decreased phosphate content demonstrated decreased degradation rates as noted previously and likely maintains a more stable surface for cell adhesion at the glass-cell interface, promoting cell adhesion.

The P40 dissolution products demonstrated no significant changes to hMSC ALP activity when applied in SM. In combination with OM- however, the P40 dissolution products demonstrated significantly increased ALP activity compared to the SM, P40

and OM- treatments. *ALPL* gene expression however, showed that OM, OM- and P40OM- were all upregulated to similar levels. This promotion of ALP protein activity, beyond that of the OM-, was likely due to the contribution of high pyrophosphate (51%) from the P40 formulation, noted to promote ALP activity and inhibit matrix mineralization. This correlated with the data in the ALZ assay which demonstrated no stain intensity despite the high levels of ALP activity observed from P40OM-. Furthermore, the levels of ALP activity in P40 and P40OM- treated samples may be masked by the levels of pyrophosphate in culture due to the competitive inhibition previously noted in the literature. Ultimately, the data presented here suggests that in a pro-osteogenic environment, P40OM- promotes strong levels of ALP gene and protein activity. This likely due to the contribution of pyrophosphate however, the increased in ALP activity observed is likely not sufficient enough to prevent excessive pyrophosphate from inhibiting matrix mineralization.

Gene expression activity of cells treated with P40 suggests minimal changes to expression when the dissolution products of P40 are applied in SM. When applied with OM- however, increases to osteogenic markers such as *RUNX2* and *MSX2* are observed, suggesting the potential initiation of osteogenic commitment. Additionally, promotion of Notch receptors and non-canonical *WNT5A* in P40OM- suggests some contribution to the attenuation of osteogenic differentiation through promotion of β-catenin degradation and inhibition of *RUNX2* activity.

In conclusion, this work highlights the disconnect between cell adhesion and cell health when testing different PBG formulations. While a formulation may demonstrate no cytotoxic effects and even promote some osteogenic effects when applied in an indirect manner, it may not retain many cells when cultured directly due to the rapid dissolution of its surface. Pyrophosphate was shown to potentially act as a double-

edged sword, promoting ALP activity while contributing to the inhibition of matrix mineralization, likely due to its oversaturation in culture by P40. Finally, despite the upregulation of *RUNX2* observed, its activity may be attenuated through the upregulation of Notch target genes *HEY1* and *HES1*. This combined with the β-catenin antagonizing activity of *WNT5A* suggests a potential negative effect on osteogenic differentiation.

Chapter 5 - Microsphere formulation mixing

5.1 Introduction

Glass microspheres of various different compositions have been shown to provide numerous advantages over fixed geometry implants such as tissue infiltration, enhanced surface area and minimally invasive delivery methods (Gupta et al., 2018; McLaren et al., 2019; Mitragotri et al., 2014). Microspheres also have several advantages over irregular shaped particles such as improved particle flow properties, increased surface area and more consistent degradation rates (Gupta et al., 2018; Mitragotri et al., 2014). Furthermore, porous microspheres offer additional advantages of increased surface area, faster degradation times and can act as scaffolds for tissue growth (Gupta et al., 2018; McLaren et al., 2019). This chapter explores the development of new PBG formulations and combinations thereof with the previously tested porous P40 formulation (chapter 4).

5.2 Aims and hypotheses

This chapter explores the development of new microsphere formulations through the replacement of magnesium for calcium in the PBG formulation $50P_2O_5{\cdot}(50\text{-}x)CaO{\cdot}(x)MgO$ (x=50, 25 and 0). Three formulations were developed (P50Mg50, P50Ca25Mg25 and P50Ca50) and their impact on *in vitro* hMSC metabolic and osteogenic activity was investigated. The tailorable nature of PBGs demonstrates their versatility with controllable degradation rates and modifiable properties. Modification of PBG formulations allows for the tailoring of degradation rates from months to days while properties of microspheres can be augmented through the addition of various ions, for example: titanium and copper to integrate radiopacity and anti-microbial capacity to the PBG microspheres (Foroutan et al., 2019; Matsumura et al., 1992). In

contrast to this flexibility is the difficulty in achieving a balance of characteristics with PBG formulations, adding titanium may allow for x-ray visualization of the microspheres within a patient but greatly decreases degradation rates as demonstrated by Abou Neel et al. (2007). Slower solubility is achievable but comes at the cost of decreased ion release rates. Studies like that of Maeno et al. (2005) have demonstrated the importance of concentration of calcium ions on osteoblast function. Showing that concentrations lower than 4 mM calcium promote proliferation of mouse osteoblasts while concentrations in the range of 6-8 mM promote mouse osteoblast differentiation. An as yet unexplored advantage of microsphere geometry is the capacity to mix different formulations of microspheres together to leverage the properties of both or several formulations. To this end, this chapter aimed to develop a faster degrading formulation that released more inorganic ions than the previously tested formulations and identify and optimize the impact on hMSC of mixing two different PBG microsphere formulations. As demonstrated in the previous chapter, a slower degrading formulation was superior for cell adhesion while its ionic degradation products provided little benefit for osteogenic differentiation. It was hypothesized that by combining microspheres of slow and fast degradation rates, sufficient ion release may be achieved to promote osteogenic differentiation.

5.3 Results

5.3.1 Material characterization

EDX analysis

To confirm the composition of the produced PBG to the target formulation, EDX was carried out. Table 5.1 confirms that the three PBG formulations are within 1-3% of the target formulation.

Table 5.1. EDX measurements of P50Mg50, P50Ca25Mg25 and P50Ca50 against target formulation (mol%) ± standard error of the mean (SEM).

		P2O5 (mol%)	CaO (mol%)	MgO (mol%)
P50Mg50	Target	50	-	50
	Measured	47.0 ± 0.7	-	53.0 ± 0.7
P50Ca25Mg25	Target	50	25	25
	Measured	50.1 ± 0.3	24.3 ± 0.4	25.6 ± 0.2
P50Ca50	Target	50	50	-
	Measured	51.0 ± 0.0	49.0 ± 0.0	-

DSC analysis

A Differential scanning calorimeter (DSC) was used to determine the thermal properties of the three glass formulations. Figure 5.1A shows the thermal profiles of the three PBGs, P50Mg50, P50Ca25Mg25 and P50Ca50 and Table 5.2 collates the T_g, T_c and T_m values for the respective formulations. A slight increase in T_g could be seen as 50% of the calcium was substituted for magnesium, shifting from 521 °C to 530 °C. However, once all the calcium was removed, the T_g onset greatly increases to 552 °C.

Increases in T_c were also observed as magnesium was added to the formulation, starting at 645 °C and increasing to 757 °C as all the calcium was replaced. The formulation with both calcium and magnesium resulted in two distinct melting peaks at 913 °C and 938 °C while the complete replacement of calcium for magnesium resulted in no melting peaks being detected at the tested temperatures.

XRD analysis

XRD analysis of the three glass formulations demonstrated no sharp crystalline peaks confirming the amorphous nature of the glasses as can be seen in Figure 5.1B.

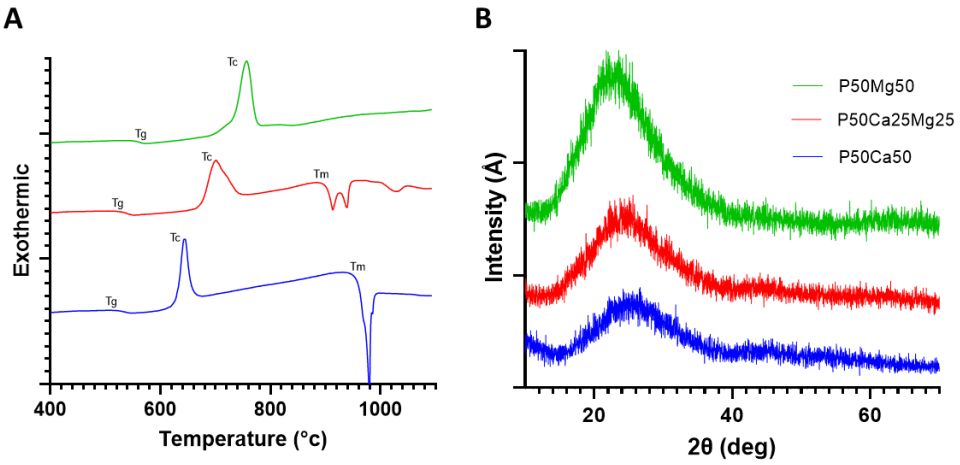


Figure 5.1. Glass characterization of P50Ca50, P50Ca50Mg50 and P50Mg50. (A) Thermal analysis traces via DSC of the PBG formulations showing T_g, T_c and T_m. (B) XRD spectra confirming the amorphous nature of P50Ca50, P50Ca50Mg50 and P50Mg50 glasses produced.

Table 5.2. Glass transition (T_g), onset of crystallisation (T_c), melting temperature (T_m) and calculated thermal processing window (Tc_{onset}) for each of the PBG glass formulations explored.

	T_g	*T_c*			*T_m*		*Window*
	Onset	Onset	1	2	1	2	Tc_{onset}- Tg
P50Mg50	552	728	757				176
P50Ca25Mg25	530	674	702		913	938	145
P50Ca50	521	625	645		978		105

^{31}P NMR Spectroscopy

NMR analysis was used to identify the distribution of Q^n species within the PBG formulations. NMR spectra for the three formulations revealed two peaks representing Q^1 and Q^2 units (Brow, 2000) (Figure 5.2). No Q^0 or Q^3 units were detected. Both P50Ca50 and P50Ca25Mg25 demonstrated nearly identical distribution of Q^1 and Q^2 species, differing only by ~1%. The complete substitution of calcium for magnesium however, increased the Q^1 species to 16.63% compared to the 6.14% and 5.30% seen in the P50Ca25Mg25 and P50Ca50 formulations (Table 5.3).

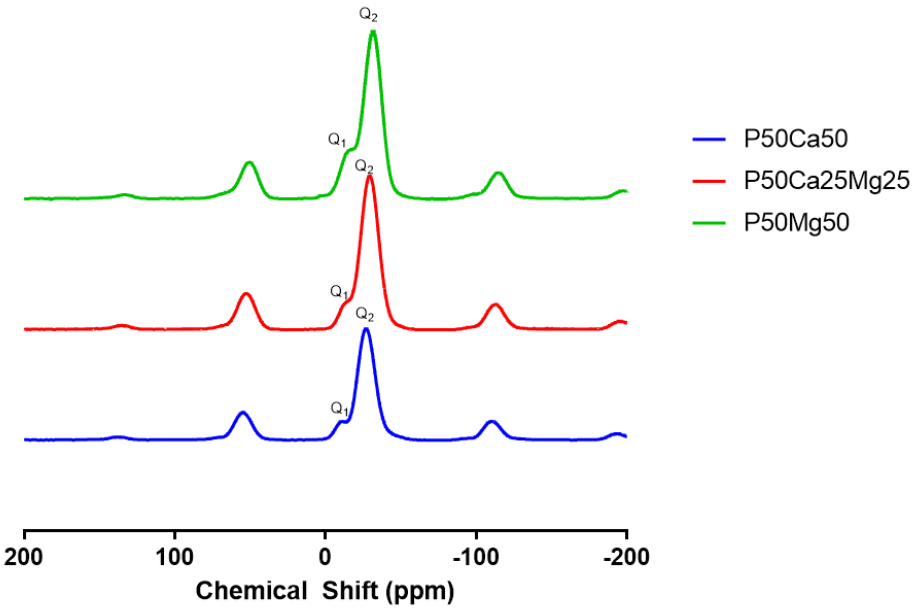


Figure 5.2. ^{31}P NMR spectra of the P50Ca50, P50Ca25Mg25 and P50Mg50 formulations. Data provided by Jeremy Titman and Alex Taylor.

Table 5.3. Distribution of Q^n species across PBG formulations

	Q^0	Q^1	Q^2
P50Ca50	0	5.30	94.70
P50Ca25Mg25	0	6.14	93.86
P50Mg50	0	16.63	83.37

5.3.2 Material Spheroidization

Using the previously described flame spheroidization method for the production of porous P40 (Hossain et al., 2018), ground glass from the P50Ca50, P50Ca25Mg25 and P50Mg50 formulations were explored for porous microsphere formation. Resin embedding and cross-sectioning revealed that pores formed within the microspheres of the three formulations, however these microspheres remained solid on the outside

as can be seen in Figure 5.3A-C. These pores also demonstrated little interconnectivity and next to no contact with the microsphere surface. Figure 5.3D demonstrates the increased viscosity of the P50Ca50 formulation which may contribute to the internalized porosity observed.

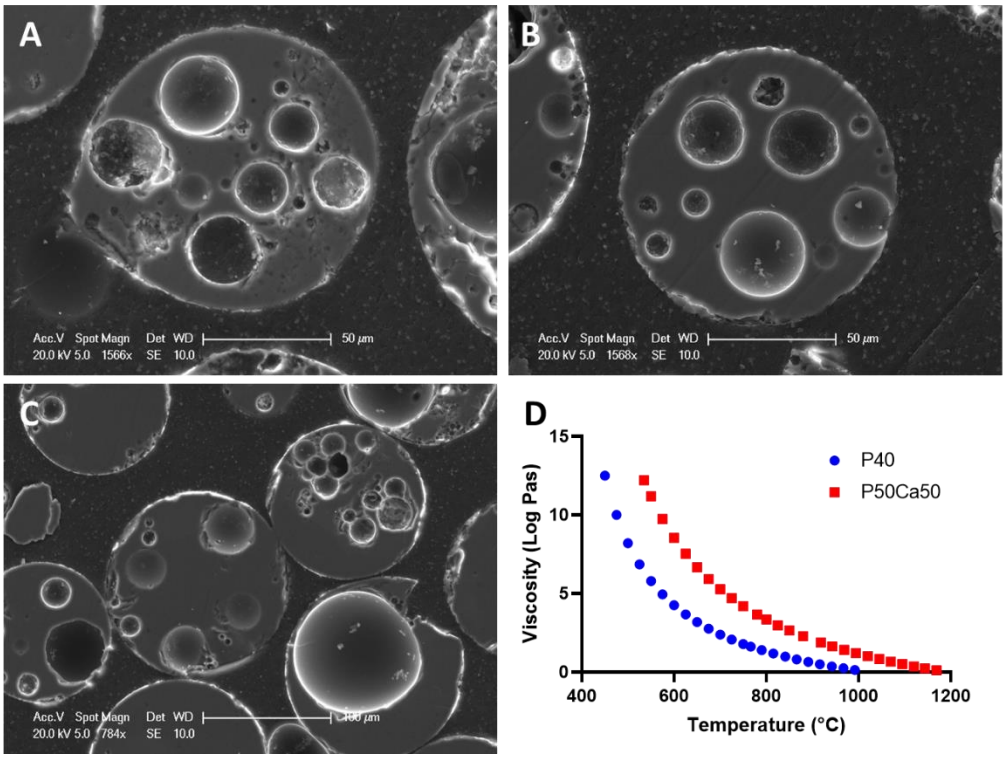


Figure 5.3. SEM scans of resin embedded sections of (A) P50Ca50, (B) P50Ca25Mg25, (C) P50Mg50 and (D) viscosity of the P40 and P50Ca50 PBGs via a high temperature viscometer. Viscosity data provided by Towhidul Islam.

5.3.3 Indirect microsphere application and mixture

5.3.3.1 Effects of microsphere degradation products on hMSC

In order to determine the effectiveness of each PBG formulation, solid PBG microspheres were indirectly tested on hMSC through the application of their dissolution products into SM. Figure 5.4A demonstrates that P50Mg50 resulted in the highest metabolic activity after 11 days while P50Ca25Mg25 and P50Ca50 resulted in almost complete loss of cells from the monolayer. Due to the necessity of calcium for the promotion of bone growth and osteogenic differentiation, P50Ca50 was utilized for subsequent combinatorial experiments.

Figure 5.4B and 5.5 demonstrates the combination of two different microsphere formulations to explore if both of their properties could be exploited. In this case, P40 was used for its previously seen non-toxic effect on hMSC in culture and P50Ca50 was used for its substantial initial dose of calcium potentially released during its dissolution. A combination of both P40 and P50Ca50 was used, substituting 0-100% of P40 with P50Ca50 to allow for the testing of various combinations of the two formulations. Figure 5.4B demonstrated that as P40 was replaced by P50Ca50, significant decreases in metabolic activity were observed compared to the SM control, even at the lowest dose of 25% P50Ca50. Higher doses of >25% substitution resulted in almost complete loss of the monolayer.

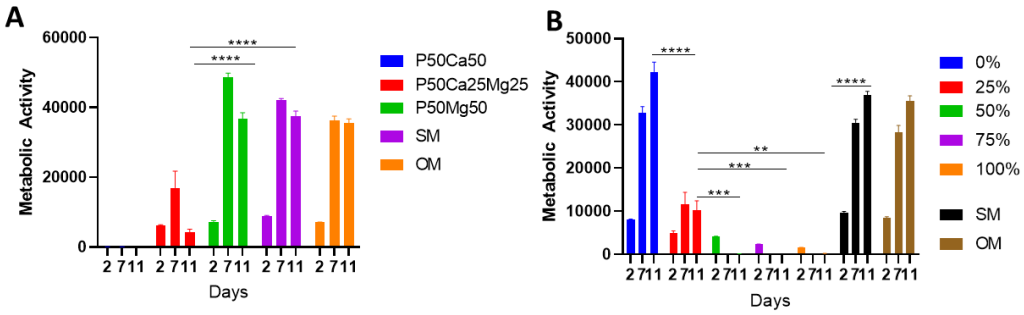


Figure 5.4. The metabolic activity of hMSC treated with the dissolution products of (A) P50Ca50, P50Ca25Mg25 and P50Mg50 and (B) mixes of 0-100% P50Ca50 mixed with P40 compared to standard media (SM) and osteogenic media (OM). **p<0.01, ***p<0.001 and ****p<0.0001. (n=3 technical replicates).

Following this, lower concentrations of P50Ca50 mixed with P40 were tested, from 0-25%. Figure 5.5A shows that adverse effects to metabolic activity were observed after >20% of P40 was substituted with P50Ca50, with 20% demonstrating significantly decreased metabolic activity compared to the SM control and the 0 and 10% mixes. Figure 5.5B and 5.5C demonstrated the tested osteogenic activity of hMSC after treatment with the various mixes. Decreasing levels of ALP activity were seen as P40 was substituted with P50Ca50, however, no significant change could be seen between 0-10%. The loss in cells from 20-25% would result in lower levels of ALP activity due to the lack of cells contributing to the assay. Interestingly, significant levels of ALZ stain intensity were seen in the 20-25% mixes compared to the 0 and 10% as well as the SM control.

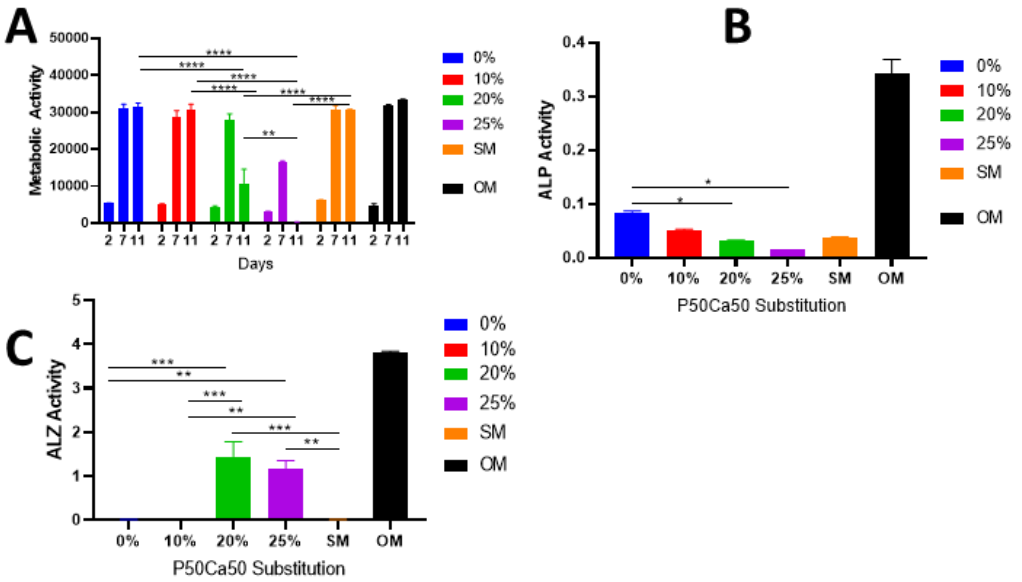


Figure 5.5. The metabolic (A; day 2, 7 and 11), ALP (B; day 11) and ALZ activity (C; day 21) of hMSC treated with the dissolution products of P40 mixed with 0-25% of P50Ca50 compared to standard medium (SM) and osteogenic medium (OM). *p<0.05, **p<0.01, ***p<0.001 and ****p<0.0001. (n=3 technical replicates).

5.3.3.2 Effects of mixed microsphere degradation products on hMSC gene expression

Due to the 10% demonstrating the best metabolic activity of all the tested mix formulations, it was carried forward for gene expression analysis using TaqMan Low Density Arrays (TLDAs). After 11 days of indirect treatment with the dissolution products of 90% P40 10% P50Ca50 in SM (henceforth referred to as Mix) and OM- (MixOM-), hMSC were collected and processed for gene expression analysis. Table 5.4 indexes all the gene groups analysed in this subsection.

Table 5.4. Index of gene groups analysed in chapter 5

Section Number	**Gene Group**
5.3.3.2.1	Proliferative
5.3.3.2.2	Integrin
5.3.3.2.3	Osteoblastic
5.3.3.2.4	Notch
5.3.3.2.5	TGF-β and BMP
5.3.3.2.6	Wnt

5.3.3.2.1 Proliferative markers

After 11 days of indirect treatment with Mix and MixOM-, proliferation gene expression markers *CCND1*, *PCNA* and *MKI67* in hMSC were observed for any changes (Figure 5.6). Mix treatment demonstrated no significant changes to expression compared to the SM control and MixOM- demonstrated significant increases to *MKI67* expression compared to the OM- control. MixOM- also demonstrated upregulation of *PCNA* and downregulation of *CCND1* compared to the SM control.

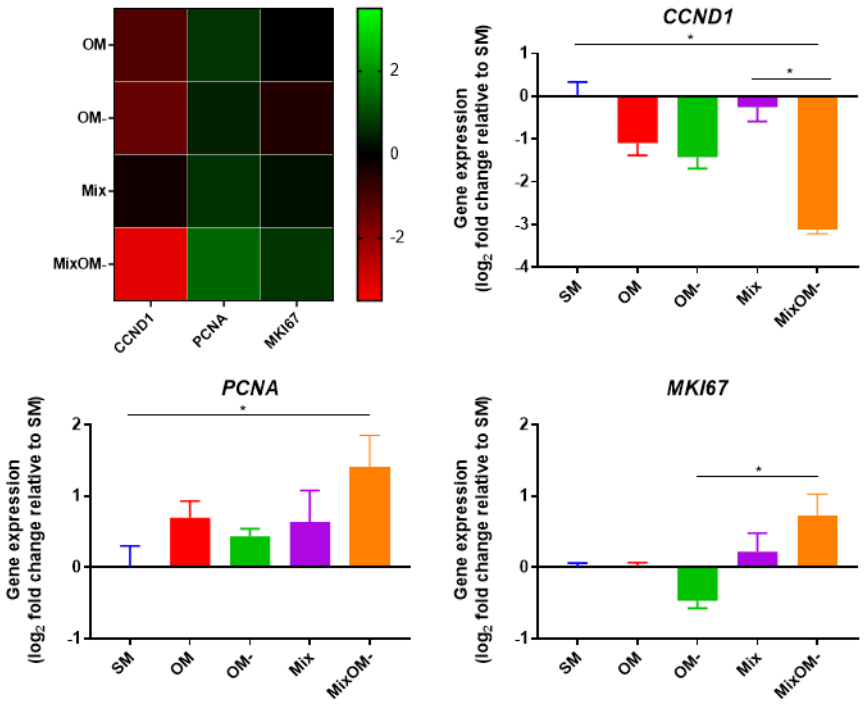


Figure 5.6. hMSC proliferation gene expression after 11 days of Mix and MixOM- treatment normalized to SM control. *p<0.05 (n=2).

5.3.3.2.2 Integrin markers

Figure 5.7 shows gene expression changes of integrin subunit markers *ITGA1*, *ITGA3* and *ITGB1* in hMSC after 11 days of indirect treatment with Mix and MixOM-. Mix treatment showed no significant changes to integrin gene expression compared to the SM control. MixOM- however, significantly upregulated *ITGA3* expression compared to the OM- control. No significant changes to *ITGA1* or *ITGB1* expression were observed in Mix or MixOM- treatments.

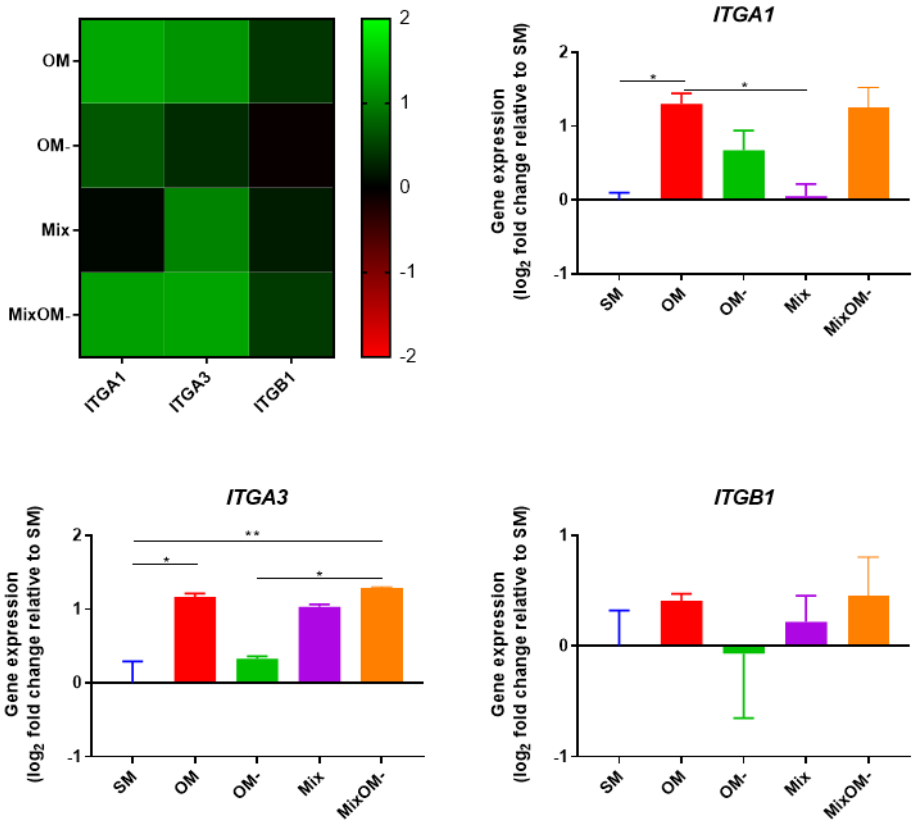


Figure 5.7. hMSC Integrin gene expression after 11 days of Mix and MixOM- treatment normalized to SM control. *p<0.05, **p<0.005 (n=2).

5.3.3.2.3 Osteoblast markers

Figure 5.8 shows gene expression changes of osteoblast markers *RUNX2, ALPL, COL1A1, BGLAP, MSX2, DLX5* and *SPP1* in hMSC after 11 days of indirect treatment with Mix and MixOM-. Additionally, while not directly influencing osteoblast differentiation *PPAR-γ* and *TNFRSF11* were also observed for changes in expression during indirect treatment with Mix and MixOM-. No significant changes to osteoblast gene expression were observed between the Mix and SM control treatments and MixOM- and OM- control treatments. MixOM- also showed significantly increased PPAR-γ expression over the SM control to levels similar to that of OM and OM-.

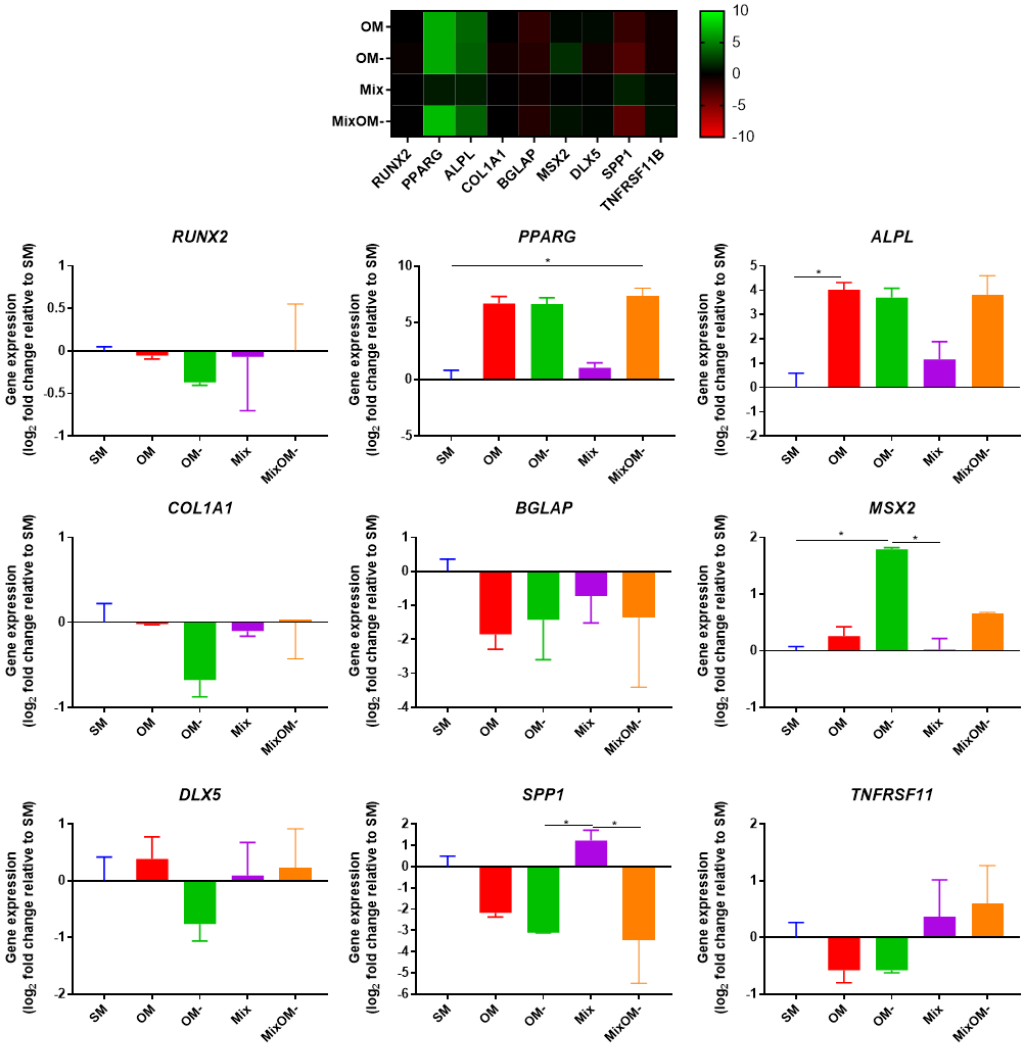


Figure 5.8. hMSC osteoblast gene expression after 11 days of Mix and MixOM- treatment normalized to SM control. *p<0.05 (n=2).

5.3.3.2.4 Notch markers

Notch gene markers were analysed for changes in expression after indirect treatment of hMSC with Mix and MixOM- after 11 days (Figure 5.9). The genes analysed included Notch receptors (*NOTCH1, NOTCH2* and *NOTCH3*), ligands (*JAG1, JAG2* and *DLL1*) and a Notch regulator (*DLL3*). Mix treatment showed no significant changes to Notch gene

expression compared to the SM control. MixOM- treatment showed significant upregulation of *NOTCH1* and *NOTCH2* compared to the OM- control. Finally, MixOM- also upregulated *NOTCH1, NOTCH3, JAG1* and *DLL3* compared to the SM control.

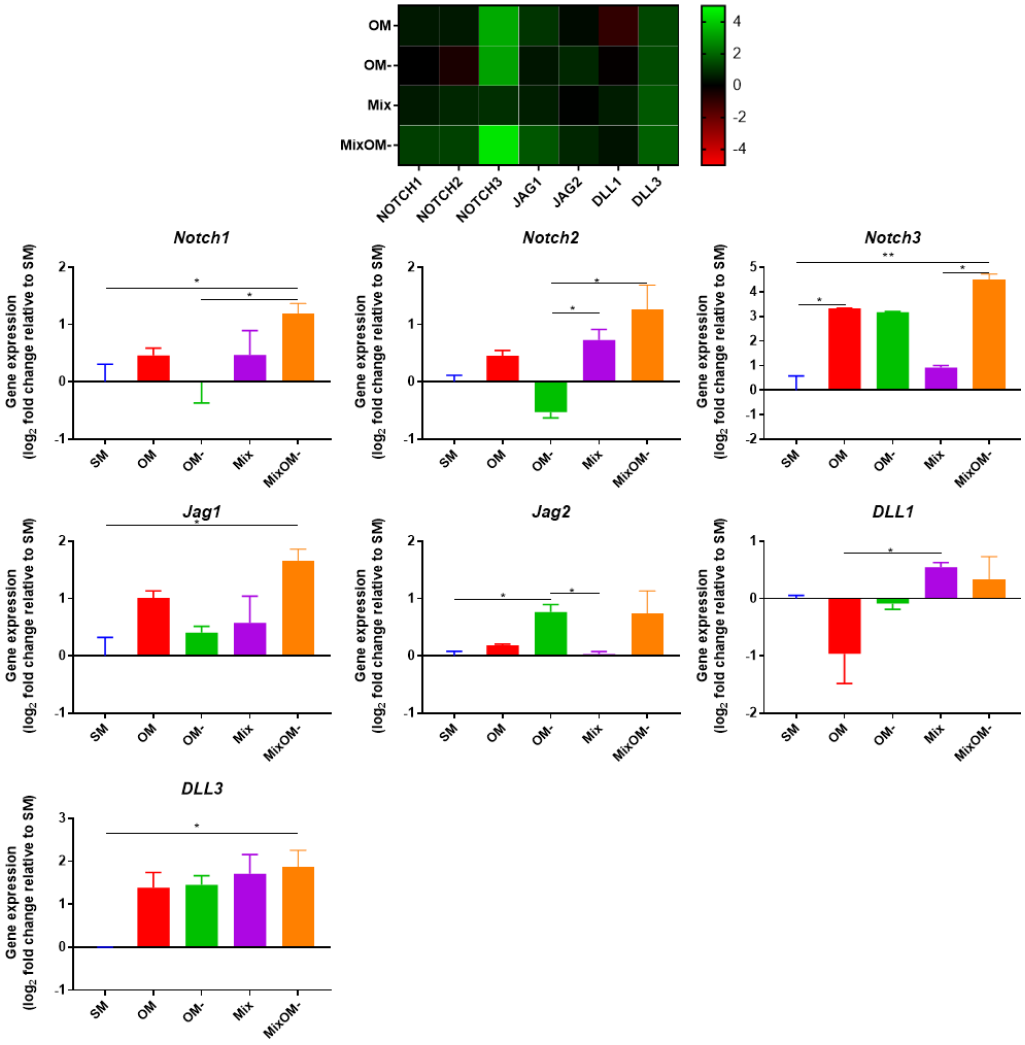


Figure 5.9. hMSC Notch gene expression after 11 days of Mix and MixOM- treatment normalized to SM control. *p<0.05, **p<0.005 (n=2).

5.3.3.2.5 TGFβ and BMP markers

TGFβ and BMP genes were analysed for changes in expression after 11 days of indirect treatment with Mix and MixOM- (Figure 5.10). Genes analysed included BMP ligands (*BMP2, BMP4* and *BMP5*), TGFβ ligands (*TGFβ1, TGFβ2, TGFβ3*), SMADs (*SMAD1, SMAD3, SMAD4, SMAD6* and *SMAD7*) and Noggin (*NOG*). Mix treatment resulted in no significant changes in gene expression compared to the SM control. MixOM- only demonstrates significant changes in the expression of *BMP4* where it was downregulated compared to the SM control.

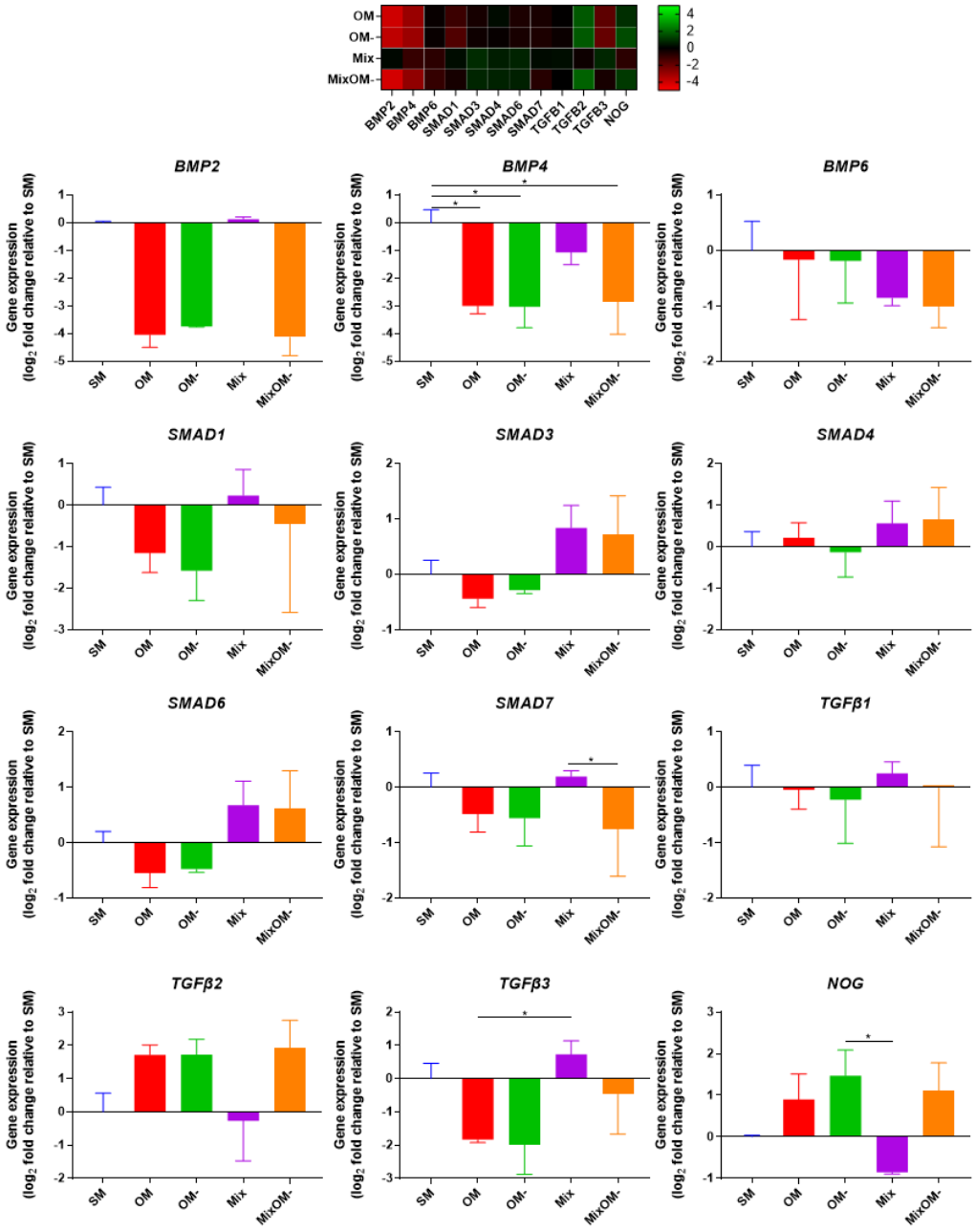


Figure 5.10. hMSC TGFβ and BMP gene expression after 11 days of Mix and MixOM- treatment normalized to SM control. *p<0.05 (n=2).

5.3.3.2.6 Wnt markers

Figure 5.11 shows the analysis of Wnt genes which were carried out after 11 days of indirect treatment with Mix and MixOM- on hMSC. Wnt co-receptors (*LRP5, LRP6, FZD1* and *ROR2*), ligands (*WNT5A*, *WNT10B*), inhibitor *SFRP1* and transcriptional activator *CTNNB1* were observed for changes in expression. Mix treatment showed upregulation of *WNT10B* compared to the SM control. MixOM- upregulated *ROR2, LRP5* and *SFRP1* compared to the OM- control. MixOM- also upregulated *CTNNB1*, *ROR2* and *SFRP1* compared to the SM control.

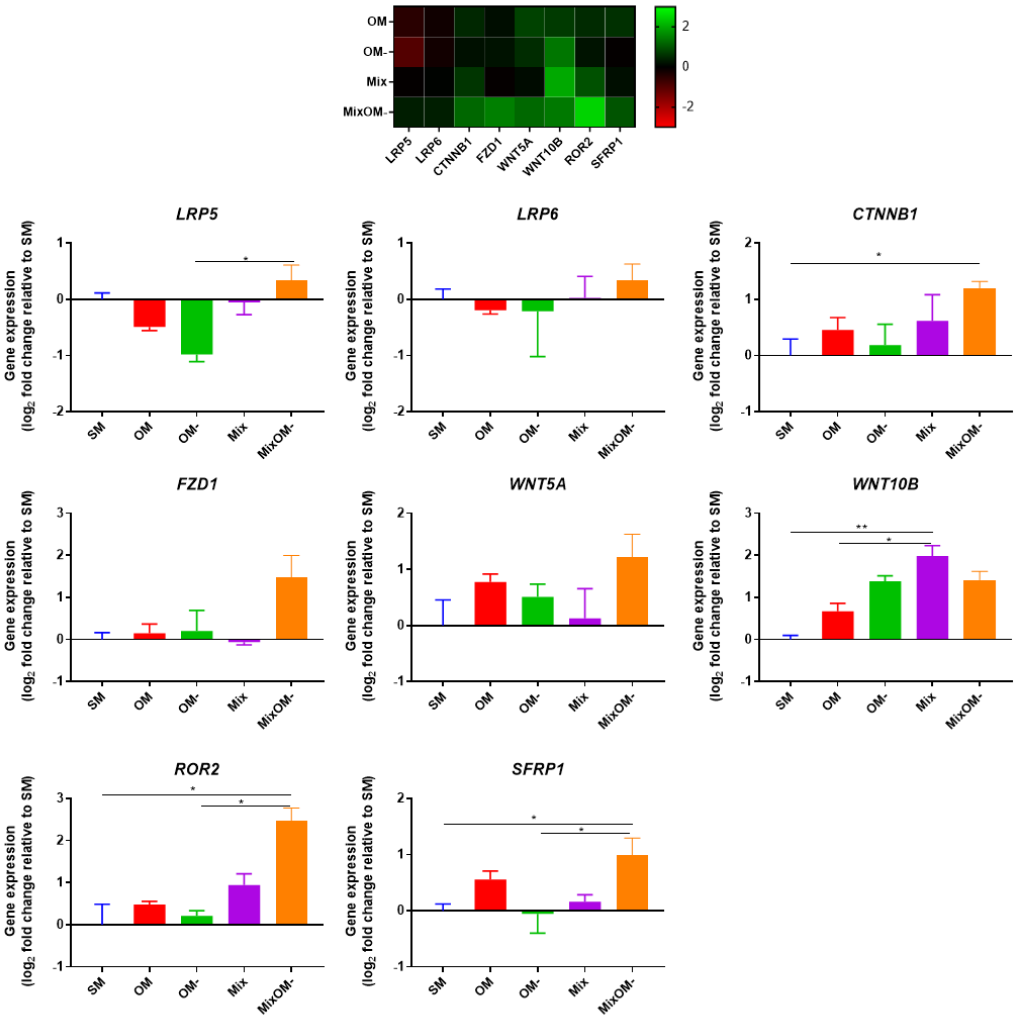


Figure 5.11. hMSC Wnt gene expression after 11 days of Mix and MixOM- treatment normalized to SM control. *p<0.05, **p<0.005 (n=2).

5.4 Discussion

PBGs allow for tailorable controlled release of inorganic ions as the glass degrades. Previous chapters highlighted the potential impacts of these ionic products on hMSC while demonstrating the benefits of slower degrading formulations on hMSC adhesion. This chapter investigates the osteogenic impact of utilizing potentially faster degrading formulations and aimed to identify the biological benefits of mixing microspheres of slower and faster degrading formulations.

5.4.1 Material characterization

No crystallization peaks were observed for all three glass formulations, confirming their amorphous nature. Thermal analysis revealed a linear increase in T_g and T_c as magnesium was added to the formulations. The thermal data presented in this study correlated with the study carried out by Ahmed et al. (2010), who showed an increase in T_c and T_g with increasing MgO content within the $40P_2O_5{\cdot}25CaO{\cdot}(0+x)MgO{\cdot}(35-x)MgO$ (x=0-30) PBG system. This increase has been attributed to increasing crosslinking density in the glass due to magnesium acting as an intermediary oxide (Okura et al., 2006). ^{31}P NMR analysis revealed a majority Q^2 distribution (>80%) and a much smaller Q^1 distribution for all three formulations. No Q^0 or Q^3 were identified. A 10% shift from Q^2 to Q^1 was identified for P50Mg50 compared to P50Ca25Mg25. While both calcium and magnesium act to depolymerize the phosphate network, the increase in Q^1 species within the P50Mg50 formulation suggests that some magnesium may be acting as an intermediary oxide (Ahmed et al., 2010).

PBG spheroidization utilizes an oxy-acetylene gas flame to allow ground PBG particles to reach a viscosity which allows it to entrap decomposing porogen gas bubbles within the molten particle. The surface tension of the viscous glass causes the particle to assume a spherical morphology as it is ejected from the flame while entrapped gas

bubbles escape to the surface to create pores (Hossain et al., 2018). P50Ca50 was demonstrated to be more viscous than previously successfully spheroidized P40 formulation. This is not unusual as Parsons et al. (2015) demonstrated an increase in viscosity with increasing phosphate content in the $(40+x)P_2O_5 \cdot 16CaO \cdot 24MgO \cdot (20-x)Na_2O$ (x=0-20) PBG system. These increases in viscosity were attributed to increases in phosphate chain length from increasing phosphate content from 40% to 50%. The increase in viscosity when using a PBG with 50% phosphate content likely entraps the decomposed porogen bubbles within the glass entirely, preventing their release before the glass cools and solidifies. As such, the internal porosity and lack of surface connecting pores were likely attributed to the increase in viscosity observed.

5.4.2 Effects of indirect treatment of PBG on hMSC

Indirect treatment of hMSC with the three PBG formulations resulted in severe loss of metabolic viability compared to the SM control in both the P50Ca50 and the P50Ca25Mg25 formulations while the P50Mg50 formulation demonstrated a similar response to the SM control at day 11.

Increasing phosphate content in PBGs has been shown to increase degradation rates in a number of studies (Uo et al., 1998b). Furthermore, studies such as those carried out by Abou Neel et al. (2007) demonstrated how increasing solubility decreased glass cytocompatibility with MG63 cells. This could explain the drastic difference in cell response seen between the previously tested P40 formulation and the new P50Ca50 and P50Ca25Mg25 tested here, as the increase in phosphate content and loss of sodium from the formulation would have resulted in increased degradation rates due to increases in phosphate glass solubility (Oueslati Omrani et al., 2015).

This increased degradation rate of P50Ca50 compared to the previously tested P40 microspheres, would have released increased concentrations of phosphate and calcium ions into the media. As discussed previously, increases of phosphate (1-7 mM) were known to induce apoptosis in osteoblast like cells (Meleti et al., 2000). Magne et al., (2003) has further elaborated on this and demonstrated the apoptotic effects of combining 4 mM phosphate and 2.4 mM calcium (through NaH_2PO_4 and Na_2HPO_4 and $CaCl_2$ supplementation). The calcium content present in the media (1.80 mM) with the calcium present in FBS, may have saturated this apoptotic pathway before the addition of supplementary calcium through PBG dissolution. Regardless, the surge of phosphate through P50Ca50 dissolution correlated with previously reported findings of phosphate concentration triggered toxicity of hMSC (>1.25 mM). Skelton et al. (2007) also explored the effects of a similar ternary PBG of the formula $50P_2O_5 \cdot (50-x)CaO \cdot XNa_2O$ (x=2-10) on primary human bone marrow MSC. All PBG formulations reported >40% cell death with no significant difference noted between the tested formulations. These results correlate with the data presented in this study though less cell death was noted in the study by Skelton et al. (2007). This difference in cell survival rates could be attributed to a number of factors such as using primary cells and keeping cells in culture for significantly longer periods of time (3-4 weeks). Furthermore, Skelton et al. (2007) cultured cells on glass discs which were immersed in culture medium for 24 hours before use due to a suggested benefit of protein absorption on adhesion, proliferation and differentiation.

Our previous studies also suggested the potential of phosphate toxicity rescue of hMSC though the addition of calcium and magnesium. While the P50Ca25Mg25 formulation resulted in some cell survival by day 7 compared to P50Ca50, by day 11, almost all the cells of the monolayer were lost. However, the P50Mg50 formulation demonstrated similar levels of metabolic activity compared to SM, correlating with the previous study

which showed no negative impact on cell metabolic activity with various magnesium concentrations (0-20 mM) or even in combination with 5 mM phosphate. Slower degrading compositions could be achieved through decreases in phosphate content, increases in calcium content or the addition of titanium or iron. Magnesium has reliably shown to benefit metabolic activity in cases of high phosphate levels on cells. This action is twofold, through slowing degradation rates by acting as a modifier oxide within the PBG structure but also by acting to rescue cells under phosphate induced stress. To prevent such severe impacts to metabolic activity in future formulations, slower, more controlled degrading formulations or compositions with increased calcium or magnesium and decreased phosphate would likely result in better monolayer health.

Following these findings, P50Ca50 microspheres were mixed at various ratios with P40 to allow for the leveraging of the properties of two different microsphere formulations, P40 which demonstrated superior metabolic activity and P50Ca50 which has a much higher calcium content. Mixing experiments demonstrated that mix ratios higher than 10% P50Ca50 resulted in significant negative impact to metabolic activity of hMSC. A 10% mix of P50Ca50 with P40 resulted in no significant decrease in cell viability by day 11 and would result in much higher levels of calcium in media than would be observed with a pure P40 application. Mixing microsphere formulations would allow for slower degrading formulations to act as cell scaffolds, allowing for tissue infiltration into a defect while faster degrading microspheres allow for optimal levels of ion release to be achieved (McLaren et al., 2019). The previously demonstrated disconnect between cell adhesion and cell health when seeded on PBG or indirectly treated with PBG dissolution products could thereby be solved through the mixing of microspheres of differing properties.

While no osteogenic activity was noted at the 10% mix, the 20% and 25% mixes demonstrated increased ALZ stain intensity over the SM control. This was unusual due to the decreased metabolic activity and impacted monolayer seen in the 20-25% treatments by day 11 as well as the minimal levels of ALP activity observed. Due to the necessity of ALP for matrix mineralization and the loss of cells seen, it is likely that the observed increase in ALZ stain intensity with higher concentrations of P50Ca50 are due to precipitation of calcium out of solution (Golub and Boesze-Battaglia, 2007). As seen previously with precursor compound testing and as demonstrated by Sage et al. (2011), when high enough concentrations of calcium (1.6 mM) and phosphate (2 mM) were achieved in solution, precipitation of calcium phosphate can occur. Furthermore, chapter 3 demonstrated that the retaining of precipitation likely occurs due to high levels of calcium (5 mM) promoting osteocalcin and osteopontin expression, two matrix proteins that have high levels of affinity for Ca^{2+} and would cause calcium deposition to be retained and slowly build up in culture over time. This retained deposition is likely what is being stained by the ALZ assay and results in significant false positive readings to matrix mineralization activity in the 20% and 25% P50Ca50:P40 mixes.

The data presented here demonstrates that P50Ca50 and P50Ca25Mg25 result in significant loss of cell viability when their dissolution products are indirectly applied to hMSC. Combination with a more stable, slower degrading formulation allows for the rescue of cell health while allowing for increased levels of calcium to be released into culture. The 90% P40 and 10% P50Ca50 mix demonstrated similar levels of metabolic activity to that of the SM control and P40 treated cells however no increases to osteogenic activity were noted.

5.4.3 Effects of indirect treatment on hMSC gene expression

5.4.3.1 Proliferation markers

Indirect application of the 90% P40 and 10% P50Ca50 Mix alone did not significantly impact proliferation markers, correlating with the lack of significant difference seen in metabolic activity of hMSC when indirectly treated with Mix. In a pro-osteogenic environment however, through the combination of Mix with OM- media, significantly decreased *CCND1* expression and increased *PCNA* expression were observed over the SM control. Additionally, *MKI67* expression was upregulated in MixOM- treated cells over OM- treated hMSC, suggesting that the combination of Mix and OM- promoted the elevation of expression beyond that of OM- treatment alone. As discussed by a number of studies, CCND1 controls cell progression through the G1 phase of the cell cycle (Ahlin et al., 2017; Baldin et al., 1993). Downregulation suggested a decrease in proliferative activity compared to the SM control however, as discussed previously, the antagonistic nature of proliferation and differentiation indicates that initiation of osteogenic differentiation may likely be due to the need of suspension of the cell cycle (Ruijtenberg and van den Heuvel, 2016; Rutkovskiy et al., 2016). In contrast, however, was the increase in *PCNA* expression of MixOM- treated cells compared to SM. PCNA however, was discussed by Maga and Hübscher (2003) to control a number of cell processes depending on the regulatory state of numerous other genes and as such may not be completely representative of an increased proliferative state. Mix treatment in SM correlates with metabolic activity data presented previously indicating similar levels of activity to that of the SM control. Mix in OM- suggests a potential decrease in proliferation due to CCND1's downregulation and the lack of significant changes from the SM control in MKI67 expression. However, due to the upregulation of MKI67 and *PCNA* due to its multifunctional nature, further timepoints may be required to confirm the effect of MixOM- on proliferative activity of hMSC.

5.4.3.2 Integrin markers

Mix caused no significant changes to integrin expression compared to the SM control while MixOM- causes increases in *ITGA3* expression compared to both SM and OM-. Clover et al. (1992) demonstrated the high levels of expression of integrins β1 (*ITGB1*), α3 (*ITGA3*) and others in osteoblast cells *in situ*. While this data demonstrated that *ITGA3* was significantly upregulated in both OM and MixOM- samples, no significant changes to *ITGB1* were seen. This difference in expression may be attributed to the use of a cell line as opposed to a primary cell source. Additionally, Clover et al. (1992) noted the different patterns of integrin expression in the literature and attributed this to the various stages of osteoblast differentiation (Bennett et al., 2001). Bennett et al. (2001) also noted increased levels of expression of integrin subunits α3 and α5 when mandibular osteoblasts were treated with vitamin D3 and hydrocortisone, known to promote differentiation in human osteoblasts (Ireland et al., 2004). Interestingly, while MixOM- demonstrates similar levels of integrin expression compared to OM, it was significantly higher than OM- in *ITGA3* expression indicating a combination of PBG dissolution products and OM- media promoting increased expression. The lack of significant *ITGB1* expression ultimately indicated an inconclusive change in integrin activity as the β1 subunit plays a key role in adhesion when combined with other subunits such as α3 and α1 within a heterodimer (Brakebusch and Fässler, 2005). More late stage timepoints could help elucidate the effectiveness of a P40 and P50Ca50 mix in promoting adhesion through integrin expression as similar levels of expression were seen in OM treated samples that demonstrated a typical osteogenic phenotype by day 21.

5.4.3.3 Osteoblastic markers

While not an osteoblastic marker, but an adipogenic marker, PPAR-γ expression was significantly upregulated by MixOM- treatment. The level of *PPAR-γ* expression was similar to that of OM and OM- treatments, once again suggesting significant contribution of dexamethasone in the MixOM- media upregulating the gene. As previously discussed, upregulation of *PPAR-γ* is a known effect of dexamethasone treatment and despite PPAR-γ being a marker for adipogenesis, dexamethasone has been used for osteogenic differentiation (Ghali et al., 2015). The OM treatment also displays similar levels of *PPAR-γ* yet by day 21 represents an osteoblast phenotype. Furthermore, Mix treatment alone did not significantly upregulate *PPAR-γ* and as such it was unlikely that the PBG contributed to the observed increase in the MixOM- treatment.

Interestingly, the increase in ALZ stain intensity observed in the 20% and 25% P50Ca50:P40 mixes was not seen in the 10% mix. Chapter 3 saw an increase in ALZ stain intensity with the 555 treatment and was suggested to be due to calcium mediated overexpression of the *BGLAP* and *SPP1* genes. The 10% mix in both SM and OM- do not demonstrate any significant upregulation to *BGLAP* or *SPP1* correlating with the lack of ALZ stain intensity seen, further suggesting that calcium content promotes expression of *BGLAP* and *SPP1* which contribute to the binding and build-up of calcium precipitate.

Ultimately, the Mix and MixOM- treatments did not demonstrate any significant changes to osteoblast gene expression compared to the SM or OM- controls respectively.

5.4.3.4 Notch markers

The Mix treatment on its own demonstrated no significant changes to Notch gene expression compared to the SM control, when combined with OM- in the MixOM- treatment however, *NOTCH1*, *NOTCH3*, *JAG1* and *DLL3* were all significantly upregulated compared to the SM control. Furthermore, *NOTCH1* and *NOTCH2* were also upregulated in MixOM- samples compared to OM- treated samples suggesting significant contribution in gene upregulation by the PBG dissolution products. MixOM- would therefore appear to promote activation of the Notch pathway, through the upregulation of receptors (*NOTCH1, NOTCH2* and *NOTCH3*) and ligand (*JAG1*). The Notch signalling has been demonstrated to inhibit osteoblast differentiation through the attenuation of RUNX2 and β-catenin signalling (Deregowski et al., 2006; Xu et al., 2015). Lawal et al. (2017) hypothesized that Notch signalling plays a role in coordinating bone formation through the maintenance of the osteoprogenitor pool. It was shown that *JAG1* deletion in osteolineage cells increases the number of osteoblast cells in culture through depletion of osteoprogenitors. Lawal et al. (2017) demonstrated that *JAG1* inhibits the transition from osteoprogenitor to pre-osteoblasts. These findings suggest that the application of MixOM- to hMSC convey an inhibitory effect on osteogenic differentiation through the Notch pathway. However, the upregulation of the divergent *DLL3* ligand contrasts with this finding as Ladi et al. (2005) have shown that *DLL3* acts as an antagonist to the Notch pathway potentially inhibiting the β-catenin suppression seen with typical Notch activation (Deregowski et al., 2006; Heuss et al., 2008; Zanotti and Canalis, 2016).

Ultimately, MixOM- treatment on hMSC appears to promote Notch signalling on day 11, however, *DLL3* may convey some inhibition of this pathway. The promotion of the Notch pathway may have negative downstream effects on osteogenic differentiation through β-catenin and RUNX2 activity suppression.

5.4.3.5 TGF-β and BMP markers

Mix treatment on hMSC revealed no significant changes to the expression of TGF-β and BMP markers compared to the SM control, however, MixOM- showed significant downregulation of *BMP4* compared to the SM control. MixOM- treated cells displayed levels of *BMP4* expression similar to that of OM- and OM in isolation, suggesting minimal contribution of the Mix dissolution products to the changes of *BMP4* gene expression. This level of expression in osteogenically differentiating cells is not unusual as Maeda et al. (2004) has demonstrated the significant upregulation of endogenous *BMP4* only during osteoblast maturation at 24+ days into culture of murine C2C12 cells.

5.4.3.6 Wnt markers

Mix treatment showed no significant changes to Wnt gene expression compared to the SM treatment with the exception of *WNT10B*, which was significantly upregulated. MixOM- on the other hand, showed significant *CTNNB1*, *ROR2* and *SFRP1* expression compared to SM and increased *LRP5* expression compared to OM-.

WN10B expression is known to decrease during adipogenic differentiation *in vitro*, through the inhibition of adipogenic factors such as PPAR-γ (Ross et al., 2000). Cawthorn et al. (2012) demonstrated that *WNT10B* expression suppresses adipogenesis and promotes osteoblastogenesis through a β-catenin dependent mechanism. However, in this study, Mix treated samples showed no decreases to expression of *PPAR-γ* compared to SM despite the significant upregulation of *WNT10B*. The study by Cawthorn et al. (2012) was carried out on murine ST2 cells in osteogenic media (10 mM β-glycerophosphate and 25 μg/mL ascorbic acid) suggesting that the osteoblastogenesis stimulating and PPAR-γ inhibiting nature of WNT10B requires a pro-osteogenic environment to function. Furthermore, β-catenin was not upregulated

in Mix treated samples, though the mechanism of adipogenic suppression and osteoblast promotion likely occurs due to the stabilization of β-catenin rather than promotion of expression similar to how WNT4 interacts with β-catenin (Lyons et al., 2004).

Contrasting to Mix treatment, MixOM- showed significantly upregulated *β-catenin* expression compared to the SM control, suggesting an impact on the canonical Wnt pathway. Conversely, the Wnt signalling inhibitor *SFRP1* was also upregulated in MixOM- treated samples (Yao et al., 2010). Activation of the Wnt pathway through Wnt ligand and receptor binding inhibits β-catenin phosphorylation through attenuation of the β-catenin destruction complex (axin-GSK3β-Ck1-APC) (Baron and Gori, 2018; Baron and Kneissel, 2013). SFRP1 on the other hand, disrupts this attenuation through the sequestering of Wnt ligands (Bodine et al., 2005). Yao et al. (2010) have also demonstrated the ability of SFRP1 to not only inhibit osteoblast maturation through the Wnt pathway, but to also attenuate the pro-osteogenic effects of PTH. Therefore, despite the upregulation of *β-catenin*, the upregulation of *SFRP1* may result in negative consequences to osteogenic differentiation. Yao et al. (2010) further demonstrated through overexpression of *SFRP1* that mice bone marrow cells exhibited 30% lower ALP activity. The upregulation of *SFRP1* correlates with data presented in chapter 3, suggesting some contribution of high calcium content to *SFRP1* upregulation and ALP inhibition. Further testing on factors downstream of β-catenin, such as lymphoid enhancer factor (LEF) or T-cell factor (TCF), may be required to determine the final activation state of the canonical Wnt pathway (Cadigan and Waterman, 2012).

A study on PBG fibres ($50P_2O_5{\cdot}40CaO_5{\cdot}5Na_2O{\cdot}5Fe_2O_3$) by Lin et al. (2020) demonstrated a significant increase in *β-catenin* expression of murine cells treated with fibres in OM

on day 7 and 21, with no significance seen on day 14. Chapter 4 previously showed that P40OM- demonstrated no significant increases to *β-catenin* expression levels at day 11 compared to SM, coinciding with the data presented by Lin et al. (2020). This suggests that the faster degrading P50Ca50 formulation, even in a 10% mix with P40 promoted significant *β-catenin* expression in the pro-osteogenic environment of OM-. A recent study by Ardeshirylajimi et al. (2018) who demonstrated similar *β-catenin* upregulation on polyphosphate treated adipose-derived MSC suggested a polyphosphate mediated Wnt-mTOR mechanism in the upregulation of *β-catenin*. The 10% P50Ca50 used contains 95% Q^2 species, suggesting a possible contribution of polyphosphates to β-catenin gene expression.

Similar to the previously seen P40OM- treatment, *ROR2* was also significantly upregulated in the MixOM- treatment. Billiard et al. (2005) demonstrated a biphasic pattern of *ROR2* expression in various cell lines representing stages of osteoblast differentiation. Pre-osteoblasts demonstrated a 1-fold increases to *ROR2* expression while early osteoblasts showed no increases in expression. Finally, a small 0.6-fold increase in expression was observed in late stage osteoblasts. MixOM- treatment showed a 2.5-fold increase in *ROR2* expression compared to the SM control. The higher levels of *ROR2* expression than that of the pre-osteoblast cells tested by Billiard et al. (2005) may be attributed to differences in timepoint (day 0 vs day 11). This data suggests that the MixOM- treated cells at day 11 may be entering the pre-osteoblast stage of differentiation based on the levels of *ROR2* expression observed and previously noted decreases in *CCND1* proliferative marker and increases to *ALPL* expression compared to the SM control. However, due to the multirole nature of ROR2 in the canonical and non-canonical Wnt pathways, its ultimate effects on osteogenic differentiation remains uncertain.

The strong upregulation of *β-catenin* represents a positive indicator for osteogenic differentiation. However, the upregulation of *SFRP1* may lead to inhibition of osteoblast commitment through the attenuation of the canonical pathways. Furthermore, the similar levels of *ROR2* expression seen with pre-osteoblast cells also correlates with early stage differentiation markers seen, suggesting that treated cells may display typical osteogenic activity at a later timepoint if not inhibited by SFRP1 and other pathways.

5.5 Summary

Material characterization data demonstrated that a typical linear increase in T_g was observed with increasing magnesium content. ^{31}P NMR analysis identified a majority Q^2 distribution (>80%) and a much smaller Q^1 distribution in all three formulations. P50Mg50 showed 10% higher Q^1 content than the P50Ca50 and P50Ca25Mg25 formulations suggesting the integration of some magnesium into the phosphate backbone, acting as an intermediary oxide. Furthermore, an expected increase in viscosity from the P40 formulation to the P50 formulations likely caused the internal only porosity observed. The high viscosity likely prevented gas escape to the surface before the PBG solidifies and resulted in the internal only porosity observed within the P50Ca50, P50Ca25Mg25 and P50Mg50 formulations. Future formulations with decreased viscosity though phosphate reduction or increased incidence time within the flame to allow for gas escape may result in successful porous spheroidization.

Significant impacts to metabolic activity are seen in the indirect testing of the P50Ca50 and P50Ca25Mg25 formulations by day 11. Increased magnesium content promoted hMSC survival as P50Ca25Mg25 displayed no significant decreases to metabolic activity on day 7 while P50Mg50 displayed metabolic activity levels similar to that of the SM control by day 11. This data correlates with precursor application data presented previously where a dose dependent phosphate toxicity was observed and additionally where cells could be rescued through application of calcium and magnesium (5 mM). Interestingly, while increasing the concentration of the P50Ca50 mix to 20% or 25% resulted in cytotoxicity and no ALP activity, increases in ALZ stain intensity were observed. This data again correlates with chapter 3 which highlighted the impact of ≥5 mM calcium in the promotion of *BGLAP* and *SPP1* matrix protein gene expression, causing the binding of calcium phosphate precipitate and resulting in a false positive ALZ stain.

Though no increases to osteogenic activity were observed in the 10% mix, optimization of the formulation for optimal cell survival before promotion of osteogenic differentiation would provide a good foundation for future modification of the formulation to further promote the intended effect. This could be achieved through decreases in phosphate toxicity through decreasing PBG solubility by increasing modifier oxide content and decreasing phosphate content. The next chapter of this thesis explores a formulation that substitutes phosphate for calcium which may promote cell survival as suggested in this chapter.

Mixing microspheres of two different formulation allowed for the leveraging of both of their respective properties, superior metabolic activity with P40 and increased calcium release with P50Ca50. Using a slower degrading porous formulation would provide better support for tissue infiltration into defects while faster degrading formulations could supply the levels of ions required for hMSC differentiation. Mix treatment in SM largely revealed no significant changes to gene expression while MixOM- treatment resulted in a decrease in proliferative marker *CCND1* and increases to *ALPL* expression compared to the SM control, suggesting the promotion of an osteogenic phenotype. Furthermore, *ROR2* expression was significantly upregulated, correlating with levels of expression seen in pre-osteoblasts.

Finally, MixOM- demonstrated gene expression resulting in conflicting effects on the β-catenin pathway. Notch signalling is likely promoted though the upregulation of *NOTCH*1, *NOTCH2* and *JAG1* in MixOM-. The Notch pathway has β-catenin and RUNX2 disrupting effects indicating potential inhibition of osteogenic commitment and differentiation. In contrast, MixOM- demonstrated potential attenuation of the Notch pathway through the upregulation of *DLL3* in addition to strongly upregulating *β*-

catenin itself. *SFRP1* upregulation is also observed. *SFRP1* inhibits β-catenin stabilization through the disruption of Wnt ligands ultimately inhibiting the Wnt pathway and thus osteogenic differentiation. Chapter 3 also demonstrated significant upregulation of *SFRP1*, this was likely attributed to high calcium content (5 mM). This correlates with the data presented here as the rapid degrading nature of P50Ca50 likely results in excess calcium, promoting the upregulation of *SFRP1*. Ultimately, despite *β-catenin* upregulation and *DLL3* mediated Notch suppression, it is likely that due to the complementary and inhibitory effects of both *SFRP1* and Notch signalling, β-catenin would be degraded leading to inhibition of osteogenic differentiation.

The *SFRP1* gene has been shown to be an unlikely antagonist to PBG mediated osteogenic differentiation, contrasting with studies that indicate high calcium levels (5 mM) are necessary for osteogenic differentiation. Future formulations with slower degradation profiles or less calcium content may result in superior osteogenic differentiation due to the increased β-catenin expression and stabilization observed without the antagonistic effects of *SFRP1*. Finally, this chapter highlighted the potential of mixing microspheres of multiple formulations, contributing to different aspects of bone growth. Slower degrading formulations may act as a scaffold to promote tissue ingrowth mixed with faster degrading formulations which may have a strong impact on cell behaviours, pushing hMSC down an osteogenic pathway.

Chapter 6 - Microsphere formulation optimization for osteogenic response

6.1 Introduction

PBGs are comprised of a network of linked tetrahedral units typically denoted by Q^n terminology. Through the addition of network modifier oxides such as CaO and MgO, depolymerization of the phosphate network occurs due to the formation of ionic bonds between the phosphate groups (Zachariasen, 1932). As increasing concentrations of modifier oxides are added to the glass, metaphosphate (Q^2), pyrophosphate (Q^1) and orthophosphate (Q^0) structures are formed. Alteration of the PBG formulation with these network modifier oxides allow for the alteration of the PBG properties from degradation rates to thermal stability as well as quantity and type of phosphate species released into solution once degraded (Ahmed et al., 2005; Knowles et al., 2005; Sharmin and Rudd, 2017).

6.2 Aims and hypotheses

PBG properties such as dissolution rates and bioactivity are strongly related to the content and variety of modifying oxides added into the formulation (Sharmin and Rudd, 2017). The previous chapter highlighted not only the negative impact of fast resorbing high phosphate content glasses on cell health, but also how formulations can vary in viscosity which impacts the porous microsphere spheroidization process, resulting in PBG microspheres with internalized porosity. This study aimed to identify the effects of a 5% substitution of phosphate content for calcium in the P50Ca25Mg25 formulation (P45Ca30Mg25; henceforth referred to as P45). It was hypothesized that a decrease in phosphate content and increase in calcium content would produce a more stable formulation by decreasing PBG solubility leading to potentially decreased cytotoxic effects on hMSC health as well as altering the formulation viscosity profile to

allow for successful production of fully porous microspheres. Furthermore, the osteogenic differentiation potential of the P45 formulation on hMSC was explored through ALP, ALZ cellular assays in addition to gene expression analysis with TaqMan Low Density Arrays (TLDAs).

6.3 Results

6.3.1 Material characterization

EDX analysis

EDX was carried out to confirm the composition of the manufactured PBG composition. Table 6.1 shows that P45 was within 1-2% of the target formulation.

Table 6.1. EDX measurements of P45 and P50Ca25Mg25 against target formulation (mol%) ± standard error of the mean (SEM).

		P_2O_5 (mol%)	CaO (mol%)	MgO (mol%)
P45	Target	45	30	25
	Measured	43.5 ± 1.0	31.3 ± 1.0	25.3± 0.1
P50Ca25Mg25	Target	50	25	25
	Measured	50.1 ± 0.3	24.3 ± 0.4	25.6 ± 0.2

DSC analysis

To identify the thermal properties of the P45 formulation, differential scanning calorimeter (DSC) analysis was carried out. Figure 6.1A showed the DSC thermal profile gathered and the T_g, T_c and T_m values are presented in Table 6.2. Thermal analysis revealed a complex trace as can be seen in Figure 6.1A with multiple crystallization and melting events. A very late T_g and T_c onset was observed at 565 °C and 625 °C, leading to a small processing window of 64 °C.

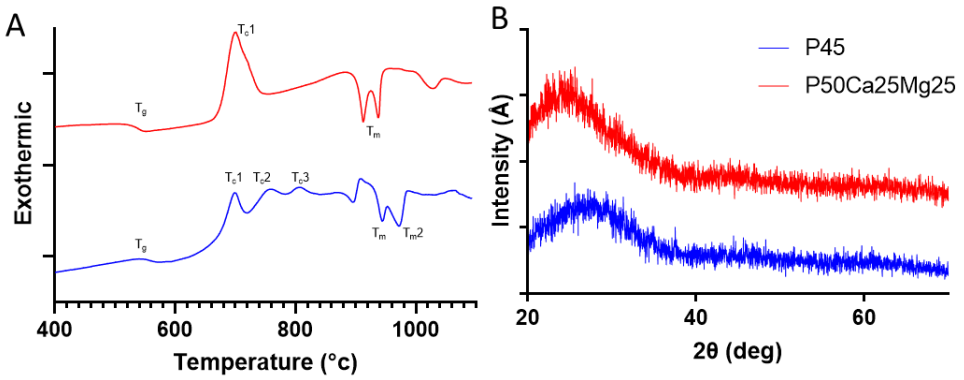


Figure 6.1. Glass characterization of P45. (A) Thermal analysis traces via DSC showing T_g, T_c and T_m. (B) XRD spectra confirming the amorphous nature of P45 and P50Ca25Mg25.

XRD analysis

XRD was used to identify crystalline peaks within the P45 formulation. Figure 6.1B showed the XRD spectra for this formulation demonstrating the lack of sharp peaks in the P45 glass, confirming its amorphous nature.

Table 6.2. Glass transition (T_g), onset of crystallization (T_c), melting temperature (T_m) and calculated thermal processing window (Tc_{onset}) for P45 and P50Ca25Mg25.

Glass Code	T_g	T_c				T_m		*Window*
	Onset	Onset	1	2	3	1	2	Tc_{onset}- Tg
P45	565	629	699	757	808	944	972	64
P50Ca25Mg25	530	674	702			913	938	145

^{31}P NMR spectroscopy

NMR analysis allows for the identification of various Q^n species within the P45 PBG formulation. The NMR spectra in Figure 6.2 showed two peaks representing Q^1 and Q^2 units (Brow, 2000). Unlike the significant Q^2 speciation observed in the P50Ca25Mg25 formulation (93.86%), decreasing the phosphate content and increasing calcium content by 5% greatly increased the Q^1 species content to 45%. Q^2 species was reduced to 55% and no Q^0 or Q^3 were detected.

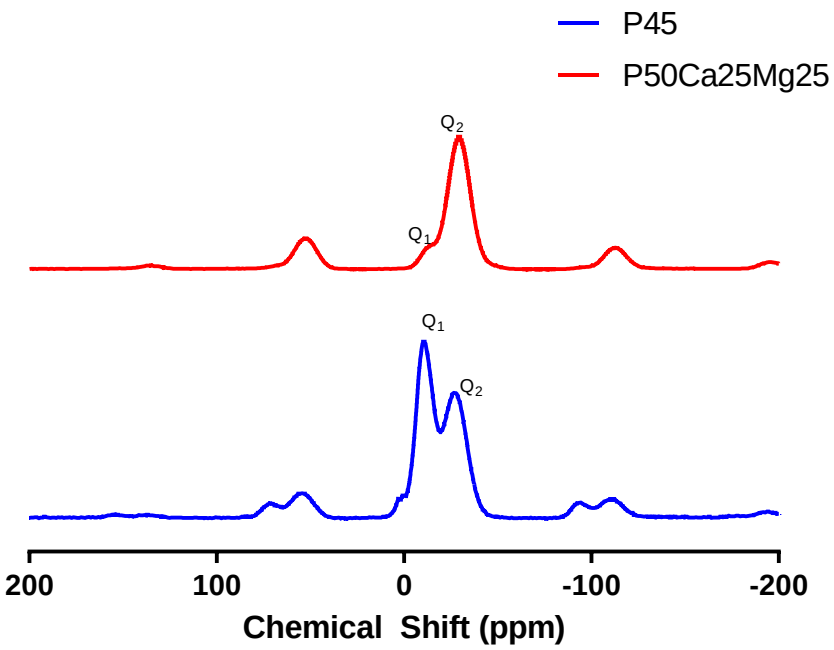


Figure 6.2. ^{31}P NMR spectra of the P45 and P50Ca25Mg25 PBG formulations. Data provided by Jeremy Titman and Alex Taylor.

Table 6.3. Distribution of Q^n species across PBG formulations

	Q^0	Q^1	Q^2
P45	0	45	55
P50Ca25Mg25	0	6	94

6.3.2 Material Spheroidization

In contrast to only having achieved internal porosity for the P50Ca50, P50Mg50 and P50Ca25Mg25 formulations, the reduction of phosphate content and increase in calcium content for P45 allowed for production of fully porous microspheres with external and interconnected pores to be formed utilizing the flame spheroidization procedure described earlier (Figure 6.3A) (Hossain et al., 2018). The porous P45 microspheres resembled the porous P40 (Figure 6.3B), both showed minimal internal only porosity that was observed with P50Ca50, P50Mg50 and P50Ca25Mg25 formulations.

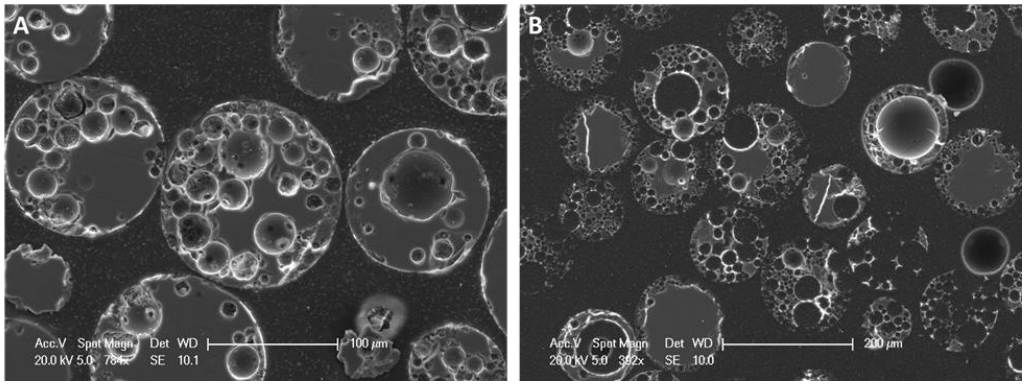


Figure 6.3. SEM scans of resin embedded sections of (A) P45 and (B) P40.

6.3.3 Indirect microsphere application

6.3.3.1 Effects of P45 microsphere degradation products on hMSC

P45 was produced by decreasing the phosphate content and increasing calcium content in P50Ca25Mg25. To identify the biological impact of P45, porous P45 degradation products were applied to hMSC every 48 hours for 21 days. Metabolic activity at day 2, 7 and 11, ALP activity at day 11 and ALZ staining intensity at day 21 were measured. Figure 6.4A demonstrated the significant increases in metabolic activity seen in the P45 treated cells compared to both the SM and OM controls on day 11. P45 also demonstrated significant ALP activity on day 11 compared to the SM control. Despite the substantial increase in ALP activity, no significant ALZ staining was observed (Figure 6.4B and 6.4C).

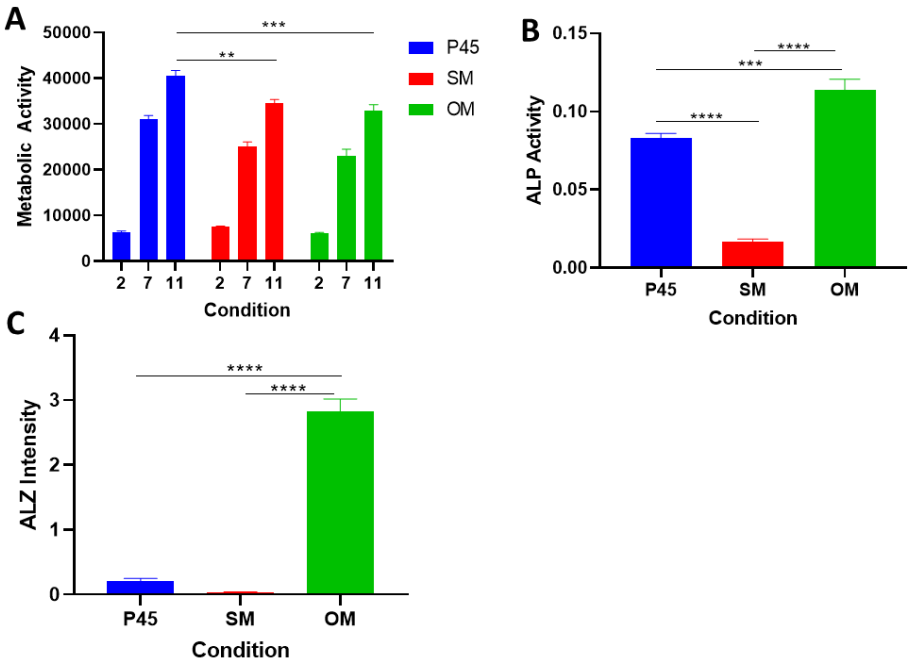


Figure 6.4. (A) The metabolic (day 2, 7 and 11), (B) ALP (day 11) and (C) ALZ intensity (day 21) of hMSC treated with the dissolution products of P45 compared to SM and OM. **p<0.01, ***p<0.001 and ****p<0.0001. (n=3).

Porous P45 was incubated in OM- medium (osteogenic media without β-glycerophosphate) to investigate the effects of the PBG degradation products in a pro-osteogenic environment without its effects being masked by phosphate supplied by β-glycerophosphate. As can be seen in Figure 6.5A, P45 demonstrated a significant increase in metabolic activity on day 11 while P45OM- (P45 in OM- medium), showed no significant changes from the P45, SM and OM- treatments. P45OM- did show increased metabolic activity compared to the OM control. Interestingly, P45OM- also demonstrated significantly more ALP activity on day 11 compared to all other

treatment conditions, however, despite this, no significant changes to ALZ staining were observed compared to P45 or the SM control (Figure 6.5B and 6.5C).

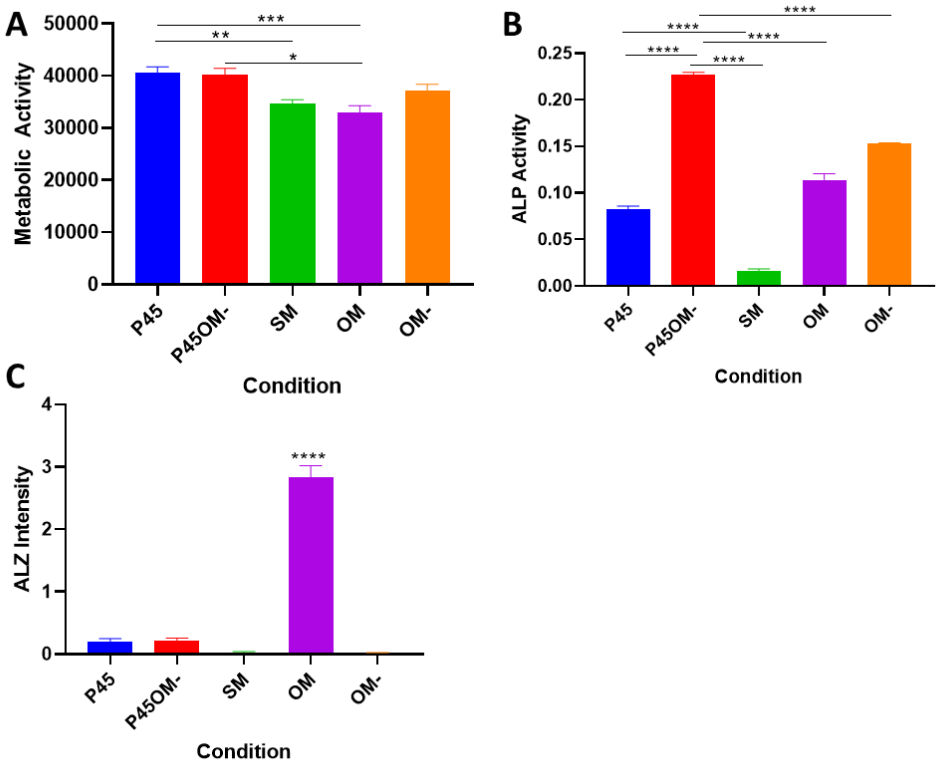


Figure 6.5. (A) The metabolic (day 2), (B) ALP (day 11) and (C) ALZ intensity (day 21) of hMSC treated with the dissolution products of P45 incubated in SM and OM- compared to SM, OM and OM- controls.*p<0.05, **p<0.01, ***p<0.001 and ****p<0.0001. (n=3 technical replicates).

6.3.3.2 Effects of mixed microsphere degradation products on hMSC gene expression

The P45 formulation in both SM and OM- demonstrated strong promotion of ALP activity compared to the SM, OM and OM- controls. Despite the ALP activity seen, no ALZ stain intensity was observed. To investigate this osteogenic activity, hMSC indirectly treated with P45 in SM and OM- were collected and carried forward for gene expression analysis using TaqMan Low Density Arrays (TLDAs). Table 6.4 indexes all the gene groups analysed in this subsection.

Table 6.4. Index of gene groups analysed in chapter 6

Section Number	**Gene Group**
6.3.3.2.1	Proliferative
6.3.3.2.2	Integrin
6.3.3.2.3	Osteoblastic
6.3.3.2.4	Notch
6.3.3.2.5	TGF-β and BMP
6.3.3.2.6	Wnt

6.3.3.2.1 Proliferative markers

Proliferation gene expression markers *CCND1*, *PCNA* and *MKI67* were observed after 11 days of indirect treatment with P45 and P45OM- (Figure 6.6). P45 treatment showed no significant changes to gene expression when compared with the SM control. An increase in *PCNA* expression was seen with P45OM- expression compared to the SM control while P45 and OM- treatments in isolation also displayed no significant changes to expression.

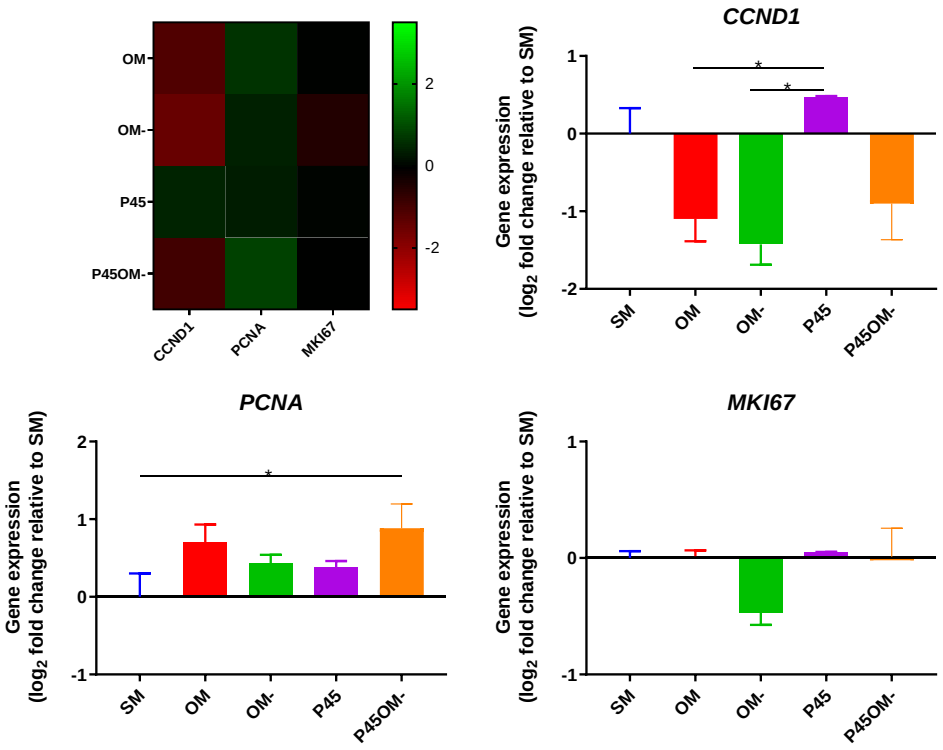


Figure 6.6. hMSC proliferation gene expression after 11 days of P45 and P45OM- treatment normalized to SM control. *p<0.05 (n=2).

6.3.3.2.2 Integrin markers

Integrin subunit markers *ITGA1*, *ITGA3* and *ITGB1* were analysed for changes in expression after 11 days of indirect treatment with P45 and P45OM- (Figure 6.7). P45 treatment demonstrated no significant changes to integrin gene expression when compared to the SM control. P45OM- showed significant increases in *ITGA3* expression over the SM control, displaying similar levels of expression to that of OM treated samples.

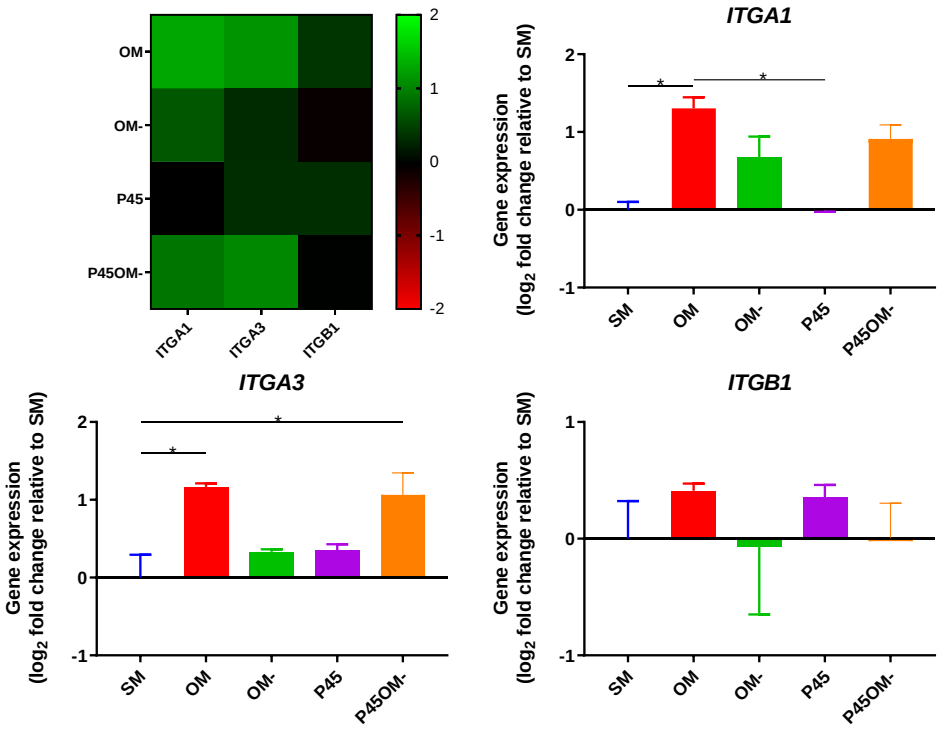


Figure 6.7. hMSC integrin gene expression after 11 days of P45 and P45OM- treatment normalized to SM control. *p<0.05 (n=2).

6.3.3.2.3 Osteoblast markers

Figure 6.8 showed the analysis of osteoblast markers *RUNX2, ALPL, COL1A1, BGLAP, MSX2, DLX5* and *SPP1* in hMSC after 11 days of treatment with P45 and P45OM-. Additionally, while not directly influencing osteoblast differentiation *PPAR-γ* and *TNFRSF11* were also observed for changes in expression during indirect treatment. No significant changes in expression are observed between P45 treatment and the SM control. A significant difference in *MSX2* expression was seen in P45OM- treated samples compared to OM-, where the latter is upregulated, P45OM- samples display levels of expression similar to that of SM. P45OM- also showed significant increases in *PPAR-γ* and *ALPL* expression and significant decreases in *BGLAP* expression compared to the SM control. No other osteogenic genes showed significant changes to expression.

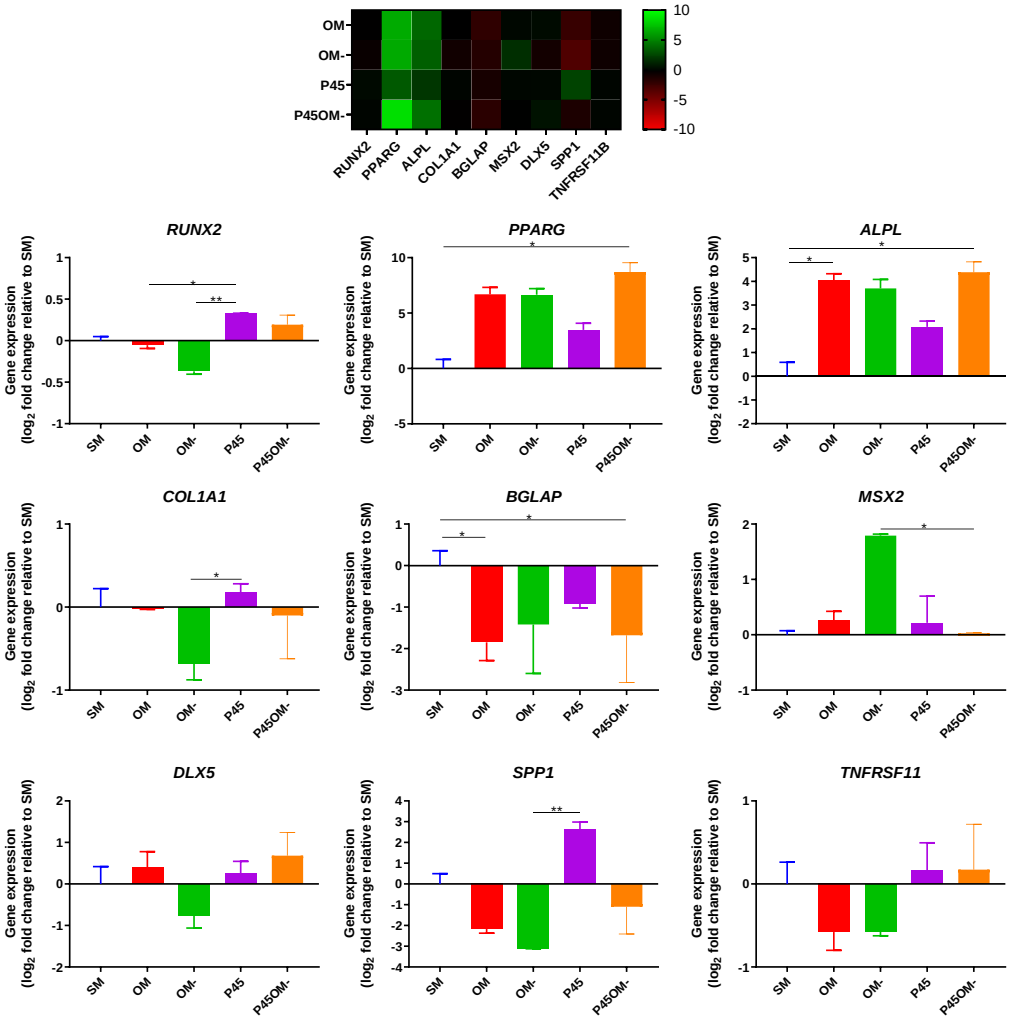


Figure 6.8. hMSC osteoblast gene expression after 11 days of P45 and P45OM- treatment normalized to SM control. *p<0.05, **p<0.005 (n=2).

6.3.3.2.4 Notch markers

Notch markers were analysed in hMSC after 11 days of treatment with P45 and P45OM- (Figure 6.9). The genes analysed included Notch receptors (*NOTCH1, NOTCH2* and *NOTCH3*), ligands (*JAG1, JAG2* and *DLL1*) and a Notch regulator (*DLL3*). P45 treated cells showed no significant changes in expression compared to the SM control. P45OM- treatments showed significant increases in *NOTCH1* and *NOTCH2* expression

compared to OM- treated cells, additionally, P45OM- treatments caused significant upregulation in *NOTCH1* and *NOTCH3* expression compared to the SM control.

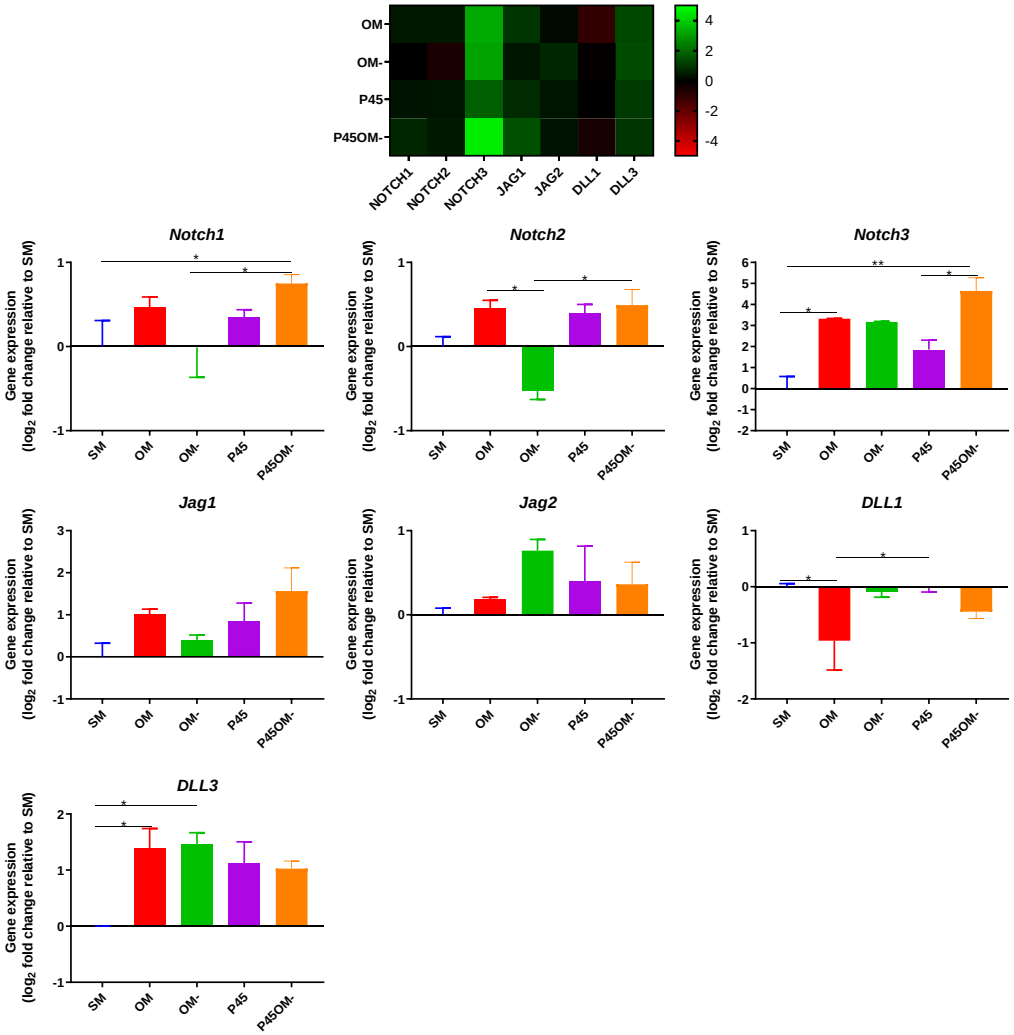


Figure 6.9. hMSC Notch gene expression after 11 days of P45 and P45OM- treatment normalized to SM control. *p<0.05, **p<0.005 (n=2).

6.3.3.2.5 TGFβ and BMP markers

TGFβ and BMP markers were investigated for changes after hMSC were treated with the dissolution products of P45 and P45OM- for 11 days (Figure 6.10). Genes analysed included BMP ligands (*BMP2, BMP4* and *BMP5*), TGFβ ligands (*TGFβ1, TGFβ2, TGFβ3*), SMADs (*SMAD1, SMAD3, SMAD4, SMAD6 and SMAD7*) and Noggin (*NOG*). P45 demonstrated no significant changes to gene expression compared to the SM control. Similarly, P45OM- demonstrated no significant changes in gene expression compared to OM-. P45OM- did show a significant decrease in *BMP4* expression compared to SM unlike the P45 treatment, which was not significantly downregulated.

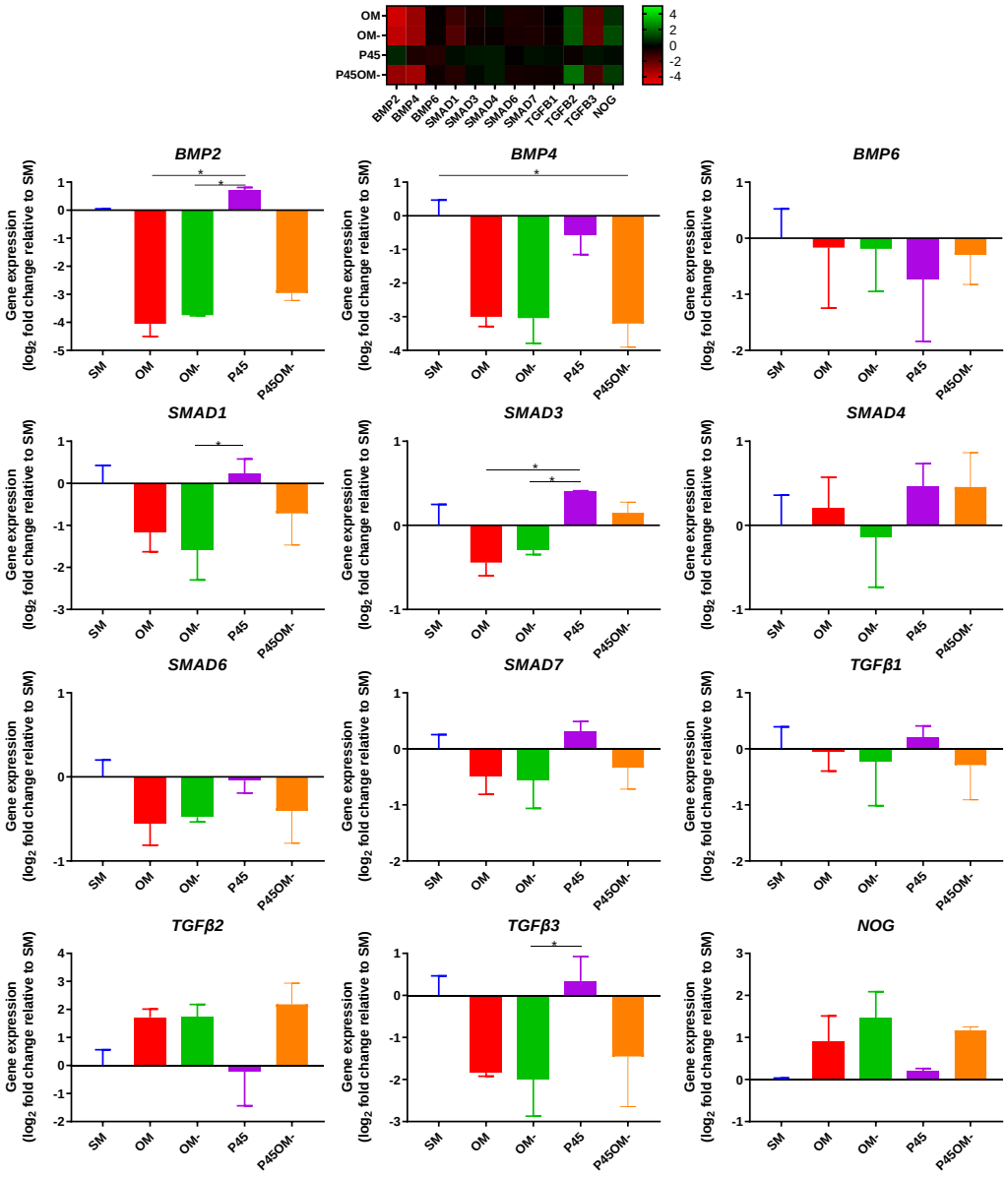


Figure 6.10. hMSC TGFβ and BMP gene expression after 11 days of P45 and P45OM- treatment normalized to SM control. *p<0.05 (n=2).

6.3.3.2.6 Wnt markers

Wnt markers were observed for changes in expression after 11 days of treatment with the dissolution products of P45 in SM or OM- (Figure 6.11). Wnt co-receptors (*LRP5, LRP6, FZD1* and *ROR2*), ligands (*WNT5A*, *WNT10B*), inhibitor *SFRP1* and transcriptional activator *CTNNB1* were observed for changes in expression. P45 treatment revealed no significant changes to gene expression compared to the SM control. P45OM- treatment significantly increased *ROR2* expression compared to OM- and the SM control. P45OM- also increased *WNT10B* expression compared to the SM control, showing similar levels of expression to that of OM-.

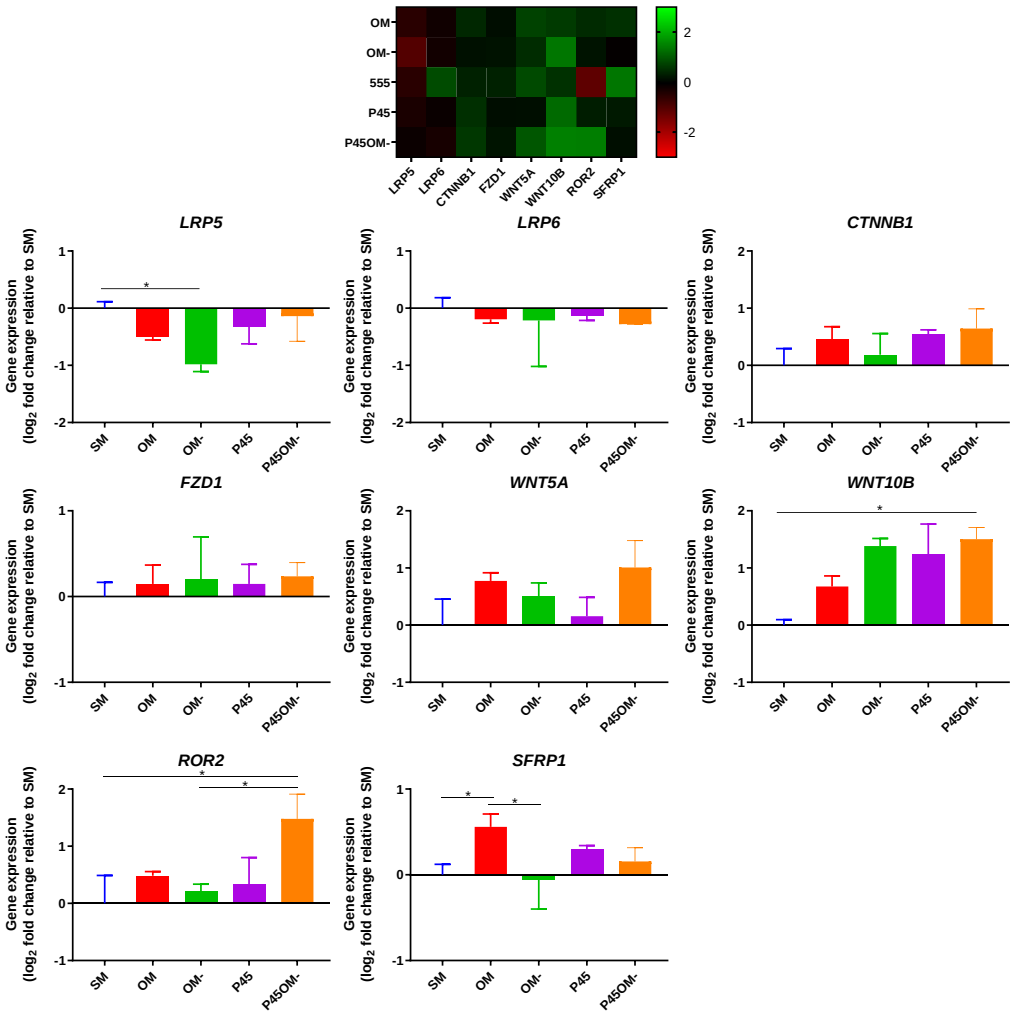


Figure 6.11. hMSC Wnt gene expression after 11 days of P45 and P45OM- treatment normalized to SM control. *p<0.05 (n=2).

6.4 Discussion

Previous chapters demonstrated the cytotoxic effects of high degradation rate owing to high phosphate content when released onto hMSC. Rescue of the phosphate treated cells was possible through high-ratio (90:10%) mixing with a slower degrading formulation (P40) or as previously shown, high doses of calcium or magnesium (5 mM of $CaCl_2$ and $MgSO_4$). Manufacturing fully porous microspheres was not successful for the P50 formulations investigated previously, which was suggested to be due to the higher viscosity of those PBG formulations, which inhibited the escape of gas released from porogen decomposition before the molten particles had cooled. This study investigated the effects of a 5% substitution of phosphate for calcium (P50Ca25Mg25 to P45Ca30Mg25) on manufacturing fully porous microspheres with interconnected pore generation and their effects on cell cytotoxicity and osteogenic differentiation.

6.4.1 Material characterization

Compositional analysis via EDX confirmed the P45 to be within 1-2% of the target formulation. The amorphous nature of the P45 formulation was also confirmed through XRD from the absence of any sharp crystallization peaks. Thermal analysis revealed a T_g and T_c onset at 565 °C and 625 °C, suggesting greatly increased glass stability, which was likely due to some integration of magnesium oxide into the phosphate backbone. Sahar and Abidin (1994) demonstrated increasing relative density with increasing MgO content in the $(70\text{-}x)P_2O_5{\cdot}30CaO{\cdot}(0+x)MgO$ (x=0-35) PBG system. Additionally, Ahmed et al. (2010) demonstrated decreasing degradation rate of PBGs with increasing MgO content and attributed this to the Mg^{2+} ions ability to integrate into the PBG as a network former due to the lower coordination number (4) compared to Ca^{2+} (6) (Sahar and Kamaruddin, 1996). Patel et al. (2017) demonstrated that Mg-O bonds demonstrate a significantly shorter bond length than Ca-O bonds,

therefore, the potential integration of Mg^{2+} into the phosphate chain backbone would result in a more stable, slower degrading PBG. Finally, a 45% Q^1 and 55% Q^2 species distribution was identified compared to the previously observed 6% Q^1 and 94% Q^2 of the P50Ca25Mg25 formulation which suggested greater depolymerization of the phosphate network due to the 5% substitution of phosphate content for calcium (Ahmed et al., 2010).

Interestingly, the 5% decrease in phosphate content from the P50 formulations likely decreased the viscosity previously seen, correlating with the study by Parsons et al. (2010) who demonstrated increasing viscosity with increasing phosphate content in the $(40+x)P_2O_5{\cdot}16CaO{\cdot}24MgO{\cdot}(20-x)Na_2O$ (x=0-20) PBG system. This decrease in viscosity likely allowed for formation of external, surface level interconnected pores due to the escape of entrapped porogen before solidification of the glass microsphere.

6.4.2 Effects of indirect treatment of PBG on hMSC

Indirect porous P45 treatment demonstrated promotion of metabolic activity in hMSC compared to both the SM and OM controls. P45 treatment significantly increased ALP activity compared to the SM treatment, and when combined with OM- media (P45OM-), demonstrated significant increases in ALP activity over the OM- and OM controls. However, despite the significant promotion of ALP activity observed, no changes to ALZ stain intensity were seen suggesting some inhibition of matrix mineralization activity.

A 5% reduction in phosphate content and increase in calcium content from P50Ca25Mg25 to P45, demonstrated a significant change to the effect of PBG dissolution products on hMSC. Where P50Ca25Mg25 revealed detrimental effects on the cell monolayer, P45 promoted cell metabolic activity beyond that of the SM

control, even with greater surface area and thus increased degradation rates due to its porous nature. As demonstrated by Abou Neel et al. (2014), glasses with lower solubility through titanium doping better supported cell growth with human osteosarcoma cells when cultured both indirectly or directly on PBG discs. Uo et al. (1998) also noted decreases in cytotoxicity of human dental pulp cells when solubility of PBG was decreased. Ahmed et al. (2004) also demonstrated the degradation profiles of a similar PBG formulation ($P_2O_5{\cdot}CaO{\cdot}Na_2O$), where phosphate content was fixed at 45, 50 and 55% and calcium and sodium content were substituted. Ahmed et al. (2004) noted significantly increased solubility from the formulations fixed at 50% phosphate content compared to the 45% phosphate content formulations. Additionally, increases in calcium (30-40%) further decreased the solubility observed. These studies correlate with the data presented in this study, as a 5% substitution of phosphate content for calcium greatly decreased the observed cytotoxicity. The negative effect of high phosphate content in PBG and thus increased solubility on cell toxicity noted in this and various other studies was likely due to the increases in phosphate content released, known for its induction of apoptosis. This was also demonstrated by Magne et al. (2003) and Meleti et al. (2000), who showed the concentration dependent apoptotic activity of phosphate (1-7 mM) on osteoblast like cells, particularly in the presence of calcium (2.4 mM, with ATDC5 cells).

Interestingly, P45 demonstrated significant promotion to ALP activity despite the suggested competitive inhibition of inorganic phosphate on ALP activity by Dean (2002). Furthermore, despite this significant ALP activity, no matrix mineralization was observed. The substantial distribution of pyrophosphate in the P45 formulation (55% Q^2) likely promoted ALP protein activity while inhibiting matrix mineralization. Inorganic pyrophosphate is a known inhibitor of matrix mineralization due to its ability to sequester calcium and bind to mineralization sites, preventing hydroxyapatite

formation and integration into the collagen matrix (Addison et al., 2007; Fleisch and Bisaz, 1962). Paradoxically, pyrophosphate is known to promote its own cleavage through upregulation of ALP expression (Pujari-Palmer et al., 2016; Xu et al., 1991). Furthermore studies such as those done by Grover et al. (2013) demonstrated that pyrophosphate in cement matrix (28 wt% calcium pyrophosphate using β-TCP, orthophosphoric acid and pyrophosphoric acid) did not inhibit mineralization *in vivo*, but instead promoted it. It was suggested that this occurred due to the simultaneous promotion of ALP activity which counteracted its mineralization inhibitory nature. In contrast, this study observed no matrix mineralization despite significant ALP activity. This could be explained due to difference in timepoint and model as the study by Grover et al. (2013) was carried out in sheep over 12 months with increases over the control not seen before 12 months. It is likely then that the lack of matrix mineralization observed in this study was caused by a combination of two issues: i) the increased ALP activity was insufficient to counteract the high levels of pyrophosphate present at the tested time point and ii) osteogenic differentiation had not progressed sufficiently to allow for matrix mineralization.

Porous P45 PBG microspheres demonstrated strong potential for promoting metabolic and ALP activity, beyond that of all previously tested formulations. Despite this matrix mineralization was still attenuated, likely in part due to the high pyrophosphate content. Further exploration of the gene expression on day 11 using TLDAs was conducted to help elucidate the cause of inhibition of matrix mineralization activity.

6.4.3 Effects of indirect treatment on hMSC gene expression

6.4.3.1 Proliferation markers

Indirect P45 treatment on hMSC for 11 days showed no changes to proliferation genes compared to the SM control. P45OM- treatment only showed a significant increase to *PCNA* expression compared to the SM control. Significant increases to metabolic activity were seen in P45 treated samples compared to the SM control while P45OM- treated samples did not demonstrate a significant change from SM. These results contrast with the changes to proliferative gene expression, suggesting increases in metabolic activity but not cell proliferation.

6.4.3.2 Integrin markers

Indirect P45 treatment caused no significant changes to integrin gene expression on day 11. P45OM- demonstrated increases to *ITGA3*, at similar levels to OM treated cells, compared to SM. Clover et al. (1992) demonstrated *in situ*, the high levels of β1 (ITGB1) and α3 (ITGA3) in osteoblast cells. The data presented here however showed a lack of significant *ITGB1* expression which suggested an inconclusive change to the promotion of integrin activity in the P45OM- treatment despite the increases to *ITGA3* seen, as β1 subunits as well as α subunits are required for the formation of functional integrin heterodimers (Brakebusch and Fässler, 2005). It is possible however, for calcium ions to bind to and promote integrin protein activation as highlighted by Xiong et al. (2002).

6.4.3.3 Osteoblastic markers

Indirect P45 treatment caused no significant changes to osteoblastic gene expression compared to the SM control. P45OM- treatment showed a significant decrease in *MSX2* expression compared to OM- treated cells, demonstrating levels of expression similar to that of the untreated SM control. P45OM- also demonstrated significant

increases to *PPAR-γ* and *ALPL* expression as well as decreases to *BGLAP* expression compared to the SM control.

As noted previously, *PPAR-γ* is not an osteoblastic marker, but an adipogenic marker. Its upregulation in osteogenic differentiation is unusual due to the antagonistic nature of the two lineages (Zhuang et al., 2016). The use of dexamethasone, a known promoter of *PPAR-γ*, is likely the cause of the increases in expression seen in OM, OM- and P45OM- treated samples. Studies such as Ghali et al. (2015) utilize 100 nM dexamethasone while still demonstrating an osteogenic phenotype. Regardless, it is unlikely that P45 contributed to the increases to *PPAR-γ* as P45 showed no significant increases to expression while P45OM- treatment showed similar levels of expression compared to OM and OM- treatments.

ALPL expression was not significantly altered in P45 treated samples while a significant increase was seen in P45OM- treated samples compared to the SM control. This data contrasts with the ALP activity data seen when hMSC were treated with P45 and P45OM-. P45 treated cells demonstrated significant increases to ALP activity compared to SM, yet no significant increases to *ALPL* gene expression were observed. Conversely, P45OM- treated cells demonstrated significant increases in ALP activity compared to SM, P45, OM- and OM treatments while *ALPL* gene expression showed similar levels of expression to that of OM and OM-, suggesting little contribution from P45 to the promotion of *ALPL* expression at the timepoint analysed. This contrasting data can be explained by the high levels of pyrophosphate within the P45 formulation. Pujari-Palmer et al. (2016) demonstrated a biphasic pattern to ALP promotion in MC3T3 cells when treated with increasing doses (0-1000 μM) of sodium pyrophosphate, showing increases in activity at 0.1 μM and 100 μM. However, increases in *ALP* gene expression were only observed at the 0.1 μM dose. Pyrophosphate was shown to increase either

or both *ALP* expression and enzymatic activity depending on the dose, which may explain the contrasting results of gene expression and enzymatic activity within this study.

BGLAP is a notable marker for osteoblast differentiation. It plays a role in the inhibition of hydroxyapatite formation (Ducy et al., 1996; Price et al., 1976). Ducy et al. (1996) demonstrated that osteocalcin null mice resulted in increased bone mass and quality. Tsao et al. (2017) demonstrated significant increases to *BGLAP* expression only at day 21 of hMSC in OM. Similarly, a significant spike in *BGLAP* expression is seen in murine MC3T3-E1 cells after 21 days of culture with PBG fibres ($50P_2O_5{\cdot}40CaO_5{\cdot}5Na_2O{\cdot}5Fe_2O_3$) in OM media. Decreased levels of *BGLAP* expression observed were not unusual due to its noted late stage role in osteoblast expression (Rutkovskiy et al., 2016; Tsao et al., 2017). Further timepoints may confirm the late stage upregulation of *BGLAP* in P45 treated cells. Chapter 3 and 5 suggested that high levels of calcium (5 mM) may play a role in the upregulation of *BGLAP* and *SPP1* which contribute to the binding and build-up of calcium phosphate in culture leading to a false positive ALZ stain. The suggested decreased degradation profile of P45 due to 5% phosphate for calcium substitution, evidenced by significantly enhanced cell survival, would release less calcium into the media. The lack of *BGLAP* and *SPP1* expression further supports the hypothesis that high levels of calcium released from PBGs can cause their upregulation.

P45 treatment demonstrated no significant alterations of osteoblastic gene expression at day 11 of treatment while P45OM- displayed levels of expression similar to that of OM- treated cells, suggesting little contribution of P45 to the observed changes in gene expression. Ultimately, P45, either in SM or OM-, did not significantly impact osteoblastic gene activity however, further experimentation may be required to conclusively state the effect of P45 on ALP due to effects pyrophosphate has on both

ALP gene expression and enzymatic activity. Pyrophosphate has also been demonstrated to strongly inhibit matrix mineralization (Addison et al., 2007; Pujari-Palmer et al., 2016) and as such, quantification of protein and pyrophosphate content may help further optimize PBG formulations in the future through the tailoring of pyrophosphate release profiles. Reduction of pyrophosphate content or slower degradation rates may result in less inhibition of matrix mineralization.

6.4.3.4 Notch markers

P45 treatment showed no significant changes to Notch gene expression compared to the SM control while P45OM- treatment demonstrated increases to *NOTCH1* and *NOTCH2* expression compared to the OM- control, suggesting contribution of the P45 degradation products to the promotion of *NOTCH1* and *NOTCH2* gene expression. *NOTCH1* and *NOTCH3* also demonstrated increased levels of expression when treated with P45OM- compared to the SM control. Deregowski et al. (2006) has demonstrated that overexpression of *NOTCH1* in murine ST2 stromal cells suppressed osteoblast differentiation through inhibition of Wnt/β-catenin signalling, likely through the destabilization of β-catenin or inhibition of its transactivating potential (Zanotti and Canalis, 2016). P45OM- demonstrates the strong promotion of Notch receptors, and no significant upregulation of *DLL3* which acts as an antagonist to the Notch pathway (Ladi et al., 2005). The promotion of the Notch pathway through upregulation of its receptors would have negative consequences for osteogenic differentiation through the suppression of β-catenin stabilization and inhibition of RUNX2 by Notch target genes, *HEY1* and *HES1* (Deregowski et al., 2006; Lin and Hankenson, 2011). The data presented in this chapter suggests that P45OM- treatment strongly promotes Notch signalling which may have negative impacts on osteogenic differentiation.

6.4.3.5 TGF-β and BMP markers

P45 treatment on hMSC revealed no significant changes to TGF-β and BMP gene expression compared to the SM control. Similarly, P45OM- demonstrated no significant changes to expression compared to the OM- control. P45OM- did show significant downregulation of *BMP4* however, this level of expression was similar to that of OM and OM- suggesting minimal contribution of P45 to the change in expression. Maeda et al. (2004) showed that *BMP4* was upregulated in late stage mature murine osteoblasts 24+ days into culture. Further timepoints may confirm increases in expression during osteoblast maturation.

6.4.3.6 Wnt markers

P45 treatment demonstrated no significant changes to Wnt gene expression compared to the SM control. P45OM- showed significant upregulation of *ROR2* compared to OM- as well as significant upregulation to *WNT10B* and *ROR2* compared to the SM control.

WNT10B upregulation is known to inhibit adipogenesis while stimulating osteoblastogenesis (Ross et al., 2000). Furthermore, Bennett et al. (2005) showed that transgenic mice expressing *WNT10B* decreased the accumulation and development of adipose tissue while promoting increased bone mass and density. However, Cawthorn et al. (2012) demonstrated through retroviral expression in ST2 cells, the ability of *WNT10B* to promote osteoblast differentiation through a β-catenin dependent mechanism. No significant increases in β-catenin were observed, furthermore the previously seen *NOTCH1* receptor upregulation would be anticipated to inhibit any remaining β-catenin activity through Notch target gene *HES1* activity as suggested by Zanotti and Canalis (2016).

Billiard et al. (2005) demonstrated changes in the levels of *ROR2* expression in various cell lines that represented stages of human osteoblast differentiation. A biphasic pattern of *ROR2* activation was observed, with pre-osteoblasts demonstrating a 1-fold increase in expression, early osteoblasts demonstrating next to no increases in expression and late osteoblasts demonstrating a 0.6-fold increase in expression. The data presented here demonstrated a 1.4-fold increase in *ROR2* expression compared to the SM control, approaching the pattern of expression seen in pre-osteoblasts. Billiard et al. (2005) suggested that WNT1 or WNT3 mediated ROR2 activation caused the initiation of an unidentified signalling cascade and that potentially inhibited β-catenin stabilization due to the sequestering of Wnt ligands away from typical LRP-FZD receptor mediated pathways.

Previous chapters suggested that high concentrations of calcium may be upregulating *SFRP1* gene expression which in turn inhibits ALP activity (Yao et al., 2010). The suggested decreased solubility of the P45 formulation compared to the P50Ca50 would therefore likely release less calcium into medium. As demonstrated in this chapter, P45 treatment in SM or OM- did not promote the expression of *SFRP1*, further suggesting the necessity of high levels of calcium in the promotion of this gene.

Taken together, P45OM- treatment could result in attenuation of β-catenin related pathways through inhibition of stabilizing mechanisms required for downstream β-catenin activity. This in combination with the upregulation of β-catenin attenuation activity by the Notch pathway may contribute to the lack of matrix mineralization observed, despite the high levels of ALP activity seen.

6.5 Summary

Material analysis of the P45 formulation revealed a higher T_g and T_c onset, likely due to magnesium acting as an intermediary oxide, integrating itself into the phosphate chain backbone, leading to the creation of a more durable structure. A large shift from Q^2 to Q^1 was also observed in the P45 formulation (45% Q^1 and 55% Q^2), likely due to increased depolymerization of the phosphate network by calcium and magnesium. The previous chapter highlighted the impact of high viscosity on the spheroidization procedure, resulting in the entrapment of decomposing porogen within the viscous glass. As suggested by the literature, decreases in phosphate content and increases in calcium content likely decreased the viscosity of the P45 formulation. This chapter has shown that by reducing the phosphate content, and likely viscosity, gas bubbles can now escape the microsphere surface before cooling and solidifying. This escape allows for the generation of interconnected pores that are not solely internalized as previously observed with the P50 formulations.

Decreasing phosphate content by 5% showed significant improvements over the previous formulations in both material and cell survival capacity. Indirect treatment of hMSC with P45 conditioned media revealed a strong promotion of metabolic and ALP activity but no promotion of matrix mineralization. The osteogenic effects were likely due to the abundance of pyrophosphate within the P45 formulation which is known to both inhibit matrix mineralization and promote ALP activity. The increases to activity alone were likely insufficient to clear the collagen matrix of bound pyrophosphate, impacting any potential matrix mineralization. Gene expression analysis revealed that the dissolution products from P45 significantly promoted ALP activity yet caused minimal changes to *ALP* gene expression. This corelated with literature which demonstrated that high levels of pyrophosphate (100 µM) may promote ALP protein activity but not gene expression. Treatment with P45OM- demonstrated the

upregulation of genes which suggest the strong attenuation of β-catenin stabilization mechanisms. The ubiquitination of β-catenin would prevent downstream genes such as *RUNX2* from being upregulated, likely contributing to the lack of matrix mineralization activity observed.

The data presented in this study further demonstrated the impact of high calcium levels on hMSC gene expression. Correlating with the data presented in chapter 3 and 5, it is likely that calcium (5 mM) promotes the expression of matrix proteins *BGLAP* and *SPP1*, along with the Wnt antagonist *SFRP1*. The promotion of *BGLAP* and *SPP1* may lead to interference with the ALZ assay while *SFRP1* has been demonstrated in the literature to strongly inhibit the Wnt pathway and may further contribute to the attenuation of β-catenin stabilization.

This study highlighted a number of key issues involved with the promotion of osteogenic differentiation with PBGs. The levels of pyrophosphate were demonstrated to be of critical importance, with excess released into medium resulting in lack of ALP upregulation and even inhibition of matrix mineralization. Furthermore, it is likely that high levels of calcium (5 mM) promote *SFRP1*, *BGLAP* and *SPP1*. Ultimately, the P45 formulation demonstrated no matrix mineralization, likely in part due to the overabundance of pyrophosphate but also due to the potential promotion of β-catenin degradation through Notch upregulation, leading to attenuation of critical osteoblastic proteins such as RUNX2.

Chapter 7 - Final Discussion

There is increasing interest in the utilization of PBGs in bone regeneration due to their tailorable degradation rates and similar composition to the inorganic phase of bone (Hoppe et al., 2011). Increasing evidence demonstrates that the ionic dissolution products from PBGs have the capacity to drive the differentiation process of hMSCs (Barradas et al., 2012; Murphy et al., 2014). This thesis aimed to demonstrate the biological impact of PBGs on hMSC and how they may regulate gene expression. This was investigated using *in vitro* testing of PBG precursor compounds, PBG dissolution products, direct seeding onto PBG disc surface and gene expression analysis utilizing TaqMan Low Density Arrays (TLDAs).

7.1 Possible role of PBGs in β-catenin destabilization

Treatment of hMSC with high concentrations of calcium in the 555 treatment (5 mM) and MixOM- treatment (10% P50Ca50) demonstrated significant upregulation of *SFRP1*. SFRP1 is a Wnt antagonist that binds to Wnt ligands, preventing them from binding to their receptor and subsequently resulting in the inhibition of β-catenin stabilization (Yao et al., 2010). Treatment with the dissolution products of all tested PBG formulations (P40, Mix and P45) demonstrated upregulation of various Notch receptors (*Notch1*, *Notch2* and *Notch3*) when in OM- compared to the SM or OM- control. Notch signalling promotes the upregulation of its target gene *HES1* which has been noted to act as a repressor for β-catenin mediated transcription (McLarren et al., 2001). The data presented in this thesis suggests that PBG dissolution products strongly promote destabilization of the β-catenin protein through two distinct mechanisms; i) upregulation of SFRP1 and ii) Notch signalling which are detailed below and illustrated in Figure 7.1.

β-catenin plays a key role in osteoblast differentiation and its inhibition has been demonstrated to attenuate osteogenic differentiation and bone formation (Glass and Karsenty, 2006; Marie, 2008). The canonical Wnt signalling pathway functions to promote the survival and action of the β-catenin protein. Wnt ligands bind to Frizzled (FZD) and low-density lipoprotein receptor (LRP) coreceptors and inhibit the GSK3 destruction complex which works to phosphorylate β-catenin. In the absence of phosphorylation by the GSK3 destruction complex, β-catenin does not get ubiquitinated, resulting in its survival (Shares et al., 2018). β-catenin is then translocated to the nucleus where it binds to LEF/TCF transcription factors which work to promote expression of key osteogenic factors such as RUNX2 (Gaur et al., 2005; Shares et al., 2018). This pathway is illustrated in Figure 7.1A.

SFRP1 acts as an antagonist to the canonical Wnt pathway by binding to Wnt proteins and inhibiting their activation (Bovolenta et al., 2008). Studies such as those done by Yao et al. (2010) and Bodine et al. (2004) demonstrated the negative impact *SFRP1* has on bone density, osteoblast maturation markers and ALP activity. Calcium has been integrated in PBG for its capacity to act as a modifier oxide but also due to the proposed benefits of calcium for osteogenic differentiation (Hoppe et al., 2011; Maeno et al., 2005). Whilst studies such as Lin et al. (2020) have demonstrated increased osteogenic differentiation in calcium containing PBG formulations, the ALP and gene expression data presented here suggests that high concentrations of calcium may contribute to the upregulation of *SFRP1* and thus the inhibition of osteogenic differentiation as illustrated in Figure 7.1B.

Notch plays a key role in determining cell fate and function. The activation of Notch receptors leads to their cleavage by the γ-secretase complex and the subsequent release of the Notch intracellular domain (NICD) (Zanotti and Canalis, 2016). The NICD

is then translocated to the nucleus and binds to mastermind-like (Maml), promoting Notch target genes, *HEY* and *HES1* (Lin and Hankenson, 2011). These genes have been demonstrated to ablate RUNX2 transcription thought he inhibition of β-catenin activity within the Wnt pathway (Deregowski et al., 2006; Hilton et al., 2008; Zamurovic et al., 2004). All tested PBG microspheres (P40, Mix and P45) within this study demonstrated some promotion of Notch receptor expression when in a pro-osteogenic environment, with only MixOM- demonstrating potential Notch signalling attenuation through the upregulation of Notch antagonist DLL3.

This study highlights the previously unexplored destabilization of β-catenin though application of PBG dissolution products and the two mechanisms by which this may occur. Confirmation of SFRP1 mediated Wnt inhibition may be achieved using calcium doses or dissolution products of PBG with increasing calcium content, delivered to hMSC where fluorescent protein tagged β-catenin, western blotting or immunofluorescence may be used to quantify or localize the protein content (Flozak et al., 2016; Kafri et al., 2016; Tan et al., 2014). Confirmation of Notch mediated β-catenin attenuation may be achieved using qRT-PCR analysis to quantify Notch target genes and Wnt target genes as well as quantifying and observing β-catenin localization as described previously (Regan and Long, 2013).

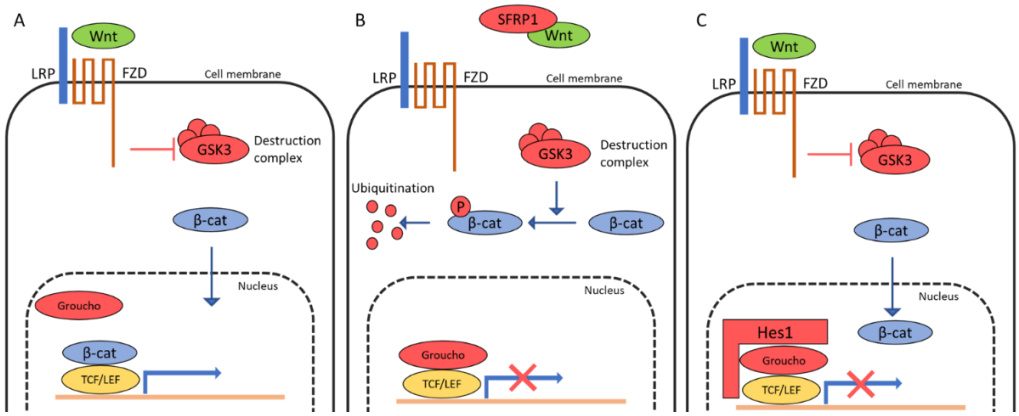


Figure 7.1. Illustration demonstrating (A) The successful activation of the Wnt pathway through the binding of a Wnt ligand to the LRP-FZD coreceptors resulting in the inhibition of the GSK3 destruction complex and accumulation of β-catenin (β-cat) in the nucleus which binds to TCF/LEF and promotes gene transcription. (B) The proposed mechanism of PBG mediated β-catenin destabilization through the binding of Wnt ligands by SFRP1, preventing them from activating the LRP-FZD coreceptors resulting in the phosphorylation and destruction of β-catenin (β-cat) by the GSK3 destruction complex. (C) The second proposed mechanism of PBG mediated β-catenin destabilization through the binding of the Notch target gene Hes1 to Groucho, preventing the accumulated β-catenin (β-cat) from Wnt signalling from promoting transcription.

7.2 Pyrophosphate and its role in matrix mineralization

The data presented here demonstrated that excess levels of phosphate anions can cause significant cell death when applied to hMSC at high doses (>1.25 mM). Chapter 3 demonstrated that this toxicity can be mitigated by doses of calcium and magnesium (5 mM). PBGs that contain less phosphate content and increased modifier oxides (MOs) such as calcium or magnesium would result in slower degradation profiles as increased depolymerization occurs with the addition of further MOs (Ahmed et al., 2018). Slower degrading PBGs would release less phosphate anions into medium whose minimized toxic effect can be further attenuated by the increased calcium and magnesium concentration.

This study demonstrated with the P40 (51% Q^1) and P45 (45% Q^1) formulation that ALP activity was significantly upregulated in the pro-osteogenic environment of OM- yet demonstrated no matrix mineralization activity. Studies have demonstrated the inhibition of pyrophosphate on hydroxyapatite formation though the blocking of matrix mineralization sites and the sequestration of calcium (Addison et al., 2015; Orriss et al., 2016). This inhibitory activity can be reversed though pyrophosphate hydrolysis by ALP to produce orthophosphate units which can be incorporated into the collagen matrix (Omelon et al., 2009; Orimo, 2010; Xu et al., 1991). Orimo (2010) suggested that the ratio of pyrophosphate and orthophosphate units may play a key role in determining successful matrix mineralization due to the ability of pyrophosphate to block matrix mineralization sites. This correlates with the study by Pujari-Palmer et al. (2016) who demonstrated that pyrophosphate may promote ALP activity and gene expression. Taken together, it is likely that pyrophosphate in culture may promote some ALP activity, however, excess pyrophosphate may saturate ALP enzyme capacity, preventing all pyrophosphate from being removed from the matrix. The high Q^1 content of the P40 and P45 formulations suggests possible contribution of

pyrophosphate ions released which may promote ALP activity whilst inhibiting matrix mineralization sites due to oversaturation. Additionally, it should be noted that other phosphate species released from PBGs such as polyphosphate and metaphosphate may contribute to the observed effects on hMSC. Many studies demonstrate that polyphosphates showed a comparable mineralization inhibiting effect to that of pyrophosphates (Hoac et al., 2013; Leyhausen et al., 1998; Omelon et al., 2013; Omelon and Grynpas, 2011), however, recent studies demonstrate polyphosphate mediated β-catenin upregulation that was similarly seen in the MixOM- formulation which contains 10% P50Ca50 (5% Q^1 and 95% Q^2) suggesting some contribution of polyphosphates to the upregulation of this gene (Ardeshirylajimi et al., 2018).

7.3 PBG design for adhesion or osteogenic differentiation

While significantly lower cell counts were observed with hMSC seeded directly onto the P40 PBG disc compared to the slower degrading P30 formulation, indirect assays with P40, P35 and P30 revealed minimal changes to cell metabolic or osteogenic activity compared to the undifferentiated control. Additionally, indirect P40 treatments demonstrated no significant downregulation of integrin gene expression. This study correlates with others in the literature indicating superior cell adhesion with decreasing solubility of the PBG formulation (Navarro et al., 2003b; Skelton et al., 2007b). However, this study also highlighted the disconnect between cell adhesion on faster degrading formulations (P40) and the impact of their dissolution products on metabolic and osteogenic activity. While a PBG formulation may behave in biocompatible or even pro-osteogenic manner when indirectly tested with PBG dissolution products, direct culture on the PBG surface may result in significant cell loss depending on the dissolution rate of the formulation. Furthermore, whilst calcium and magnesium ions released from the P40, P35 and P30 formulations may interact with and promote integrin mediated adhesion, the reductions of phosphate content in the P35 and P30 formulations could result in a decreased degradation profile and thus release less calcium and magnesium ions into the culture media (Tharmalingam and Hampson, 2016; Xiong et al., 2002). Ultimately, it was likely that the degradation of the glass disc surface itself caused detachment and loss of cells from the PBG surface (Navarro et al., 2003b). This disconnect poses a problem for the design of PBG microspheres for the promotion of osteogenic differentiation and bone growth, due to the conflicting goals of providing the cell sufficient dissolution products required to elicit a biological response and designing a PBG formulation with a slow enough degradation profile to support cell adhesion. This hypothesis correlated with the data presented by Abou Neel et al. (2014) who demonstrated the culture of human

osteosarcoma (HOS) cells on glass discs with increasing titanium content ($50P_2O_5 \cdot 30CaO \cdot (20\text{-}x)Na_2O \cdot (x)TiO$, x=0, 5, 10 and 15). It was demonstrated that while glasses with titanium content (and thus lower solubility) provided a more stable surface for cell adhesion and growth, all glasses with titanium demonstrated no significant changes to osteoblastic genes or ALP activity compared to the tissue culture plastic control.

The data presented here also highlighted the previously unexplored potential of PBG microsphere mixing. Utilizing P50Ca50 and porous P40 in a 10:90 mix allowed for significant cell survival whilst increasing the calcium content released from the microsphere mix. Likewise, utilization of two distinct PBG formulations, a slow degrading PBG to act as a cell scaffold and fast degrading PBG for enhanced ion release in combination may alleviate the disconnect observed when attempting to design a single PBG formulation for conflicting goals.

7.4 Future work

The data presented here highlights key challenges within PBG development for tissue engineering applications that had previously not been explored. Future optimizations to the PBG formulation may aim to tackle these issues to develop a formulation that elicits a stronger osteogenic response. Pyrophosphate content release may be reduced through the decrease of PBG solubility, through the addition of titanium or decreasing Q^1 content though reductions in phosphate content. An investigation into the use of lithium as a MO may prove to be an interesting solution to the observed promotion of β-catenin destabilization genes, due to lithium's demonstrated ability to inhibit the GSK3 destruction complex (Li et al., 2017). The GSK3 destruction complex is the major enactor of β-catenin destabilization through phosphorylation, and its inhibition may result in less attenuation by SFRP1 and increased accumulation of β-catenin in the nucleus. Exploration of a secondary, slower degrading formulation to act as a cell scaffold may provide a more suitable surface for cell adhesion.

Measurement of osteogenic activity for cells treated with PBG dissolution products proved to be challenging due to the demonstrated blocking of matrix mineralization though potential pyrophosphate and polyphosphate activity as well as transcriptional upregulation of matrix proteins *BGLAP* and *SPP1*. While blocking of matrix mineralization may mask potential osteogenic activity, *BGLAP* and *SPP1* could promote the detection of false positives through their affinity for calcium, resulting in the build-up of non-biological deposition (Sage et al., 2011; Zoch et al., 2016). Utilization of a non-calcium based osteogenic assay such collagen staining using sirius red (Nie et al., 2016) or osteonectin immunocytochemistry stains (Junker et al., 2010) may help elucidate the contribution of PBGs to osteogenic differentiation despite any mineralization blocking activity that may be present. Protein quantification of ALP through protein quantification kits or western blotting may also help identify the

contribution of PBG dissolution products to ALP protein activity while alleviating the concerns of the ALP and ALZ assays (Pujari-Palmer et al., 2016; Yamaza et al., 2018). Finally, while gene expression analysis is a useful tool for identifying PBG mediated gene expression changes within the cells, validation of post-transcriptional protein levels would confirm the effects of the gene expression changes observed. Immunocytochemistry or western blotting may help identify the changes in protein levels and combining these with gene expression data would generate stronger evidence of the effects of PBG dissolution products on osteogenic activity.

7.5 Final conclusions

This thesis has demonstrated novel findings into the effect of PBG on mesenchymal progenitors. PBG dissolution treatments demonstrated promotion β-catenin destabilization through Notch signalling and *SFRP1* upregulation, which in turn inhibits osteogenic differentiation through inhibition of β-catenin mediated *RUNX2* upregulation and activity. Additionally, pyrophosphate was demonstrated to likely act as a double-edged sword, both promoting ALP activity while inhibiting matrix mineralization when oversaturated, suggesting that a potential balance between pyrophosphate and orthophosphate that must be met to promote an overall net positive effect on matrix mineralization. Microsphere mixing was demonstrated to be a novel approach in developing and optimizing PBG microspheres for different functions in a unified goal of promoting both a surface for cell adhesion and dissolution products for differentiation. Taken together the results present a strong foundation for the development of next generation PBG formulations that could promote osteogenic differentiation and bone growth.

References:

Abou Neel, E.A., Chrzanowski, W., Knowles, J.C., 2014. Biological performance of titania containing phosphate-based glasses for bone tissue engineering applications. Mater. Sci. Eng. C 35, 307–313. https://doi.org/10.1016/j.msec.2013.10.029

Abou Neel, E.A., Mizoguchi, T., Ito, M., Bitar, M., Salih, V., Knowles, J.C., 2007. In vitro bioactivity and gene expression by cells cultured on titanium dioxide doped phosphate-based glasses. Biomaterials 28, 2967–2977. https://doi.org/10.1016/j.biomaterials.2007.03.018

Abou Neel, E.A., Pickup, D.M., Valappil, S.P., Newport, R.J., Knowles, J.C., 2009. Bioactive functional materials: a perspective on phosphate-based glasses. J Mater Chem 19, 690–701. https://doi.org/10.1039/B810675D

Acampora, D., Merlo, G.R., Paleari, L., Zerega, B., Postiglione, M.P., Mantero, S., Bober, E., Barbieri, O., Simeone, A., Levi, G., 1999. Craniofacial, vestibular and bone defects in mice lacking the Distal-less-related gene Dlx5. Development 126, 3795–3809.

Adams, C.S., Mansfield, K., Perlot, R.L., Shapiro, I.M., 2001. Matrix Regulation of Skeletal Cell Apoptosis ROLE OF CALCIUM AND PHOSPHATE IONS. J. Biol. Chem. 276, 20316–20322. https://doi.org/10.1074/jbc.M006492200

Addison, W.N., Azari, F., Sørensen, E.S., Kaartinen, M.T., McKee, M.D., 2007. Pyrophosphate Inhibits Mineralization of Osteoblast Cultures by Binding to Mineral, Up-regulating Osteopontin, and Inhibiting Alkaline Phosphatase Activity. J. Biol. Chem. 282, 15872–15883. https://doi.org/10.1074/jbc.M701116200

Addison, W.N., Nelea, V., Chicatun, F., Chien, Y.-C., Tran-Khanh, N., Buschmann, M.D., Nazhat, S.N., Kaartinen, M.T., Vali, H., Tecklenburg, M.M., Franceschi, R.T., McKee, M.D., 2015. Extracellular matrix mineralization in murine MC3T3-E1 osteoblast cultures: an ultrastructural, compositional and comparative analysis with mouse bone. Bone 71, 244–256. https://doi.org/10.1016/j.bone.2014.11.003

Ahlin, C., Lundgren, C., Embretsén-Varro, E., Jirström, K., Blomqvist, C., Fjällskog, M.-L., 2017. High expression of cyclin D1 is associated to high proliferation rate and increased risk of mortality in women with ER-positive but not in ER-

negative breast cancers. Breast Cancer Res. Treat. 164, 667–678. https://doi.org/10.1007/s10549-017-4294-5

Ahmed, I., Lewis, M., Olsen, I., Knowles, J.C., 2004. Phosphate glasses for tissue engineering: Part 1. Processing and characterisation of a ternary-based P2O5–CaO–Na2O glass system. Biomaterials 25, 491–499. https://doi.org/10.1016/S0142-9612(03)00546-5

Ahmed, I., Lewis, M.P., Nazhat, S.N., Knowles, J.C., 2005. Quantification of Anion and Cation Release from a Range of Ternary Phosphate-based Glasses with Fixed 45 mol% P2O5. J. Biomater. Appl. 20, 65–80. https://doi.org/10.1177/0885328205049396

Ahmed, I., Parsons, A., Jones, A., Walker, G., Scotchford, C., Rudd, C., 2010. Cytocompatibility and effect of increasing MgO content in a range of quaternary invert phosphate-based glasses. J. Biomater. Appl. 24, 555–575. https://doi.org/10.1177/0885328209102761

Ahmed, I., Parsons, A., Rudd, C., Nazhat, S.N., Knowles, J., Guerry, P., Smith, M.E., 2008. Comparison of phosphate-based glasses in the range 50P2O5-(50 - X)CaO-xNa2O prepared using different precursors. Glass Technol. - Eur. J. Glass Sci. Technol. Part A 49, 63–72.

Ahmed, I., Ready, D., Wilson, M., Knowles, J.C., 2006. Antimicrobial effect of silver-doped phosphate-based glasses. J. Biomed. Mater. Res. A 79A, 618–626. https://doi.org/10.1002/jbm.a.30808

Ahmed, I., Ren, H., Booth, J., 2018. Developing Unique Geometries of Phosphate-Based Glasses and their Prospective Biomedical Applications. Johns. Matthey Technol. Rev. 63. https://doi.org/10.1595/205651319X15426460058863

Akino, K., Mineta, T., Fukui, M., Fujii, T., Akita, S., 2003. Bone morphogenetic protein-2 regulates proliferation of human mesenchymal stem cells. Wound Repair Regen. 11, 354–360. https://doi.org/10.1046/j.1524-475X.2003.11507.x

Allen, M.R., Burr, D.B., 2019. Chapter 5 - Bone Growth, Modeling, and Remodeling, in: Burr, D.B., Allen, M.R. (Eds.), Basic and Applied Bone Biology (Second Edition). Academic Press, pp. 85–100. https://doi.org/10.1016/B978-0-12-813259-3.00005-1

Aquino-Martínez, R., Artigas, N., Gámez, B., Rosa, J.L., Ventura, F., 2017. Extracellular calcium promotes bone formation from bone marrow mesenchymal stem cells by amplifying the effects of BMP-2 on SMAD signalling. PLoS ONE 12. https://doi.org/10.1371/journal.pone.0178158

Ardeshirylajimi, A., Golchin, A., Khojasteh, A., Bandehpour, M., 2018. Increased osteogenic differentiation potential of MSCs cultured on nanofibrous structure through activation of Wnt/β-catenin signalling by inorganic polyphosphate. Artif. Cells Nanomedicine Biotechnol. 46, S943–S949. https://doi.org/10.1080/21691401.2018.1521816

Babenko, L.P., Zholobak, N.M., Shcherbakov, A.B., Voychuk, S.I., Lazarenko, L.M., Spivak, M.Y., 2012. Antibacterial activity of cerium colloids against opportunistic microorganisms in vitro. Mikrobiolohichnyi Zhurnal Kiev Ukr. 1993 74, 54–62.

Baino, F., Hamzehlou, S., Kargozar, S., 2018. Bioactive Glasses: Where Are We and Where Are We Going? J. Funct. Biomater. 9. https://doi.org/10.3390/jfb9010025

Baldin, V., Lukas, J., Marcote, M.J., Pagano, M., Draetta, G., 1993. Cyclin D1 is a nuclear protein required for cell cycle progression in G1. Genes Dev. 7, 812–821. https://doi.org/10.1101/gad.7.5.812

Baron, R., Gori, F., 2018. Targeting WNT signaling in the treatment of osteoporosis. Curr. Opin. Pharmacol., • Respiratory • Musculoskeletal 40, 134–141. https://doi.org/10.1016/j.coph.2018.04.011

Baron, R., Kneissel, M., 2013. WNT signaling in bone homeostasis and disease: from human mutations to treatments. Nat. Med. 19, 179–192. https://doi.org/10.1038/nm.3074

Barradas, A.M.C., Fernandes, H.A.M., Groen, N., Chai, Y.C., Schrooten, J., van de Peppel, J., van Leeuwen, J.P.T.M., van Blitterswijk, C.A., de Boer, J., 2012. A calcium-induced signaling cascade leading to osteogenic differentiation of human bone marrow-derived mesenchymal stromal cells. Biomaterials 33, 3205–3215. https://doi.org/10.1016/j.biomaterials.2012.01.020

Beck, G.R., Zerler, B., Moran, E., 2000. Phosphate is a specific signal for induction of osteopontin gene expression. Proc. Natl. Acad. Sci. U. S. A. 97, 8352–8357.

Beederman, M., Lamplot, J.D., Nan, G., Wang, J., Liu, X., Yin, L., Li, R., Shui, W., Zhang, H., Kim, S.H., Zhang, W., Zhang, J., Kong, Y., Denduluri, S., Rogers, M.R., Pratt, A., Haydon, R.C., Luu, H.H., Angeles, J., Shi, L.L., He, T.-C., 2013. BMP signaling in mesenchymal stem cell differentiation and bone formation. J. Biomed. Sci. Eng. 6, 32–52. https://doi.org/10.4236/jbise.2013.68A1004

Bellido, T., 2014. Osteocyte-Driven Bone Remodeling. Calcif. Tissue Int. 94, 25–34. https://doi.org/10.1007/s00223-013-9774-y

Bennett, C.N., Longo, K.A., Wright, W.S., Suva, L.J., Lane, T.F., Hankenson, K.D., MacDougald, O.A., 2005. Regulation of osteoblastogenesis and bone mass by Wnt10b. Proc. Natl. Acad. Sci. U. S. A. 102, 3324–3329. https://doi.org/10.1073/pnas.0408742102

Bennett, J.H., Carter, D.H., Alavi, A.L., Beresford, J.N., Walsh, S., 2001. Patterns of integrin expression in a human mandibular explant model of osteoblast differentiation. Arch. Oral Biol. 46, 229–238. https://doi.org/10.1016/s0003-9969(00)00114-x

Berebichez-Fridman, R., Gómez-García, R., Granados-Montiel, J., Berebichez-Fastlicht, E., Olivos-Meza, A., Granados, J., Velasquillo, C., Ibarra, C., 2017. The Holy Grail of Orthopedic Surgery: Mesenchymal Stem Cells-Their Current Uses and Potential Applications. Stem Cells Int. 2017, 2638305. https://doi.org/10.1155/2017/2638305

Berebichez-Fridman, R., Montero-Olvera, P.R., 2018. Sources and Clinical Applications of Mesenchymal Stem Cells. Sultan Qaboos Univ. Med. J. 18, e264–e277. https://doi.org/10.18295/squmj.2018.18.03.002

Billiard, J., Way, D.S., Seestaller-Wehr, L.M., Moran, R.A., Mangine, A., Bodine, P.V.N., 2005. The Orphan Receptor Tyrosine Kinase Ror2 Modulates Canonical Wnt Signaling in Osteoblastic Cells. Mol. Endocrinol. 19, 90–101. https://doi.org/10.1210/me.2004-0153

Bitar, M., Salih, V., Mudera, V., Knowles, J.C., Lewis, M.P., 2004. Soluble phosphate glasses: in vitro studies using human cells of hard and soft tissue origin. Biomaterials 25, 2283–2292.

Block, T.J., Marinkovic, M., Tran, O.N., Gonzalez, A.O., Marshall, A., Dean, D.D., Chen, X.-D., 2017. Restoring the quantity and quality of elderly human mesenchymal stem cells for autologous cell-based therapies. Stem Cell Res. Ther. 8. https://doi.org/10.1186/s13287-017-0688-x

Bobis, S., Jarocha, D., Majka, M., 2006. Mesenchymal stem cells: characteristics and clinical applications. Folia Histochem. Cytobiol. 44, 215–230.

Bodine, P.V.N., Billiard, J., Moran, R.A., Ponce-de-Leon, H., McLarney, S., Mangine, A., Scrimo, M.J., Bhat, R.A., Stauffer, B., Green, J., Stein, G.S., Lian, J.B., Komm, B.S., 2005. The Wnt antagonist secreted frizzled-related protein-1 controls osteoblast and osteocyte apoptosis. J. Cell. Biochem. 96, 1212–1230. https://doi.org/10.1002/jcb.20599

Bodine, P.V.N., Zhao, W., Kharode, Y.P., Bex, F.J., Lambert, A.-J., Goad, M.B., Gaur, T., Stein, G.S., Lian, J.B., Komm, B.S., 2004. The Wnt antagonist secreted frizzled-related protein-1 is a negative regulator of trabecular bone formation in adult mice. Mol. Endocrinol. Baltim. Md 18, 1222–1237. https://doi.org/10.1210/me.2003-0498

Bohner, M., Lemaitre, J., 2009. Can bioactivity be tested in vitro with SBF solution? Biomaterials 30, 2175–2179. https://doi.org/10.1016/j.biomaterials.2009.01.008

Bonewald, L.F., 2005. Generation and function of osteocyte dendritic processes. J. Musculoskelet. Neuronal Interact. 5, 321–324.

Boskey, A.L., 2013. Bone composition: relationship to bone fragility and antiosteoporotic drug effects. BoneKEy Rep. 2. https://doi.org/10.1038/bonekey.2013.181

Bovolenta, P., Esteve, P., Ruiz, J.M., Cisneros, E., Lopez-Rios, J., 2008. Beyond Wnt inhibition: new functions of secreted Frizzled-related proteins in development and disease. J. Cell Sci. 121, 737–746. https://doi.org/10.1242/jcs.026096

Boyan, B., Schwartz, Z., 2006. Response of Musculoskeletal Cells to Biomaterials. J. Am. Acad. Orthop. Surg. 14.

Brakebusch, C., Fässler, R., 2005. β 1 integrin function in vivo: Adhesion, migration and more. Cancer Metastasis Rev. 24, 403–411. https://doi.org/10.1007/s10555-005-5132-5

Brow, R.K., 2000. Review: the structure of simple phosphate glasses. J. Non-Cryst. Solids 263–264, 1–28. https://doi.org/10.1016/S0022-3093(99)00620-1

Brunner, M., Millon-Frémillon, A., Chevalier, G., Nakchbandi, I.A., Mosher, D., Block, M.R., Albigès-Rizo, C., Bouvard, D., 2011. Osteoblast mineralization requires β1 integrin/ICAP-1–dependent fibronectin deposition. J. Cell Biol. 194, 307–322. https://doi.org/10.1083/jcb.201007108

Buckwalter, J.A., Glimcher, M.J., Cooper, R.R., Recker, R., 1996. Bone biology. I: Structure, blood supply, cells, matrix, and mineralization. Instr. Course Lect. 45, 371–386.

Bunker, B.C., Arnold, G.W., Wilder, J.A., 1984. Phosphate glass dissolution in aqueous solutions. J. Non-Cryst. Solids 64, 291–316. https://doi.org/10.1016/0022-3093(84)90184-4

Cadigan, K.M., Waterman, M.L., 2012. TCF/LEFs and Wnt Signaling in the Nucleus. Cold Spring Harb. Perspect. Biol. 4. https://doi.org/10.1101/cshperspect.a007906

Cai, Y., Chen, Y., Hong, X., Liu, Z., Yuan, W., 2013. Porous microsphere and its applications [WWW Document]. Int. J. Nanomedicine. URL https://www.dovepress.com/porous-microsphere-and-its-applications-peer-reviewed-article-IJN (accessed 3.13.20).

Calabrese, G., Giuffrida, Raffaella, Fabbi, C., Figallo, E., Lo Furno, D., Gulino, R., Colarossi, C., Fullone, F., Giuffrida, Rosario, Parenti, R., Memeo, L., Forte, S., 2016. Collagen-Hydroxyapatite Scaffolds Induce Human Adipose Derived Stem Cells Osteogenic Differentiation In Vitro. PLoS ONE 11. https://doi.org/10.1371/journal.pone.0151181

Carano, R.A.D., Filvaroff, E.H., 2003. Angiogenesis and bone repair. Drug Discov. Today 8, 980–989. https://doi.org/10.1016/S1359-6446(03)02866-6

Carreira, A.C., Lojudice, F.H., Halcsik, E., Navarro, R.D., Sogayar, M.C., Granjeiro, J.M., 2014. Bone Morphogenetic Proteins: Facts, Challenges, and Future Perspectives. J. Dent. Res. 93, 335–345. https://doi.org/10.1177/0022034513518561

Cawthorn, W.P., Bree, A.J., Yao, Y., Du, B., Hemati, N., Martinez-Santibañez, G., MacDougald, O.A., 2012. Wnt6, Wnt10a and Wnt10b inhibit adipogenesis and stimulate osteoblastogenesis through a β-catenin-dependent mechanism. Bone 50, 477–489. https://doi.org/10.1016/j.bone.2011.08.010

Champlin, R., 2003. Selection of Autologous or Allogeneic Transplantation. Holl.-Frei Cancer Med. 6th Ed.

Chang, G., Boone, S., Martel, D., Rajapakse, C.S., Hallyburton, R.S., Valko, M., Honig, S., Regatte, R.R., 2017. MRI assessment of bone structure and microarchitecture. J. Magn. Reson. Imaging 46, 323–337. https://doi.org/10.1002/jmri.25647

Chang, S.-F., Chang, T.-K., Peng, H.-H., Yeh, Y.-T., Lee, D.-Y., Yeh, C.-R., Zhou, J., Cheng, C.-K., Chang, C.A., Chiu, J.-J., 2009. BMP-4 Induction of Arrest and Differentiation of Osteoblast-Like Cells via p21CIP1 and p27KIP1 Regulation. Mol. Endocrinol. 23, 1827–1838. https://doi.org/10.1210/me.2009-0143

Chen, G., Deng, C., Li, Y.-P., 2012. TGF-β and BMP Signaling in Osteoblast Differentiation and Bone Formation. Int. J. Biol. Sci. 8, 272–288. https://doi.org/10.7150/ijbs.2929

Chen, J., Long, F., 2013. β-catenin promotes bone formation and suppresses bone resorption in postnatal growing mice. J. Bone Miner. Res. Off. J. Am. Soc. Bone Miner. Res. 28, 1160–1169. https://doi.org/10.1002/jbmr.1834

Chen, W., Villa-Diaz, L.G., Sun, Y., Weng, S., Kim, J.K., Lam, R.H.W., Han, L., Fan, R., Krebsbach, P.H., Fu, J., 2012. Nanotopography Influences Adhesion, Spreading, and Self-renewal of Human Embryonic Stem Cells. ACS Nano 6, 4094–4103. https://doi.org/10.1021/nn3004923

Clover, J., Dodds, R.A., Gowen, M., 1992. Integrin subunit expression by human osteoblasts and osteoclasts in situ and in culture. J. Cell Sci. 103, 267–271.

Coleman, J.E., 1992. Structure and mechanism of alkaline phosphatase. Annu. Rev. Biophys. Biomol. Struct. 21, 441–483. https://doi.org/10.1146/annurev.bb.21.060192.002301

Cooke, J.P., Losordo, D.W., 2002. Nitric Oxide and Angiogenesis. Circulation 105, 2133–2135. https://doi.org/10.1161/01.CIR.0000014928.45119.73

Corsi, K.A., Schwarz, E.M., Mooney, D.J., Huard, J., 2007. Regenerative medicine in orthopaedic surgery. J. Orthop. Res. 25, 1261–1268. https://doi.org/10.1002/jor.20432

Dahl, S.G., Allain, P., Marie, P.J., Mauras, Y., Boivin, G., Ammann, P., Tsouderos, Y., Delmas, P.D., Christiansen, C., 2001. Incorporation and distribution of strontium in bone. Bone 28, 446–453. https://doi.org/10.1016/S8756-3282(01)00419-7

Dalby, M.J., Bonfield, W., Di Silvio, L., 2003. Enhanced HAPEX topography: Comparison of osteoblast response to established cement. J. Mater. Sci. Mater. Med. 14, 693–697. https://doi.org/10.1023/A:1024959632082

Danoux, C., Pereira, D., Döbelin, N., Stähli, C., Barralet, J., van Blitterswijk, C., Habibovic, P., 2016. The Effects of Crystal Phase and Particle Morphology of Calcium Phosphates on Proliferation and Differentiation of Human Mesenchymal Stromal Cells. Adv. Healthc. Mater. 5, 1775–1785. https://doi.org/10.1002/adhm.201600184

Danoux, C.B.S.S., Bassett, D.C., Othman, Z., Rodrigues, A.I., Reis, R.L., Barralet, J.E., van Blitterswijk, C.A., Habibovic, P., 2015. Elucidating the individual effects of calcium and phosphate ions on hMSCs by using composite materials. Acta Biomater. 17, 1–15. https://doi.org/10.1016/j.actbio.2015.02.003

De, A., 2011. Wnt/Ca2+ signaling pathway: a brief overview. Acta Biochim. Biophys. Sin. 43, 745–756. https://doi.org/10.1093/abbs/gmr079

Dean, R.L., 2002. Kinetic studies with alkaline phosphatase in the presence and absence of inhibitors and divalent cations. Biochem. Mol. Biol. Educ. 30, 401–407. https://doi.org/10.1002/bmb.2002.494030060138

Deb, S., Wang, M., Tanner, K.E., Bonfield, W., 1996. Hydroxyapatite-polyethylene composites: effect of grafting and surface treatment of hydroxyapatite. J. Mater. Sci. Mater. Med. 7, 191–193. https://doi.org/10.1007/BF00119729

Deregowski, V., Gazzerro, E., Priest, L., Rydziel, S., Canalis, E., 2006. Notch 1 Overexpression Inhibits Osteoblastogenesis by Suppressing Wnt/β-Catenin but Not Bone Morphogenetic Protein Signaling. J. Biol. Chem. 281, 6203–6210. https://doi.org/10.1074/jbc.M508370200

Donnelly, H., Dalby, M.J., Salmeron-Sanchez, M., Sweeten, P.E., 2018. Current approaches for modulation of the nanoscale interface in the regulation of cell behavior. Nanomed. 14, 2455–2464. https://doi.org/10.1016/j.nano.2017.03.020

Dorozhkin, S.V., 2010. Bioceramics of calcium orthophosphates. Biomaterials 31, 1465–1485. https://doi.org/10.1016/j.biomaterials.2009.11.050

Downey, P.A., Siegel, M.I., 2006. Bone Biology and the Clinical Implications for Osteoporosis. Phys. Ther. 86, 77–91. https://doi.org/10.1093/ptj/86.1.77

Ducy, P., Desbois, C., Boyce, B., Pinero, G., Story, B., Dunstan, C., Smith, E., Bonadio, J., Goldstein, S., Gundberg, C., Bradley, A., Karsenty, G., 1996. Increased bone formation in osteocalcin-deficient mice. Nature 382, 448–452. https://doi.org/10.1038/382448a0

Duncan, R.L., Akanbi, K.A., Farach-Carson, M.C., 1998. Calcium signals and calcium channels in osteoblastic cells. Semin. Nephrol. 18, 178–190.

El Bialy, I., Jiskoot, W., Reza Nejadnik, M., 2017. Formulation, Delivery and Stability of Bone Morphogenetic Proteins for Effective Bone Regeneration. Pharm. Res. 34, 1152–1170. https://doi.org/10.1007/s11095-017-2147-x

Evans, M.J., Kaufman, M.H., 1981. Establishment in culture of pluripotential cells from mouse embryos. Nature 292, 154–156. https://doi.org/10.1038/292154a0

Fairbairn, N.G., Meppelink, A.M., Ng-Glazier, J., Randolph, M.A., Winograd, J.M., 2015. Augmenting peripheral nerve regeneration using stem cells: A review of current opinion. World J. Stem Cells 7, 11–26. https://doi.org/10.4252/wjsc.v7.i1.11

Felfel, R.M., Ahmed, I., Parsons, A.J., Palmer, G., Sottile, V., Rudd, C.D., 2013. Cytocompatibility, degradation, mechanical property retention and ion release profiles for phosphate glass fibre reinforced composite rods. Mater. Sci. Eng. C Mater. Biol. Appl. 33, 1914–1924. https://doi.org/10.1016/j.msec.2012.12.089

Feng, X.-H., Derynck, R., 2005. SPECIFICITY AND VERSATILITY IN TGF-β SIGNALING THROUGH SMADS. Annu. Rev. Cell Dev. Biol. 21, 659–693. https://doi.org/10.1146/annurev.cellbio.21.022404.142018

Fleisch, H., Bisaz, S., 1962. Mechanism of Calcification: Inhibitory Role of Pyrophosphate. Nature 195, 911–911. https://doi.org/10.1038/195911a0

Florencio-Silva, R., Sasso, G.R. da S., Sasso-Cerri, E., Sim&#xf5, Es, M.J., Cerri, P.S., rgio, 2015. Biology of Bone Tissue: Structure, Function, and Factors That Influence Bone Cells [WWW Document]. BioMed Res. Int. https://doi.org/10.1155/2015/421746

Flozak, A.S., Lam, A.P., Gottardi, C.J., 2016. A Simple Method to Assess Abundance of the β-Catenin Signaling Pool in Cells. Methods Mol. Biol. Clifton NJ 1481, 49–60. https://doi.org/10.1007/978-1-4939-6393-5_6

Foroutan, F., McGuire, J., Gupta, P., Nikolaou, A., Kyffin, B.A., Kelly, N.L., Hanna, J.V., Gutierrez-Merino, J., Knowles, J.C., Baek, S.-Y., Velliou, E., Carta, D., 2019. Antibacterial Copper-Doped Calcium Phosphate Glasses for Bone Tissue Regeneration. ACS Biomater. Sci. Eng. 5, 6054–6062. https://doi.org/10.1021/acsbiomaterials.9b01291

Franks, K., Abrahams, I., Georgiou, G., Knowles, J.C., 2001. Investigation of thermal parameters and crytallisation in a ternary CaO–Na2O–P2O5-based glass system. Biomaterials 22, 497–501. https://doi.org/10.1016/S0142-9612(00)00207-6

Gao, H., Tan, T., Wang, D., 2004. Dissolution Mechanism and Release Kinetics of Phosphate Controlled Release Glasses in Aqueous Medium. J. Control. Release Off. J. Control. Release Soc. 96, 29–36. https://doi.org/10.1016/j.jconrel.2003.12.031

Gaur, T., Lengner, C.J., Hovhannisyan, H., Bhat, R.A., Bodine, P.V.N., Komm, B.S., Javed, A., Wijnen, A.J. van, Stein, J.L., Stein, G.S., Lian, J.B., 2005. Canonical WNT Signaling Promotes Osteogenesis by Directly Stimulating Runx2 Gene Expression. J. Biol. Chem. 280, 33132–33140. https://doi.org/10.1074/jbc.M500608200

Gerber, H.-P., Ferrara, N., 2000. Angiogenesis and Bone Growth. Trends Cardiovasc. Med. 10, 223–228. https://doi.org/10.1016/S1050-1738(00)00074-8

Ghali, O., Broux, O., Falgayrac, G., Haren, N., van Leeuwen, J.P., Penel, G., Hardouin, P., Chauveau, C., 2015. Dexamethasone in osteogenic medium strongly induces adipocyte differentiation of mouse bone marrow stromal cells and increases

osteoblast differentiation. BMC Cell Biol. 16, 9. https://doi.org/10.1186/s12860-015-0056-6

Glass, D.A., Karsenty, G., 2006. Molecular Bases of the Regulation of Bone Remodeling by the Canonical Wnt Signaling Pathway, in: Current Topics in Developmental Biology. Academic Press, pp. 43–84. https://doi.org/10.1016/S0070-2153(05)73002-7

Golub, E.E., Boesze-Battaglia, K., 2007. The role of alkaline phosphatase in mineralization. Curr. Opin. Orthop. 18, 444–448. https://doi.org/10.1097/BCO.0b013e3282630851

González, M.A., Gonzalez-Rey, E., Rico, L., Büscher, D., Delgado, M., 2009. Treatment of experimental arthritis by inducing immune tolerance with human adipose-derived mesenchymal stem cells. Arthritis Rheum. 60, 1006–1019. https://doi.org/10.1002/art.24405

Gregory, C.A., Gunn, W.G., Peister, A., Prockop, D.J., 2004. An Alizarin red-based assay of mineralization by adherent cells in culture: comparison with cetylpyridinium chloride extraction. Anal. Biochem. 329, 77–84. https://doi.org/10.1016/j.ab.2004.02.002

Grover, L.M., Wright, A.J., Gbureck, U., Bolarinwa, A., Song, J., Liu, Y., Farrar, D.F., Howling, G., Rose, J., Barralet, J.E., 2013. The effect of amorphous pyrophosphate on calcium phosphate cement resorption and bone generation. Biomaterials 34, 6631–6637. https://doi.org/10.1016/j.biomaterials.2013.05.001

Grynpas, M.D., Marie, P.J., 1990. Effects of low doses of strontium on bone quality and quantity in rats. Bone 11, 313–319. https://doi.org/10.1016/8756-3282(90)90086-E

Gunawidjaja, P.N., Mathew, R., Lo, A.Y.H., Izquierdo-Barba, I., García, A., Arcos, D., Mattias Edén, M.V.-R., 2012. Local structures of mesoporous bioactive glasses and their surface alterations in vitro: inferences from solid-state nuclear magnetic resonance. Philos. Transact. A Math. Phys. Eng. Sci. 370, 1376–1399. https://doi.org/10.1098/rsta.2011.0257

Gupta, D., Hossain, K.M.Z., Ahmed, I., Sottile, V., Grant, D.M., 2018. Flame-Spheroidized Phosphate-Based Glass Particles with Improved Characteristics for Applications in Mesenchymal Stem Cell Culture Therapy and Tissue Engineering. ACS Appl. Mater. Interfaces 10, 25972–25982. https://doi.org/10.1021/acsami.8b05267

Haque, P., Parsons, A.J., Barker, I.A., Ahmed, I., Irvine, D.J., Walker, G.S., Rudd, C.D., 2010. Interfacial properties of phosphate glass fibres/PLA composites: Effect of the end functionalities of oligomeric PLA coupling agents. Compos. Sci. Technol., ICCM-17: Composites In Biomedical Applications 70, 1854–1860. https://doi.org/10.1016/j.compscitech.2010.06.012

Hauge, E.M., Qvesel, D., Eriksen, E.F., Mosekilde, L., Melsen, F., 2001. Cancellous Bone Remodeling Occurs in Specialized Compartments Lined by Cells Expressing Osteoblastic Markers. J. Bone Miner. Res. 16, 1575–1582. https://doi.org/10.1359/jbmr.2001.16.9.1575

Hench, L.L., 2006. The story of Bioglass®. J. Mater. Sci. Mater. Med. 17, 967–978. https://doi.org/10.1007/s10856-006-0432-z

Hench, L.L., 1980. Biomaterials. Science 208, 826–831. https://doi.org/10.1126/science.6246576

Hench, L.L., Splinter, R.J., Allen, W.C., Greenlee, T.K., 1971. Bonding mechanisms at the interface of ceramic prosthetic materials. J. Biomed. Mater. Res. 5, 117–141. https://doi.org/10.1002/jbm.820050611

Hench, L.L., Thompson, I., 2010. Twenty-first century challenges for biomaterials. J. R. Soc. Interface 7, S379–S391. https://doi.org/10.1098/rsif.2010.0151.focus

Heuss, S.F., Ndiaye-Lobry, D., Six, E.M., Israël, A., Logeat, F., 2008. The intracellular region of Notch ligands Dll1 and Dll3 regulates their trafficking and signaling activity. Proc. Natl. Acad. Sci. 105, 11212–11217. https://doi.org/10.1073/pnas.0800695105

Hilton, M.J., Tu, X., Wu, X., Bai, S., Zhao, H., Kobayashi, T., Kronenberg, H.M., Teitelbaum, S.L., Ross, F.P., Kopan, R., Long, F., 2008. Notch signaling maintains bone marrow mesenchymal progenitors by suppressing osteoblast differentiation. Nat. Med. 14, 306–314. https://doi.org/10.1038/nm1716

Hoac, B., Kiffer-Moreira, T., Millán, J.L., McKee, M.D., 2013. Polyphosphates inhibit extracellular matrix mineralization in MC3T3-E1 osteoblast cultures. Bone 53, 478–486. https://doi.org/10.1016/j.bone.2013.01.020

Hodges, R.M., MacDonald, N.S., Nusbaum, R., Stearns, R., Ezmirlian, F., Spain, P., McArthur, C., 1950. The Strontium Content of Human Bones. J. Biol. Chem. 185, 519–524.

Holleville, N., Matéos, S., Bontoux, M., Bollerot, K., Monsoro-Burq, A.-H., 2007. Dlx5 drives Runx2 expression and osteogenic differentiation in developing cranial

suture mesenchyme. Dev. Biol. 304, 860–874. https://doi.org/10.1016/j.ydbio.2007.01.003

Hoppe, A., Güldal, N.S., Boccaccini, A.R., 2011. A review of the biological response to ionic dissolution products from bioactive glasses and glass-ceramics. Biomaterials 32, 2757–2774. https://doi.org/10.1016/j.biomaterials.2011.01.004

Hoppe, U., Kranold, R., Stachel, D., Barz, A., Hannon, A., 2000. Variation in P-O Bonding in Phosphate Glasses -A Neutron Diffraction Study. Z. Für Naturforschung A 55. https://doi.org/10.1515/zna-2000-3-401

Horwitz, E.M., Le Blanc, K., Dominici, M., Mueller, I., Slaper-Cortenbach, I., Marini, F.C., Deans, R.J., Krause, D.S., Keating, A., International Society for Cellular Therapy, 2005. Clarification of the nomenclature for MSC: The International Society for Cellular Therapy position statement. Cytotherapy 7, 393–395. https://doi.org/10.1080/14653240500319234

Hossain, K.M.Z., Hasan, M., Felfel, R., Ahmed, I., 2014. Development of phosphate-based glass fibers for biomedical applications. pp. 104–115. https://doi.org/10.4155/EBO.13.352

Hossain, K.M.Z., Patel, U., Ahmed, I., 2015. Development of microspheres for biomedical applications: a review. Prog. Biomater. 4, 1–19. https://doi.org/10.1007/s40204-014-0033-8

Hossain, K.M.Z., Patel, U., Kennedy, A.R., Macri-Pellizzeri, L., Sottile, V., Grant, D.M., Scammell, B.E., Ahmed, I., 2018. Porous calcium phosphate glass microspheres for orthobiologic applications. Acta Biomater. 72, 396–406. https://doi.org/10.1016/j.actbio.2018.03.040

Hott, M., Noel, B., Bernache-Assolant, D., Rey, C., Marie, P.J., 1997. Proliferation and differentiation of human trabecular osteoblastic cells on hydroxyapatite. J. Biomed. Mater. Res. 37, 508–516.

Hu, Y., Du, Y., Jiang, H., Jiang, G.-S., 2014. Cerium promotes bone marrow stromal cells migration and osteogenic differentiation via Smad1/5/8 signaling pathway. Int. J. Clin. Exp. Pathol. 7, 5369–5378.

Huang, W., Yang, S., Shao, J., Li, Y.-P., 2007. Signaling and transcriptional regulation in osteoblast commitment and differentiation. Front. Biosci. J. Virtual Libr. 12, 3068–3092.

Hung, H.-C., Chang, G.-G., 2001. Differentiation of the slow-binding mechanism for magnesium ion activation and zinc ion inhibition of human placental alkaline phosphatase. Protein Sci. Publ. Protein Soc. 10, 34–45.

Hurley, L.S., 1981. Teratogenic aspects of manganese, zinc, and copper nutrition. Physiol. Rev. 61, 249–295.

Ireland, D.C., Bord, S., Beavan, S.R., Compston, J.E., 2004. Hydrocortisone increases the rate of differentiation of cultured human osteoblasts. J. Cell. Biochem. 91, 594–601. https://doi.org/10.1002/jcb.10756

Ishitani, T., Kishida, S., Hyodo-Miura, J., Ueno, N., Yasuda, J., Waterman, M., Shibuya, H., Moon, R.T., Ninomiya-Tsuji, J., Matsumoto, K., 2003. The TAK1-NLK mitogen-activated protein kinase cascade functions in the Wnt-5a/Ca(2+) pathway to antagonize Wnt/beta-catenin signaling. Mol. Cell. Biol. 23, 131–139. https://doi.org/10.1128/mcb.23.1.131-139.2003

Islam, M.T., Felfel, R.M., Abou Neel, E.A., Grant, D.M., Ahmed, I., Hossain, K.M.Z., 2017. Bioactive calcium phosphate–based glasses and ceramics and their biomedical applications: A review. J. Tissue Eng. 8. https://doi.org/10.1177/2041731417719170

Jäger, M., Hernigou, P., Zilkens, C., Herten, M., Li, X., Fischer, J., Krauspe, R., 2010. Cell therapy in bone healing disorders. Orthop. Rev. 2, e20. https://doi.org/10.4081/or.2010.e20

Jeong, B.-C., Kim, H.-J., Bae, I.-H., Lee, K.-N., Lee, K.-Y., Oh, W.-M., Kim, S.-H., Kang, I.-C., Lee, S.-E., Koh, G.-Y., Kim, K.-K., Koh, J.-T., 2010. COMP-Ang1, a chimeric form of Angiopoietin 1, enhances BMP2-induced osteoblast differentiation and bone formation. Bone 46, 479–486. https://doi.org/10.1016/j.bone.2009.09.019

Jilka, R.L., 2003. Biology of the basic multicellular unit and the pathophysiology of osteoporosis. Med. Pediatr. Oncol. 41, 182–185. https://doi.org/10.1002/mpo.10334

Julien, M., Magne, D., Masson, M., Rolli-Derkinderen, M., Chassande, O., Cario-Toumaniantz, C., Cherel, Y., Weiss, P., Guicheux, J., 2007. Phosphate stimulates matrix Gla protein expression in chondrocytes through the extracellular signal regulated kinase signaling pathway. Endocrinology 148, 530–537. https://doi.org/10.1210/en.2006-0763

Jung, W.K., Koo, H.C., Kim, K.W., Shin, S., Kim, S.H., Park, Y.H., 2008. Antibacterial Activity and Mechanism of Action of the Silver Ion in Staphylococcus aureus

and Escherichia coli. Appl. Environ. Microbiol. 74, 2171–2178. https://doi.org/10.1128/AEM.02001-07

Junker, J.P.E., Sommar, P., Skog, M., Johnson, H., Kratz, G., 2010. Adipogenic, Chondrogenic and Osteogenic Differentiation of Clonally Derived Human Dermal Fibroblasts. Cells Tissues Organs 191, 105–118. https://doi.org/10.1159/000232157

Kafri, P., Hasenson, S.E., Kanter, I., Sheinberger, J., Kinor, N., Yunger, S., Shav-Tal, Y., 2016. Quantifying β-catenin subcellular dynamics and cyclin D1 mRNA transcription during Wnt signaling in single living cells. eLife 5, e16748. https://doi.org/10.7554/eLife.16748

Kanatani, M., Sugimoto, T., Kano, J., Chihara, K., 2002. IGF-I mediates the stimulatory effect of high phosphate concentration on osteoblastic cell proliferation. J. Cell. Physiol. 190, 306–312. https://doi.org/10.1002/jcp.10067

Kanis, J.A., McCloskey, E.V., Johansson, H., Cooper, C., Rizzoli, R., Reginster, J.-Y., 2013. European guidance for the diagnosis and management of osteoporosis in postmenopausal women. Osteoporos. Int. 24, 23–57. https://doi.org/10.1007/s00198-012-2074-y

Kasuga, T., 2005. Bioactive calcium pyrophosphate glasses and glass-ceramics. Acta Biomater. 1, 55–64. https://doi.org/10.1016/j.actbio.2004.08.001

Kawano, Y., Kypta, R., 2003. Secreted antagonists of the Wnt signalling pathway. J. Cell Sci. 116, 2627–2634. https://doi.org/10.1242/jcs.00623

Kelmendi-Doko, A., Rubin, J.P., Klett, K., Mahoney, C., Wang, S., Marra, K.G., 2017. Controlled dexamethasone delivery via double-walled microspheres to enhance long-term adipose tissue retention. J. Tissue Eng. 8, 2041731417735402. https://doi.org/10.1177/2041731417735402

Khoshniat, S., Bourgine, A., Julien, M., Petit, M., Pilet, P., Rouillon, T., Masson, M., Gatius, M., Weiss, P., Guicheux, J., Beck, L., 2011a. Phosphate-dependent stimulation of MGP and OPN expression in osteoblasts via the ERK1/2 pathway is modulated by calcium. Bone 48, 894–902. https://doi.org/10.1016/j.bone.2010.12.002

Khoshniat, S., Bourgine, A., Julien, M., Petit, M., Pilet, P., Rouillon, T., Masson, M., Gatius, M., Weiss, P., Guicheux, J., Beck, L., 2011b. Phosphate-dependent stimulation of MGP and OPN expression in osteoblasts via the ERK1/2 pathway is modulated by calcium. Bone 48, 894–902. https://doi.org/10.1016/j.bone.2010.12.002

Kim, Y.-P., Lee, G.-S., Kim, J.-W., Kim, M.S., Ahn, H.-S., Lim, J.-Y., Kim, H.-W., Son, Y.-J., Knowles, J.C., Hyun, J.K., 2015. Phosphate glass fibres promote neurite outgrowth and early regeneration in a peripheral nerve injury model. J. Tissue Eng. Regen. Med. 9, 236–246. https://doi.org/10.1002/term.1626

Kläning, E., Christensen, B., Sørensen, E.S., Vorup-Jensen, T., Jensen, J.K., 2014. Osteopontin binds multiple calcium ions with high affinity and independently of phosphorylation status. Bone 66, 90–95. https://doi.org/10.1016/j.bone.2014.05.020

Knowles, J., Ahmed, I., Lewis, M., 2005. Quantification of anions and cations from ternary phosphate based glasses with fixed 50 and 55 mol% P2O5 using ion chromatography. Phys. Chem. Glas. 46, 547–552.

Knowles, J.C., 2003. Phosphate based glasses for biomedical applications. J. Mater. Chem. 13, 2395–2401. https://doi.org/10.1039/B307119G

Ko, Y.H., Hong, S., Pedersen, P.L., 1999. Chemical mechanism of ATP synthase. Magnesium plays a pivotal role in formation of the transition state where ATP is synthesized from ADP and inorganic phosphate. J. Biol. Chem. 274, 28853–28856. https://doi.org/10.1074/jbc.274.41.28853

Kokubo, T., 1998. Apatite formation on surfaces of ceramics, metals and polymers in body environment. Acta Mater. 46, 2519–2527. https://doi.org/10.1016/S1359-6454(98)80036-0

Komori, T., Yagi, H., Nomura, S., Yamaguchi, A., Sasaki, K., Deguchi, K., Shimizu, Y., Bronson, R.T., Gao, Y.-H., Inada, M., Sato, M., Okamoto, R., Kitamura, Y., Yoshiki, S., Kishimoto, T., 1997. Targeted Disruption of Cbfa1 Results in a Complete Lack of Bone Formation owing to Maturational Arrest of Osteoblasts. Cell 89, 755–764. https://doi.org/10.1016/S0092-8674(00)80258-5

Kuroda, Y., Kawai, T., Goto, K., Matsuda, S., 2019. Clinical application of injectable growth factor for bone regeneration: a systematic review. Inflamm. Regen. 39. https://doi.org/10.1186/s41232-019-0109-x

Ladi, E., Nichols, J.T., Ge, W., Miyamoto, A., Yao, C., Yang, L.-T., Boulter, J., Sun, Y.E., Kintner, C., Weinmaster, G., 2005. The divergent DSL ligand Dll3 does not activate Notch signaling but cell autonomously attenuates signaling induced by other DSL ligands. J. Cell Biol. 170, 983–992. https://doi.org/10.1083/jcb.200503113

Landi, E., Logroscino, G., Proietti, L., Tampieri, A., Sandri, M., Sprio, S., 2008. Biomimetic Mg-substituted hydroxyapatite: from synthesis to in vivo behaviour. J. Mater. Sci. Mater. Med. 19, 239–247. https://doi.org/10.1007/s10856-006-0032-y

Lapa, A., Cresswell, M., Jackson, P., Boccaccini, A.R., 2020. Phosphate glass fibres with therapeutic ions release capability – a review. Adv. Appl. Ceram. 119, 1–14. https://doi.org/10.1080/17436753.2018.1564413

Lawal, R.A., Zhu, X., Batey, K., Hoffman, C.M., Georger, M.A., Radtke, F., Hilton, M.J., Xing, L., Frisch, B.J., Calvi, L.M., 2017. Notch Ligand Jagged1 Regulates the Osteoblastic Lineage by Maintaining the Osteoprogenitor Pool. J. Bone Miner. Res. Off. J. Am. Soc. Bone Miner. Res. 32, 1320–1331. https://doi.org/10.1002/jbmr.3106

Le Blanc, K., Mougiakakos, D., 2012. Multipotent mesenchymal stromal cells and the innate immune system. Nat. Rev. Immunol. 12, 383–396. https://doi.org/10.1038/nri3209

Lee, M.-H., Kim, Y.-J., Yoon, W.-J., Kim, J.-I., Kim, B.-G., Hwang, Y.-S., Wozney, J.M., Chi, X.-Z., Bae, S.-C., Choi, K.-Y., Cho, J.-Y., Choi, J.-Y., Ryoo, H.-M., 2005. Dlx5 specifically regulates Runx2 type II expression by binding to homeodomain-response elements in the Runx2 distal promoter. J. Biol. Chem. 280, 35579–35587. https://doi.org/10.1074/jbc.M502267200

Lee, M.N., Hwang, H.-S., Oh, S.-H., Roshanzadeh, A., Kim, J.-W., Song, J.H., Kim, E.-S., Koh, J.-T., 2018. Elevated extracellular calcium ions promote proliferation and migration of mesenchymal stem cells via increasing osteopontin expression. Exp. Mol. Med. 50, 142. https://doi.org/10.1038/s12276-018-0170-6

Lerner, U.H., Ohlsson, C., 2015. The WNT system: background and its role in bone. J. Intern. Med. 277, 630–649. https://doi.org/10.1111/joim.12368

Leyhausen, G., Lorenz, B., Zhu, H., Geurtsen, W., Bohnensack, R., Müller, W.E.G., Schröder, H.C., 1998. Inorganic Polyphosphate in Human Osteoblast-like Cells. J. Bone Miner. Res. 13, 803–812. https://doi.org/10.1359/jbmr.1998.13.5.803

LI, J., WANG, G.-B., FENG, X., ZHANG, J., FU, Q., 2016. Effect of gallium nitrate on the expression of osteoprotegerin and receptor activator of nuclear factor-κB ligand in osteoblasts in vivo and in vitro. Mol. Med. Rep. 13, 769–777. https://doi.org/10.3892/mmr.2015.4588

Li, L., Peng, X., Qin, Y., Wang, R., Tang, J., Cui, X., Wang, T., Liu, W., Pan, H., Li, B., 2017. Acceleration of bone regeneration by activating Wnt/β-catenin signalling

pathway via lithium released from lithium chloride/calcium phosphate cement in osteoporosis. Sci. Rep. 7, 1–12. https://doi.org/10.1038/srep45204

Lin, G.L., Hankenson, K.D., 2011. Integration of BMP, Wnt, and Notch signaling pathways in osteoblast differentiation. J. Cell. Biochem. 112, 3491–3501. https://doi.org/10.1002/jcb.23287

Lin, X., Chen, Q., Xiao, Y., Gao, Y., Ahmed, I., Li, M., Li, H., Zhang, K., Qiu, W., Liu, X., Boccaccini, A.R., Qian, A., 2020. Phosphate glass fibers facilitate proliferation and osteogenesis through Runx2 transcription in murine osteoblastic cells. J. Biomed. Mater. Res. A 108, 316–326. https://doi.org/10.1002/jbm.a.36818

Lindfors, N.C., Koski, I., Heikkilä, J.T., Mattila, K., Aho, A.J., 2010. A prospective randomized 14-year follow-up study of bioactive glass and autogenous bone as bone graft substitutes in benign bone tumors. J. Biomed. Mater. Res. B Appl. Biomater. 94, 157–164. https://doi.org/10.1002/jbm.b.31636

Liu, Y., Bhat, R.A., Seestaller-Wehr, L.M., Fukayama, S., Mangine, A., Moran, R.A., Komm, B.S., Bodine, P.V.N., Billiard, J., 2007. The Orphan Receptor Tyrosine Kinase Ror2 Promotes Osteoblast Differentiation and Enhances ex Vivo Bone Formation. Mol. Endocrinol. 21, 376–387. https://doi.org/10.1210/me.2006-0342

Lukomska, B., Stanaszek, L., Zuba-Surma, E., Legosz, P., Sarzynska, S., Drela, K., 2019. Challenges and Controversies in Human Mesenchymal Stem Cell Therapy [WWW Document]. Stem Cells Int. https://doi.org/10.1155/2019/9628536

Lyons, J.P., Mueller, U.W., Ji, H., Everett, C., Fang, X., Hsieh, J.-C., Barth, A.M., McCrea, P.D., 2004. Wnt-4 activates the canonical beta-catenin-mediated Wnt pathway and binds Frizzled-6 CRD: functional implications of Wnt/beta-catenin activity in kidney epithelial cells. Exp. Cell Res. 298, 369–387. https://doi.org/10.1016/j.yexcr.2004.04.036

Macri-Pellizzeri, L., De Melo, N., Ahmed, I., Grant, D., Scammell, B., Sottile, V., 2018. Live Quantitative Monitoring of Mineral Deposition in Stem Cells Using Tetracycline Hydrochloride. Tissue Eng. Part C Methods 24, 171–178. https://doi.org/10.1089/ten.tec.2017.0400

Maeda, K., Kobayashi, Y., Udagawa, N., Uehara, S., Ishihara, A., Mizoguchi, T., Kikuchi, Y., Takada, I., Kato, S., Kani, S., Nishita, M., Marumo, K., Martin, T.J., Minami, Y., Takahashi, N., 2012. Wnt5a-Ror2 signaling between osteoblast-lineage cells and osteoclast precursors enhances osteoclastogenesis. Nat. Med. 18, 405–412. https://doi.org/10.1038/nm.2653

Maeda, S., Hayashi, M., Komiya, S., Imamura, T., Miyazono, K., 2004. Endogenous TGF-β signaling suppresses maturation of osteoblastic mesenchymal cells. EMBO J. 23, 552–563. https://doi.org/10.1038/sj.emboj.7600067

Maeno, S., Niki, Y., Matsumoto, H., Morioka, H., Yatabe, T., Funayama, A., Toyama, Y., Taguchi, T., Tanaka, J., 2005. The effect of calcium ion concentration on osteoblast viability, proliferation and differentiation in monolayer and 3D culture. Biomaterials 26, 4847–4855. https://doi.org/10.1016/j.biomaterials.2005.01.006

Maga, G., Hübscher, U., 2003. Proliferating cell nuclear antigen (PCNA): a dancer with many partners. J. Cell Sci. 116, 3051–3060. https://doi.org/10.1242/jcs.00653

Magne, D., Bluteau, G., Faucheux, C., Palmer, G., Vignes-Colombeix, C., Pilet, P., Rouillon, T., Caverzasio, J., Weiss, P., Daculsi, G., Guicheux, J., 2003. Phosphate is a specific signal for ATDC5 chondrocyte maturation and apoptosis-associated mineralization: possible implication of apoptosis in the regulation of endochondral ossification. J. Bone Miner. Res. 18, 1430–1442.

Maier, J.A.M., Bernardini, D., Rayssiguier, Y., Mazur, A., 2004. High concentrations of magnesium modulate vascular endothelial cell behaviour in vitro. Biochim. Biophys. Acta BBA - Mol. Basis Dis. 1689, 6–12. https://doi.org/10.1016/j.bbadis.2004.02.004

Maisonpierre, P.C., Suri, C., Jones, P.F., Bartunkova, S., Wiegand, S.J., Radziejewski, C., Compton, D., McClain, J., Aldrich, T.H., Papadopoulos, N., Daly, T.J., Davis, S., Sato, T.N., Yancopoulos, G.D., 1997. Angiopoietin-2, a natural antagonist for Tie2 that disrupts in vivo angiogenesis. Science 277, 55–60.

Marie, P.J., 2008. Transcription factors controlling osteoblastogenesis. Arch. Biochem. Biophys., Highlight Issue: Bone Remodeling: Facts and Perspectives 473, 98–105. https://doi.org/10.1016/j.abb.2008.02.030

Marie, P.J., 2003. Optimizing bone metabolism in osteoporosis: insight into the pharmacologic profile of strontium ranelate. Osteoporos. Int. 14, 9–12. https://doi.org/10.1007/s00198-002-1344-5

Marie, P.J., Hott, M., Modrowski, D., De Pollak, C., Guillemain, J., Deloffre, P., Tsouderos, Y., 1993. An uncoupling agent containing strontium prevents bone loss by depressing bone resorption and maintaining bone formation in estrogen-deficient rats. J. Bone Miner. Res. Off. J. Am. Soc. Bone Miner. Res. 8, 607–615. https://doi.org/10.1002/jbmr.5650080512

Marks, S.C., Popoff, S.N., 1988. Bone cell biology: The regulation of development, structure, and function in the skeleton. Am. J. Anat. 183, 1–44. https://doi.org/10.1002/aja.1001830102

Marquez, M.P., Alencastro, F., Madrigal, A., Jimenez, J.L., Blanco, G., Gureghian, A., Keagy, L., Lee, C., Liu, R., Tan, L., Deignan, K., Armstrong, B., Zhao, Y., 2017. The Role of Cellular Proliferation in Adipogenic Differentiation of Human Adipose Tissue-Derived Mesenchymal Stem Cells. Stem Cells Dev. 26, 1578–1595. https://doi.org/10.1089/scd.2017.0071

Marsell, R., Einhorn, T.A., 2009. The role of endogenous bone morphogenetic proteins in normal skeletal repair. Injury, Bone Morphogenetic Proteins: Applications in Orthopaedic and Trauma Surgery 40, S4–S7. https://doi.org/10.1016/S0020-1383(09)70003-8

Massagué, J., Seoane, J., Wotton, D., 2005. Smad transcription factors. Genes Dev. 19, 2783–2810. https://doi.org/10.1101/gad.1350705

Matamoros-Veloza, A., Hossain, K.M.Z., Scammell, B.E., Ahmed, I., Hall, R., Kapur, N., 2020. Formulating injectable pastes of porous calcium phosphate glass microspheres for bone regeneration applications. J. Mech. Behav. Biomed. Mater. 102, 103489. https://doi.org/10.1016/j.jmbbm.2019.103489

Matsumura, H., Sueyoshi, M., Atsuta, M., 1992. Radiopacity and physical properties of titanium-polymethacrylate composite. J. Dent. Res. 71, 2–6. https://doi.org/10.1177/00220345920710010201

Matsunaga, T., Weihrauch, D.W., Moniz, M.C., Tessmer, J., Warltier, D.C., Chilian, W.M., 2002. Angiostatin Inhibits Coronary Angiogenesis During Impaired Production of Nitric Oxide. Circulation 105, 2185–2191. https://doi.org/10.1161/01.CIR.0000015856.84385.E9

McKee, M.D., Nanci, A., 1996. Osteopontin at mineralized tissue interfaces in bone, teeth, and osseointegrated implants: Ultrastructural distribution and implications for mineralized tissue formation, turnover, and repair. Microsc. Res. Tech. 33, 141–164. https://doi.org/10.1002/(SICI)1097-0029(19960201)33:2<141::AID-JEMT5>3.0.CO;2-W

McLaren, J.S., Macri-Pellizzeri, L., Hossain, K.M.Z., Patel, U., Grant, D.M., Scammell, B.E., Ahmed, I., Sottile, V., 2019. Porous Phosphate-Based Glass Microspheres Show Biocompatibility, Tissue Infiltration, and Osteogenic Onset in an Ovine Bone Defect Model. ACS Appl. Mater. Interfaces 11, 15436–15446. https://doi.org/10.1021/acsami.9b04603

McLarren, K.W., Theriault, F.M., Stifani, S., 2001. Association with the Nuclear Matrix and Interaction with Groucho and RUNX Proteins Regulate the Transcription Repression Activity of the Basic Helix Loop Helix Factor Hes1. J. Biol. Chem. 276, 1578–1584. https://doi.org/10.1074/jbc.M007629200

Mechiche Alami, S., Gangloff, S.C., Laurent-Maquin, D., Wang, Y., Kerdjoudj, H., 2016. Concise Review: In Vitro Formation of Bone-Like Nodules Sheds Light on the Application of Stem Cells for Bone Regeneration. STEM CELLS Transl. Med. 5, 1587–1593. https://doi.org/10.5966/sctm.2015-0413

Meleti, Z., Shapiro, I.M., Adams, C.S., 2000. Inorganic phosphate induces apoptosis of osteoblast-like cells in culture. Bone 27, 359–366. https://doi.org/10.1016/S8756-3282(00)00346-X

Merwin, G.E., 1986. Bioglass middle ear prosthesis: preliminary report. Ann. Otol. Rhinol. Laryngol. 95, 78–82. https://doi.org/10.1177/000348948609500117

Mikami, Y., Lee, M., Irie, S., Honda, M.J., 2011. Dexamethasone modulates osteogenesis and adipogenesis with regulation of osterix expression in rat calvaria-derived cells. J. Cell. Physiol. 226, 739–748. https://doi.org/10.1002/jcp.22392

Mitragotri, S., Burke, P.A., Langer, R., 2014. Overcoming the challenges in administering biopharmaceuticals: formulation and delivery strategies. Nat. Rev. Drug Discov. 13, 655–672. https://doi.org/10.1038/nrd4363

Mould, A.P., Akiyama, S.K., Humphries, M.J., 1995. Regulation of Integrin α5β1-Fibronectin Interactions by Divalent Cations EVIDENCE FOR DISTINCT CLASSES OF BINDING SITES FOR Mn2+, Mg2+, AND Ca2+. J. Biol. Chem. 270, 26270–26277. https://doi.org/10.1074/jbc.270.44.26270

Muguruma, Y., Hozumi, K., Warita, H., Yahata, T., Uno, T., Ito, M., Ando, K., 2017. Maintenance of Bone Homeostasis by DLL1-Mediated Notch Signaling. J. Cell. Physiol. 232, 2569–2580. https://doi.org/10.1002/jcp.25647

Murphy, W.L., McDevitt, T.C., Engler, A.J., 2014. Materials as stem cell regulators. Nat. Mater. 13, 547–557. https://doi.org/10.1038/nmat3937

Nakamura, S., Matsumoto, T., Sasaki, J.-I., Egusa, H., Lee, K.Y., Nakano, T., Sohmura, T., Nakahira, A., 2010. Effect of calcium ion concentrations on osteogenic differentiation and hematopoietic stem cell niche-related protein expression in osteoblasts. Tissue Eng. Part A 16, 2467–2473. https://doi.org/10.1089/ten.TEA.2009.0337

Navarro, M., Ginebra, M.-P., Clément, J., Salvador, M., Gloria, A., Planell, J.A., 2003a. Physicochemical Degradation of Titania-Stabilized Soluble Phosphate Glasses for Medical Applications. J. Am. Ceram. Soc. 86, 1345–1352. https://doi.org/10.1111/j.1151-2916.2003.tb03474.x

Navarro, M., Ginebra, M.-P., Planell, J.A., 2003b. Cellular response to calcium phosphate glasses with controlled solubility. J. Biomed. Mater. Res. A 67, 1009–1015. https://doi.org/10.1002/jbm.a.20014

Nie, B., Ao, H., Chen, C., Xie, K., Zhou, J., Long, T., Tang, T., Yue, B., 2016. Covalent immobilization of KR-12 peptide onto a titanium surface for decreasing infection and promoting osteogenic differentiation. RSC Adv. 6, 46733–46743. https://doi.org/10.1039/C6RA06778F

Oishi, I., Suzuki, H., Onishi, N., Takada, R., Kani, S., Ohkawara, B., Koshida, I., Suzuki, K., Yamada, G., Schwabe, G.C., Mundlos, S., Shibuya, H., Takada, S., Minami, Y., 2003. The receptor tyrosine kinase Ror2 is involved in non-canonical Wnt5a/JNK signalling pathway. Genes Cells 8, 645–654. https://doi.org/10.1046/j.1365-2443.2003.00662.x

Okamoto, T., Aoyama, T., Nakayama, T., Nakamata, T., Hosaka, T., Nishijo, K., Nakamura, T., Kiyono, T., Toguchida, J., 2002. Clonal heterogeneity in differentiation potential of immortalized human mesenchymal stem cells. Biochem. Biophys. Res. Commun. 295, 354–361. https://doi.org/10.1016/s0006-291x(02)00661-7

Okura, T., Miyachi, T., Monma, H., 2006. Properties and vibrational spectra of magnesium phosphate glasses for nuclear waste immobilization. J. Eur. Ceram. Soc., Proceedings of the International Symposium on Inorganic and Environmental Materials, Eindhoven, NL, October 2004 26, 831–836. https://doi.org/10.1016/j.jeurceramsoc.2005.07.031

Olivares-Navarrete, R., Lee, E.M., Smith, K., Hyzy, S.L., Doroudi, M., Williams, J.K., Gall, K., Boyan, B.D., Schwartz, Z., 2017. Substrate Stiffness Controls Osteoblastic and Chondrocytic Differentiation of Mesenchymal Stem Cells without Exogenous Stimuli. PLOS ONE 12, e0170312. https://doi.org/10.1371/journal.pone.0170312

Olorunniji, F., Igunnu, A., Adebayo, J., Arise, R., Malomo, S., 2007. Cofactor Interactions In The Activation Of Tissue Non-Specific Alkaline Phosphatase: Synergistic Effects Of Zn2+ And Mg2+ Ions. Biokem. ISSN 0795-8080 Vol 19 Num 2 19. https://doi.org/10.4314/biokem.v19i2.56422

Omelon, S., Ariganello, M., Bonucci, E., Grynpas, M., Nanci, A., 2013. A Review of Phosphate Mineral Nucleation in Biology and Geobiology. Calcif. Tissue Int. 93, 382–396. https://doi.org/10.1007/s00223-013-9784-9

Omelon, S., Georgiou, J., Henneman, Z.J., Wise, L.M., Sukhu, B., Hunt, T., Wynnyckyj, C., Holmyard, D., Bielecki, R., Grynpas, M.D., 2009. Control of Vertebrate Skeletal Mineralization by Polyphosphates. PLoS ONE 4. https://doi.org/10.1371/journal.pone.0005634

Omelon, S., Grynpas, M., 2011. Polyphosphates Affect Biological Apatite Nucleation. Cells Tissues Organs 194, 171–175. https://doi.org/10.1159/000324845

Oner, G., Bhaumick, B., Bala, R.M., 1984. Effect of zinc deficiency on serum somatomedin levels and skeletal growth in young rats. Endocrinology 114, 1860–1863. https://doi.org/10.1210/endo-114-5-1860

Orimo, H., 2010. The Mechanism of Mineralization and the Role of Alkaline Phosphatase in Health and Disease. J. Nippon Med. Sch. 77, 4–12. https://doi.org/10.1272/jnms.77.4

Orriss, I.R., Arnett, T.R., Russell, R.G.G., 2016. Pyrophosphate: a key inhibitor of mineralisation. Curr. Opin. Pharmacol., Musculoskeletal 28, 57–68. https://doi.org/10.1016/j.coph.2016.03.003

Oryan, A., Kamali, A., Moshiri, A., Eslaminejad, M.B., 2017. Role of Mesenchymal Stem Cells in Bone Regenerative Medicine: What Is the Evidence? Cells Tissues Organs 204, 59–83. https://doi.org/10.1159/000469704

Otto, F., Thornell, A.P., Crompton, T., Denzel, A., Gilmour, K.C., Rosewell, I.R., Stamp, G.W.H., Beddington, R.S.P., Mundlos, S., Olsen, B.R., Selby, P.B., Owen, M.J., 1997. Cbfa1, a Candidate Gene for Cleidocranial Dysplasia Syndrome, Is Essential for Osteoblast Differentiation and Bone Development. Cell 89, 765–771. https://doi.org/10.1016/S0092-8674(00)80259-7

Oueslati Omrani, R., Kaoutar, A., El Jazouli, A., Krimi, S., Khattech, I., Jemal, M., Videau, J.-J., Couzi, M., 2015. Structural and thermochemical properties of sodium magnesium phosphate glasses. J. Alloys Compd. 632, 766–771. https://doi.org/10.1016/j.jallcom.2015.01.297

Park, K.H., Choi, Y., Yoon, D.S., Lee, K.-M., Kim, D., Lee, J.W., 2018. Zinc Promotes Osteoblast Differentiation in Human Mesenchymal Stem Cells Via Activation of the cAMP-PKA-CREB Signaling Pathway. Stem Cells Dev. 27, 1125–1135. https://doi.org/10.1089/scd.2018.0023

Parsons, A.J., Ahmed, I., Rudd, C.D., Cuello, G.J., Pellegrini, E., Richard, D., Johnson, M.R., 2010. Neutron scattering and ab initio molecular dynamics study of cross-linking in biomedical phosphate glasses. J. Phys. Condens. Matter Inst. Phys. J. 22, 485403. https://doi.org/10.1088/0953-8984/22/48/485403

Parsons, A.J., Sharmin, N., Shaharuddin, S.I.S., Marshall, M., 2015a. Viscosity profiles of phosphate glasses through combined quasi-static and bob-in-cup methods. J. Non-Cryst. Solids 408, 76–86. https://doi.org/10.1016/j.jnoncrysol.2014.10.014

Parsons, A.J., Sharmin, N., Shaharuddin, S.I.S., Marshall, M., 2015b. Viscosity profiles of phosphate glasses through combined quasi-static and bob-in-cup methods. J. Non-Cryst. Solids 408, 76–86. https://doi.org/10.1016/j.jnoncrysol.2014.10.014

Patel, U., Macri-Pellizzeri, L., Zakir Hossain, K.M., Scammell, B.E., Grant, D.M., Scotchford, C.A., Hannon, A.C., Kennedy, A.R., Barney, E.R., Ahmed, I., Sottile, V., 2019. In vitro cellular testing of strontium/calcium substituted phosphate glass discs and microspheres shows potential for bone regeneration. J. Tissue Eng. Regen. Med. 13, 396–405. https://doi.org/10.1002/term.2796

Patel, U., Moss, R.M., Hossain, K.M.Z., Kennedy, A.R., Barney, E.R., Ahmed, I., Hannon, A.C., 2017. Structural and physico-chemical analysis of calcium/strontium substituted, near-invert phosphate based glasses for biomedical applications. Acta Biomater. 60, 109–127. https://doi.org/10.1016/j.actbio.2017.07.002

Paunesku, T., Mittal, S., Protić, M., Oryhon, J., Korolev, S.V., Joachimiak, A., Woloschak, G.E., 2001. Proliferating cell nuclear antigen (PCNA): ringmaster of the genome. Int. J. Radiat. Biol. 77, 1007–1021. https://doi.org/10.1080/09553000110069335

Phetfong, J., Sanvoranart, T., Nartprayut, K., Nimsanor, N., Seenprachawong, K., Prachayasittikul, V., Supokawej, A., 2016. Osteoporosis: the current status of mesenchymal stem cell-based therapy. Cell. Mol. Biol. Lett. 21. https://doi.org/10.1186/s11658-016-0013-1

Pi, M., Faber, P., Ekema, G., Jackson, P.D., Ting, A., Wang, N., Fontilla-Poole, M., Mays, R.W., Brunden, K.R., Harrington, J.J., Quarles, L.D., 2005. Identification of a Novel Extracellular Cation-sensing G-protein-coupled Receptor. J. Biol. Chem. 280, 40201–40209. https://doi.org/10.1074/jbc.M505186200

Poole, K.E.S., Compston, J.E., 2006. Osteoporosis and its management. BMJ 333, 1251–1256. https://doi.org/10.1136/bmj.39050.597350.47

Price, P.A., Otsuka, A.A., Poser, J.W., Kristaponis, J., Raman, N., 1976. Characterization of a gamma-carboxyglutamic acid-containing protein from bone. Proc. Natl. Acad. Sci. 73, 1447–1451. https://doi.org/10.1073/pnas.73.5.1447

Puchtler, H., Meloan, S.N., Terry, M.S., 1969. On the history and mechanism of alizarin and alizarin red S stains for calcium. J. Histochem. Cytochem. Off. J. Histochem. Soc. 17, 110–124. https://doi.org/10.1177/17.2.110

Pujari-Palmer, M., Pujari-Palmer, S., Lu, X., Lind, T., Melhus, H., Engstrand, T., Karlsson-Ott, M., Engqvist, H., 2016. Pyrophosphate Stimulates Differentiation, Matrix Gene Expression and Alkaline Phosphatase Activity in Osteoblasts. PLOS ONE 11, e0163530. https://doi.org/10.1371/journal.pone.0163530

Regan, J., Long, F., 2013. Notch Signaling and Bone Remodeling. Curr. Osteoporos. Rep. 11, 126–129. https://doi.org/10.1007/s11914-013-0145-4

Robling, A.G., Castillo, A.B., Turner, C.H., 2006. Biomechanical and Molecular Regulation of Bone Remodeling. Annu. Rev. Biomed. Eng. 8, 455–498. https://doi.org/10.1146/annurev.bioeng.8.061505.095721

Rochefort, G.Y., Pallu, S., Benhamou, C.L., 2010. Osteocyte: the unrecognized side of bone tissue. Osteoporos. Int. 21, 1457–1469. https://doi.org/10.1007/s00198-010-1194-5

Rodrigues, A.I., Leonor, I.B., Reis, R.L., van Blitterswijk, C., Habibovic, P., 2014. Stimulatory effects of inorganic ions on osteogenesis in vitro, in: Journal of Tissue Engineering and Regenerative Medicine. Presented at the Journal of Tissue Engineering and Regenerative Medicine.

Ross, S.E., Hemati, N., Longo, K.A., Bennett, C.N., Lucas, P.C., Erickson, R.L., MacDougald, O.A., 2000. Inhibition of adipogenesis by Wnt signaling. Science 289, 950–953. https://doi.org/10.1126/science.289.5481.950

Roura, S., Bagó, J.R., Soler-Botija, C., Pujal, J.M., Gálvez-Montón, C., Prat-Vidal, C., Llucià-Valldeperas, A., Blanco, J., Bayes-Genis, A., 2012. Human Umbilical Cord Blood-Derived Mesenchymal Stem Cells Promote Vascular Growth In Vivo. PLoS ONE 7. https://doi.org/10.1371/journal.pone.0049447

Rozario, T., DeSimone, D.W., 2010. The extracellular matrix in development and morphogenesis: A dynamic view. Dev. Biol., Special Section: Morphogenesis 341, 126–140. https://doi.org/10.1016/j.ydbio.2009.10.026

Rubin, H., 1975. Central role for magnesium in coordinate control of metabolism and growth in animal cells. Proc. Natl. Acad. Sci. 72, 3551–3555. https://doi.org/10.1073/pnas.72.9.3551

Ruijtenberg, S., van den Heuvel, S., 2016. Coordinating cell proliferation and differentiation: Antagonism between cell cycle regulators and cell type-specific gene expression. Cell Cycle 15, 196–212. https://doi.org/10.1080/15384101.2015.1120925

Rutkovskiy, A., Stensløkken, K.-O., Vaage, I.J., 2016. Osteoblast Differentiation at a Glance. Med. Sci. Monit. Basic Res. 22, 95–106. https://doi.org/10.12659/MSMBR.901142

Sage, A.P., Lu, J., Tintut, Y., Demer, L.L., 2011. Hyperphosphatemia-induced nanocrystals upregulate the expression of bone morphogenetic protein-2 and osteopontin genes in mouse smooth muscle cells in vitro. Kidney Int. 79, 414–422. https://doi.org/10.1038/ki.2010.390

Sahar, M.R., Abidin, A.Z., 1994. Some properties of CaO-MgO-P2O5 glasses. J. Mater. Sci. Lett. 13, 227–229. https://doi.org/10.1007/BF00571758

Sahar, M.R., Kamaruddin, N., 1996. The phase equilibrium of binary MgO- and CaO-phosphate glasses. J. Mater. Sci. Lett. 15, 1932–1934. https://doi.org/10.1007/BF00274340

Saltman, P.D., Strause, L.G., 1993. The role of trace minerals in osteoporosis. J. Am. Coll. Nutr. 12, 384–389.

Samee, N., de Vernejoul, M.-C., Levi, G., 2007. Role of DLX regulatory proteins in osteogenesis and chondrogenesis. Crit. Rev. Eukaryot. Gene Expr. 17, 173–186. https://doi.org/10.1615/critreveukargeneexpr.v17.i3.10

Sasaki, K., Murakami, T., Kawasaki, M., Takahashi, M., 1987. The cell cycle associated change of the Ki-67 reactive nuclear antigen expression. J. Cell. Physiol. 133, 579–584. https://doi.org/10.1002/jcp.1041330321

Schliephake, H., 2013. Clinical Efficacy of Growth Factors to Enhance Tissue Repair in Oral and Maxillofacial Reconstruction: A Systematic Review: Clinical Efficacy of Growth Factors. Clin. Implant Dent. Relat. Res. 17. https://doi.org/10.1111/cid.12114

Sghayyar, H.N.M., Lim, S.S., Ahmed, I., Lai, J.Y., Cheong, X.Y., Chong, Z.W., Lim, A.F.X., Loh, H.-S., 2020. Fish biowaste gelatin coated phosphate-glass fibres for wound-healing application. Eur. Polym. J. 122, 109386. https://doi.org/10.1016/j.eurpolymj.2019.109386

Shares, B.H., Busch, M., White, N., Shum, L., Eliseev, R.A., 2018. Active mitochondria support osteogenic differentiation by stimulating β-catenin acetylation. J. Biol. Chem. 293, 16019–16027. https://doi.org/10.1074/jbc.RA118.004102

Sharmin, N., Rudd, C.D., 2017. Structure, thermal properties, dissolution behaviour and biomedical applications of phosphate glasses and fibres: a review. J. Mater. Sci. 52, 8733–8760. https://doi.org/10.1007/s10853-017-0784-4

Shih, P.Y., Ding, J.Y., Lee, S.Y., 2003. 31P MAS-NMR and FTIR analyses on the structure of CuO-containing sodium poly- and meta-phosphate glasses. Mater. Chem. Phys. 80, 391–396. https://doi.org/10.1016/S0254-0584(03)00098-1

Shoback, D., Chen, T.H., Pratt, S., Lattyak, B., 1995. Thapsigargin stimulates intracellular calcium mobilization and inhibits parathyroid hormone release. J. Bone Miner. Res. Off. J. Am. Soc. Bone Miner. Res. 10, 743–750. https://doi.org/10.1002/jbmr.5650100511

Shorr, E., Carter, A.C., 1952. The usefulness of strontium as an adjuvant to calcium in the remineralization of the skeleton in man. Bull. Hosp. Joint Dis. 13, 59–66.

Shu, R., McMullen, R., Baumann, M.J., McCabe, L.R., 2003. Hydroxyapatite accelerates differentiation and suppresses growth of MC3T3-E1 osteoblasts. J. Biomed. Mater. Res. A 67, 1196–1204. https://doi.org/10.1002/jbm.a.20021

Silver, I.A., Murrills, R.J., Etherington, D.J., 1988. Microelectrode studies on the acid microenvironment beneath adherent macrophages and osteoclasts. Exp. Cell Res. 175, 266–276. https://doi.org/10.1016/0014-4827(88)90191-7

Sims, N.A., Martin, T.J., 2020. Chapter 10 - Coupling of bone formation and resorption, in: Bilezikian, J.P., Martin, T.J., Clemens, T.L., Rosen, C.J. (Eds.), Principles of Bone Biology (Fourth Edition). Academic Press, pp. 219–243. https://doi.org/10.1016/B978-0-12-814841-9.00010-5

Skelton, K.L., Glenn, J.V., Clarke, S.A., Georgiou, G., Valappil, S.P., Knowles, J.C., Nazhat, S.N., Jordan, G.R., 2007a. Effect of ternary phosphate-based glass compositions on osteoblast and osteoblast-like proliferation, differentiation and death in vitro. Acta Biomater. 3, 563–572. https://doi.org/10.1016/j.actbio.2006.11.008

Skelton, K.L., Glenn, J.V., Clarke, S.A., Georgiou, G., Valappil, S.P., Knowles, J.C., Nazhat, S.N., Jordan, G.R., 2007b. Effect of ternary phosphate-based glass compositions on osteoblast and osteoblast-like proliferation, differentiation and death in vitro. Acta Biomater. 3, 563–572. https://doi.org/10.1016/j.actbio.2006.11.008

Sodek, J., Ganss, B., McKee, M.D., 2000. Osteopontin. Crit. Rev. Oral Biol. Med. Off. Publ. Am. Assoc. Oral Biol. 11, 279–303. https://doi.org/10.1177/10454411000110030101

Solomons, C.C., Styner, J., 1969. Osteogenesis imperfecta: Effect of magnesium administration on pyrophosphate metabolism. Calcif. Tissue Res. 3, 318–326. https://doi.org/10.1007/BF02058674

Srivastava, S., Kumar, N., Thakur, R.S., Roy, P., 2013. Role of vanadium (V) in the differentiation of C3H10t1/2 cells towards osteoblast lineage: a comparative analysis with other trace elements. Biol. Trace Elem. Res. 152, 135–142. https://doi.org/10.1007/s12011-013-9602-2

Stendig-Lindberg, G., Koeller, W., Bauer, A., Rob, P.M., 2004. Experimentally induced prolonged magnesium deficiency causes osteoporosis in the rat. Eur. J. Intern. Med. 15, 97–107. https://doi.org/10.1016/j.ejim.2004.01.003

Strazic Geljic, I., Melis, N., Boukhechba, F., Schaub, S., Mellier, C., Janvier, P., Laugier, J.-P., Bouler, J.-M., Verron, E., Scimeca, J.-C., 2018. Gallium enhances reconstructive properties of a calcium phosphate bone biomaterial. J. Tissue Eng. Regen. Med. 12, e854–e866. https://doi.org/10.1002/term.2396

Strobel, L.A., Hild, N., Mohn, D., Stark, W.J., Hoppe, A., Gbureck, U., Horch, R.E., Kneser, U., Boccaccini, A.R., 2013. Novel strontium-doped bioactive glass nanoparticles enhance proliferation and osteogenic differentiation of human bone marrow stromal cells. J. Nanoparticle Res. 15, 1780. https://doi.org/10.1007/s11051-013-1780-5

Suri, C., Jones, P.F., Patan, S., Bartunkova, S., Maisonpierre, P.C., Davis, S., Sato, T.N., Yancopoulos, G.D., 1996. Requisite role of angiopoietin-1, a ligand for the TIE2 receptor, during embryonic angiogenesis. Cell 87, 1171–1180.

Suzuki, T., Miyamoto, T., Fujita, N., Ninomiya, K., Iwasaki, R., Toyama, Y., Suda, T., 2007. Osteoblast-specific Angiopoietin 1 overexpression increases bone mass. Biochem. Biophys. Res. Commun. 362, 1019–1025. https://doi.org/10.1016/j.bbrc.2007.08.099

Takahashi, K., Tanabe, K., Ohnuki, M., Narita, M., Ichisaka, T., Tomoda, K., Yamanaka, S., 2007. Induction of pluripotent stem cells from adult human fibroblasts by defined factors. Cell 131, 861–872. https://doi.org/10.1016/j.cell.2007.11.019

Talaat, W.M., Ghoneim, M.M., Salah, O., Adly, O.A., 2018. Autologous Bone Marrow Concentrates and Concentrated Growth Factors Accelerate Bone Regeneration After Enucleation of Mandibular Pathologic Lesions. J. Craniofac. Surg. 29, 992–997. https://doi.org/10.1097/SCS.0000000000004371

Tan, C.W., Gardiner, B.S., Hirokawa, Y., Smith, D.W., Burgess, A.W., 2014. Analysis of Wnt signaling β-catenin spatial dynamics in HEK293T cells. BMC Syst. Biol. 8, 44. https://doi.org/10.1186/1752-0509-8-44

Terkeltaub, R.A., 2001. Inorganic pyrophosphate generation and disposition in pathophysiology. Am. J. Physiol. Cell Physiol. 281, C1–C11.

Tharmalingam, S., Daulat, A.M., Antflick, J.E., Ahmed, S.M., Nemeth, E.F., Angers, S., Conigrave, A.D., Hampson, D.R., 2011. Calcium-sensing Receptor Modulates Cell Adhesion and Migration via Integrins. J. Biol. Chem. 286, 40922–40933. https://doi.org/10.1074/jbc.M111.265454

Tharmalingam, S., Hampson, D.R., 2016. The Calcium-Sensing Receptor and Integrins in Cellular Differentiation and Migration. Front. Physiol. 7. https://doi.org/10.3389/fphys.2016.00190

Thiele, S., Rachner, T.D., Rauner, M., Hofbauer, L.C., 2016. WNT5A and Its Receptors in the Bone-Cancer Dialogue. J. Bone Miner. Res. 31, 1488–1496. https://doi.org/10.1002/jbmr.2899

Topol, L., Jiang, X., Choi, H., Garrett-Beal, L., Carolan, P.J., Yang, Y., 2003. Wnt-5a inhibits the canonical Wnt pathway by promoting GSK-3-independent beta-catenin degradation. J. Cell Biol. 162, 899–908. https://doi.org/10.1083/jcb.200303158

Tošić, M., Nikolić, J., Grujić, S., Zivanovic, V., Zildžović, S.N., Matijašević, S.D., Smiljanić, S., 2013. Dissolution behavior of a polyphosphate glass into an aqueous solution under static leaching conditions. J. Non-Cryst. Solids 362, 185–194. https://doi.org/10.1016/j.jnoncrysol.2012.11.024

Tsao, Y.-T., Huang, Y.-J., Wu, H.-H., Liu, Y.-A., Liu, Y.-S., Lee, O.K., 2017. Osteocalcin Mediates Biomineralization during Osteogenic Maturation in Human Mesenchymal Stromal Cells. Int. J. Mol. Sci. 18. https://doi.org/10.3390/ijms18010159

Ullah, I., Subbarao, R.B., Rho, G.J., 2015. Human mesenchymal stem cells - current trends and future prospective. Biosci. Rep. 35. https://doi.org/10.1042/BSR20150025

Uo, M., Mizuno, M., Kuboki, Y., Makishima, A., Watari, F., 1998a. Properties and cytotoxicity of water soluble Na2O–CaO–P2O5 glasses. Biomaterials 19, 2277–2284. https://doi.org/10.1016/S0142-9612(98)00136-7

Uo, M., Mizuno, M., Kuboki, Y., Makishima, A., Watari, F., 1998b. Properties and cytotoxicity of water soluble Na2O–CaO–P2O5 glasses. Biomaterials 19, 2277–2284. https://doi.org/10.1016/S0142-9612(98)00136-7

van Gestel, N.A.P., Geurts, J., Hulsen, D.J.W., van Rietbergen, B., Hofmann, S., Arts, J.J., 2015. Clinical Applications of S53P4 Bioactive Glass in Bone Healing and Osteomyelitic Treatment: A Literature Review. BioMed Res. Int. 2015. https://doi.org/10.1155/2015/684826

van Gestel, N.A.P., Schuiringa, G.H., Hennissen, J.H.P.H., Delsing, A.C.A., Ito, K., van Rietbergen, B., Arts, J.J., Hofmann, S., 2019. Resorption of the calcium phosphate layer on S53P4 bioactive glass by osteoclasts. J. Mater. Sci. Mater. Med. 30, 94. https://doi.org/10.1007/s10856-019-6295-x

van Zoelen, E.J., Duarte, I., Hendriks, J.M., van der Woning, S.P., 2016. TGFβ-induced switch from adipogenic to osteogenic differentiation of human mesenchymal stem cells: identification of drug targets for prevention of fat cell differentiation. Stem Cell Res. Ther. 7, 123. https://doi.org/10.1186/s13287-016-0375-3

Verron, E., Masson, M., Khoshniat, S., Duplomb, L., Wittrant, Y., Baud'huin, M., Badran, Z., Bujoli, B., Janvier, P., Scimeca, J.-C., Bouler, J.-M., Guicheux, J., 2010. Gallium modulates osteoclastic bone resorption in vitro without affecting osteoblasts. Br. J. Pharmacol. 159, 1681–1692. https://doi.org/10.1111/j.1476-5381.2010.00665.x

Vidal-Puig, A.J., Considine, R.V., Jimenez-Liñan, M., Werman, A., Pories, W.J., Caro, J.F., Flier, J.S., 1997. Peroxisome proliferator-activated receptor gene expression in human tissues. Effects of obesity, weight loss, and regulation by insulin and glucocorticoids. J. Clin. Invest. 99, 2416–2422.

Visconti, R., Iversen, T., Cottrell, J., 2019. A Review of Dysregulated Osteoblast and Osteoclast Coupling in Bone Disease and Failure. J. Bone Res. 7, 1–14. https://doi.org/10.35248/2572-4916.19.7.201

Vo, T.N., Kasper, F.K., Mikos, A.G., 2012. Strategies for Controlled Delivery of Growth Factors and Cells for Bone Regeneration. Adv. Drug Deliv. Rev. 64, 1292–1309. https://doi.org/10.1016/j.addr.2012.01.016

Wang, J., Wang, Q., Cui, Y., Liu, Z.Y., Zhao, W., Wang, C.L., Dong, Y., Hou, L., Hu, G., Luo, C., Chen, J., Lu, Y., 2012. Knockdown of cyclin D1 inhibits proliferation, induces apoptosis, and attenuates the invasive capacity of human glioblastoma cells. J. Neurooncol. 106, 473–484. https://doi.org/10.1007/s11060-011-0692-4

Wang, Y., Pan, J., Zhang, Y., Li, X., Zhang, Z., Wang, P., Qin, Z., Li, J., 2019. Wnt and Notch signaling pathways in calcium phosphate-enhanced osteogenic differentiation: A pilot study. J. Biomed. Mater. Res. B Appl. Biomater. 107, 149–160. https://doi.org/10.1002/jbm.b.34105

Wazer, J., Fluck, E., 1959. Principles of Phosphorus Chemistry. VI. Reorganization of Quadruply Connected Monophosphorus Compounds. Part B. The Chlorophosphoric Acids. J. Am. Chem. Soc. - J AM CHEM SOC 81. https://doi.org/10.1021/ja01533a004

Weber, J.M., Calvi, L.M., 2010. Notch Signaling and the Bone Marrow Hematopoietic Stem Cell Niche. Bone 46, 281–285. https://doi.org/10.1016/j.bone.2009.08.007

Wei, X., Yang, X., Han, Z., Qu, F., Shao, L., Shi, Y., 2013. Mesenchymal stem cells: a new trend for cell therapy. Acta Pharmacol. Sin. 34, 747–754. https://doi.org/10.1038/aps.2013.50

Willson, T., Nelson, S.D., Newbold, J., Nelson, R.E., LaFleur, J., 2015. The clinical epidemiology of male osteoporosis: a review of the recent literature. Clin. Epidemiol. 7, 65–76. https://doi.org/10.2147/CLEP.S40966

Wolf, F.I., Cittadini, A., 1999. Magnesium in cell proliferation and differentiation. Front. Biosci. J. Virtual Libr. 4, D607-617.

Wu, M., Chen, G., Li, Y.-P., 2016. TGF-β and BMP signaling in osteoblast, skeletal development, and bone formation, homeostasis and disease. Bone Res. 4, 1–21. https://doi.org/10.1038/boneres.2016.9

Xiong, J.-P., Stehle, T., Zhang, R., Joachimiak, A., Frech, M., Goodman, S.L., Arnaout, M.A., 2002. Crystal Structure of the Extracellular Segment of Integrin αVβ3 in Complex with an Arg-Gly-Asp Ligand. Science 296, 151–155. https://doi.org/10.1126/science.1069040

Xu, J., Li, Z., Hou, Y., Fang, W., 2015. Potential mechanisms underlying the Runx2 induced osteogenesis of bone marrow mesenchymal stem cells. Am. J. Transl. Res. 7, 2527–2535.

Xu, Y., Cruz, T.F., Pritzker, K.P., 1991. Alkaline phosphatase dissolves calcium pyrophosphate dihydrate crystals. J. Rheumatol. 18, 1606–1610.

Xue, W., Dahlquist, K., Banerjee, A., Bandyopadhyay, A., Bose, S., 2008. Synthesis and characterization of tricalcium phosphate with Zn and Mg based dopants. J. Mater. Sci. Mater. Med. 19, 2669–2677. https://doi.org/10.1007/s10856-008-3395-4

Xynos, I.D., Edgar, A.J., Buttery, L.D.K., Hench, L.L., Polak, J.M., 2001. Gene-expression profiling of human osteoblasts following treatment with the ionic products of Bioglass® 45S5 dissolution. J. Biomed. Mater. Res. 55, 151–157. https://doi.org/10.1002/1097-4636(200105)55:2<151::AID-JBM1001>3.0.CO;2-D

Yamaguchi, M., 1998. Role of zinc in bone formation and bone resorption. J. Trace Elem. Exp. Med. 11, 119–135. https://doi.org/10.1002/(SICI)1520-670X(1998)11:2/3<119::AID-JTRA5>3.0.CO;2-3

Yamaza, H., Sonoda, S., Nonaka, K., Kukita, T., Yamaza, T., 2018. Pamidronate decreases bilirubin-impaired cell death and improves dentinogenic dysfunction of stem cells from human deciduous teeth. Stem Cell Res. Ther. 9, 303. https://doi.org/10.1186/s13287-018-1042-7

Yang, C., Su, H., Liao, X., Han, C., Yu, T., Zhu, G., Wang, X., Winkler, C.A., O'Brien, S.J., Peng, T., 2018. Marker of proliferation Ki-67 expression is associated with transforming growth factor beta 1 and can predict the prognosis of patients with hepatic B virus-related hepatocellular carcinoma. Cancer Manag. Res. 10, 679–696. https://doi.org/10.2147/CMAR.S162595

Yang, F., Yang, D., Tu, J., Zheng, Q., Cai, L., Wang, L., 2011. Strontium Enhances Osteogenic Differentiation of Mesenchymal Stem Cells and In Vivo Bone Formation by Activating Wnt/Catenin Signaling. STEM CELLS 29, 981–991. https://doi.org/10.1002/stem.646

Yao, W., Cheng, Z., Shahnazari, M., Dai, W., Johnson, M.L., Lane, N.E., 2010. Overexpression of Secreted Frizzled-Related Protein 1 Inhibits Bone Formation and Attenuates Parathyroid Hormone Bone Anabolic Effects. J. Bone Miner. Res. 25, 190–199. https://doi.org/10.1359/jbmr.090719

Yoshizawa, S., Brown, A., Barchowsky, A., Sfeir, C., 2014a. Role of magnesium ions on osteogenic response in bone marrow stromal cells. Connect. Tissue Res. 55 Suppl 1, 155–159. https://doi.org/10.3109/03008207.2014.923877

Yoshizawa, S., Brown, A., Barchowsky, A., Sfeir, C., 2014b. Role of magnesium ions on osteogenic response in bone marrow stromal cells. Connect. Tissue Res. 55, 155–159. https://doi.org/10.3109/03008207.2014.923877

Yoshizawa, S., Brown, A., Barchowsky, A., Sfeir, C., 2014c. Magnesium ion stimulation of bone marrow stromal cells enhances osteogenic activity, simulating the effect of magnesium alloy degradation. Acta Biomater. 10, 2834–2842. https://doi.org/10.1016/j.actbio.2014.02.002

Yuan, H., de Bruijn, J.D., Zhang, X., van Blitterswijk, C.A., de Groot, K., 2001. Bone induction by porous glass ceramic made from Bioglass® (45S5). J. Biomed. Mater. Res. 58, 270–276. https://doi.org/10.1002/1097-4636(2001)58:3<270::AID-JBM1016>3.0.CO;2-2

Yuasa, M., Yamada, T., Taniyama, T., Masaoka, T., Xuetao, W., Yoshii, T., Horie, M., Yasuda, H., Uemura, T., Okawa, A., Sotome, S., 2015. Dexamethasone Enhances Osteogenic Differentiation of Bone Marrow- and Muscle-Derived Stromal Cells and Augments Ectopic Bone Formation Induced by Bone Morphogenetic Protein-2. PLOS ONE 10, e0116462. https://doi.org/10.1371/journal.pone.0116462

Zachariasen, W.H., 1932. THE ATOMIC ARRANGEMENT IN GLASS. J. Am. Chem. Soc. 54, 3841–3851. https://doi.org/10.1021/ja01349a006

Zamurovic, N., Cappellen, D., Rohner, D., Susa, M., 2004. Coordinated activation of notch, Wnt, and transforming growth factor-beta signaling pathways in bone morphogenic protein 2-induced osteogenesis. Notch target gene Hey1 inhibits mineralization and Runx2 transcriptional activity. J. Biol. Chem. 279, 37704–37715. https://doi.org/10.1074/jbc.M403813200

Zanotti, S., Canalis, E., 2016. Notch Signaling and the Skeleton. Endocr. Rev. 37, 223–253. https://doi.org/10.1210/er.2016-1002

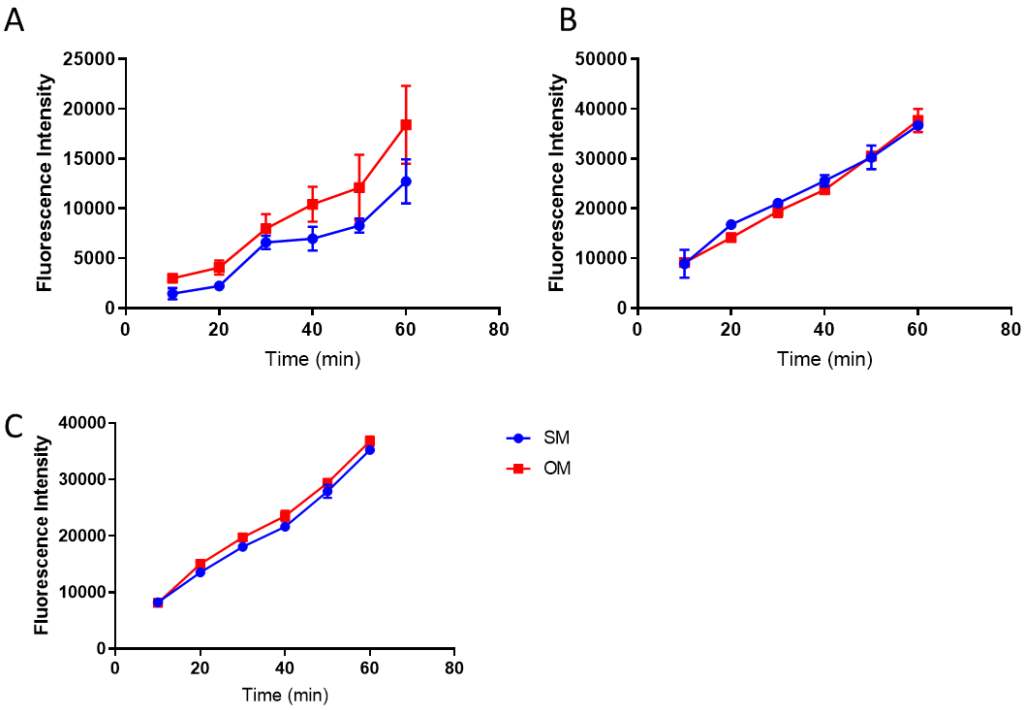
Zhang, A.-X., Yu, W.-H., Ma, B.-F., Yu, X.-B., Mao, F.F., Liu, W., Zhang, J.-Q., Zhang, X.-M., Li, S.-N., Li, M.-T., Lahn, B.T., Xiang, A.P., 2007. Proteomic identification of differently expressed proteins responsible for osteoblast differentiation from human mesenchymal stem cells. Mol. Cell. Biochem. 304, 167–179. https://doi.org/10.1007/s11010-007-9497-3

Zhang, J., Liu, C., Li, Y., Sun, J., Wang, P., Di, K., Zhao, Y., 2010. Effect of cerium ion on the proliferation, differentiation and mineralization function of primary mouse osteoblasts in vitro. J. Rare Earths 28, 138–142. https://doi.org/10.1016/S1002-0721(09)60067-3

Zhuang, H., Zhang, X., Zhu, C., Tang, X., Yu, F., Shang, G.W., Cai, X., 2016. Molecular Mechanisms of PPAR-γ Governing MSC Osteogenic and Adipogenic Differentiation. Curr. Stem Cell Res. Ther. 11, 255–264. https://doi.org/10.2174/1574888x10666150531173309

Zoch, M.L., Clemens, T.L., Riddle, R.C., 2016. New insights into the biology of osteocalcin. Bone 82, 42–49. https://doi.org/10.1016/j.bone.2015.05.046

Appendix I – PrestoBlue Optimization

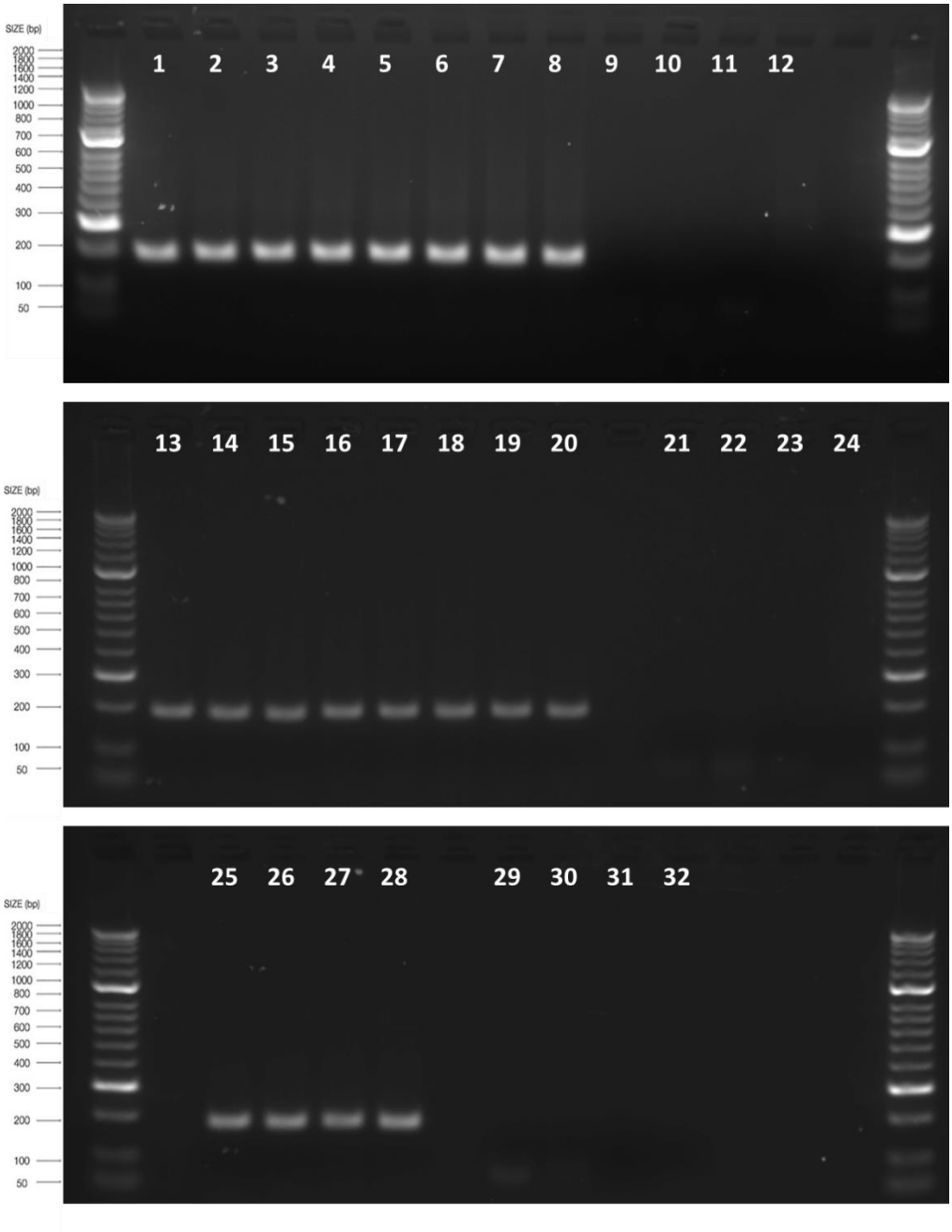


Appendix Figure 1. PrestoBlue optimization at day 2, 7 and 11 on hMSC culture. 40 minutes was the selected incubation time due to being within the linear phase.

Appendix II – cDNA validation

Appendix Table 1. Housekeeping gene primers used for cDNA validation

	B-Actin
Forward	TCACCCACACTGTGCCCATCTACGA
Reverse	CAGCGGAACCGCTCATT GCCAATGG



Appendix Figure 2. cDNA validation of hMSC samples by RT-PCR and gel electrophoresis. Successful validation of SM (1, 13), OM (2,14), OM- (3, 15), 555 (4, 16), P40 (5, 17), P40OM- (6, 18), Mix (7, 19), MixOM- (8, 20), P45 (25, 27) and P45OM- (26, 28) samples against no tissue control (9, 21,29), RT negative (10, 22, 30), RNA negative (11, 23, 31) and PCR negative (12, 24, 32).